Characterisation of the LH2 complexes of *Allochromatium vinosum*

Kirsty Anne Hacking
BSc.(Hons.)

Submitted in fulfilment of the requirements for the degree of Doctor of Philosophy

School of Molecular, Cellular and Systems Biology

College of Medical, Veterinary and Life Sciences

University of Glasgow

2015

Author's declaration

This thesis is an original composition which describes work performed entirely by myself unless otherwise cited or acknowledged. Its contents have not previously been submitted for any other degree. The research for this degree was preformed between 2011 and 2015.

Signature……

Printed Name ……

Abstract

Purple photosynthetic bacteria contain a highly efficient light-harvesting system of LH2 and LH1 complexes, consisting of peptides, bacteriochlorophyll, and carotenoids, which allow cells to grow photosynthetically under different environmental conditions.

Allochromatium (Alc.) vinosum is a sulphur purple photosynthetic bacterium that was found to produce several different LH2 complex types under different growth and nutritional conditions. These LH2 complexes have been identified as the B800-820, B800-840, and B800-850. All of the LH2 complex types of *Alc. vinosum* were confirmed as heterogeneous forming part of the basis of the unusual split B800 peak due to two potential B800 binding sites on the alpha peptides. This work produced CD data to suggest that excitonic coupling of the B800 BChl occurs and Monte Carlo simulations produced in conjunction with this work indicated that this would also contribute to the splitting of the band observed. The carotenoids of the spirilloxanthin pathway were identified within all of the LH2 complexes, however, the specific carotenoid composition varied depending on the LH2 complex type.

Unlike most purple photosynthetic bacteria, *Alc. vinosum* is able to produce LH2 complexes in the absence of carotenoid biosynthesis. Carotenoidless LH complexes are ideal for the process of reconstitution, often used to elucidate structure function relationships within complexes. Carotenoidless LH2 complexes were produced and used for proof of concept reversible dissociation studies. This work identified the B800-850 LH2 complex as a reconstitution candidate for further work.

Acknowledgements

This whole process has been a wonderful, but at times very trying time in my life. All the experiences I've had and the people I've met over this time have helped me grow as an individual and I would like to profusely thank Prof. Richard Cogdell for giving me this opportunity.

I would also like to thank the EPSCR and PARC for providing my funding for this work.

I would like to thank the whole Cogdell lab, old and new, but especially thanks to Dr Anne-Marie Carey from the bottom of my heart, I could always rely on you for a laugh or a deep hippy conversation. You were a role model I could look up to and a bastion of support. A big thanks to Dr Khuram Ashraf for being willing to read, and re-read through multiple drafts of this thesis and always trying to help me out whenever he could, with a kind word or a good giggle. Thanks to Dr Sarah Henry for designing the primers for the CrtI^{-} mutant, I wish I'd managed to make the carotenoid minus mutant. I'd like to thank all members of the Cogdell lab for their help and good humour throughout my years here: Dr Alastair Gardiner, June Southall, Dr Rachel Mulvaney, Dr Heiko Lokstein, Dr Aleks Roszak and Laura Cranston. I'd like to extend my thanks to my lab buddies on the Level 2 of the GBRC who were always good for some much needed banter and a good gurn when I went by (but I am still waiting for Síle Johnsons headshots).

I'd like to thank Dr Sharon Kelly for her help with the CD and advice on keeping calm and maintaining perspective. The biscuits were also always appreciated! A big thank you to Dr Bill Mullen for tolerating my questions on the Tandem MS-MS and putting up with my impromptu visits. Many thanks to Prof. Harry Frank, Dr Nikki Magdaong and Dr Amy LaFountain, all such lovely and kind people who were wonderful to collaborate with and I'd happily have them come back to visit.

A particular thank you has to go out to the friends who have rallied to me when this all got too much. I'd like to thank Holly for being a wonderful sister, always ready with a cookie, a kind ear, and more than a small dose of weird to remind

me that there's nothing wrong with still being about 5 years old mentally. Thanks to Annabel Campbell for the Friday evenings with a glass of wine and all the dog hugs I needed to keep me going. Thanks to Julie Riddell for fueling me with pancakes and sass (all the sass!), as well as thanks to Dr Hazel Bracken for always being willing to, quite literally, give me a good kick to keep me going! And a massive thank you to Kim Boney for being who she is and keeping me motivated when I really didn't feel I could keep going, even if you did have to tape me to my desk at times. You had faith in me when I had none, and that means a lot.

I would also like to thank my family, who I have not been able to see as much as I would have liked to over the last few years. I have received overwhelming love and support from them all. I'd like to thank my mum, Celia Hacking, for always listening to my calls even when she doesn't know what I'm talking about, and my dad, Dr Derek Hacking, for helping me with the physics and maths that have always scuppered me. I'd like to thank my siblings for tolerating my moods and distant contact: Zanne Hacking, Simon Hacking, Peter Hacking, and Lyn Tallon. I'd also like to say to my nephews and nieces; Danny, Calan, Maïlys, Iona, and the newest addition James, that Aunty Kirsty will be free to come play much more often now!

Without you all I would not have made it!

"*Ne perds pas l'occasion de voir quelque chose de beau. La beauté,*

C'est la signature de Dieu" - Charles Kingsley

Table of contents

List of tables

List of figures

List of Abbreviations

^{1*}	Singlet excited state
^{3*}	Triplet excited state
α	Alpha
ß	Beta
Alc. vinosum	*Allochromatium vinosum*
Amp	Ampicillin
AU	Arbitrary units
B800	BChl with absorption maximum at ~ 800 nm
B820	BChl with absorption maximum at ~ 820 nm
B850	BChl with absorption maximum at ~ 850 nm
BChl	Bacteriochlorophyll
CD	Circular Dichroism
CMC	Critical micelle concentration
CO_2	Carbon dioxide
Cyt C	Cytochrome c
DDM	Dodecyl maltoside
DM	Decyl maltoside
DTT	Dithiothreitol
E.coli	*Escherichia coli*
EDTA	Ethylenediaminetetraacetic acid
Kana	Kanamycin
LB	Luria Broth
LDAO	lauryl dimethylamine oxide
LH1	Light-harvesting complex 1
LH2	Light-harvesting complex 2
LT	Low temperature (77 K)
OD	Optical density
OG	Octyl glucoside
PCR	Polymerase chain reaction
RC	Reaction centre
RT	Room temperature (25 ℃)
SDCG	Sucrose density centrifugation gradient
SDC	Sucrose density centrifugation
SDS PAGE	Sodium dodecyl sulphate polyacrylamide gel electrophoresis
SEC	Size Exclusion Chromatography
SOE	Splice, Overlap, Extension
SHL40	Sulphide, high light, 40 ◦C growth conditions
SHL30	Sulphide, high light, 30 ◦C growth conditions
SLL40	Sulphide, low light, 40 ◦C growth conditions
SLL30	Sulphide, low light, 30 ◦C growth conditions
THL40	Thiosulphate, high light, 40 ◦C growth conditions
THL30	Thiosulphate, high light, 30 ◦C growth conditions
TLL40	Thiosulphate, low light, 40 ◦C growth conditions
TLL30	Thiosulphate, low light, 30 ◦C growth conditions

Chapter 1 - Introduction

1.1 Photosynthesis

Photosynthesis is one of the most important processes on Earth as it is essential for life. Photosynthesis provides the energy input for nearly all ecosystems by converting solar energy into a chemical form. Multiple organisms such as plants and algae have evolved to perform photosynthesis whereby solar energy is absorbed and used to fix carbon dioxide and reduce it into carbohydrates with oxygen as the by-product. The production of oxygen and the harnessing of solar energy for life highlight the importance of photosynthesis and its role in Earths ecosystems.

The main focus in early photosynthesis research was on oxygenic photosynthesis i.e. plants, which began in the beginning of the 17th century (1). Jan Baptista van Helmont (1580-1644) deduced from a simple weighing experiment that trees don't build their mass from parts in the soil but from the water they absorb. The phlogiston theory, postulated at the end of the 17th century by Joachim Becher (1635-1682), identified phlogiston as the flammable substance that is released into the air by substances upon combustion (2). Many scientists subscribed to this theory including Joseph Priestley (1733-1804) who applied this to experiments on the ability of plants to 'dephlogisticate' air. He found that, upon the addition of a sprig of mint, a candle would burn again for a brief period of time inside a container of air that had previously been 'phlogisticated'. This identified "dephlogistigated air" or, according to Lavoisier's pneumatic theory, oxygen as a product of the plant and integral for a candle to burn. Jan Ingenhousz (1730-1799) discovered that light was integral to the production of oxygen by plants as in darkness they "phlogisticate" the air like a candle. Jean Senebier (1742-1809) noted that plants require carbon dioxide (or 'fixed air') in order to "dephlogisticate" the air but it was Nicolas-Theodore de Saussure in the 19th century who deduced that the plants increase of mass is derived from both water and carbon dioxide. It was only with Sergei Winogradskys (1856-1953) development of the Winogradsky column in the 1880's (3) that the realm of photosynthesis began to substantially expand to include bacterial photosynthesis. A Winograsky column is a column of pond water and sediment that is enriched for the growth of pond bacteria and algae. Different layers of

added sediment create gradients of both oxygen and sulphur down the column, selecting for the growth of different species. The Winogradsky column allowed scientists such as Cornelius van Niel to grow up anoxygenic sulphur bacteria in the laboratory.

It was the study and contrast between the oxygenic phototrophs and the sulphur using phototrophs that aided van Niel in the 1920's to conclude that the production of oxygen is not from the splitting of carbon dioxide, rather it is due to the splitting of water (4). By comparing oxygenic and anoxygenic sulphur consuming phototrophs, van Niel (1931) determined that while oxygenic phototrophs produced oxygen as a by-product, purple sulphur bacteria used reduced sulphur compounds and produced sulphur as their by-product. This allowed van Niel to determine the general equation for photosynthesis (Equation 1) wherein a molecule, such as water (Equation 2) or a reduced sulphur compound (Equation 3), is used as an electron donor for the reduction of carbon dioxide.

General equation for photosynthesis as determined by van Niel (4), where A is a suitable electron donor, such as H_2O, thiosulphate, or a reduced carbon compound.

$$CO_2 + 2H_2A + \text{light energy} = C(H_2O)_n + H_2O + 2A \quad (1)$$

The most common form of photosynthesis, oxygenic photosynthesis, evolved to use water as the electron donor, and results in diatomic oxygen as the oxidised end product (Equation 2). This is the form of photosynthesis that occurs in plants and algae.

The equation for oxygenic photosynthesis, as determined by van Niel (4), with water as the electron donor producing diatomic oxygen as the by-product.

$$CO_2 + 2H_2O + \text{light energy} = C(H_2O)_n + H_2O + O_2 \quad (2)$$

Alternatively, if the electron donor is an inorganic substrate this produces a different oxidised by-product, forming the basis of anoxygenic photosynthesis. Anoxygenic photosynthesis is the form observed in photosynthetic bacteria and can use a variety of different electron donor molecules. The electron donor can be a variety of different inorganic molecules, such as hydrogen sulphide (5, 6), or organic molecules, such as succinate (7, 8). Equation 3 shows the overall

equation if the electron donor is hydrogen sulphide, creating a by-product of sulphur.

The equation for anoxygenic photosynthesis, as determined by van Niel (4), with hydrogen sulphide as the electron donor producing elemental sulphur as the by-product.

$$CO2 + 2H_2S + \text{light energy} = C(H_2O)_n + H_2O + 2S^0 \quad (3)$$

There are several groups of organisms that are able to grow photosynthetically. These are plants, cyanobacteria, algae, and halobacteria as well as purple and green photosynthetic bacteria. The archaean halobacteria harvest energy from sunlight but are not conventional phototrophs as they do not use chlorophyll light-harvesting systems, rather protein light-driven proton pumps unlike the other organisms listed (9).

1.2 Purple photosynthetic bacteria

Purple photosynthetic bacteria are one of the model organisms used to study photosynthesis due to their simplicity, ease of growth and the robustness of their photosynthetic apparatus. Previously, purple photosynthetic bacteria were classified into two groups depending on whether or not they metabolised sulphur compounds. Modern molecular techniques have illuminated further distinctions, showing that the photosynthetic bacteria fall into three subgroups alphaproteobacteria, betaproteobacteria and gammaproteobacteria (10). It is the alpha and betaproteobacteria subtypes that make up the non-sulphur contingent of purple photosynthetic bacteria while the sulphur bacteria are placed within the gammaproteobacteria (11)(Table 1.1).

Table 1.1 Examples of common purple photosynthetic bacterial species from the subtypes alphaproteobacteria and gammaproteobacteria, which are referenced in this work. (11)

Subtype	Alphaproteobacteria	Gammaproteobacteria
Family	Rhodospirillaceae	Chromatiaceae
Species	*Rhodopseudomonas (Rps.) palustris*	(Previously *Chromatium*) *Allochromatium (Alc.) vinosum*
	Rhodopseudomonas (Rps.) viridis	*Allochromatium (Alc.) minutissimum*
	Rhodopseudomonas (Rps.) acidophila	
		Marichromatium (Mch.) purpuratum
	Rhodobacter (Rba.) capsulatus	
	Rhodobacter (Rba.) spheroides	
		Thermochromatium (Tch.) tepidum
	Phaeospirillum (Phs.) molischianum	
	Rhodospirillum (Rsp.) rubrum	

Alpha-, beta-, and gammaproteobacteria require anaerobic conditions in order to grow photosynthetically. It is under low oxygen partial pressures that they produce the structures and complexes required for photosynthesis (12-14), such as the intracytoplasmic membrane (ICM). Structures such as the ICM are not present when the purple photosynthetic bacterium grows chemoheterotrophically (15). The ICM is a continuous membrane that is distinct from the inner membrane and is used to house the light reactions of the bacterium (11). The structure of the ICM varies between different species of bacteria, forming lamellae in some and chromatophores in others (16). Purple photosynthetic bacteria grow photosynthetically when they inhabit low oxygen environments such as the bottom of ponds and stagnant water (Figure 1.1). They inhabit the stratum below the oxygenic phototrophs, such as algae and cyanobacteria. A consequence of this is that the wavelengths of light that reach the purple photosynthetic bacteria are limited due to being filtered through these oxygenic, chlorophyll containing phototrophs. Chlorophyll containing organisms absorb wavelengths in the blue and red parts of the incident solar spectrum. This results in only the green and NIR wavelengths of light reaching the organisms in the lower layers of water. For this reason, purple photosynthetic bacteria use pigments that are able to absorb light in the green

and near infrared (NIR) regions of the absorption spectrum and use it for photosynthesis.

Purple sulphur and non-sulphur bacteria occupy different layers within bodies of water (Figure 1.1). Purple sulphur bacteria occupy the very bottom of ponds as decaying matter sinks to the bottom. It is this decaying matter that is the source of the reduced sulphur compounds that purple sulphur bacteria use as electron donors. Purple non-sulphur bacteria inhabit the stratum above the sulphur bacteria (17).

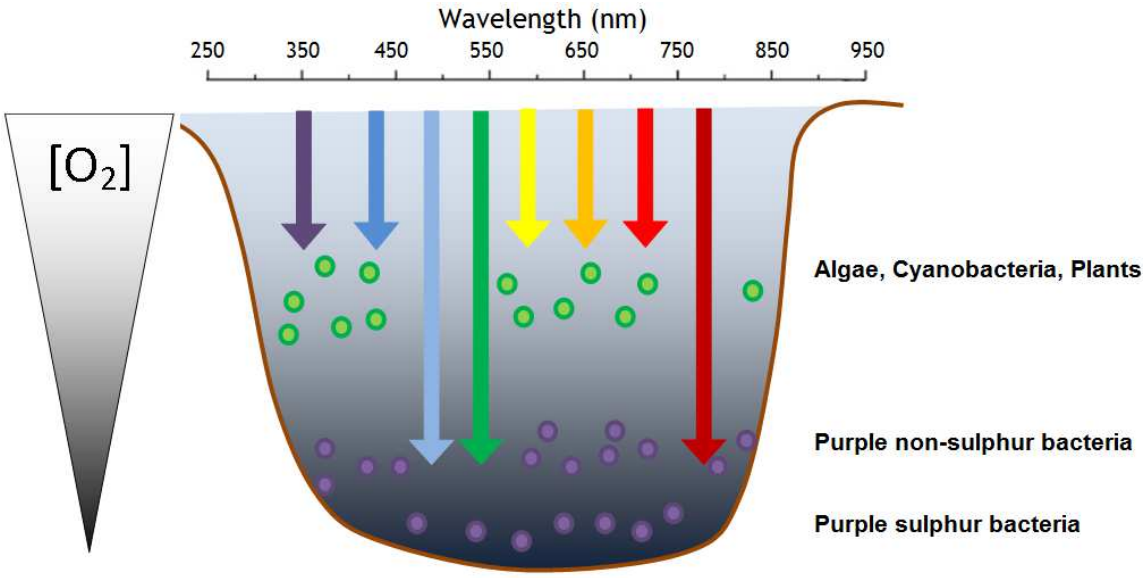

Figure 1.1 Schematic diagram of a pond containing different phototrophs; algae, cyanobacteria, and purple photosynthetic bacteria.
The different wavelengths of light shown on the axis across the top are represented by coloured arrows. These different wavelengths of light are filtered through the chlorophyll containing algae and cyanobacteria present in the upper layers of the water. These phototrophs are oxygenic, producing oxygen that results in an oxygen gradient as further from the oxygenic phototrophs the level of oxygen greatly reduces. The purple photosynthetic bacteria require low oxygen concentrations to photosynthesise and so they occupy the lower layers of water, where the level of oxygen is lowest. The wavelengths of light that penetrate through the chlorophyll containing phototrophs are the blue, green and near infrared regions of the absorption, which reach the purple photosynthetic bacteria at the bottom of the pond. Purple sulphur bacteria inhabit the deepest parts of the pond in order to access the sulphur compounds released by decaying material, whereas purple non-sulphur bacteria inhabit the layer of water above the purple sulphur bacteria.

1.2.1 An overview of the light reactions of purple photosynthetic bacteria

Historically, photosynthesis has been split into two sets of reactions, the light and dark reactions. The light reactions involve the harvesting of light energy by pigments; in purple photosynthetic bacteria the light energy is then converted

into ATP molecules and a reduced cofactor, $NADH_2$. The dark reactions use the ATP and $NADH_2$ to fix and reduce simple organic molecules into sugars (18).

The light reactions are based within the ICM in purple photosynthetic bacteria (11) while the dark reactions occur free in solution within the cytoplasm. Incident photons are absorbed by an array of light-harvesting complexes within the ICM of the photosynthetic bacterium. These complexes consist of proteins that contain bacteriochlorophyll (BChl) and carotenoid pigments. The pigments absorb light energy and funnel it down an energy gradient to a central reaction centre (RC) where a charge separation occurs across the membrane, effectively 'trapping' the solar energy in a chemical form.

The charge separation in the RC powers a series of REDOX reactions involving other protein complexes bound within the ICM (Figure 1.2) that lead to the formation of a proton motive force (PMF). As a result of the primary charge separation reactions, a quinone is reduced to a quinol. The quinol is subsequently released into the membrane where it reduces the cytochrome b/c_1 complex (19) translocating two protons across the membrane, creating a PMF. The electrons from the quinol reduce the cytochrome c complex (20), which then reduces the RC to prepare it for more charge separation. It is the PMF that provides the driving force for the ATPsynthase (21, 22) complex in order to create ATP.

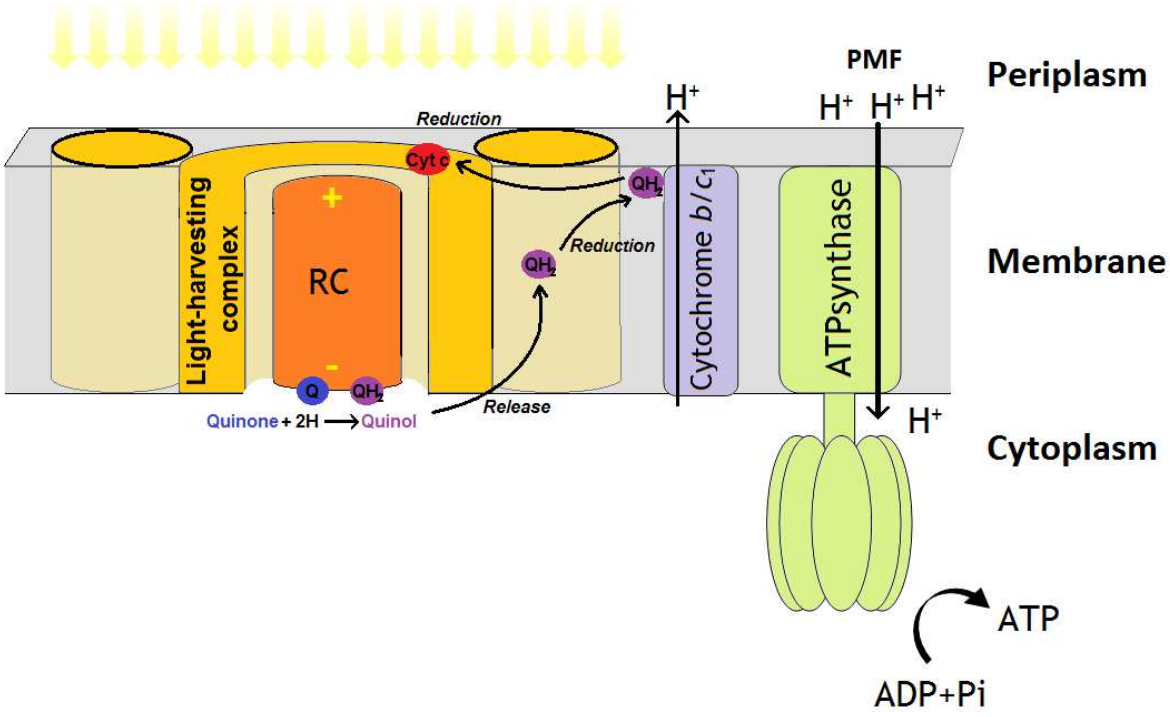

Figure 1.2 Schematic diagram showing the proteins within the ICM of purple photosynthetic bacteria that are involved in the light-dependant reactions.
These membrane bound complexes harvest light energy and convert it into ATP and $NADPH_2$ for the dark reactions. The energy is absorbed by the light-harvesting complexes that funnel the energy to the reaction centre (RC). This energy is used by the RC to create a charge separation across the membrane to fuel the reduction of a quinone. The oxidation of the quinone by the cytochrome b/c_1 complex (19) translocates two protons across the membrane into the periplasm, creating a proton motive force (PMF). The electrons are transferred to the cytochrome c complex (20), which reduces the RC. The PMF is used by the ATP synthase complex to create ATP (22).

1.3 Purple bacterial photosynthetic light-harvesting machinery

The first stage of the light reactions is the absorption of solar energy, and this is performed by light-harvesting complexes. The light harvesting complexes sit peripherally to the RC and act like an energy funnel absorbing the solar energy and transferring it down an energy gradient to the RC. This increases the cross section of solar energy captured for use by the RC for charge separation.

The light-harvesting complexes and RC consist of bacteriochlorophyll (BChl) and carotenoid pigments packaged within a protein scaffold. These complexes form arrays within the membrane (23, 24) that allows easy energy transfer from the peripheral light-harvesting machinery to the reaction centre.

When one of the pigments absorbs a photon, an electron is excited to a higher energy level (Figure 1.3 S_1 or S_2). The energy is then transferred on or is

dissipated through several photosynthetically non-productive processes. In the light-harvesting complexes energy transfer occurs from the first excited singlet state and in reaction centres this excited state is used to drive the first electron transfer reaction. The processes involved in the electron excitation and relaxation are easily visualised using a Jablonski diagram (Figure 1.3). The excitation of an electron by a photon stimulates the electron out of the ground state and into a higher energy singlet excitation level (Figure 1.3, heavy black lines dubbed S_1 and S_2). Electrons in the singlet excitation level are able to decay back to the ground state progressively or, preferably in photosynthesis, transfer the energy on or be transferred on. Each energy level contains multiple smaller vibrational states, (Figure 1.3, light dashed lines). The energy of the electron dissipates through several different non-radiative and radiative processes. Non-radiative modes of energy dissipation include vibrational relaxation and internal conversion. Energy lost within an energy state as the electron falls down the vibrational states is referred to as vibrational relaxation, while the movement of an electron down to another energy level is internal conversion. A change in the spin multiplicity, whereby the electron spin reverses direction, causes the electron to move from a singlet excitation state to a triplet excitation state. This is termed intersystem crossing (Figure 1.3 ISC, S_1 to T_1). The triplet excited electron and its partner in the ground state have parallel spins resulting in the transition to the ground state being forbidden due to the Pauli Exclusion Principle (25). This results in the triplet excitation state being long lived in comparison to the singlet state, milliseconds in comparison to nanoseconds in the case of bacteriochlorophyll (26). Fluorescence and phosphorescence are forms of radiative energy dissipation that occur if the energy cannot be transferred on by excitation energy transfer. Fluorescence occurs from singlet excitation states and occurs at a slightly longer wavelength than the position of the absorption band due to energy loss from internal conversion and vibrational relaxation. Phosphorescence is the release of the energy from the triplet excitation states and so occurs over a much longer period of time.

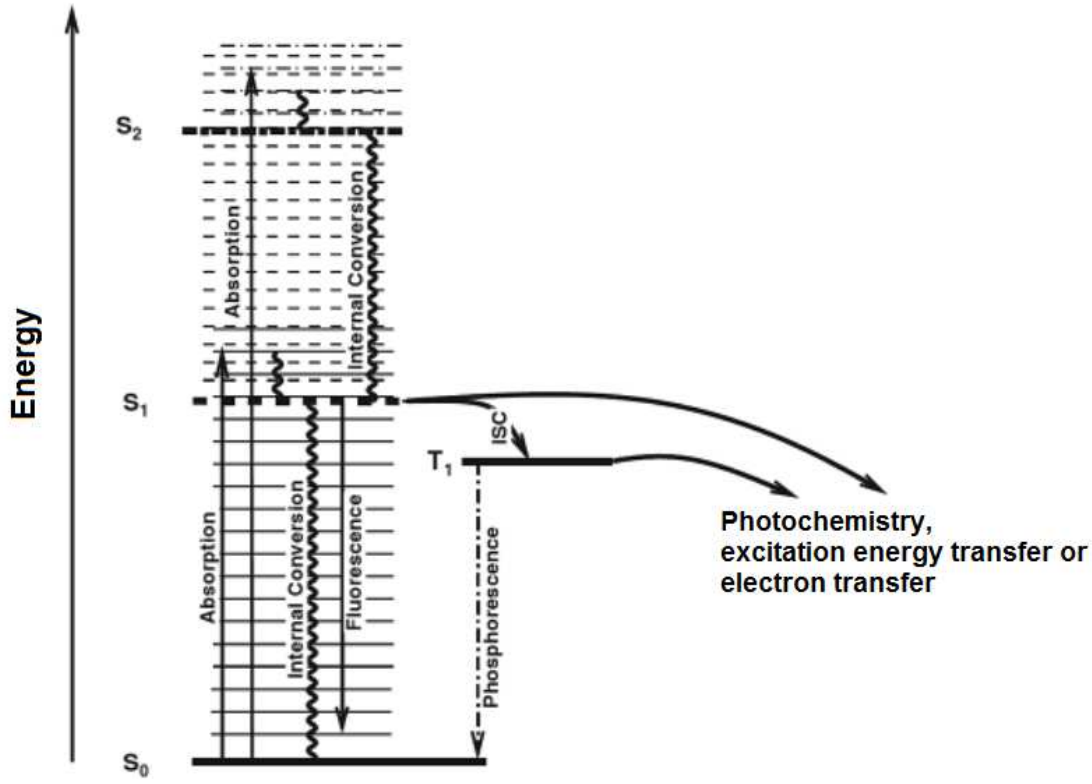

Figure 1.3 Jablonski diagram (27) showing the electron excited singlet (S_1 and S_2) and triplet (T_1) states and the different modes of energy decay that return the electron to the ground state (S_0).
Excitation by a photon (absorption) excites the electron from the ground state into the S_1, S_2, or S_3 states. The energy dissipates in non-radiative (internal conversion, vibrational relaxation, and intersystem crossing) and radiative methods (fluorescence, and phosphorescence). Vibrational relaxation is the dissipation of energy as the electron relaxes down the different vibrational states within the energy state. Internal conversion is the dissipation of the energy allowing the electron to fall down an energy state. Upon a change of the spin multiplicity of the electron changes the electron from a singlet (S_1) state to a triplet state (T_1), this is referred to as intersystem crossing (ISC). The radiative modes of energy dissipation are fluorescence and phosphorescence to return the electron to the ground state energy level.

1.3.1 **Pigments**

The major light-harvesting pigment of purple photosynthetic bacteria is BChl. Six types of BChl have been identified in nature; BChl a, b (28), c , d, e, and g (29), but purple photosynthetic bacteria are only known to possess BChl a and b (30). The BChl molecule can be separated into two basic parts – the hydrophobic tail and the bacteriochlorin ring (Figure 1.4). The bacteriochlorin ring consists of five macrocycles, (I, II, III, IV, and V) with a central Mg^{2+} ion. It is the bacteriochlorin ring that contains the conjugated system of π-bonds that forms the chromophore. The chromophore is the part of the pigment molecule that absorbs light energy. The structure of BChl a is shown in figure 1.4 and the green box shows the group that is substituted between BChl a and BChl b (28). The effect of this change is that BChl b produces a more red-shifted absorption spectrum

than BChl a due to an increase in the length of the π-bond system. The hydrophobic tail increases the hydrophobic nature of the BChl molecule and can be either a geranylgeraniol group (31) or a phytol group (28) (Figure 1.4). The main structural difference between the two hydrophobic tail types is the presence of double bonds in the geranylgeranyl group that are absent in the phytyl tail. There is no functional difference between the two hydrophobic tail groups.

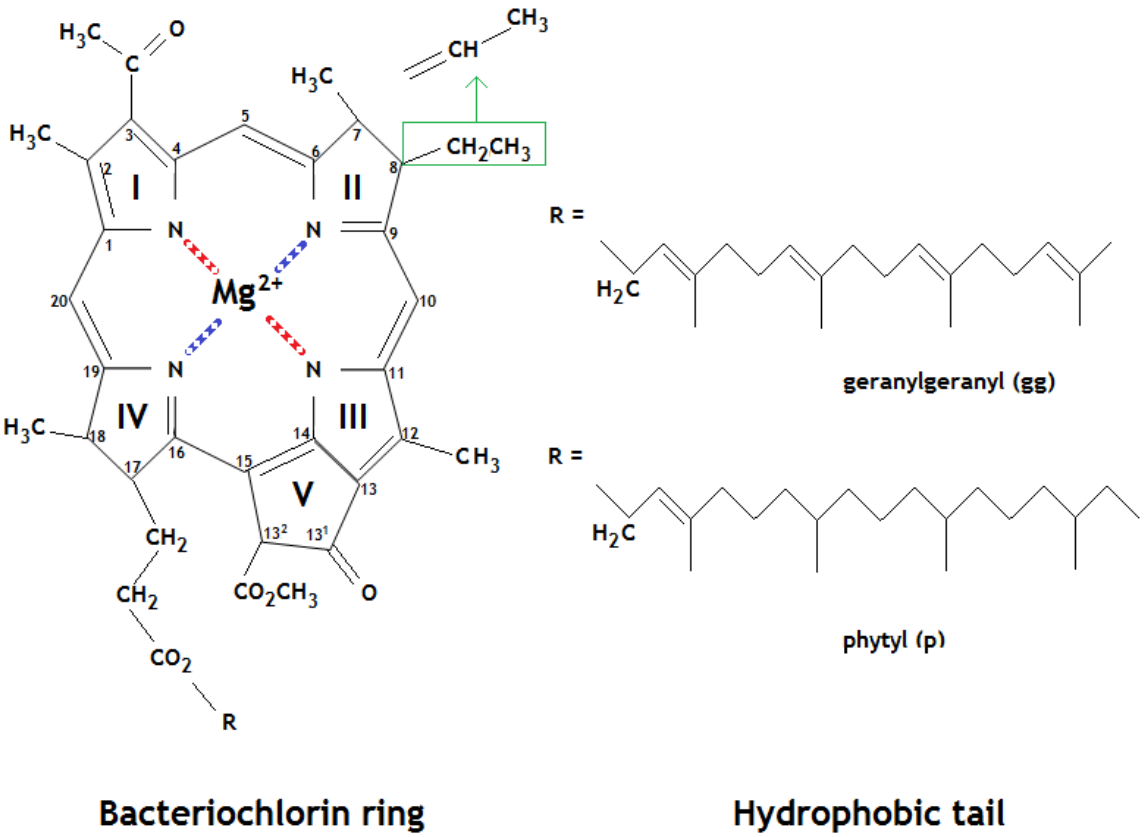

Figure 1.4 Structure of BChl a showing the bacteriochlorin ring and the two potential hydrophobic tail groups that are found as the R group.
The two hydrophobic tail groups that have been observed on the BChl a molecule are a geranylgeranyl (31) or a phytyl (28) **tail**. The phytyl tail is one carbon longer than the geranylgeranyl but only contains one double bond. The geranylgeranyl group contains the same double bond as the phytyl as well as three more. The hydrophobic tail does not contain a chromophore. The main chromophore of the BChl is the bacteriochlorin ring, which contains the Qx (red) and Qy (blue) transition dipole moments. Both BChl a and b have been found in purple photosynthetic bacteria, the difference between BChl a and BChl b is the substitution of the group outlined in green box (28, 32).

The spectrum of free monomeric BChl in inorganic solvents contains four main absorption peaks dubbed the Qy, Qx, Bx, and By peaks (Figure 1.5 blue spectrum)(33). These absorption bands relate to transition dipoles on the BChl ring. The Bx and By are often referred to by the joint term Soret peak. The transition dipoles that absorb in the red and NIR, the Qx and Qy, have a specific

position on the bacteriochlorin ring perpendicular to each other (Figure 1.4 red and blue lines, respectively).

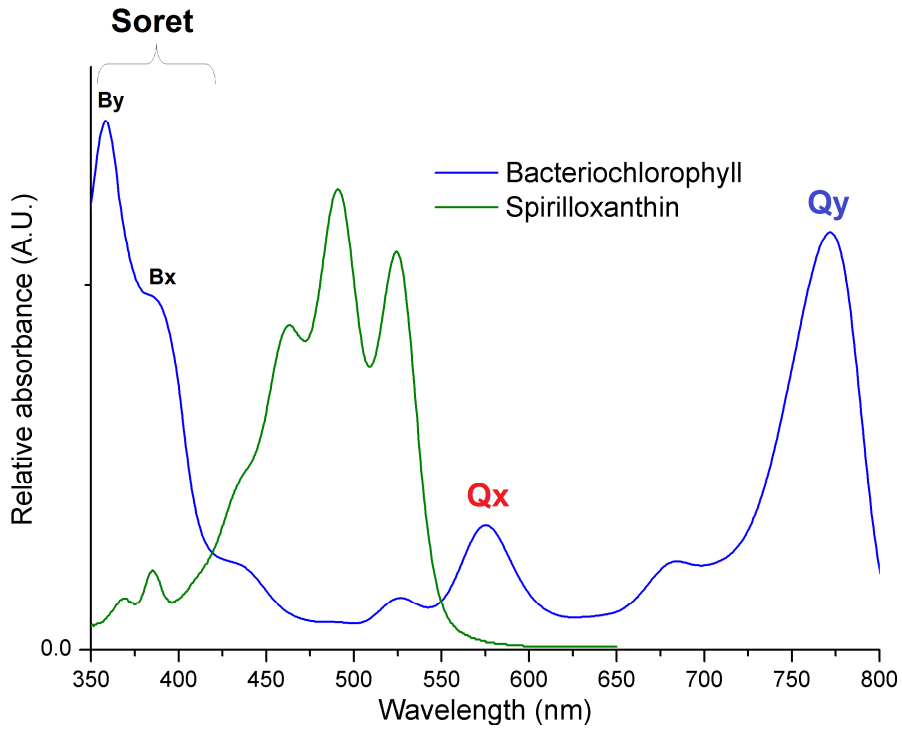

Figure 1.5 Absorption spectra of BChl a (blue) and the carotenoid spirilloxanthin (green) in acetone.
The BChl absorption spectrum consists of multiple peaks that relate to transition dipole moments, Qy, Qx, Bx, and By, and the carotenoid produces three absorption peaks in the region of 400-550 nm. The transition dipole moments of the By and Bx are known by the joint term Soret peak. The position of the peaks of both the carotenoid and BChl depends on the type of pigment and the polarizability and polarity of its environment. In acetone, the different peaks of the BChl centre at 772 nm (Qy), 580 nm (Qx) and ~370 (Soret), and the three spirilloxanthin peaks centre at 465 nm, 492 nm, and 525 nm.

The position of the Qy transition of BChl is sensitive to a variety of factors. When free in solution, the Qy band is affected by the polarity of the solvent it is suspended in (34). Aggregation of the BChl pigments causes a red-shift of the Qy absorption band, which increases with the number of BChl within the aggregate.

When bound within a protein scaffold additional factors affect the position of the Qy transition dipole, due to the effects of nearby protein residues. Deformations of the bacteriochlorin macrocycle, such as doming, can occur due to steric hindrance from nearby residues. This doming can shift the Qy absorption peak, while also affecting the duration of excitation times. The rotation of the C3-acetyl group relative to the chromophore π-bond system causes shifts in the absorption spectrum, this can occur due to residues forming

hydrogen bonds to the C3-acetyl or 13^1 keto carbonyl groups (35). Within the protein scaffold the BChl can be held in proximity to each other, and the BChl can effectively form an aggregate, allowing excitonic coupling to occur that produces a red-shift of the Qy peaks (36).

Carotenoids are the other pigment type present within the light-harvesting complexes of purple photosynthetic bacteria. Carotenoids are hydrophobic, long chain hydrocarbons that are desaturated to form a conjugated double bond system. It is the conjugated π-bond system that forms the chromophore (Figure 1.6 green highlighting) (37) allowing the molecule to absorb light in the visible region of the spectrum between 400-550 nm (Figure 1.5 green spectrum). Factors that affect the position and line profile of the carotenoid absorption spectrum include the length of the conjugated double bond system as well as any chemical modifications present on the chromophore. The longer the chromophore (the more repeats of double/single bonds present in tandem in the molecule) the more red-shifted the peaks observed in the absorption spectrum.

Figure 1.6 Structure of the carotenoid spirilloxanthin with the conjugated double bond system highlighted in green.
It is the conjugated double bond system that constitutes the chromophore. The number of π bonds is described using the term n =, in this case spirilloxanthin n = 13.

Three peaks are observed in the absorption spectra of carotenoids from purple photosynthetic bacteria in the 450-600 nm region of the absorption spectrum (Figure 1.5 green spectrum). The positions of the absorption bands of the carotenoid are sensitive to the polarity and polarizability of the solvent they are suspended in (38). When the carotenoid is bound within a protein, the protein environment of the carotenoid affects the position of the absorption bands observed.

Carotenoids perform three functions in the light-harvesting complexes of purple photosynthetic bacteria; light-harvesting (39), structural stability (32, 40), and

photoprotection (41-44). The light absorbed by the carotenoid can be utilised by the light-harvesting complex to drive photosynthesis. The energy absorbed stimulates an electron within the carotenoid into a singlet excitation state. This energy is then transferred on to one of the singlet excitation states of the bound BChl (Figure 1.7). When bound within a light-harvesting complex, different carotenoids have different levels of efficiency in their ability to harvest light and transfer this energy on to the BChl. Generally, it has been observed that carotenoids containing shorter chromophores are associated with higher energy transfer efficiencies in light-harvesting complexes (45-47). The excited electrons are excited to the S_2 state within the carotenoid, as the S_1 state is a forbidden 'dark' state due to its symmetry with the S_0 state (48, 49).

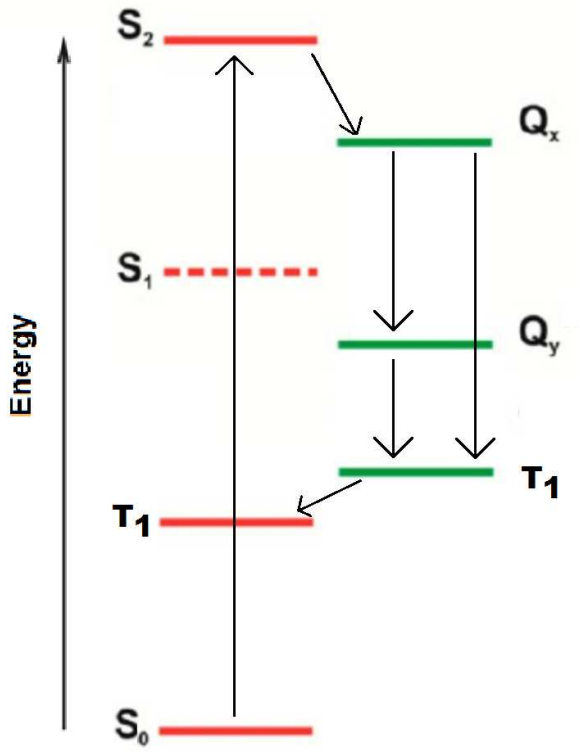

Figure 1.7 Jablonski diagram of the carotenoid and BChl singlet and triplet energy levels. The carotenoid singlet (S_1 and S_2) and triplet energy states (T_1) (red lines) and the energy states of the transition dipole moments (Qx and Qy) and the triplet excitation state (T_1) of the BChl (green lines). Electrons are excited to the S_2 state within the carotenoid, as the S_1 state is a forbidden 'dark' state due to its symmetry (48, 49). The energy can then be passed on to the Qx or Qy energy levels of the BChl. If triplet excitation states are formed due to intersystem crossing, these are quenched by the carotenoid due to the lower energy of the carotenoid T_1 energy state (42).

The transfer of energy between the carotenoids and the BChl allows not just the transfer of singlet excitation states to the BChl but the quenching of triplet excitation states from the BChl (46, 50). This is because the triplet excitation

state of the carotenoid is of a lower energy than the triple excitation state of BChl (Figure 1.7) (51). If the excited electron in singlet excited BChl (Equation 5) changes its spin due to intersystem crossing, it then enters a triplet state as outlined in section 1.2 (Equation 6). This triplet state is able to form singlet oxygen due to its long lived nature (Equation 7). Singlet oxygen is highly reactive and so detrimental to the bacterium (52).

Singlet excition of BChl

$$BChl + hv \rightarrow {}^{1}BChl^{*} \quad (5)$$

ISC of singlet excited BChl to triplet excited BChl

$${}^{1}BChl^{*} \rightarrow {}^{3}BChl^{*} \quad (6)$$

Formation of singlet oxygen from triplet excited BChl

$${}^{3}BChl^{*} + hv \rightarrow {}^{3}BChl^{*} + \Delta_{g}O_{2^{*}} \quad (7)$$

The carotenoid is able to quench triplet excited BChl and prevent the formation of singlet oxygen (Equation 8)(46, 50). This occurs by Dexter energy transfer. The carotenoids are then able to release this energy as heat (Equation 9) (42).

Transfer of triplet excited state to carotenoid

$${}^{3}BChl^{*} + Car \rightarrow BChl + {}^{3}Car^{*} \quad (8)$$

The dissipation of carotenoid triplet state as heat

$${}^{3}Car^{*} \rightarrow Car + heat \quad (9)$$

The carotenoids are also able to quench singlet oxygen (42, 53, 54). The quenching of both BChl triplet excitation states and singlet oxygen prevents the degradation of the BChl and the toxic effects of reactive oxygen species formed from singlet oxygen (52).

1.3.2 **Purple photosynthetic reaction centres**

Early work on the RC by Okamura et al., (55) identified three peptides that were named the Light (L), Medium (M) and Heavy chains (H) after the relative molecular weights observed after analysis by SDS PAGE. In 1985, the reaction centre from *Rps. viridis* was the first membrane protein to have its structure solved by H. Michel et al (56), for which the Nobel prize was awarded in 1988

(57). This structure elucidated the fact that the RC consists of BChl, bacteriopheophytin (BPh) and carotenoid pigments bound within a protein complex consisting of the three protein subunits L, M, H, and, in the case of *Rps. viridis*, a cytochrome c. The L and M peptides bind BChl and bacteriopheophytin pigments in position for effective light-driven electron transfer that creates the charge separation across the membrane.

1.3.3 **Purple photosynthetic bacterial peripheral light-harvesting complexes**

The RC is surrounded by light-harvesting complexes to increase the cross section of the solar spectrum that is captured for use by the RC. These complexes come in two types, the light-harvesting complex 1 (LH1) and the light-harvesting complex 2 (LH2). All purple photosynthetic bacteria contain the LH1 complex and most but not all contain the LH2 complex (Figure 1.8). The LH2 is a smaller peripheral light-harvesting complex that absorbs light energy at shorter wavelengths than LH1 and transfers the energy onto the LH1 (58). The LH1 is always found in a 1:1 ratio with the RC as it directly surrounds the RC (59-61), for this reason the two complexes are referred to as the LH1/RC “core” complex.

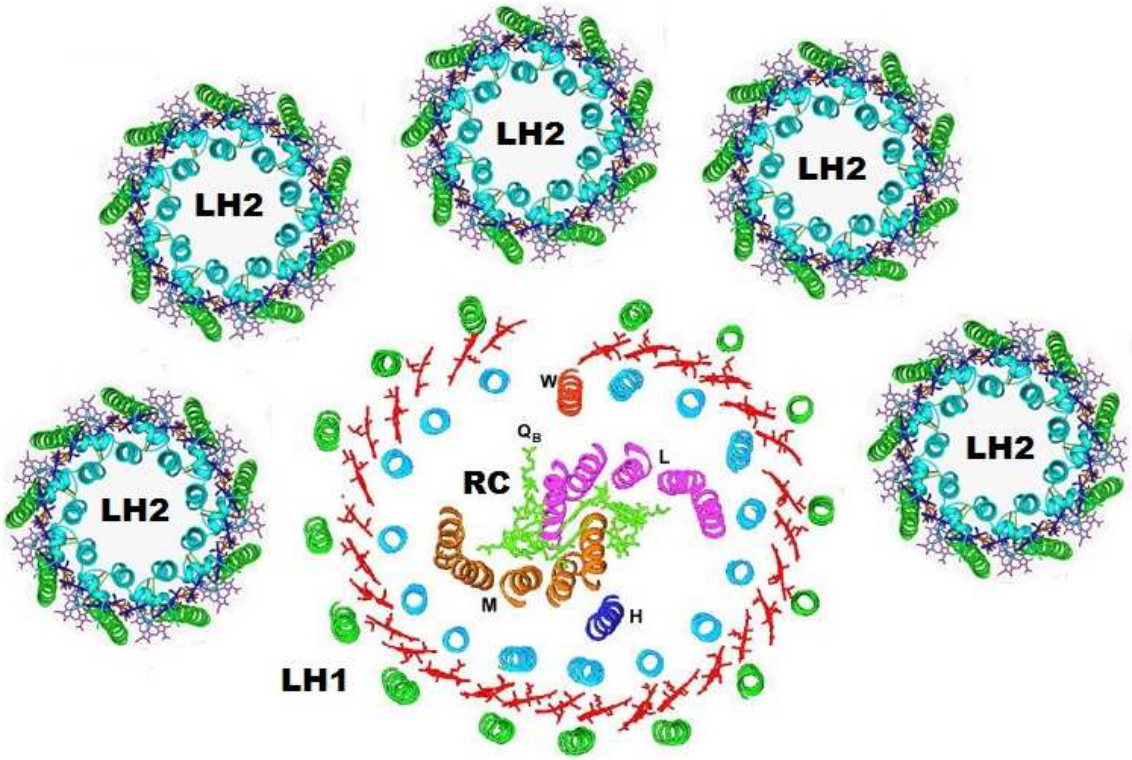

Figure 1.8 Diagram showing the LH1/RC "core" and LH2 light-harvesting machinery of purple photosynthetic bacteria.
The light-harvesting complex 2 (LH2) complexes shown are the repeats of the nonamer B800-850 LH2 from *Rps. acidophila* (62, 63) with proteins shown in cyan (alpha peptide) and green (beta peptide), and pigments in blue, purple (BChl), and orange (carotenoid). The light-harvesting complex 1 (LH1) shown is the *Rps. palustris* structure (60) and is an elliptical complex consisting of 15 subunits with the protein W helix at the gap in the ring. The LH1 proteins are shown in cyan (alpha peptide) and green (beta peptide) with BChl pigments in dark red, and the carotenoids not shown. The reaction centre (RC) sits in the middle of the LH1 complex, with proteins in orange (M peptide), pink (L peptide), and blue (H peptide) and BChl pigments in green. Solar energy is absorbed at shorter wavelengths by the LH2 complex, which then transfers the energy down an energy gradient onto the LH1 complex. The LH1 complex then transfers this energy onto the RC, which is then used by the RC to create a charge separation across the membrane.

Both the LH1 and LH2 form rings that are based on a similar modular principle, as they consist of oligomers of alpha/beta polypeptide heterodimer subunits that span the membrane once and form a scaffold for non-covalently bound pigments.

The pigments bound within the light-harvesting complexes, carotenoids and BChl, absorb at different wavelengths than the free pigments due to 'tuning' by the protein scaffold they are bound to. The differences in the positions of the Qy bands of the BChl populations are due to differences in their site energies, as well as due to pigment-pigment interactions. The site energy of the BChl is defined by the different H bonding of the peptides to the BChl, which varies depending on the peptide residues present within the BChl binding site. In

addition to the site energy, pigment-pigment interactions can shift the position of the Qy peak.

This effect is most prominent when contrasting the absorption spectrum of the LH1/RC “core” and LH2 (Figure 1.9). The absorption spectrum of the LH1/RC “core” complex is cumulative of the absorption from the small number of pigments bound within the RC and the larger number of pigments bound within the LH1. Figure 1.9 shows the room temperature absorption spectra of the LH1/RC “core” and LH2 complexes from *Rps. acidophila*. The BChl Qy peaks of the LH1/RC “Core” complex absorb at 760 nm (RC), 800 nm (RC) and 885 nm (LH1), while the BChl Qy peaks of the LH2 absorb at 800 nm and 863 nm. The positions of the peaks in the absorption spectrum of the different light-harvesting complexes vary depending on the species of bacterium. There are no chemical modifications to the BChl to cause the difference in the wavelength position of the Qy, it is nearly entirely due to the differences in the protein binding and the larger number of aggregated BChl.

The carotenoid absorption peaks are shown in green on the absorption spectrum (Figure 1.5). Carotenoids fulfil their three roles of light-harvesting, photoprotection and structural stability to different degrees depending on the requirements of the bacterium and light-harvesting complex. Bacteria that inhabit deeper waters will rely on the light-harvesting capabilities of the carotenoid more due to the poor light-transmission of NIR wavelengths through water (64), and some bacteria produce alternative carotenoids with shorter chromophores to produce more efficient energy transfer (47). Drews et al, (1971) and Clayton (1963) found that carotenoidless LH1 and RC complexes could form as long as the bacteria were grown in the complete absence of any oxygen, thus preventing the formation of any reactive oxygen species. This suggests that the purpose of carotenoids in the LH1/RC “core” complex is predominantly photoprotective. Carotenoids have been found to be integral in the formation of the LH2 complex (40) as in their absence the polypeptides fail to aggregate into a full LH2 complex. It was suggested that this may be due to the hydrophobicity of the carotenoid stabilising the heterodimer subunit.

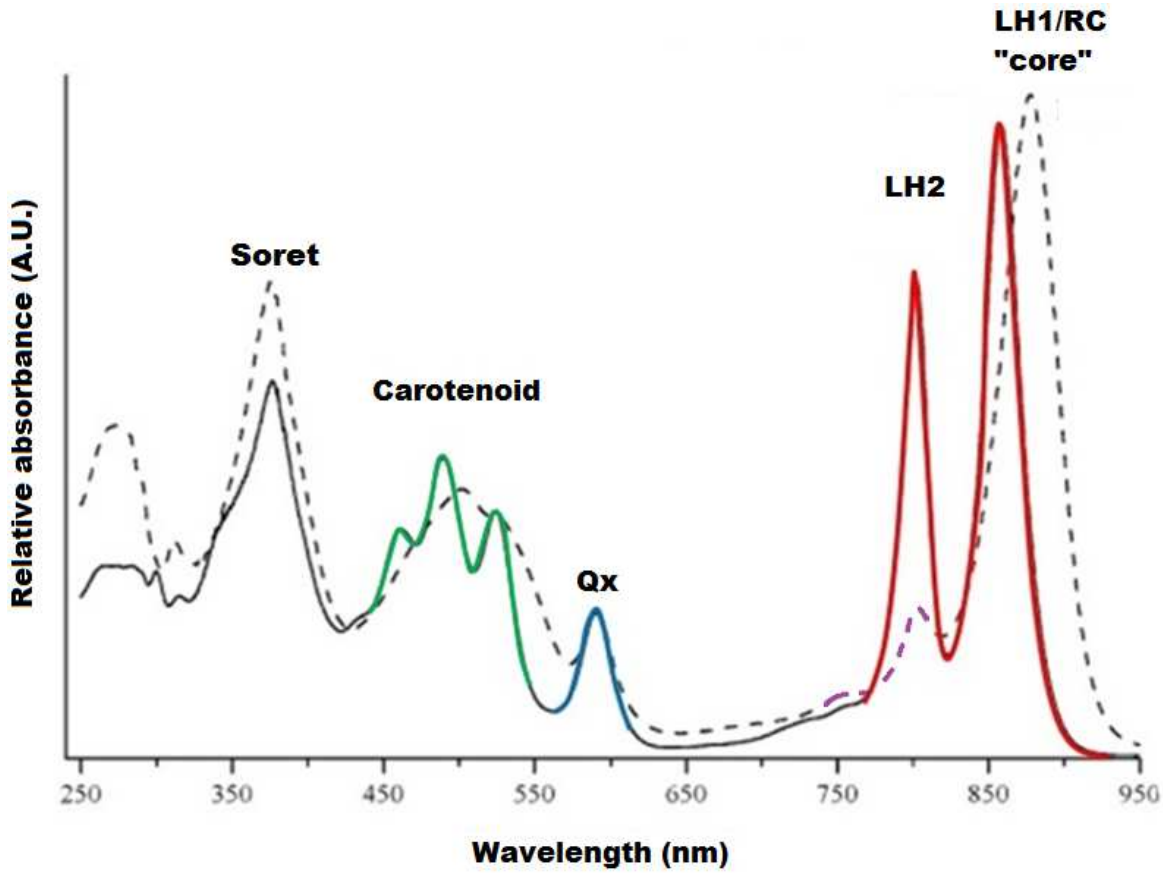

Figure 1.9 Normalised absorption spectra of the LH1/RC "core" and LH2 complexes from *Rps. acidophila* (65).
The LH2 absorption spectrum (solid line) shows the absorption of the bound BChl at ~ 370 nm (Soret peak), ~590 nm (Qx, blue), 800 nm and 863 nm (Qy, red), and the absorption of the bound carotenoid at ~460 nm, ~490 nm, and 525 nm (green). The LH1 absorption spectrum (dotted line) shows the absorption of the LH1 bound BChl at ~ 370 nm (Soret peak), 595 nm (Qx), and at 885 nm (Qy), and the bound carotenoid peaks between 450-550 nm. The absorption of the reaction centre is shown in purple at ~ 760 nm, and 800 nm.

The LH1/RC "core" and LH2 complexes form part of the basis of how purple photosynthetic bacteria adapt to changes in light-conditions. Purple photosynthetic bacteria optimise their light-harvesting capacity in different environmental conditions by controlling the amount and size of photosynthetic units (the number of light-harvesting BChl pigments present per RC)(66). This is achieved by exerting control over the formation of the ICM and the LH2:LH1 ratio (13, 65, 67). Under high light the ratio is low, but under low light conditions the ratio increases as the number of LH2 complexes increases to optimise the energy capture of the light-harvesting complexes. For a full discussion see the recent review (14).

1.3.3.1 Light-harvesting complex 1 (LH1)

Early work on the LH1 found the presence of two polypeptides, alpha and beta, present in a 1:1 ratio (68), with two BChl and one carotenoid (23) per alpha and beta. Determination of the structures confirmed previous biophysical findings (69) that the alpha and beta peptides form heterodimer subunits that traverse the membranes once and non-covalently bind BChl and carotenoid pigments (Figure 1.10). The alpha and beta polypeptides are encoded for by the *puf* operon (70, 71). In each heterodimer subunit of the LH1 there is a single carotenoid and a pair of BChls, which are excitonically coupled. These excitonically coupled BChl produce the absorption peak that centres at the longest wavelength, at 885 nm in *Rps. acidophila* (72), in the NIR observed in the absorption spectrum (Figure 1.9). The specific position of the NIR absorption maximum observed depends on the bacterium the LH1 has been produced by.

The LH1 structure directly surrounds the RC and funnels the energy absorbed by the LH2 complexes into the RC. The LH1/RC "core" complex is known to be dimeric in some species, such as *Rba. sphaeroides* (73-75), and monomeric in others (60, 61). The structure for the LH1 complex from *Rps. palustris* was solved by X-ray crystallography (60) (Figure 1.10) and showed it to be monomeric and consisting of 15 repeating heterodimer subunits. The LH1 from *Rps. palustris* was determined to be elliptical with a gap facilitated by the helix protein W. Protein W is thought to be homologous to the pufX helix within *Rba. sphaeroides* (75) that is key in creating the gap in the LH1 that allows the quinol to be released into the membrane to reduce the cytochrome b/c_1 complex. The 3 Å structure of the LH1/RC from *Tch. tepidum* (61) showed no such gap, with an additional alpha/beta heterodimer subunit in place of protein W helix.

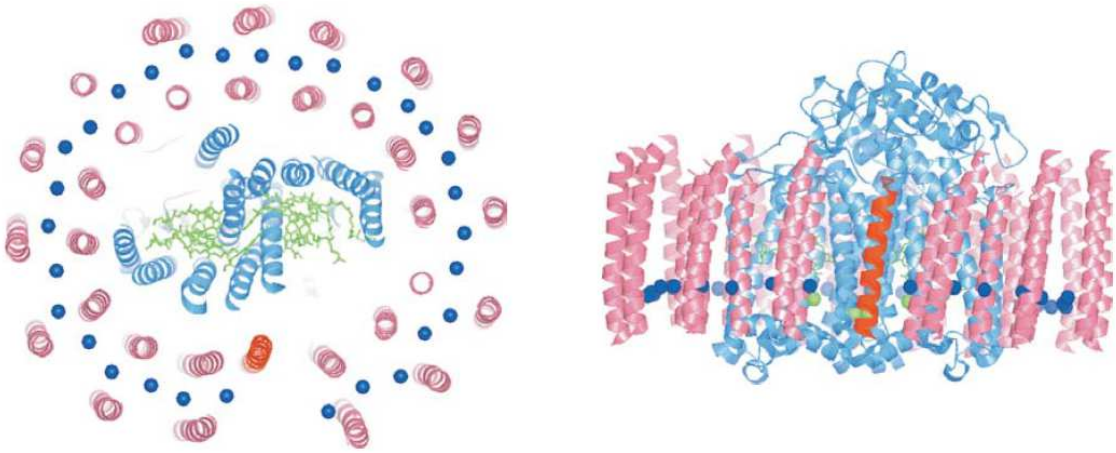

Figure 1.10 X-ray crystallography structure of monomeric elliptical 15-mer LH1 structure surrounding the RC complex from *Rps. palustris* (60) (PDB 1PYH).
The alpha and beta peptides of the LH1 complex are show in pink, with the BChl shown by their Mg^{2+} ion (blue sphere). The protein W is shown as the single red helix at the gap of the LH1. The RC peptides are shown in blue, and the bound pigments of the reaction centre are shown in green as sticks. Left: top view of the complex, and Right: side view through the membrane of the complex.

1.3.3.2 Light-harvesting complex 2 (LH2)

The LH2 complexes consist of a ring of repeating heterodimer subunits (Figure 1.11). The heterodimer subunits are formed from alpha (Figure 1.11 cyan) and beta (Figure 1.11 green) polypeptides (5-6 kDa) (63, 69, 76), which are coded by *puc* genes (10, 77-79), in a 1:1 ratio creating a scaffold for the BChl and carotenoid pigments.

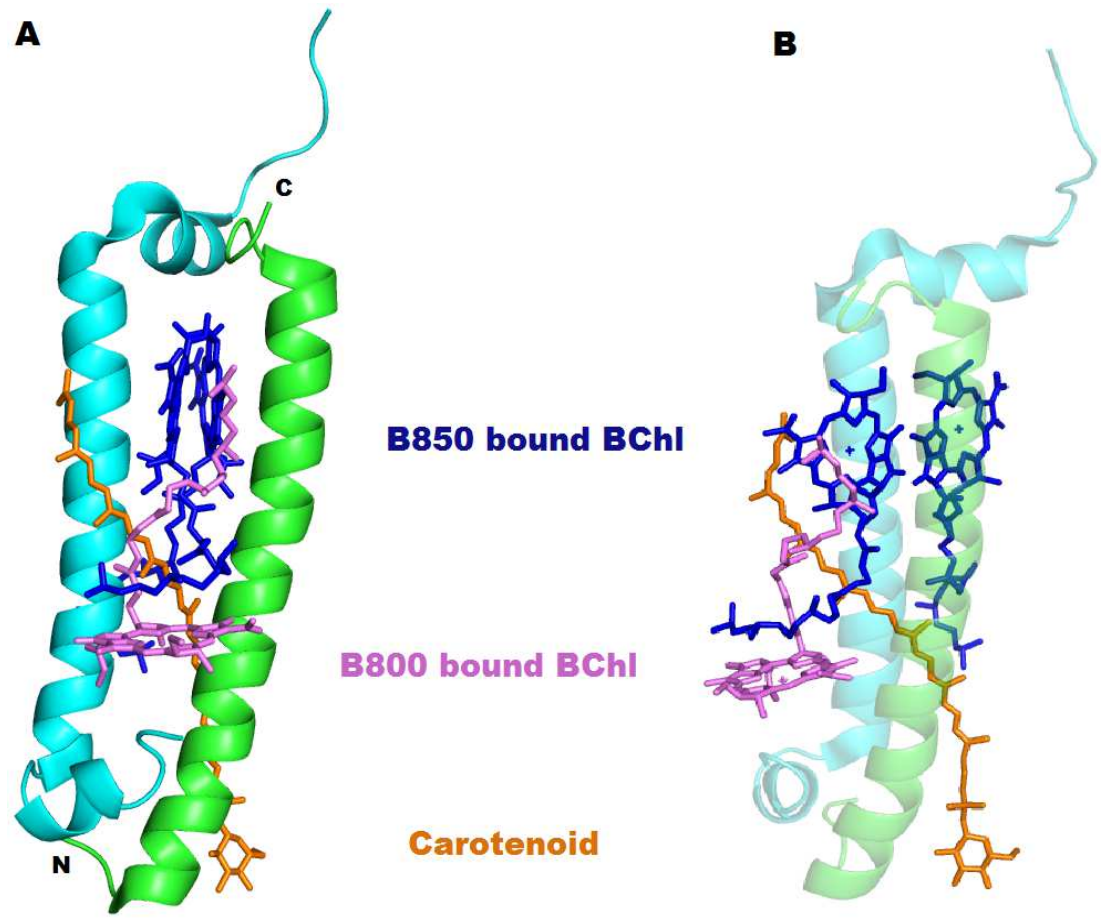

Figure 1.11 Side view of the heterodimer subunit from the B800-850 LH2 complex from *Rps. acidophila* (63)(PDB 1KZU) showing A: peptides and bound BChl and carotenoid, and B: peptides shown transparent with a change in angle to show the pigment arrangement. The alpha (cyan) and beta (green) peptides traverse the membrane once and bind BChl that absorb as part of the B850 BChl (dark blue) and the B800 BChl monomer (purple). The carotenoid (orange) interdigitates between the hydrophobic tails of the BChl and the polypeptides, providing added stability due to its hydrophobic nature. The bacteriochlorin ring of the B800 monomer sits parallel to the membrane while the hydrophobic tail angles up toward the B850 BChl. The B850 BChl sit perpendicular to the plane of the membrane, with the tails angled down towards the B800 BChl.

The current structural understanding of LH2 complexes show it to be a nonamer in the case of *Rhodopseudomonas (Rps.) acidophila* (62, 63)(Figure 1.12) or an octamer in the case of *Phaeospirillum (Phs.) molischianum* (80) and *Marichromatium (Mch.) purpuratum* (81). Unlike in the LH1 complex there are three BChl per heterodimer subunit (62, 63, 69, 80, 82) that form a dimer and a monomer. The monomeric BChl (Figure 1.11 and Figure 1.12 purple) sits with its bacteriochlorin ring perpendicular to the transmembrane alpha helices of the α/ß polypeptides, while the dimerised BChl (Figure 1.11 and Figure 1.12 blue) sit parallel to the helices. As in the LH1 heterodimer subunits, there is a single non-covalently bound carotenoid per heterodimer subunit (83) (Figure 1.11 and Figure 1.12 orange).

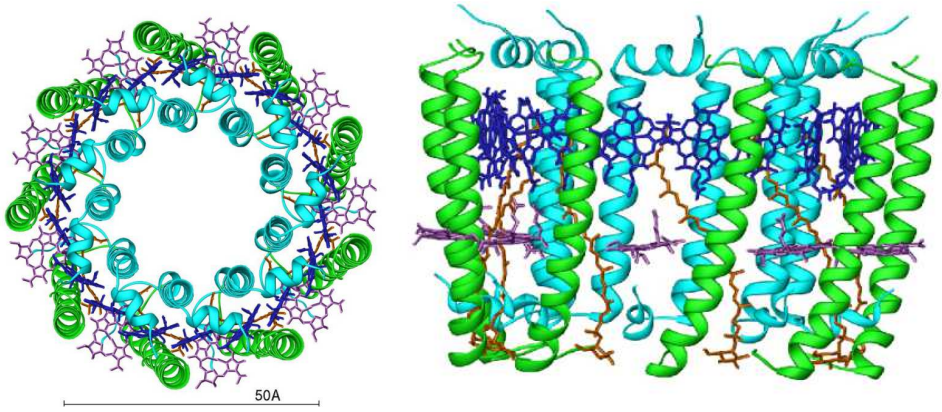

Figure 1.12 X-ray crystallography structure of the nonameric B800-850 LH2 complex type from *Rps. acidophila* (PDB 1KZU)(63).
The alpha (cyan) and beta (green) peptides form a protein scaffold for the B800 BChl (purple), B850 BChl (blue), and the carotenoids (orange). The top view structure shows the nonameric structure with the alpha peptides forming the internal protein ring, and the beta peptides forming the outer protein ring. The bacteriochlorin rings of the B800 BChl sit parallel to the membrane and thus the bacteriochlorin ring is easily visualised at this angle. The bacteriochlorin rings of the B850 BChl sit perpendicular to the membrane and so they appear side on at this angle. This shows the overlap between all the B850 BChl that allows the excitonic coupling of the molecules. The side view of the structure shows the repeating heterodimer subunit of the LH2 complex. The phytyl tails of the BChl interdigitate with the carotenoid, adding stability. This proximity is also required for energy transfer from the carotenoid to the BChl as well as the quenching of BChl triplet excitation states.

It is these two populations of BChl that produce the two different Qy absorption bands in NIR at ~ 800 nm (monomeric BChl) and ~ 850 nm (dimeric BChl) and thus are referred to as the B800 and B850 BChl respectively (34, 84). The difference in the positions of the Qy bands of the two BChl populations are due to differences in their site energies and the strength of interactions between pigments (85). The dimeric BChl are excitonically coupled across the ring, which shifts the position of their Qy further to the red than the B800 BChl. The LH2 complexes that absorb in these relative positions are often referred to as a B800-850 complex due to the position of these absorption bands.

The B850 BChl are non-covalently bound in place by conserved histidines on both the alpha and beta polypeptides (Figure 1.13). The overlap of the III and V cycles is clearly observed in the structure, allowing the excitonic coupling of the BChl. The polypeptide binds the BChl that is closest to the opposite peptide, i.e. the alpha peptide binds to the BChl closest to the beta peptide. The BChl bound to the alpha peptide is dubbed αBChl and the BChl bound to the beta peptide, ßBChl. These BChl are further held in place and tuned by H bonds from trp45 and Tyr44 on the alpha peptide. These residues form H bonds to the C3-acetyl group

on the BChl (35, 36, 62, 63, 86, 87). The 13^1 keto carbonyl group on the V cycle is also known to be important in binding and stabilising the BChl but not in the B800-850 LH2 complex type from *Rps. acidophila* (32, 88).

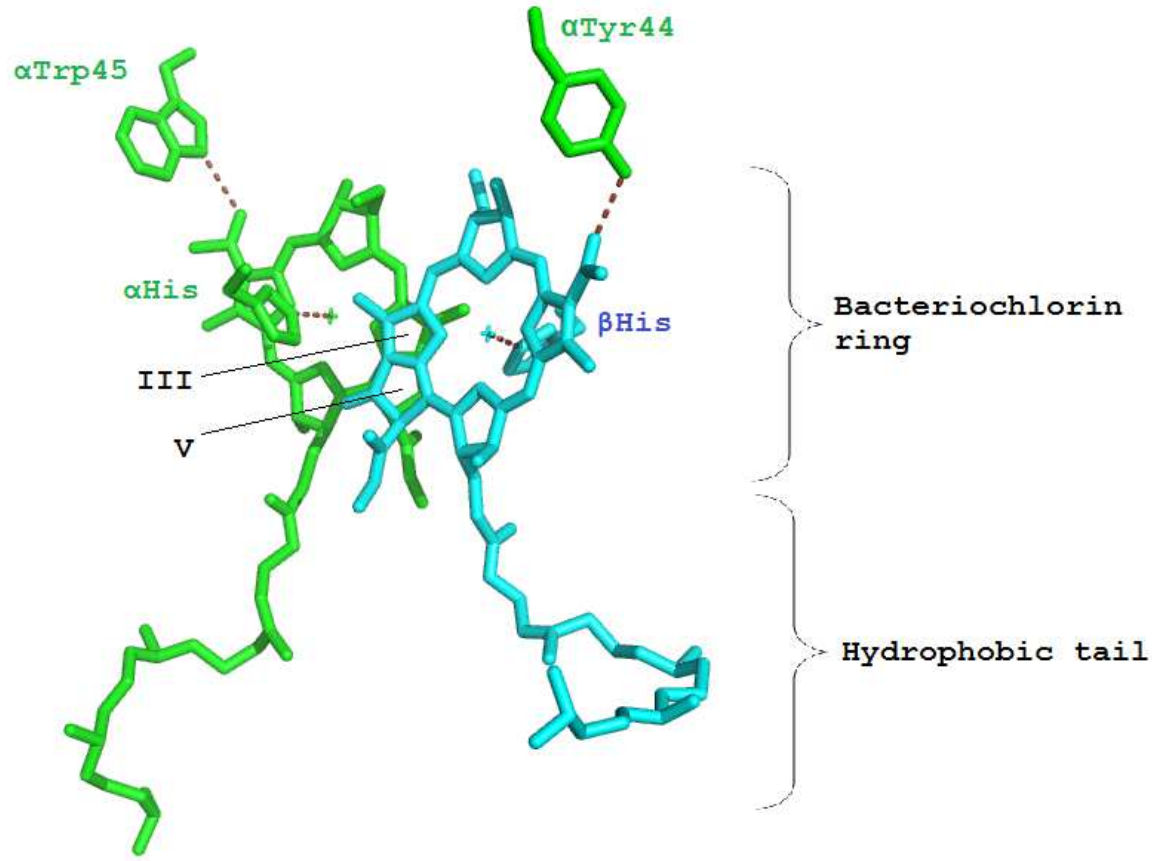

Figure 1.13 Stick view of the dimerised BChl from the B800-850 LH2 complex type from *Rps. acidophila* 10050 (PDB 1KZU)(63).
The BChl and residues associated with the alpha peptide are shown in green, while the BChl and residues associated with the beta peptide are shown in cyan. The histidine residues that coordinate with the central Mg^{2+} ion from both the alpha and beta peptides are shown as αHis and βHis respectively. The trp45 residue from the alpha peptide from this heterodimer subunit H bonds to the C3-acetyl group of the αBChl. The Tyr44 residue from the alpha peptide of the following heterodimer subunit forms an H bond with the C3-acetyl group of the βBChl. This figure shows the overlap in the III and V cycles of the bacteriochlorin ring, which are essential to the excitonic coupling of the dimerised BChl across the whole of the LH2 ring. The distances between the dimerised BChl within the heterodimer subunit is 8.7 Å, while between the BChl in between heterodimer subunits the distances are 9.7 Å.

The factors that affect the position of the Qy peaks produce a relatively unique absorption spectrum from different light-harvesting complexes. This provides a method of identification as well as an assay of the complexes intactness, purity and concentration.

The carotenoids of LH2 complexes are in the *trans* conformation (24, 89-91), as steric hindrance in the *cis* conformation prevents the heterodimer subunit

formation. *Cis* isomerisation can be identified by the presence of *cis* peaks at approximately ~ 370 nm in the absorption spectrum of a carotenoid (Figure 1.5) (92). As previously described, one of the key functions of the carotenoid is structural stability as it sits between the two peptides within the LH2 and interdigitates with the hydrophobic tail of the B800 BChl (65).

1.3.3.3 Adaptations of the LH2 complex for low light conditions

When some bacteria grow under low light conditions they adapt their light-harvesting machinery to compensate for the lower levels of energy reaching them. To do this, some purple photosynthetic bacteria have been found to produce alternative LH2 complex types. *Rps. acidophila* strains 7050 and 7750 (93) and *Phs. molischianum* (94, 95) produce a low light adapted LH2 complex, sometimes referred to as the LH3 complex, which absorbs at 800 nm and ~ 820 nm and has thus been dubbed the B800-820 LH2 complex type (Figure 1.14).

The advantages of the blue shift of the absorption peak from ~ 850 nm to 820 nm is the reduction in the back transfer of energy from the LH1/RC “core” complex to the LH2 complex (96). The reduction in back transfer results in a more efficient energy transfer process, which is important under conditions where the amount of light is limited.

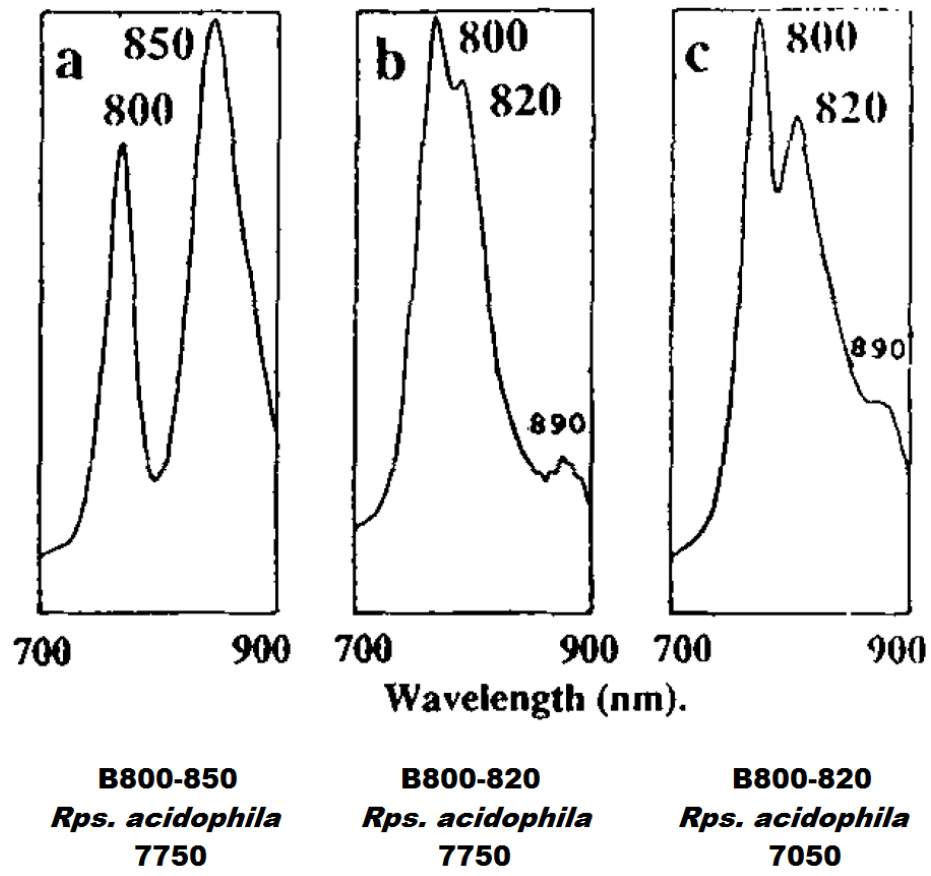

Figure 1.14 NIR absorption spectra (97) of the B800-850 LH2 complex type produced by *Rps. acidophila* 7750 under high light conditions, the B800-820 LH2 complex type produced by *Rps. acidophila* 7750 under low light conditions, and the B800-820 produced by *Rps. acidophila* 7050 under low light conditions.

Under low light conditions both strain 7050 and 7750 change to producing a B800-820 LH2 complex with NIR absorption peaks that centre at 800 nm and 820 nm. The LH1/RC "core" peak at 890 nm does not change under different growth conditions. The B800-820 LH2 complex reduces the amount of energy back transfer from the LH1 complex, thus increasing the efficiency of the process.

Changes in carotenoid composition are also observed due to changes in growth conditions, such as the shift from rhodopin glucoside to rhodopinal glucoside in *Rsp. acidophila* 7050 under low light conditions (98). Rhodopinal glucoside absorbs at a longer wavelength with broader peaks than rhodopin glucoside suggesting that a shift to longer wavelength improves the level of energy capture (47, 93). Additionally, rhodopinal glucoside more efficiently transfers energy on from the carotenoid to the BChl (47).

The determination of the B800-820 LH2 complex type from *Rps. acidophila* 7050 (99) confirmed findings from previous mutagenesis studies (35, 86) of the structural basis for the difference in the Qy absorption of the dimeric BChl between the B800-850 and B800-820 LH2 complex types. The shift from 850 nm to 820 nm is due to a change in hydrogen bonding from the alpha peptide to the

B850 BChl. In the B800-820 LH2 complex the αTyr44 and αTrp45 residues (Figure 1.15 blue) are replaced by phenylalanine and leucine respectively (Figure 1.15 red) (99). This means that the H bonds present in the B800-850 LH2 complex type can no longer form and this changes the site energy of the BChl. Additionally, the residue at position 41 on the α peptide in the B800-850, a phenylalanine, is replaced by a tyrosine in the B800-820 LH2 complex. This residue forms an H bond with the C3 acetyl group of the αBChl causing a rotation of the C3-acetyl group relative to their position in the B800-850 LH2, causing the blue-shift of the absorption band of the Qy band.

Both the C3-acetyl and $C13^1$-keto group of the ßBChl are unbound, and the $C13^1$-keto of the αBChl is unbound. In the B800-820 LH2 complex type the C3-acetyl of the αBChl is H bonded to αTyr41. This change of H bonding causes a rotation of the C3-acetyl groups of the B820 BChl to torsion angle (C2-C3-C31-O31) is 132° for the αBChl and 135° for the ßBChl (99), while the equivalent angles in the B850 BChl are αBChl 166° and ßBChl 156° (63). The rotation of the C3-acetyl moves a π-bond out of alignment, effectively shortening the series of conjugated double bonds and thus the chromophore. This blue shifts the Qy absorption of the BChl.

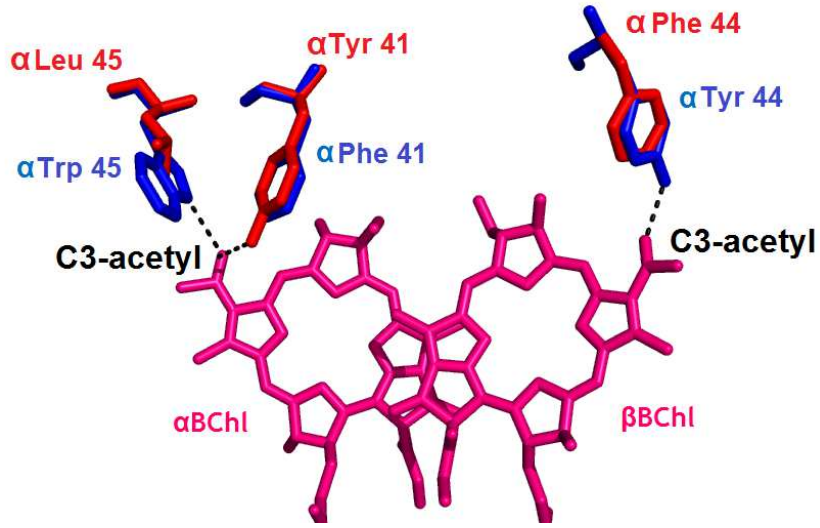

Figure 1.15 Comparision of the residues involved in the hydrogen bonding in the B800-820 (99)(PDB 1IJD) and B800-850 LH2 complex (62, 63)(PDB 1KZU) types from *Rps. acidophila*. Residues from the B820 alpha peptide (red) and from the B850 alpha peptide (blue) that bind to the dimeric BChl are shown. The structural comparison shows the differences between the residues contained on the different polypeptides involved in the H bonding of the BChl between the two LH2 complex types. The residues that form H bonds with the C3-acetyl of the BChl on the B800-850 alpha peptide are Trp45 and Tyr44, these are substituted by the Leu45, and Phe44 in the B800-820 LH2 complex. This removes the potential for H bonding of these residues in the B800-820 LH2 complex. The Phe41 residue of the B800-850 LH2 complex is replaced by Tyr41 in the B800-820. This allows H bonding to the C3-acetyl group of the BChl. Structures were overlaid using Pymol version 1.6 and bonds identified (63, 99) shown by dashed lines.

Some bacteria such as *Rps. palustris* are able to produce heterogenous LH2 complexes (100, 101) wherein the alpha and beta composition of the different heterodimer subunits is non-identical. The bacterium must possess several *puc* operons in order to express different alpha and beta polypeptides. In the case of *Rps. palustris*, five *puc* operons have been identified (102). *Rps. palustris* produces a B800-850 LH2 complex when grown under high light conditions and an alternative LH2 when grown under low light conditions (103-106). Both the high light LH2 complex (Figure 1.16 top panel) and low light LH2 complexes (Figure 1.16 bottom panel) produce absorption peaks in the NIR at 800 nm and 856 nm, however the 800 nm peak of the low light LH2 is of a higher intensity and the 856 nm peak is reduced to a broad low intensity peak. This reduction in the intensity of the 856 nm peak most probably produces a similar effect to the blue shift of the 850 nm peak in the *Rps. acidophila*, in reducing the level of energy transfer back from the LH1/RC "core" complex. The broadening of the 856 nm absorption peak is a by-product of the heterogeneity of the low light LH2 complex. The NIR absorption spectrum of the low light LH2 is cumulative of both 824 nm and 856 nm absorption peaks (101, 104, 106). This is due to the presence

of heterodimer subunits that produce a 856 nm absorption peak and heterodimer subunits that produce a 824 nm absorption peak contained within the same LH2 complex (101).

The structural basis for the change in the absorption appears to be similar to that observed between the B800-850 and B800-820 LH2 complexes from *Rps. acidophila*. The change in the site energy of some of the BChl is due to the inclusion of an additional alpha peptide in the low light LH2. At the relative positions α44 and α45 the alpha peptide has the residues replaced with phenylalanine and methionine (107). These residues are unable to form H bonds with the C3-acetyl group of the BChl allowing this group to rotate out of the plane of the bacteriochlorin ring and effectively shorten the chromophore (99). This blue shifts the absorption of the excitonically coupled BChl within the heterodimer subunits that contain this alpha peptide to 824 nm.

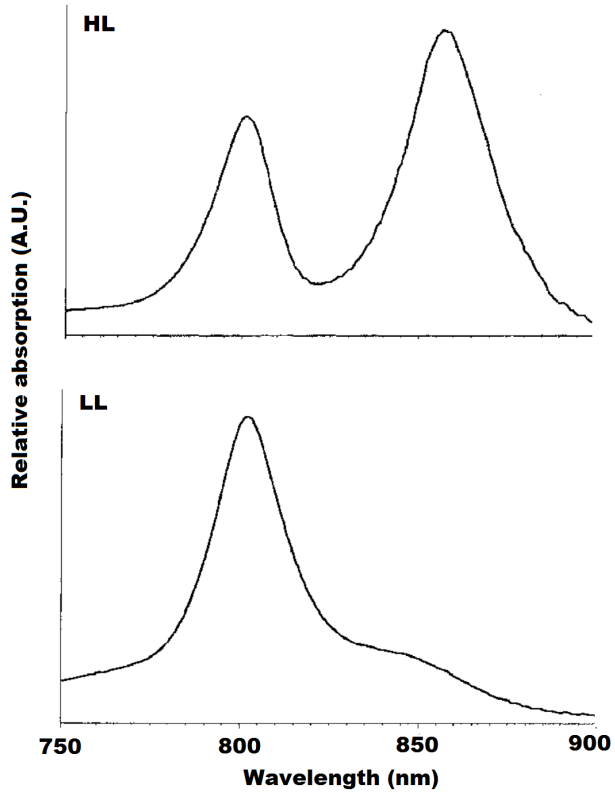

Figure 1.16 Room temperature NIR absorption spectra for the LH2 complexes produced by *Rps. palustris* under high light (HL, 7000 lux or 95 µmol m^{-2} s^{-1}) and low light (LL, 90-300 lux or 2- 5 µmol m^{-2} s^{-1}) conditions (107).
Rps. palustris produces an LH2 complex with Qy peaks that centre at 800 nm and 856 nm under HL conditions. Under LL conditions, *Rps. palustris* produces an LH2 complex with Qy peaks that centre at 800 nm with a broad maximum at 856 nm. The broad 856 nm peak in the LL LH2 complex is due to the heterogeneity of the LH2 complex producing peaks at both 824 nm and 856 nm (104). The reduction in intensity of this peak results in a reduction in the back transfer of energy from the LH1/RC "core" complex, therefore increasing the efficiency of the energy transfer process under low light conditions.

Currently all of the high resolution structures determined have been for homogeneous LH2 complexes (62, 63, 80, 99). Heterogeneous LH2 complex types provide an alternative mode of adapting to different growth conditions in some cases, such as *Phs. molischianum*, producing intermediate complexes between the B800-820 (94) and B800-850 (95).

1.4 *Allochromatium (Alc.) vinosum*

Allochromatium (Alc.) vinosum, previously *Chromatium vinosum* Strain D, is a sulphur purple photosynthetic bacterium from the gammaproteobacterium subtype. *Alc. vinosum* has been studied for the last six decades for its diverse sulphur metabolism as well as its variable absorption spectra. *Alc. vinosum* cells produce different absorption spectra depending on the nutritional and

environmental conditions under which they are grown (5, 6, 108, 109). These studies observed substantial variation in the Qy absorption peaks in the NIR of the membranes prepared from *Alc. vinosum* grown under different growth conditions. *Alc. vinosum* is affected by temperature, light intensity and sulphur source, meaning that the absorption spectra were not well reproduced between different studies (Figures 1.17-1.19). Bril (1959) prepared chromatophores with peaks at ~ 800 nm, ~ 850 nm, and a shoulder at ~ 890 nm from cells grown in the presence of thiosulphate (Figure 1.17). It was observed that the height of the ~850 peak varied and a reduction in peak intensity was accompanied by a blue-shift of the peak.

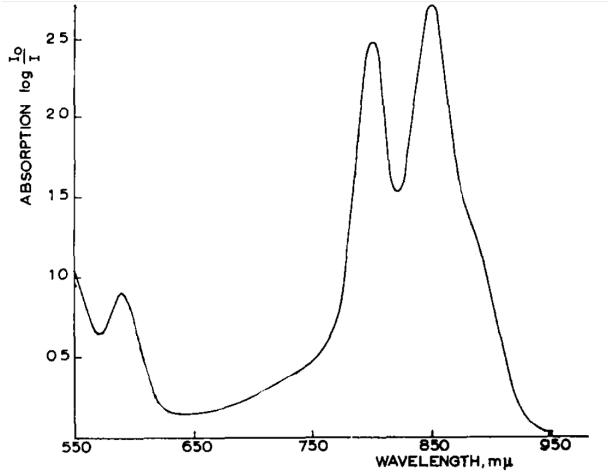

Figure 1.17 Absorption spectrum of *Alc. vinosum* chromatophores from cells grown in the presence of thiosulphate (110).
This early work shows chromophores from cells grown in the presence of thiosulphate but without a careful check on temperature or light intensity. The NIR absorption peaks observed centre at ~ 800 nm and ~ 850 nm with a shoulder at approximately 890 nm. The ~850 nm peak is the highest intensity peak, followed by the ~ 800 nm peak. The ~800nm and ~850 nm most probably are produced by an LH2 complex type, and the shoulder at ~ 890 nm by an LH1 complex type.

Work by Cusanoviche (111) identified the peaks of *Alc. vinosum* at 805 nm, 845 nm, and 888 nm, with the 805 nm peak substantially higher than the 845 nm peak (Figure 1.18). Chromatophores were from cells grown at 35 ℃ ± 2 ℃ at 50 footcandles (~ 8 μmol m^{-2} s^{-1}).

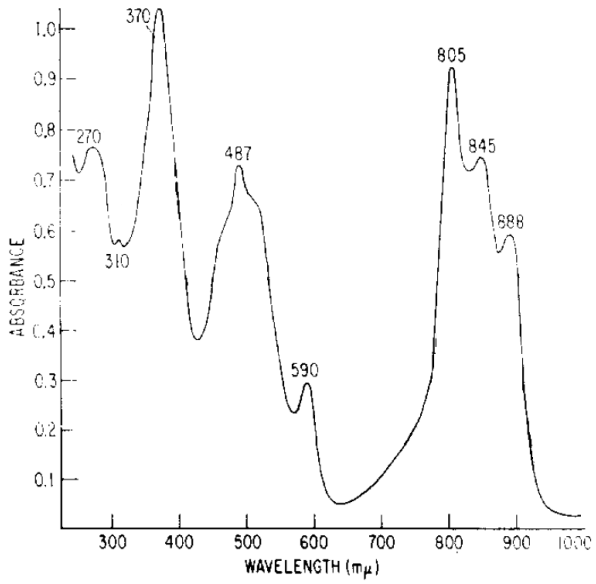

Figure 1.18 Absorption spectrum of *Alc. vinosum* chromatophores from cells cultured with succinic acid as the carbon source, at 35 ℃ ±2 ℃, at 50 footcandles (~ 8 µmol m^{-2} s^{-1}) (111). The NIR absorption peaks observed centre at 805 nm, 845 nm and 888 nm. The 805 nm peak is the highest peak present followed by the 845 nm and finally the 888 nm peak. The 805nm and 845 nm peaks most probably are produced by an LH2 complex type, and the peak at 888 nm by an LH1 complex type.

The NIR absorption spectrum observed in cells grown in the presence of both thiosulphate and sodium sulphide in the study by (108) showed peaks at ~800 nm, ~ 820 nm, and 890 nm (Figure 1.19).

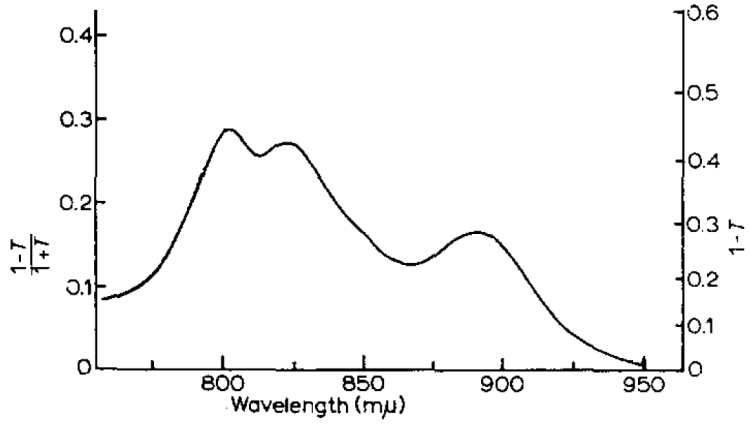

Figure 1.19 Absorption spectrum of *Alc. vinosum* chromatophores (108) from cells grown on Hendley medium (112) containing both sodium thiosulphate and sodium sulphide. This early work shows chromophores from cells grown in the presence of thiosulphate and sulphide but without a careful check on temperature or light intensity. The NIR absorption peaks observed centre at ~ 800 nm, ~ 820 nm, and ~ 890 nm. The ~800nm and ~820 nm most probably are produced by an LH2 complex type, and the peak at ~ 890 nm by an LH1 complex type.

The peaks at ~ 800 nm and ~ 890 nm appear to have varied minimally in previous work, but the third peak present in the NIR red-shifts by up to 30 nm between different studies. Without knowing the parameters for all three growth factors it is impossible to determine how different conditions affect the NIR spectrum observed from previous work. The changes in the absorption have been determined to be due to changes in the LH2 complexes produced (113), but the correlations between different nutritional and growth conditions are not fully understood.

Previous work (113-115) has determined that there are several LH2 complex types observed in *Alc. vinosum*; a B800-850, B800-820, and a B800-840 LH2 complex type. These LH2 complexes have been postulated as being heterogeneous both structurally and spectrally (116) and all of them produce an unusual split B800 absorption band (113, 115). Recent work (10) sequenced and annotated the full genome of *Alc. vinosum* identifying six potential *puc* genes pairs, which code alpha and beta apoproteins and provide the basis for several LH2 complex types and potentially for heterogeneous complexes (113).

Alc. vinosum has been previously reported as producing the carotenoids of the spirilloxanthin series; lycopene, anhydrorhodovibrin, spirilloxanthin, and rhodopin (11, 117, 118).

The ring size of the LH2 complex types from *Alc. vinosum* has been postulated to be larger than the current nonamer structure (115). Kereiche *et al* (2008) used EM to identify two populations of different sizes of LH2 complexes from *Alc. vinosum*, one of which was identified as potentially an octomer/nonamer and the other as a 12-mer or 13-mer. In light of further work (119) a 13-mer has been postulated as not as energetically stable as a 8, 9, 10 or 12-mer, suggesting that the some of LH2 complex types of *Alc. vinosum* are 12-mers.

1.5 Reconstitution

Determination of the structure of a complex shows how different structural elements are situated relative to each other but does not convey information on the interactions between different structural elements within a complex. One method of elucidating the interactions between different structural elements is

to substitute different parts and observe the changes in the function of the complex. This can be done using the process of reconstitution.

Reconstitution is an established biochemical technique whereby a structure is remade from its individual component parts in order to 1) test the understanding of how the structure forms and 2) to elucidate relationships between different component parts. A reconstitution protocol has been successfully developed for the LH1 complex originally by the Loach group (32, 68, 120-123) and has been instrumental in the understanding of different integral parts of the LH1 complex.

Reconstitution has been used to infer and identify key structural interactions and moieties for protein binding and LH1 formation (32), which have been confirmed upon structure determination, supporting the validity of the technique (32, 121). For example, reconstitution of bacteriopheophytin into the LH1 complex highlighted the importance of the central magnesium ion, as in its absense the LH1 failed to form (121). The determination of the LH1 structure (60) showed the coordination bonds from the conserved histidine residues to the Mg^{2+} of the BChl are key in holding the heterodimer subunits together. Other BChl analogues were reconstituted and confirmed the importance of the C3-acetyl and $C13^1$ ketocarbonyl groups on the BChl for protein binding (32).

During the process of dissociation and re-association, an intermediate in the formation of the LH1 from *Rsp. rubrum*, the B820, was identified and isolated (120, 122-124). The B820 is the heterodimer subunit of the LH1 complex and was named for the NIR absorption maximum of the *Rsp. rubrum* heterodimer subunit at 820 nm. Factors that were identified as important in the dissociation of the smaller B820 complex into the constituent parts were concentration, temperature, pH and the detergent used (32, 68, 122, 125).

The Loach process of LH1 reconstitution (Figure 1.20) involves the dissociation of the native complex (Figure 1.20, stage 1) using detergent (Figure 1.20, stage 2). This results in the component parts being free in solution (Figure 1.20, stage 3). The B820 intermediate is reformed by diluting the detergent concentration (Figure 1.20, stage 4). The reformation of the B820 intermediate is fairly rapid upon detergent dilution. The addition of carotenoid (Figure 1.20, stage 5) pushes the equilibrium towards whole complex formation (Figure 1.20, stage 6). Re-

association of the complete LH1 complex is a slower process, requiring hours after a further reduction in detergent concentration. The process can also be performed using the individually sourced component parts to create the light-harvesting complex from scratch (Figure 1.20, stages 3-6). This allows alternative non-native components to be substituted and the resulting effects on the ability of the complex, firstly, to form and then to function, will give useful data on the importance of the substituted component. The yields from reversible dissociation are often higher (~ 80 %) than reconstitution from constituent parts (20 %), due in part to degradation of the proteins and pigments during their extraction (121). The protocol of reconstitution was only able to be developed after suitably gentle and effective detergents were commercially available such as octyl glucoside (OG) and lauryl maltoside (126).

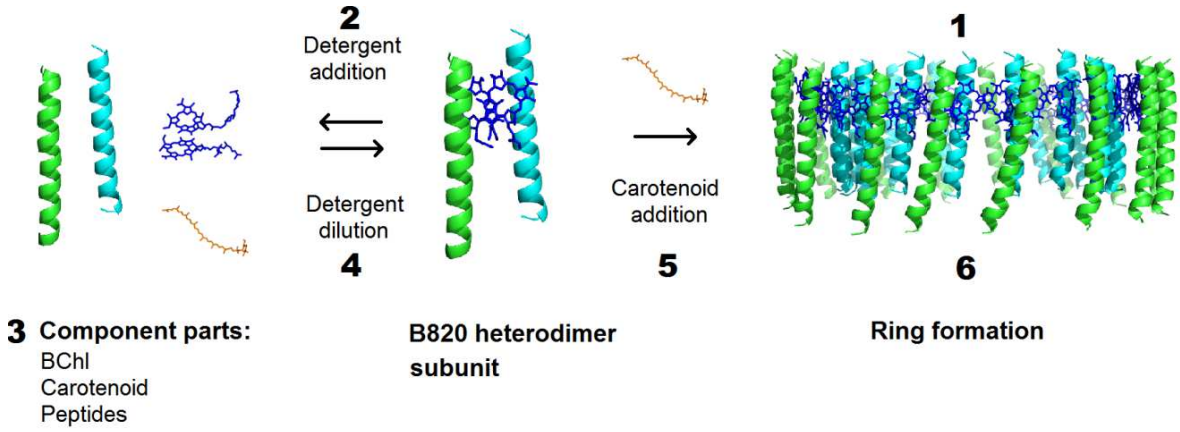

Figure 1.20 Process of reconstitution using the LH1 complex type from *Rps. palustris* (PDB IPYH)(60) as an example.
The α peptides (cyan) and β peptides (green) with carotenoid (orange), and BChl (blue) are added in after individual sourcing for de novo reconstitution, or dissociated from the LH1 complex for reversible dissociation. The process of reversible dissociation starts with a complete complex (1) that is dissociated through the addition of detergent (2). The component parts of the complex are then free in solution (3), this stage is the beginning of de novo reconstitution. The detergent concentration is then reduced (4) to encourage the component parts to form the B820 heterodimer subunit. Upon carotenoid addition (5) the heterodimer subunits oligomerise into a full complex (6).

The reconstitution technique developed by the Loach group has been applied to the LH1 of *Rsp. rubrum* (32, 120, 123), *Rba. sphaeroides* (68), and *Rba. capsulatus* (125) but has only had limited success with the LH2 from *Rsp. molischianum* (127) and *Alc. minuitissimum* (128).

Reversible dissociation was found to work best in the absence of carotenoids (68, 120, 121, 125) as this allows the complex to be fully dissociated effectively. The addition of carotenoid in either *de Novo* reconstitution or reversible dissociation

moves the equilibrium towards complex reformation (122, 129). For this reason, carotenoidless LH1 complexes have been used previously. Carotenoidless mutant strains have been isolated from *Rba. spheroides* R26.1 (130), *Rsp. rubrum* G9 (131), and *Rba. capsulatus* SB203E (132) but are not available for all species. The carotenoid biosynthesis inhibitor diphenylamine (DPA) has been used (83, 133-135) in lieu of carotenoidless mutants. DPA inhibits the enzyme phytoene desaturase (CrtI) that performs the progressive desaturation of phytoene to lycopene (Figure 1.21), therefore preventing the formation of the conjugated double bond system that forms the chromophore (37). Z-carotene is the first carotenoid visible to the human eye, appearing yellow.

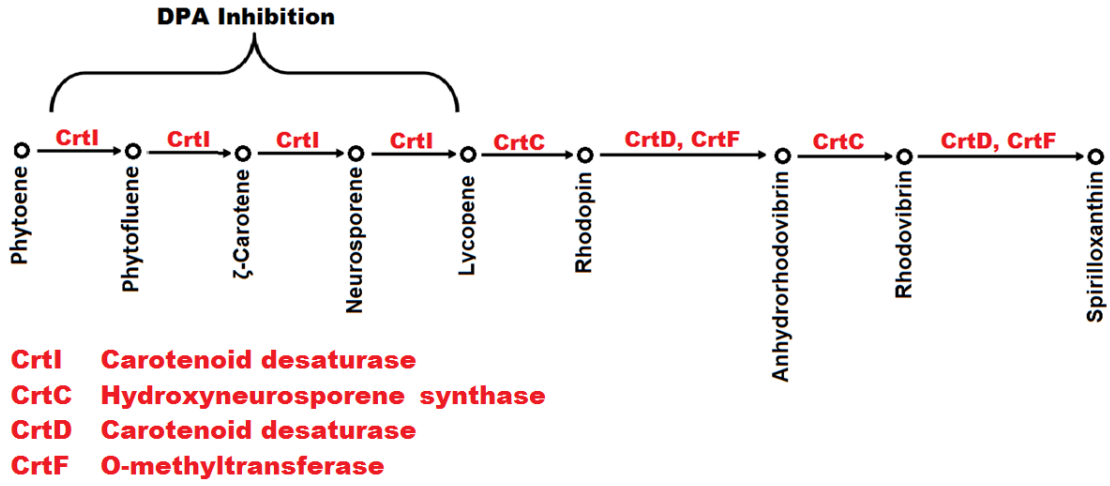

Figure 1.21 The carotenoid biosynthesis pathway of spirilloxanthin.
Carotenoids and carotenoid precursors are shown in black, while enzymes acting in the pathway are shown in red. The enzymes involved consist of three enzyme types CrtI/CrtD (Carotenoid desaturases), CrtC (Hydroxyneurosporene synthase), and CrtF type (O-methyltransferase family 2). The phytoene desaturase (CrtI) enzyme desaturates the chromaphore of the colourless carotenoid pre-cursors phytoene, phytofluene, and the coloured carotenoids ζ-carotene and neurosporene. Lycopene is then processed by carotenoid 1,2-hydratase (CrtC) to rhodopin. Rhodopin can be converted to anhydrorhodovibrin by two enzymes, 1-hydroxycarotenoid 3,4-desaturase (CrtD) and demethylspheroidene O-methyltransferase (CrtF). This can then be converted into rhodovibrin by carotenoid 1,2-hydratase (CrtC) and then to spirilloxanthin via 1-hydroxycarotenoid 3,4-desaturase (CrtD) and demethylspheroidene O-methyltransferase (CrtF) (37, 136). The enzyme affected by the carotenoid biosynthesis inhibitor diphenylamine (DPA)(133) is shown on the diagram. The phytoene desaturase enzyme is involved in multiple steps and so the inhibition is of all of these stages. The result of DPA inhibition is the build up of the carotenoid precursor phytoene.

Previous work has also used benzene washes to extract the carotenoid from LH1 complexes to make a carotenoidless complex (121).

1.5.1 **Reconstitution of the LH2 complex**

Reconstitution of LH2 peptides has only been achieved with the LH2 from *Phs. molischianum* (127) and from *Alc. minuitissium* (128) and this was postulated to be due to the fact that these peptides show strong homology with the peptides of LH1. The importance of the carotenoid in the structural stability of the LH2 complex (40) has been postulated as one of the reasons why the reconstitution protocol has not been successful, as in the absence of carotenoids the LH2 fails to form in many purple photosynthetic bacteria (40, 130, 132).

Early work (134) using the carotenoid biosynthesis inhibitor DPA showed that *Alc. vinosum* was able to grow and produce NIR spectra that indicated that the LH2 complexes were still able to form. More recent work (135, 137) on *Alc. minutissimum*, a very close relative of *Alc. vinosum* (138), found that it was able to grow and produce LH2 in the presence of DPA. This work found that in the absence of coloured carotenoids phytoene was not substituted (137). This suggests *Alc. vinosum* may be a promising species from which a viable LH2 reconstitution protocol could be developed. This could allow a variety of modifications that would be useful to discern not only the basis of the variation between the different LH2 complex types of *Alc. vinosum* but differences in other LH2 using synthetic components and a variety of biophysical and spectroscopic techniques.

1.6 Thesis aims

The overall aim of this work was to develop an effective reconstitution protocol for the LH2 complex type as has been developed for the LH1 complex. This would provide a method for elucidating structure-function interactions within the LH2 complex. Research suggested that the LH2 complexes from *Alc. vinosum* are potential candidates for a reconstitution strategy as they appear to produce LH2 complexes under carotenoid biosynthesis inhibiting conditions. Early in this work it became apparent that the understanding of the LH2 complexes of *Alc. vinosum* had not been revisited since the determination of an LH2 structure (62, 63, 80, 99) and the annotation of the genome (10). For this reason, a substantial amount of characterisation work had to be done.

- The first aim was to determine the LH2 complex types produced by *Alc. vinosum* under different growth and nutritional conditions. This involves the development and optimisation of a purification protocol to separate the different LH2 complex mixes produced under different growth conditions. A substantial question to be answered is whether the different LH2 complex types form a continuum between the B800-820 and B800-850, and the B800-840 is an intermediate, or whether these are all distinct LH2 complexes types.

- The second aim was to understand the basis of the variations observed between the different LH2 complex types of *Alc. vinosum* and the LH2 of other species. This will cover the peptide composition and carotenoid content of the different LH2 complex types as well as work towards understanding the unusual electronic and structural arrangement of the B800 BChl that gives rise to the origin of the split B800 peak.

- The third aim of this work was to identify an LH2 reconstitution candidate. As discussed in section 1.4, the initial stage of reconstitution work best in the absence of carotenoids. To determine which of the LH2 complex types of *Alc. vinosum* are stable in the absence of carotenoids, cultures will be grown in the presence of DPA under different growth conditions and the LH2 complexes produced purified. As DPA can be toxic in high concentrations other routes for carotenoidless complexes will be tested including solvent extraction of the standard complex and the creation of a genetic ‘knock-out’. Due to time restraints a full reconstitution protocol could not be developed but reversible dissociation experiments were conducted as proof of concept.

Chapter 2 - Methods and Materials

2.1 Glycerol stocks

Original *Alc. vinosum* strain D cells, DSM 180, were given as a gift from Prof. Phil Thornber, these cells were then aliquoted into 25 % (v/v) glycerol and stored at -80℃. Glycerol stocks were re-suspended in thiosulphate media (6) and cultured in high light conditions between 30℃ and 40℃ in an 8 ml container. Once grown, these cells were used to inoculate two 20 ml universal bottles containing thiosulphate media and grown in the same conditions. After further growth the universal cultures were used to inoculate larger volumes of thiosulphate media until the cultures were grown in 500 ml flat bottles. This was the starting point for cultures to be grown under specific growth conditions.

2.2 Standard growth conditions and cell harvesting

Alc. vinosum strain D was grown anaerobically in the light on media containing either 0.5 mM sodium sulphide (denoted with an S)(5) or 18.8 mM sodium thiosulphate (denoted with a T) (6) as an electron donor under several growth conditions. Cultures were grown under high light (denoted as HL) between 60-150 µmol s^{-1} m^{-2}, low light (denoted as LL) at 2 µmol s^{-1} m^{-2}, high temperature (40 °C) or standard temperature (30 °C). Cultures grown in low light conditions at 40 °C were grown in a water bath to maintain the temperature. Cells were cultured and used to inoculate fresh, sterile media twice before cells were harvested to ensure the spectra observed were indicative of the standard spectral phenotype for those growth conditions. Cultures were grown in 500 ml flat bottles or a 10 L pot for 2-3 days under high light conditions, or two weeks under low light conditions. Cells were harvested by centrifugation at 1250 xg for 25 mins and washed with MES, 100 mM KCl solution, pH 6.8 to remove residual media. Cells were then re-suspended in fresh MES, 100 mM KCl, pH 6.8 solution if frozen or re-suspended in 20 mM Tris-HCl, pH 8.0 if used immediately.

2.3 Membrane preparation

Harvested cells were homogenised to remove cell clumps before being lysed by three passages through a French press at 950 psi, in the presence of $MgCl_2$ and

DNase1 (bovine Deoxyribonuclease I, Sigma-Aldrich)(139). The lysate was centrifuged for 10 minutes at 2000 xg to remove unbroken cells and cell debris and then the supernatant was spun for 1 hour at 200,000 xg to pellet the membranes. The supernatant was discarded at this stage. Membranes were resuspended in 20 mM Tris-HCl, pH 8.0 (this buffer was used throughout the process unless otherwise stated) to an optical density (OD) of 25 at the Qy absorbance maximum. For different growth conditions the Qy absorbance maximum position varies, therefore for membranes prepared from T/S HL40 growth conditions were diluted to Qy_{856nm} = 25, for S HL30 growth conditions Qy_{853nm} = 25, for T HL30 growth conditions Qy_{850nm} = 25, and for T/S LL30 growth conditions Qy_{802nm} = 25.

2.4 *Allochromatium vinosum* LH2 Purification optimisation

The first stage in purification of the LH2 complex is sucrose density centrifugation. Sucrose density centrifugation gradients separate the larger LH1/RC 'core' complexes from the smaller LH2 complexes according to the density at which they equilibrate to. The density of the LH2 and LH1/RC 'core' complexes are dependant on the size of the detergent micelle they are suspended within, meaning that sucrose concentrations vary for each detergent.

2.4.1 LDAO and DM solubilisation trials

n-Dodecyl-ß-D-maltoside (DDM) detergent has previously been used successfully as both a solubilising detergent and a working detergent with *Alc. vinosum* (113) but did not completely solubilise the membranes. This was apparent as after centrifugation the unsolubilised pellet was still pigmented. For this reason two detergents that have been used on other purple photosynthetic membranes were trialled. Lauryldimethylamine oxide (LDAO) (63, 120, 140, 141) and decyl maltoside (DM) (81) were tested for their ability to extract the light-harvesting complexes as well as for their effects on the complexes. Membranes at OD_{856} 50 from *Alc. vinosum* cells grown in thiosulphate media at high light and 40 °C were solubilised with either 1 % LDAO (v/v) or 1.5 % DM (w/v) at room temperature and agitated for 1 hour. Membranes were then centrifuged for 60 min at 20,000 xg to pellet any unsolubilised material. The supernatant containing the

solubilised light-harvesting complexes was then decanted. The level of solubilisation was assayed by whether the pellet was pigmented. Room temperature absorption spectra were recorded using a Shimadzu UV-1700 PharmaSpec to determine the effect of solubilisation with 1 % LDAO (v/v) and 1.5 % DM (w/v) on the different light-harvesting complexes. Sucrose density centrifugation gradients were set up in 12 ml Beckman tubes with sucrose concentrations of 0.2, 0.4, 0.6, 0.8, and 1 M (2 ml volume for all concentrations) in the presence of 0.1 % LDAO (v/v) and 1 ml LDAO solubilised light-harvesting complexes were aliquoted on top of the 0.2 M sucrose layer. For DM solubilised membranes, sucrose density centrifugation gradients were set up with sucrose concentrations of 1.2, 1.4, 1.6, 1.8, and 2.0 M (2 ml volume for all concentrations) in the presence of 0.15 % DM (w/v) and 1 ml DM solubilised light-harvesting complexes were aliquoted on top of the 1.2 M sucrose layer. Sucrose density centrifugation gradients were spun at 200,000 xg for 12-16 hours to separate the light-harvesting complexes. Presence or absence of the LH1/RC "core" and LH2 complexes was determined visually by observation of pigmented bands.

2.4.2 Optimisation of sucrose density centrifugation gradients after solubilisation in dodecyl maltoside

Previous work (113) that used DDM during extraction and purification of the LH2 complexes of *Alc. vinosum* used sucrose concentrations of 0.6, 0.8, 1.0, and 1.2 M with volumes of 5.5 ml, 6 ml, 6 ml, and 5.5 ml respectively. All sucrose concentrations contained 20 mM Tris-HCl, pH 8.0, and 0.02 % DDM. These volumes of sucrose concentrations between 0.6 – 1.2 M resulted in poor separation of the LH1/RC "core" and LH2 complexes and so alternative volumes were tested.

Membranes at OD_{856} 50 from *Alc. vinosum* cells grown in thiosulphate media at high light and 40 °C were solubilised in 2 % DDM (w/v) and left agitating at room temperature for 90 min. Solubilised membranes were then centrifuged for 60 min at 20,000 xg to pellet any unsolubilised material. The supernatant (1 ml) was then loaded on top of sucrose density gradients consisting of volumes of 3 ml, 8 ml, 8 ml, and 3 ml of 0.6 M, 0.8 M, 1.0, and 1.2 M sucrose concentrations respectively. Supernatant (1 ml) was also loaded on a second set of sucrose

gradients set up with volumes of 3 ml, 6 ml, 6 ml, 6 ml, and 3 ml of 0.6 M, 0.8 M, 0.9 M, 1.0 M, and 1.2 M sucrose concentrations respectively. Sucrose density gradients were then centrifuged at 200,000 xg for 16 hours to separate the light-harvesting complexes. The separation of the LH1/RC "core" and LH2 complexes was assayed by eye.

2.5 Purification protocol for the LH2 complex types of *Alc. vinosum*

The LH2 complex types of *Alc. vinosum* were purified in dodecyl maltoside (DDM) for characterisation work as the LH2 complexes were stable, or in decyl maltoside (DM) for reconstitution studies in order to be able to perform a detergent exchange into octyl glucoside (OG) or DDM where required.

2.5.1 Solubilisation using the detergent dodecyl maltoside and sucrose density centrifugation to separate the light-harvesting complexes

All characterisation work used the detergent DDM during the purification of the LH2 complex types. Membranes were solubilised with n-Dodecyl-ß-D-maltoside (DDM, Glycon) at 2 % (w/v) at room temperature and were agitated for 90 minutes. Unsolubilised material was then pelletted by centrifugation for 20 minutes at 20,000 xg. Solubilised material was then loaded onto sucrose density centrifugation step gradients set to 0.6 M, 0.8 M, 1.0 M and 1.2 M sucrose (at 3 ml, 8 ml, 8 ml, and 3 ml respectively) and centrifuged for 14 hours at 200,000 xg. The discrete LH2 band was then decanted and the absorption spectrum recorded. The crude LH2 fraction was either used immediately for anion exchange chromatography or frozen at -20 ℃.

2.5.2 Solubilisation using the detergent decyl maltoside and sucrose density centrifugation to separate the light-harvesting complexes

All reconstitution work used the detergent DM during the purification of the LH2 complex types. Membranes were solubilised with Decyl-ß-D-maltoside (DM, Glycon) at 1.5 % (w/v) at room temperature and were agitated for 60 mins. Unsolubilised material was then pelletted by centrifugation for 20 minutes at 20,000 xg. Solubilised material was then loaded onto sucrose density

centrifugation step gradients set to 1.0 M, 1.2 M, 1.4 M and 1.6 M sucrose (at 3 ml, 8 ml, 8 ml, and 3 ml respectively) and centrifuged for 14 hours at 200,000 xg. The discrete LH2 band was then decanted and the absorption spectrum recorded. The crude LH2 fraction was either used immediately for anion exchange chromatography or frozen at -20℃.

2.5.3 Anion exchange chromatography to separate the different LH2 complex types of *Alc. vinosum*

Anion exchange chromatography was performed using Poros 20 HQ resin (packed at 2600 psi) on a BioCad 700E perfusion workstation (Applied Biosystems). The anion exchange protocol and methods for each LH2 complex type is identical regardless of whether DM or DDM detergent is used with the exception of the detergent present in the equilibration and elution buffers. Solution A was the equilibration buffer and consisted of 20 mM Tris-HCl, pH 8.0, while the elution buffer, solution B, consisted of 20 mM Tris-HCl, pH 8.0, and 1 M NaCl. Both solution A and B contained either 0.02 % DDM or 0.15 % DM depending on the detergent present in the crude LH2 fraction. The crude LH2 fraction from sucrose density centrifugation was thawed and filtered through a 0.2 μM filter (Sartorius stedim) to remove any particulates that could block the lines. The crude LH2 sucrose density centrifugation fraction (5 ml) was injected at OD_{802} (S/T LL30, SLL40), OD_{803} (S/T HL30,), or OD_{848} (S/T HL40) into the loop. The automated system injected the sample onto the column at 0 mM NaCl and the sucrose was washed from the sample and column. The elution program consisted of alternating gradients and steps to wash the sample and elute the different LH2 complex types. The different LH2 complex types elute at different NaCl concentrations and so depending on the mix of LH2 complexes produced under different growth conditions, different methods were used.

2.5.3.1 Anion exchange chromatography program for the B800-850 LH2 complex types produced under S/T HL40 growth conditions

To purify the B800-850 LH2 complex type produced under high light, 40℃ growth conditions the following step-gradients were used; a wash step for 10 column volumes (CV) at 0 mM NaCl. The first gradient step from 0 mM to 100 mM over 5 CV and held at 100 mM for 5 CV. The concentration of NaCl was increased to 250 mM over 5 CV and held for 2 more CV. The NaCl was increased to 310 mM

over 5 CV and maintained at 310 mM for a further 3 CV. The NaCl concentration was increased to 500 mM over 10 CV and maintained for 5 CV. To then clean the column the NaCl concentration was increased to 1000 mM over 5 CV. This method was named Alvin-SandThio-HL40-800-850-method-3.met.

2.5.3.2 Anion exchange chromatography program for the B800-820 and B800-840p LH2 complex types produced under T HL30, T LL40, and S/T LL30 growth conditions

To purify the B800-820 and B800-840 LH2 complex types produced under thiosulphate high light, 30℃, or thiosulphate, low light, 40℃, or low light, 30℃ growth conditions the following step-gradient program was used; a wash step for 10 column volumes (CV) at 0 mM NaCl. The first gradient step from 0 mM NaCl to 100 mM over 5 CV and held at 100 mM for 5 CV. The concentration of NaCl was increased to 240 mM over 5 CV and held for 12 CV more. The NaCl was increased to 260 mM over 2.5 CV and maintained at 260 mM for a further 9 CV. The NaCl concentration was increased to 500 mM over 10 CV and maintained for 5 CV. To then clean the column the NaCl was increased 1000 mM over 5 CV. This method was named Alvin-800-820-and800-840-method.met.

2.5.3.3 Anion exchange chromatography program for the B800-820 and B800-850 LH2 complex types produced under S HL30 and S LL40 growth conditions

To purify the B800-820 and B800-850a LH2 complex types produced under sulphide high light, 30℃, or sulphide, low light, 40℃ growth conditions the following step-gradient program was used; a wash step for 10 column volumes (CV) at 0 mM NaCl. The first gradient step from 0 mM NaCl to 100 mM over 3 CV and held at 100 mM for 5 CV. The concentration of NaCl was increased to 240 mM over 5 CV and held for 12 more CV. The NaCl was increased to 260 mM over 2.5 CV and maintained at 260 mM for a further 9 CV. The NaCl was increased to 310 mM over 5 CV and maintained for 5 CV. The NaCl concentration was increased to 500 mM over 10 CV and maintained for 2 CV. To clean the column the NaCl was increased to 1000 mM over 5 CV. This method was named Alvin-SHL 30 - exp03-6-02-13.met.

2.5.4 Size exclusion chromatography for the LH2 complex types of *Alc. vinosum*

Following anion exchange chromatography, size exclusion chromatography (SEC) was used to desalt the sample and to separate any remaining contaminants according to their size. The SEC protocol and methods for each LH2 complex type is identical regardless of whether DM or DDM detergent is used with the exception of the detergent present in the equilibration/elution buffer. Elution buffer was 20 mM Tris-HCl, pH 8.0 with either 0.02 % DDM (w/v) or 0.15 % DM (w/v). SEC was performed using a Superdex G200 column (GE Healthcare) on an AKTAprime plus system (GE Healthcare) at 0.5 ml/min at an average pressure of 0.29 psi.

2.6 Steady state absorption, transmittance and fluorescence spectroscopy

Room temperature absorption spectroscopy was performed with a Shimadzu UV-1700 PharmaSpec. Buffers contained 20 mM Tris-HCl (pH 8) for membrane samples with addition 0.02 % DDM for LH2 samples for characterisation, 0.15 % DM for LH2 samples prepared for reconstitution, or 0.7 % octyl glucoside (OG) for LH2 samples during reconstitution. All spectra were taken at an OD between 0.1 and 1 A.U. and were normalised at the Qx band (590 nm), where appropriate. Peak positions were determined using Origin 8, and the position of absorption shoulders determined by checking the ASCII files directly. Shouders in absorption are denoted by a ~ preceding the wavelength at which the absorption rapidly drops.

Fluorescence excitation and emission spectra were recorded with a 1 cm path length cuvette using a Spex 1681 0.22m Fluorolog spectrometer. Samples were diluted with 20 mM Tris-HCl buffer, pH 8.0 with 0.02 % DDM, 0.15 % DM or 0.7 % OG. Fluorescence spectroscopy must be done at very low concentrations to avoid self-absorbance of the fluorescence, so all samples were run at an OD of 0.07. Emission spectra were recorded for the B800-850c, B800-850a, B800-840p and B800-820 LH2 complex types after excitation at 488 nm. Two samples of B800-820 LH2 complex type were sourced from low light 30℃ growth conditions, one sample purified from cells grown in the presence of thiosulphate and the other

from cells grown in the presence of sulphide. Two samples of classic B800-850 LH2 complex types were purified from cells cultured at high light 40℃ growth conditions, one in the presence of sulphide and the other in thiosulphate. The alternative B800-850 was purified from cells grown in the presence of sulphide in high light at 30℃. The B800-840p was purified from *Alc. vinosum* grown under thiosulphate in high light at 30℃ growth conditions. The carotenoid depleted B800-850 LH2 complex was sourced from *Alc. vinosum* grown under sulphide in high light at 30℃ growth conditions in the presence of 75 μM DPA.

2.7 Circular dichroism (CD) spectroscopy

CD experiments were performed at room temperature using a JASCO, J-810 spectrophotometer at 20℃ with a photomultiplier sensitive between 400 -1000 nm. The NIR spectra were recorded between 750 nm and 900 nm, while the green region of the spectra was recorded between 300-600 nm to observe the carotenoid binding. Samples were run at OD 4 in a 0.2 cm cell. System parameters were 20 nm/min, 2 scans (averaged at end), 2 second response, with a 60 μm band width.

Circular dichroism was used on purified B800-820, B800-840p and B800-850c LH2 complex types from *Alc. vinosum* and compared to the standard B800-850 LH2 complex from *Rps. acidophila* 10050. The B800-820 LH2 complex type was purified from thiosulphate low light 30℃ growth conditions. The B800-850c LH2 complex types were purified from cells cultured in thiosulphate high light 40℃ growth conditions. The alternative B800-850 was purified from cells grown in the presence of sulphide in high light at 30℃. The carotenoid depleted B800-850 LH2 complex was sourced from *Alc. vinosum* grown under sulphide in high light at 30℃ growth conditions in the presence of 75 μM DPA. B800-850 LH2 complex from *Rps. acidophila* 10050 was grown and purified as per (93).

2.8 SDS PAGE

Membranes, crude LH2 extracts from sucrose density centrifugation gradients (SDCG) and purified LH2 complex types were analysed by SDS PAGE analysis. Proteins in membrane samples were denatured in 1 x Laemmli sample buffer (BioRad), 20mM Dithiothreitol (DTT) and additional 2 % SDS (v/v) and heated for

20 min at 70℃. SDCG and purified LH2 complex types were denatured in 1 x Laemmli sample buffer (BioRad) and heated for 5 min at 90℃. After denaturation, all samples were spun at 16,600 xg in a bench top centrifuge to pellet any large aggregated material. Samples were run for 27 minutes at 150 V on an anykD gel polyacrylamide gel (BioRad) with BioRad precision plus dual Xtra protein standards consisting of 12 recombinant proteins of 2, 5, 10, 15, 20, 25, 37, 50, 75, 100, 150, and 250 kDa.

2.9 Tandem MS-MS of the standard and carotenoid depleted B800-850a with Dr Bill Mullen

Tandem MS-MS was used to determine the differences in peptide composition between the alternative B800-850 (B800-850a) and the classic B800-850 (B800-850c). Both the standard B800-850a and carotenoid depleted B800-850a LH2 complexes were analysed to ensure that there were no protein changes due to the inhibition by DPA. The B800-850a was purified from SHL30 growth conditions and peptides extracted and sent to Dr Bill Mullen for tandem MS-MS mass spectroscopy. Peptides were extracted using chloroform/methanol 1:1 (v/v) with 0.1 M ammonium acetate for preferential alpha peptide extraction, and with the addition of 10 % (v/v) acetic acid for preferential beta peptide extraction. In the absence of acetic acid, only a small proportion of the betas are extracted but the addition of acetic acid causes methylation of the alphas. This means that two samples must be prepared to ensure that all peptides are extracted and identified. The extract was then passed through a sephadex LH60 resin (Amersham Biosciences) column and pooled according to its A_{280}. The full spectrum of the pooled fractions was acquired before pooling to ensure there were no pigments present as they block the HPLC. The pooled sample was then dried under nitrogen gas and stored at -20℃ if for 1-2 weeks, or at -80℃ if for longer.

Samples were analysed on a Dionex Ultimate 3000 RSLS nano flow system (Dionex, Camberly UK). After loading (5 µl) onto a Dionex 0.1×20 mm 5 µm C18 nano trap column at a flowrate of 5 µl/min in 98% 0.1% formic acid and 2% acetonitrile, sample was eluted onto an Acclaim PepMap C18 nano column 75 µm×15 cm, 2 µm 100 Å at a flow rate of 0.3 µl/min. The trap and nano flow column were maintained at 35°C. The samples were eluted with a gradient of

solvent A:98% 0.1% formic acid, 2% acetonitrile verses solvent B: 80% acetonitrile, 20% 0.1% formic acid starting at 35% B for 5 minutes rising to 45% B after 15 min and finally to 80%B after 40 min. The column was then washed and re-equilibrated prior to the next injection.

The eluant was ionized using a Proxeon nano spray ESI source operating in positive ion mode into an Orbitrap Velos FTMS (Thermo Finnigan, Bremen, Germany). Ionization voltage was 2.6 kV and the capillary temperature was 250°C. The mass spectrometer was operated in MS/MS mode scanning from 400 to 1800 amu. The top 5 multiply charged ions were selected from each scan for MS/MS analysis using HCD at 40% collision energy. The resolution of ions in MS1 was 60,000 and 7,500 for MS2.

MS and MS/MS data files were searched, in this case, against Uniprot Allochromatium + Vinosum database using SEQUEST (by using Thermo Proteome Discoverer), with no enzyme specified. Peptide data were extracted using high peptide confidence and top one peptide rank filters. No static modification set Oxidation of Methionine and Proline (M, P) as variable modifications and a peptide mass tolerance of ± 10 ppm and a fragment mass tolerance of ± 0.05 Da and allow for a maximum of two missed cleavage. Determine the false discovery rates by reverse database searches and empirical analyses of the distributions of mass deviation, whereby Ion Scores can be used to establish score and mass accuracy filters.

2.10 Carotenoid extraction, purification and analysis by thin layer chromatography (TLC)

Carotenoids were extracted from purified B800-820, B800-840p and B800-850c LH2 complex types and the LH1/RC “Core” from from *Alc. vinosum*. The B800-820 LH2 complex type was purified from thiosulphate low light 30℃ growth conditions. The B800-850c LH2 complex types were purified from cells cultured in thiosulphate high light 40℃ growth conditions. The alternative B800-840p was purified from cells grown in the presence of thiosulphate in high light at 30℃.

All carotenoid extractions were performed in low light conditions. Carotenoids were extracted from 100 µl of OD 100 purified LH2 complex types using 4 ml of

7:2 acetone/methanol. The LH2 acetone/methanol mix was left for 10 min at room temperature before 2 ml pet ether (40.60 bp) was added. The addition of 4-5 ml of warm salty water causes the carotenoid to partition into the pet ether layer, which is then decanted off. The pet ether layer is then washed with another 4-5 ml of warm salty water to remove any residual acetone. The carotenoid mix is then dried down under nitrogen and resuspended in diethyl ether. Carotenoid mixes from each of the LH2 complex types, and the LH1 were spotted onto a TLC plate using a glass pipette and separated using 90:10 pet ether/acetone (v/v) as the mobile phase.

Individual carotenoids preliminarily identified as part of the carotenoid complement of the LH2 complexes were extracted from known sources to confirm their identities. Lycopene, spirilloxanthin, anhydrorhodovibrin, and rhodopin were extracted as described from tomato paste, *Rsp. rubrum S1*, and *Alc. vinosum* strain D respectively. TLC plates were used to separate the carotenoids in the crude extracts and bands were scraped from the plates. In the case of anhydrorhodovibrin, multiple TLC plates were used to accumulate enough anhydrorhodovibrin to acquire an accurate absorption spectrum. The identities of the carotenoids were confirmed using absorption spectra and hydrophobic character. Carotenoids from the purified B800-850 LH2 complex from THL40 growth conditions were extracted and ran parallel to the Purified carotenoids, which were run using 90:10 pet ether/acetone (v/v).

2.11 Production of a carotenoid minus B800-850 using the carotenoid biosynthesis inhibitor diphenylamine (DPA)

Diphenylamine (DPA) inhibits the carotenoid biosynthesis pathway in purple photosynthetic bacteria by inhibiting the enzyme phytoene desaturase (133). DPA degrades when exposed to white light, so cultures were grown beneath a red filter during inhibition studies.

2.11.1 Establishing the sensitivity of *Alc. vinosum* to DPA and the effective concentration range for producing fully carotenoidless LH2

Cultures were grown with either thiosulphate or sulphide media in the presence of 10-100 μM DPA to establish the DPA concentration range that effectively inhibits the production of carotenoid in *Alc. vinosum*. *Alc. vinosum* cultures were grown at 40 °C in 60-80 μmol s^{-1} m^{-2} light conditions in autoclaved 100 ml flat-sided bottles. DPA is not very soluble in water and so was dissolved in ethanol and aliquoted into the cultures to a final DPA concentration of 10 μM, 20 μM, 30 μM, 40 μM, 50 μM, 60 μM, 70 μM, 80 μM, 90 μM, or 100 μM. A control culture was grown under the same conditions with an equal volume of ethanol to the culture grown at the highest DPA concentration. Cultures were incubated at 40℃ in darkness for 24 hours to allow the oxygen present to be respired, and then cultures were grown behind a red light filter. Cultures were compared visually and by absorption spectroscopy to assay the level of carotenoid inhibition and the effects on the light-harvesting complexes.

2.11.2 Production of the carotenoid depleted B800-850 LH2 complex type

The DPA concentration range of 65-75 μM produced carotenoid depleted B800-850 LH2 complex type from the high light 40℃ and 30℃ growth conditions, which was consistent with previous work (83, 134, 135). Cultures were grown in sterile 500 ml flat-sided bottles in either thiosulphate (6) or sulphide (5) media under high light (60-80 μmol s^{-1} m^{-2}) or low light (2 μmol s^{-1} m^{-2}) conditions at 40 °C or 30 °C. DPA was dissolved in ethanol to a concentration of 10 mM and added to cultures with the inoculum, to a final concentration of between 65-75 μm. Cultures were incubated at 30℃ in darkness for 24 hours to allow the oxygen present to be respired, and then cultures were grown behind a red light filter. *Alc. vinosum* cells were harvested as outlined in section 2.2. Cells were lysed using a Sanyo Soniprep 150 sonicator due to low volumes of harvested cells being insuffient for French press lysis. Cells were homogenised and lysed, in the presence of $MgCl_2$ and DNase1 (bovine Deoxyribonuclease I, Sigma-Aldrich) and then sonicated at 10 microns for 10 cycles of 30 seconds. Membranes were then prepared as outlined in section 2.3. Membranes were resuspended in 20 mM Tris-HCl, pH 8.0 to an OD_{856} of 25.

The B800-850 LH2 complexes were purified as per section 2.5 in either DDM for characterisation or DM for reconstitution studies. Absorption spectra and photos were taken to show the preferential incorporation of carotenoid.

2.12 Production of a carotenoid minus *Alc. vinosum* mutant

The creation of a carotenoid minus strain of *Alc*. vinosum allows the production of fully carotenoidless LH2 complexes without the need of the toxic inhibitor DPA.

2.12.1 Genomic extraction

Serial dilutions of cultures were plated on 1.5 % agar in thiosulphate media (6) and grown at anaerobically at 28 ℃ under 60 µmol m^{-1} s^{-2} conditions. Fifteen to twenty colonies were picked and used to inoculate 5 ml thiosulphate media. Cultures were grown overnight at 28 ℃ under 60 µmol m^{-1} s^{-2} conditions and cultures were centrifuged at 2550 xg for 15 minutes, 4 ℃, to pellet the whole cells. DNA was isolated and prepared using standard procedures (142). In brief, supernatant was removed and pellet incubated at 37 ℃ for 1 hour in 1 ml fresh lysis buffer (0.2 M Tris-HCl, 0.5 M NaCl, 0.01 M EDTA, 1 % SDS, 1 M sodium acetate). To break down proteins present, the sample was incubated at 50 ℃ in 100 µg/ml proteinase K until clear. The sample was then incubated at 37 ℃ for 30 minutes in 20 µg/ml RNAse A. The sample was mixed with an equal volume of phenol:chloroform:IAA (25:24:1 v/v) forming a milky suspension. This was spun at 16,000 xg for 5 minutes. The upper phase of the sample was decanted and 0.2 volumes 10 M ammonium acetate, and then 600 µl absolute ethanol (AR grade) were added. DNA was pelleted at 16,000 xg for 30 minutes, and supernatant removed. The pellet was then washed in 70 % ethanol, and spun for 16,000 xg for a further 10 minutes. The final DNA pellet was air dried for 15-20 minutes before being resuspended in DNAse and RNAse free water at 40 ℃ overnight. Genomic DNA was then stored at -20 ℃.

2.12.2 Creation of the CrtI^{-} Genomic 'knock-out' using Splice-Overlap-Extension method

Two genes in *Alc. vinosum* have been putatively assigned as the CrtI gene that produces phytoene desaturase for the biosynthesis of the carotenoid precursor phytoene (10), Alvin 2566 and Alvin 2570. Alvin 2566 (2,894,906…9,896,402 bp) was selected to be knocked out first. Upstream (US) forward and reverse, and downstream (DS) forward and reverse primers were designed by Dr Sarah Henry and produced by Eurofins Scientific to create flanking sequences to the identified CrtI gene (Table 2.1). EcoRI and HindIII restriction sites were incorporated into the US forward and DS reverse primers respectively.

Table 2.1 Upstream (US) and downstream (DS) forward and reverse primers showing the incorporated restriction enzyme sites (blue)

Name	5^1-3^1 sequence
US forward with EcoRI	ACAGAATTCGAAGGCGAGGATGATGAGC
US reverse	CGGTCAGGTCGGCATCAGAACCATGACTC
DS forward	CTGATGCCGACCTGACCGTCGACAACGACG
DS reverse with HindIII	ACTAAGCTTTCATCGATGTCGATCACCAG

The US and DS flanking sequences were denatured for 10 seconds at 98℃, annealed for 20 seconds at 60℃, and extended for 30 seconds at 72℃ with Phusion polymerase (Biolabs) PCR on a Biorad C1000 Thermal Cycler. These steps were repeated for 30 cycles. PCR products were then separated using gel electrophoresis and extracted using a gel extraction kit (Thermo scientific).

A gradient PCR reaction was conducted to determine the appropriate annealing temperature for the US segment of DNA. The annealing temperature was varied across a set of 8 reaction tubes, from 50℃ to 68℃ (68℃, 67℃, 64.9℃, 57℃, 53.5℃, 52℃, and 50℃). The US product was denatured for 10 seconds at 95℃, annealed for 20 seconds, and extended for 1 minute at 72℃ with MyTaq polymerase (Bioline) on a Biorad C1000 Thermal Cycler for 29 cycles. The PCR products were then analysed by gel electrophoresis as outlined in section 2.12.3.

The US and DS products were then annealed using a splice overlap extension program (SOE) PCR (143). US and DS sections were denatured at 90℃ for 10

seconds, annealed at 37 ℃ for 20 seconds, and extended at 72 ℃ for 1 minute in the absence of DNA polymerase. This results in the annealing of the two complementary codons at the 3^1 end of the sense US segment, and the anti-sense 3^1 end of the DS segment. After the SOE program is run, Phusion polymerase (Biolabs) was added and a PCR program, as outlined for the individual US and DS segments, was run. This resulted in a blunt ended insert consisting of the joined US and DS sequences with two codons in the centre, of 780 bp (Figure 2.1). This is the CrtI$^-$ insert that can then be ligated into a vector.

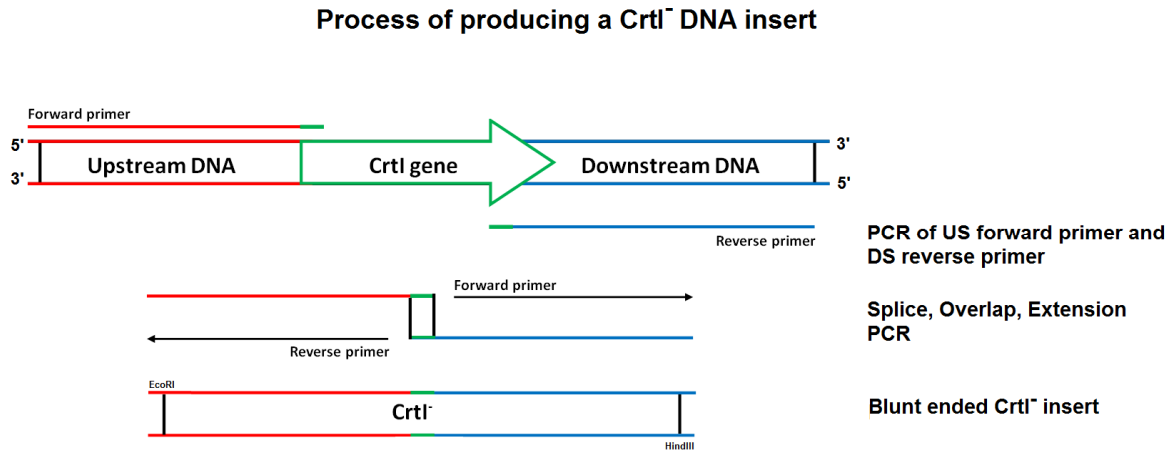

Figure 2.1 Basic schematic showing the process of producing a CrtI- DNA insert using a Splice Overlap Extension (SOE) method.
This process proceeds by the duplication of the upstream and downstream regions of the DNA around the CrtI-, phytoene desaturase, gene. These are amplified by PCR and then annealed using the splice, overlap, extension method. The products are then extended using DNA polymerase creating a blunt ended CrtI$^-$ instert.

2.12.3 DNA gel electrophoresis

DNA PCR and digestion products were checked using 1 % agarose (Roche) gels with SYBR® Safe DNA gel stain (Invitrogen) run in 1x TAE buffer on a RunOne (Embi Tec) electrophoresis tank at 100 volts. DNA was run parallel to a 1kb DNA ladder (Promega).

2.12.4 Ligation of the CrtI$^-$ into pJET1.2/blunt vector and transformation of DH5α cells

The blunt ended CrtI$^-$ was subcloned into pJET1.2/blunt (Thermo Scientific) as per the manufacturer instructions using T4 DNA ligase (Thermo Scientific). The insert was used to transform DH5α strain *E.coli* cells using heat shock treatment. Competent DH5α cells were thawed on ice before 4 µl of the pJET1.2/blunt-CrtI$^-$

was aliquoted into the cells and stirred, gently, once. Cells were left on ice for 15 min before they were placed in a 42 ℃ water bath for 30-60 seconds. Cells were then returned to ice for 5 min to recover before 250-400 µl warm LB was aliquoted into the cells. The transformed cells were then incubated for 1 hr at 37 ℃ while agitated. Cells were then plated onto an LB agar plate (100 mM ampicillin) and incubated overnight at 37 ℃. Transformed colonies produced were then picked and transferred to liquid LB (100 mM ampicillin) for overnight growth. Glycerol stocks of transformed cells were created using 1 ml 50 % glycerol (v/v) and 1 ml transformed cells. Plasmids were extracted using the Thermo Scientific miniprep kit and sent for sequencing to confirm that the insert sequence was correct.

2.12.5 Sequential and simultaneous digests of the pJET1.2/blunt-CrtI$^-$ vector using HindIII and EcoRI

The pJET1.2/blunt-CrtI$^-$ was digested with HindIII (Roche) and EcoRI (Roche) in buffer B (Roche) at 37 ℃ overnight producing a CrtI$^-$ insert with 'sticky ends'. The digested DNA was separated on the 1 % agarose gel and the band at ~780 bp was excised and then extracted using a gel extraction kit (Thermo Scientific).

As there is a HindIII restriction site present on the pJET1.2/blunt vector, this potentially slows the rate of cleavage by the HindIII enzyme of the restriction site of the CrtI$^-$ insert. Sequential digests were performed to determine whether this was a factor in low CrtI$^-$ yields. PJET1.2/blunt-CrtI$^-$ was digested for 1 hour at 37 ℃ with EcoRI (Roche) before the digested products were separated on a 1 % agarose gel, excised and purified using a gel extraction kit (Thermoscientific). The Eco RI cleaved pJET1.2/blunt-CrtI$^-$ was then digested overnight at 37 ℃ with HindIII (Roche). The digested products were separated on a 1 % agarose gel before being excised and purified using a gel extraction kit (Thermoscientific).

The simultaneous digests were repeated and the digestion products were extracted using a Qiagen gel extraction kit as there were potential issues with contamination from the Thermoscientific gel extraction kit.

A Thermo Scientific Nanodrop 1000 spectrophotometer was used to confirm the levels of DNA present after gel extractions as well as to assay the purity of the DNA acquired.

2.12.6 Ligation of the CrtI$^-$ with 'sticky ends' into pK18MobsacB vector and transformation of JM109 cells

The CrtI- insert with 'sticky ends' was ligated into the pK18MobsacB (144) vector using Promega T4 ligase for 5 min at room temperature and then overnight at 4℃. The ligated pK18MobsacB-CrtI$^-$ construct was used to transform competent *E.coli* JM109 cells using heat shock treatment as previously described. Transformed cells were then plated onto LB plates with 30 µg/ml kanamycin, 6 µl 1 M IPTG, 40 µl 20 mg/ml X-GAL (145) to induce the lac operon, and then incubated overnight at 37℃. Colonies were used to inoculate 5 ml of LB with 30 µg/ml kanamycin and grown overnight at 37℃.

2.13 Trials to determine whether extraction of carotenoids by solvent mixes can produce carotenoid depleted light-harvesting complexes

Due to the difficulty producing carotenoidless B800-820 using DPA it was decided to try to remove the carotenoid from the already formed complex. Carotenoids can be extracted from membrane bound LH complexes using benzene (Clayton and Sistrom 1978) and previous work has successfully depleted the carotenoids present in the LH1 (121). Benzene is highly toxic and so toluene was substituted due to its lower toxicity. Toluene is less polar than benzene, which may affect the level of extraction of carotenoids, therefore to compensate for this additional polar solvents were added at low percentages. Acetone, ethyl acetate, diethyl ether and petroleum ether, at 1 %, 5 % or 10 % (v/v) were used to increase the polarity of the solvent mix. The solvent mixes were added to 1 mg freeze dried chromatophores from sulphide low light grown 30℃ *Alc. vinosum* cultures. The carotenoids were extracted with 1 ml of solvent-mix, which was stirred and then left for 10 minutes at room temperature. Membranes were spun at 5000 xg to pellet the chromatophores and the supernatant was decanted. A further 1 ml of solvent-mix was used to resuspend the pellet, and the mixture was stirred and left for a further 10 min. Membranes were pelleted

by centrifugation at 5000 xg and the supernatant decanted. The pellet was then resuspended in 20 mM Tris-HCl, pH. 8.0.

To determine the full complement of carotenoids contained within 1 mg of chromatophores, carotenoids were extracted using 100 % acetone as carotenoids have good solubility in acetone (146). Membranes were washed in 1 ml acetone and pelleted by centrifugation at 5000 xg twice before being resuspended in Tris-HCl, pH 8.0. Absorption spectra of both the supernatant and the re-suspended membranes were recorded to assess the level of carotenoid extracted and the intactness of the light-harvesting complexes present within the membranes.

2.14 Reconstitution and reversible dissociation studies

The carotenoid depleted B800-850 LH2 complex was used for proof of concept reversible dissociation and reconstitution trials.

2.14.1 Carotenoid extraction and purification by alumina chromatography for reconstitution studies

Processes such as reconstitution (122) require higher purity and quantity carotenoids than can be acquired for a TLC plate. For this reason alumina chromagraphy was used to produce larger quantities of pure carotenoids. All carotenoid extractions were performed in low light conditions. The carotenoids used in reversible dissociation studies were lycopene, spirilloxanthin, and rhodopin. These carotenoids were extracted and purified from tomoto paste, *Rsp. rubrum* S1 chromatophores (147), and *Alc. vinosum* strain D chromatophores respectively. Carotenoids were extracted using 7:2 acetone/methanol, which was stirred and left for 10 min at room temperature to extract the majority of the carotenoids from the chromatophores. This was followed by the addition of 2 ml pet ether (40.60 bp) followed by 4-5 ml of warm salty water. The pet ether layer containing carotenoid was decanted off and re-washed with warm salty water to remove any residual acetone. The carotenoid mix is then dried down under nitrogen and re-suspended in pet ether for immediate alumina chromatography.

The carotenoid sample was purified using alumina column chromatography. The solid phase, alumina (aluminium oxide, Merck), was deactivated by the addition of 10 µl of water per 1 g of alumina. The addition of water reduces the number of polar sites available on the alumina, limiting its ability to retain organic compounds and preventing the carotenoid binding too strongly to the resin and failing to elute. The deactivated alumina was then poured into the vertical glass column as a slurry of alumina in the mobile phase, PET ether. The alumina column was flushed with 5 volumes of PET ether prior to addition of sample. Following the addition of the carotenoid sample, carotenoids were eluted with increasing concentrations of diethyl ether as diethyl ether is more polar than PET ether. Fractions were collected by hand, and assayed using absorption spectroscopy. Fractions were pooled according to the carotenoid peak positions and the low intensity of their *cis* peaks and carotenoids were used for reversible dissociation immediately after purification. The absorbance spectrum of each fraction was taken to quantify the quality of the samples by examining the *cis* peaks present. *Cis* absorption peaks are produced by carotenoid in the *cis* isomer form (37).

2.14.2 Dissociation of standard B800-850 LH2 complexes by LDAO, OG and DM

Standard B800-850 LH2 complexes from *Alc. vinosum* were produced by cells grown under THL40 growth conditions and purified in DM as described in section 2.5.2. The DM was dialysed out and replaced by either 0.1 % lauryldimethylamine oxide (LDAO) (v/v), 0.7 % n-octyl-ß-D-glucoside (OG) (w/v), or 0.15 % decyl maltoside (DM) (w/v) by centrifugation in a 50 kDa molecular weight cut off filter. Absorption spectroscopy was used to monitor the state of the LH2 complexes and determine whether full detergent exchange had occurred. Once the Qy peaks stopped shifting position, an additional 5 volumes of the CMC of appropriate detergent in 20 mM Tris, pH 8.0 was run through the sample. Following this, the concentrations of the detergents were increased to 2 % LDAO (v/v), 4.15 % DM (w/v), or 5 % OG (w/v) and the sample left at room temperature for 60 min before the absorption spectrum was acquired. The sample was then left overnight at room temperature and then a further absorption spectrum was recorded to monitor the intactness of the complexes.

2.14.3 Reversible dissociation of carotenoid depleted B800-850 LH2 complexes by LDAO and OG

Carotenoid depleted B800-850 LH2 complex was produced by *Alc. vinosum* grown under SHL30 growth conditions in the presence of 75 µM DPA, and purified in DM as described in section 2.5.2. The DM was dialysed out and replaced by 0.7 % OG (w/v) or 0.1 % LDAO (v/v) by centrifugation in a 50 kDa molecular weight cut off filter. Absorption spectroscopy was used to monitor the state of the LH2 complexes and determine whether full detergent exchange had occurred. Once the Qy peaks stopped shifting position, an additional 5 volumes of the CMC of appropriate detergent in 20 mM Tris, pH 8.0 was run through the sample. Following this, the concentrations of the detergents were increased to 2 % LDAO (v/v), or 5 % OG (w/v) and the sample left at room temperature for 60 min before the absorption spectrum was acquired. The sample was then left overnight at room temperature and then another absorption spectrum was recorded to monitor the intactness of the complexes. As dissociation appeared to have occurred, the concentration of detergent was reduced to the CMC (0.1 % LDAO (v/v) or 0.7 % OG (w/v)) and the absorption spectrum acquired to determine whether dissociation had been reversed.

2.14.4 Reversible dissociation of carotenoid depleted B800-850 LH2 complexes by OG and the addition of carotenoid

Carotenoid depleted B800-850 LH2 complex was produced by *Alc. vinosum* grown under SHL30 growth conditions in the presence of 75 µM DPA, and purified in DM as described in section 2.5.2. The DM was dialysed out and replaced by 0.7 % n-octyl-ß-D-glucoside (OG) by centrifugation in a 50 kDa molecular weight cut off filter. Absorption spectroscopy was used to monitor the state of the LH2 complexes and determine whether full detergent exchange had occurred. To ensure full detergent exchange, an additional 5 volumes of buffer/detergent were run through the sample until the Qy peak position was unchanged in the absorption spectrum. The B800-850 LH2 sample was concentrated to a volume of 200 µl at OD 20. The concentration of OG was increased to 5 % (w/v) by addition of 50 µl 20 % OG (w/v) to dissociate the LH2 complexes, which were left overnight at room temperature to fully dissociate. To begin to re-associate the LH2 complexes they were placed on ice in the dark and the detergent

concentration was reduced. Tris-HCl (pH 8.0) was added in 250 µl increments until the volume was 1 ml, and the OG concentration was 1.175 % (w/v). At 4℃ the CMC of OG is 1 %, resulting in the sample being just above the CMC. Freshly prepared carotenoid, as described in section 2.14.1, was added in acetone in 10 µl increments. The initial experiment using spirilloxanthin did not do this under nitrogen but in further experiments, with lycopene and rhodopin, carotenoid was added under a stream of nitrogen gas to prevent carotenoid and BChl degradation. Carotenoid was added every 10 min to prevent a build up of acetone in the solution as this negatively affected re-association. The Hamilton syringe used to inject carotenoid into solution was placed within the solution and used to stir in the carotenoid. This ensured the carotenoid entered the solution as otherwise the acetone formed a layer on top of the solution, and carotenoid was found to bind to the plastic of the eppendorf tube after acetone evaporation. After carotenoid was added in excess and the volume had been returned to 1 ml the sample was progressively diluted to 0.33 % OG. Dilutions were performed with 250 µl Tris-HCl (pH 8.0) and the sample was returned to ice beneath a stream of nitrogen gas. At 0.33 % OG (w/v) the sample was left at 4℃ overnight to allow complex reformation. After the sample had re-associated the complex was detergent exchanged into 0.02 % DDM by centrifugation. After reversible dissociation with rhodopin and lycopene the sample was purified by sucrose density sucrose centrifugation in 12 ml tubes, overnight at 200, 000 xg, at 4℃. Volumes used were 1 ml, 4 ml, 4 ml, and 1 ml of 0.6 M, 0.8 M, 1.0 M, and 1.2 M sucrose concentrations respectively, with 20 mM Tris-HCl (pH 8.0), 0.02 % DDM (w/v). Sucrose density centrifugation gradients were photographed and the LH2 band was decanted and the absorption spectrum acquired. Fluorescence emission and excitation spectra were acquired at OD 0.07 for the pre-RD sample and the post-RD sample. LH2 complexes were excited at 485 nm for fluorescence emission spectra and monitored for emission at 850 nm for excitation spectra.

2.14.5 De novo reconstitution of the B800-850 LH2 complex from *Alc. vinosum*

2.14.5.1 Purification of protein and pigment components

The alpha and beta peptides were extracted from purified freeze dried B800-850 LH2 complex using a solution of chloroform-methanol (1:1) in the presence of

ammonium acetate (0.1 M)(148). This technique preferentially extracts α peptides in addition to some ß peptides (121), which was thought sufficient for preliminary experiments. The alpha and beta peptides were extracted and separated from the pigments using a sephadex LH60 resin (Amersham Biosciences) column. The column was equilibriated in chloroform-methanol (1:1), and ammonium acetate (0.1 M) and the sample was injected onto the column and eluted by gravity flow. The absorption spectra of the fractions were measured to determine the concentration of protein, and to ensure no pigments were pooled with the peptides. The alpha and beta peptides were then dried under nitrogen and stored at –20 ˚C. The number of absorbing amino acid residues in each of the α and ß peptide sequences from *Alc. vinosum* was calculated and multiplied by its respective extinction coefficient (tyrosine 1490 M^{-1} cm^{-1}, tryptophan 5500 M^{-1} cm^{-1}, and cystine 125 M^{-1} cm^{-1}) (149, 150) and averaged across the twelve peptides to determine the average extinction coefficient of 15,823 M^{-1} cm^{-1}. The A_{280} was then divided by 15,823 M^{-1} cm^{-1} to determine the protein concentration used.

Spirilloxanthin was extracted and purified as described in section 2.14.1 and the A_{486} recorded to determine the concentration of spirilloxanthin using the extinction coefficient of 94 M-1 cm-1 (151).

Previous work found that a phytol tail instead of the geranylgeranyl group on the BChl made no difference in the ability of the complex to form (121) so BChl can be sourced from bacteria that produce different BChl a analogues. Previous work also found that whether the pigments were added in acetone or methanol made no difference to the ability of the complex to reform (32). Bacteriochlorophyll (BChl) was extracted from *Rsp. rubrum* G9 mutant using a methanol wash. Methanol was added to freeze dried G9, which was then centrifuged at 5000 xg for 10 min to pellet membrane and peptide debris. The supernatant containing BChl was decanted off and the A_{770} recorded to determine the concentration using the extinction coefficient 76 M^{-1} cm^{-1} (152). The BChl was then dried down under nitrogen and stored at 4 ˚C.

2.14.5.2 *De Novo* reconstitution

Extracted peptides were thawed and re-solubilised in 20 % OG (w/v), 20 mM Tris-HCl, pH 8.0, to ensure the peptides were fully dissociated and solubilised. The concentration of OG was then reduced to 1 % by the addition of Tris-HCl, pH 8.0, with a final peptide concentration was 6 µM. Spirilloxanthin was added in acetone to a final concentration of 7 µM while the sample was agitated under a stream of nitrogen gas. Following carotenoid addition, the OG concentration was further diluted to 0.7 % by the addition of Tris-HCl, ph 8.0, and the sample was left on ice for 10 min. Extracted BChl was re-suspended in acetone and added to a final concentration of 6 µM and the sample left to agitate for 10 minutes more on ice. Following pigment addition the concentration of OG was reduced by progressive additions of 20 mM Tris-HCl, pH 8.0, until the OG concentration reached 0.66 % and the sample left overnight at 4 ℃.

To purify the reconstituted sample, a 1 g De52 (Whatman) resin column was equilibrated in 20 mM Tris, pH 8.0, and 0.7 % OG and sample was aliquoted on top of the column. The sample was then washed with elution buffer consisting of 20 mM Tris, pH 8.0, 0.7 % OG and increasing NaCl concentrations. The NaCl concentrations used to wash the reconstituted sample were 100 mM NaCl, 250 mM NaCl, 500 mM NaCl, 1 M NaCl, and 2 M NaCl.

Chapter 3 - Establishment of *Allochromatium (Alc.) vinosum* growth conditions, LH2 complex purification and LH2 complex types produced under different growth conditions.

3.1 Introduction

The aim of the work in this chapter was to revisit the light-harvesting complexes of *Alc. vinosum* in light of recent structural and genomic understanding to see what types of LH2 can be made and characterised. One of the main questions was to discover whether the LH2 complex types of *Alc. vinosum* are discrete or whether they form a continuum of intermediate complexes.

Early work on *Alc. vinosum* strain D (5, 6, 109, 146, 153) found that different growth conditions produced cells with different NIR spectra as described in Introduction section 1.3. These variations reflected a change in the complement of light-harvesting complexes produced. It was hypothesised at the time that these changes in the absorbance of the light-harvesting machinery were adaptive in order to optimise the light-harvesting capability of the bacterium under different growth conditions.

Since this early work, there has been the successful structural determination of the LH2 (62, 72, 80, 99, 154) and LH1/RC "core" (59-61) complexes from several bacteria. This has helped allow us to understand the structural basis for the absorbance of the light-harvesting complexes.

Recent work (10) has fully annotated the genome of *Alc. vinosum* and identified six *puc* gene pairs that can code for the LH2 alphas and betas. This means that *Alc. vinosum* has, potentially, the capacity to form heterogeneous LH2 complexes, wherein the heterodimer subunits that make up the single ring of an LH2 complex are non-identical. This type of heterogeneity has been observed in the LH2 complexes of other purple photosynthetic bacteria such as *Rsp. palustris* (101) and *Phs. molischianum* (95).

3.2 Characterisation of *Alc. vinosum* spectral changes under different growth conditions

The absorption peaks observed in the NIR relate to the light-harvesting complexes (outlined in Introduction section 1.2.3) that are present in the photosynthetic membrane. Therefore, variations observed in the absorption spectra relate to changes in the light-harvesting machinery. The absorption peaks observed in the membranes of *Alc. vinosum* can be tentatively allocated to structures that are analogous to the LH1/RC "core" and LH2 structures determined from other species. The absorption peak that centres at the longest wavelength is the LH1/RC "core" complex, while all other peaks will correspond to BChl molecules bound within the LH2 complex types present. The absorption maxima centred at ~ 800 nm will correspond to the monomeric B800 BChl, while the more red-shifted LH2 peaks will relate to the excitonically coupled BChl, dubbed "B850-like" after the *Rsp. acidophila* model LH2.

To begin to determine the level of variation expressed by *Alc. vinosum* under different growth conditions, cultures were grown in either sulphide or thiosulphate media under different growth conditions (outlined in materials and methods section 2.2). Cells were then harvested and membranes were prepared as per materials and methods section 2.2 and 2.3. The NIR absorbance spectra of a diluted sample of membranes from cells grown under different growth conditions were recorded.

3.2.1 Room temperature absorption spectra of the membranes from *Alc. vinosum* grown under different growth conditions

In membranes prepared from all growth conditions a broad peak is observed in the absorption spectra at ~ 800 nm relating to the B800 BChl, with an apex at 807 nm (Figures 3.1 and 3.2). In figure 3.1, the effects of temperature and light intensity on the light-harvesting complexes produced by *Alc. vinosum* grown in the presence of sulphide (S) are observed. Distinct peaks of equal intensity are observed at 807 and 822 ± 0.5 nm in membranes produced under low light conditions at 30℃ (LL30, cyan). The LH1/RC "core" peak is positioned at 890 ± 0.5 nm. The LH1/RC "Core" peak is of a much lower intensity than the other two peaks. When *Alc. vinosum* is cultured in low light intensity at 40℃ (LL40, blue), the "B850-like" peak centres at 853 ± 0.5 nm and is of higher intensity than the

807 nm peak while the LH1/RC "core" peak is slightly blue-shifted and obscured as a shoulder. When *Alc. vinosum* is grown at high light intensity and 30℃ (HL30, green) the peaks produced from the light-harvesting complexes of *Alc. vinosum* centre at the same wavelengths as those produced under LL40 conditions but are of a lower intensity relative to the 807 nm peak. When *Alc. vinosum* is grown in high light intensity at 40℃ (HL40, dotted line) the "B850-like" peak shifts centres further to the red, to 856 ± 0.5 nm, while the LH1/RC "core" centres at 888 ± 0.5 nm, both are of a higher intensity than the 807 nm peak.

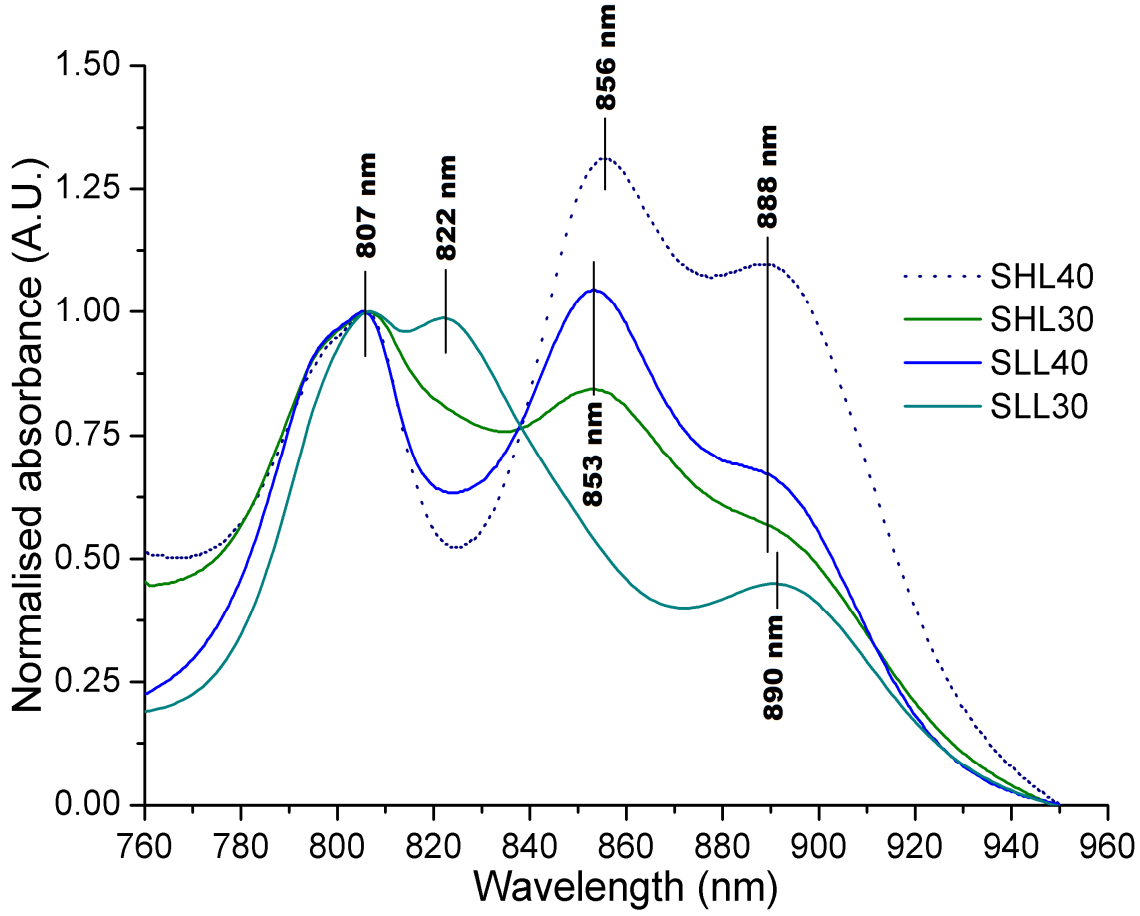

Figure 3.1 Room temperature NIR absorption spectra of *Alc. vinosum* membranes prepared from cells grown in the presence of sulphide (S) under different growth conditions (HL: High light, LL: Low light, 30℃ or 40℃).
Membranes from *Alc. vinosum* grown under SHL40 (dotted line) growth conditions produce three peaks in the NIR at 807 ± 0.5 nm, 856 ± 0.5 nm, and 888 ± 0.5 nm. The 856 nm peak and 888 nm peaks are of a higher intensity than the 807 nm peaks. Membranes from *Alc. vinosum* grown under SHL30 (green) growth conditions produce two peaks in the NIR at 807 ± 0.5 nm, 853 ± 0.5 nm, and a shoulder at ~ 890 ± 0.5 nm. The 853 nm peak and 890 shoulder are of a lower intensity than the 807 peak. Membranes from *Alc. vinosum* grown under SLL40 (blue) growth conditions produce two peaks in the NIR at 807 ± 0.5 nm, 853 ± 0.5 nm and a shoulder at ~890 ± 0.5 nm. The 853 nm peak is of a higher intensity than the 807 peaks while the 888 peak is of a lower intensity. Membranes from *Alc. vinosum* grown under SLL30 (cyan) growth conditions produce three peaks in the NIR at 807 ± 0.5 nm, 822 ± 0.5 nm and 890 ± 0.5 nm. The 822 nm peak is of equal intensity to the B800 peak and the 890 shoulder is of a lower intensity than the 807 peak.

In figure 3.2, the effects on the light-harvesting complexes produced by *Alc. vinosum* grown in the presence of thiosulphate under different light intensities and temperatures are shown. When *Alc. vinosum* is cultured under low light, 30℃ growth conditions (LL30, pink) the NIR absorption peaks of the LH2 B800 BChl and LH1/RC "core" produced centre at 807 nm and 890 ± 0.5 nm respectively, while the LH2 "B850-like" BChl peak is obscured as a shoulder at ~ 818 nm. Both the LH1/RC "core" and the "B850-like" peak are of a lower intensity relative to the B800 peak. This relationship between the B800 peak and those of the "B850-like" and LH1/RC "core" is observed in membranes from cells grown in all thiosulphate growth conditions bar those grown in high light at 40℃. When *Alc. vinosum* cells are cultured in low light intensity at 40℃ (LL40, purple) the "B850-like" BChl peak centres at 846 ± 0.5 nm, and a LH1/RC "core" is slightly blue-shifted to 888 ± 0.5 from where it has been observed in membranes from other conditions. In membranes from cells cultured under high light 30℃ (HL30, red) growth conditions the "B850-like"and LH1/RC "core" peaks centre at 849 ± 0.5 nm and 889 ± 0.5 nm respectively. The membranes from cells grown in high light intensity at 40℃ (THL40, dark red) produce the most red-shifted "B850-like" peak of all the LH2 complex types, which centres at 857 ± 0.5 nm and is at a higher intensity than that of the 807 nm peak. The LH1/RC "core" peak is positioned at 890 ± 0.5 nm and is also of a higher intensity relative to the 807 nm peak.

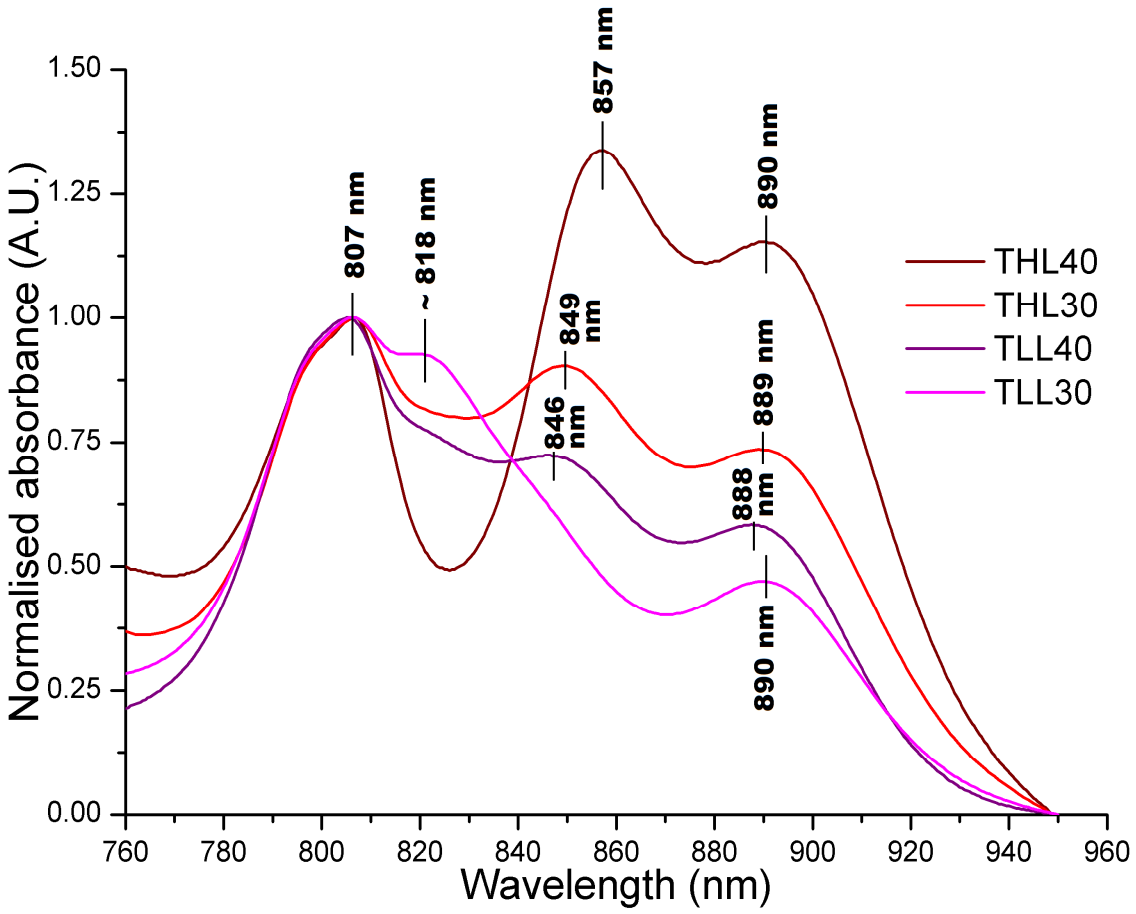

Figure 3.2 Room temperature NIR absorption spectra of *Alc. vinosum* membranes from cells grown in the presence of thiosulphate (T) under different growth conditions (HL: High light, LL: Low light, 30℃ or 40℃).
Membranes from *Alc. vinosum* grown under THL40 (dark red) growth conditions produce three peaks in the NIR at 807 ± 0.5 nm, 857 ± 0.5 nm, and 890 ± 0.5 nm. The 857 nm peak and 890 peaks are of a higher intensity than the 807 peak. Membranes from *Alc. vinosum* grown under THL30 (red) growth conditions produce two peaks in the NIR at 807 ± 0.5 nm, 849 ± 0.5 nm, and a shoulder at 889 ± 0.5 nm. The 849 nm peak and the 889 nm shoulder are of a lower intensity than the 807 peak. Membranes from *Alc. vinosum* grown under TLL40 (purple) growth conditions produce two peaks in the NIR at 807 ± 0.5 nm, 846 ± 0.5 nm and a shoulder at 888 ± 0.5 nm. The 846 nm peak and 888 shoulder are of a higher intensity than the 807 peak. Membranes from *Alc. vinosum* grown under TLL30 (pink) growth conditions produce two peaks in the NIR at 807 ± 0.5 nm and 890 ± 0.5 nm with a shoulder at ~818 ± 0.5 nm. The ~ 818 nm shoulder and 890 peak are of a lower intensity than the 807 peak.

In summary, the B800 BChl present as a broad peak with an apex at 807 nm throughout all growth conditions, and the absorption peak associated with the LH1/RC "core" shows low variation, centring at 889 ± 1 nm in membranes produced under all growth conditions. As the temperature or light intensity of the growth conditions is increased, regardless of sulphur source, a red shift of the middle of the three peaks in the NIR, associated with the excitonically coupled "B850-like" BChl of the LH2 complex, is observed. The "B850-like" peak red-shifts from ~818 nm (TLL30), to 822 ± 0.5 nm (SLL30), 846 ± 0.5 nm (TLL40), 849 nm ± 0.5 (THL30), 853 ± 0.5 nm (SLL40 and SHL30), with the highest values

at 856-857 ± 0.5 nm (THL40 and SHL40). This would imply a high level of variation in the LH2 complex types produced, specifically in the binding of the excitonically coupled BChl within the LH2 complex types.

3.2.2 Low temperature (77 K) absorption spectra of the membranes from *Alc. vinosum* grown under different growth conditions

Reducing the temperature at which absorption spectra are recorded narrows and red-shifts some of the absorption bands observed, which improves the resolution of peaks in cases where several peaks overlap. Samples were sent to our collaborator, Darek Niedzwiedzki at Washington University, to record steady state low temperature absorption spectra, at 77 K, of the membranes from various growth conditions in order to obtain higher resolution spectra (Figures 3.3 and 3.4). Low temperature absorption spectra were only acquired for membranes from *Alc. vinosum* cells grown under high light 40℃, high light 30℃, and low light 30℃ growth conditions as at the time of low temperature absorption acquisition the set up for low light 40℃ growth conditions had not been developed.

Figure 3.3 shows the low temperature absorption spectra of membranes prepared from cells grown under different growth conditions in the presence of sulphide. The narrowing of the absorption bands that occurs at low temperatures allows us to distinguish the split B800 peaks present at ~ 800 nm, centred at 797 nm and the other at 808 nm. These peak positions are the same for membranes produced under all growth conditions and the 808 nm peak is always of a higher intensity than the 797 nm peak. In membranes from SLL30 (Figure 3.3 cyan) growth conditions the “B850-like” maximum observed centres at 822 nm and produces a shoulder at ~860 nm that was not visible in the absorption spectrum measured at room temperature. The LH1/RC “Core” peak centres at 909 nm. Membranes from SHL30 (Figure 3.3 green) growth conditions produce a “B850-like” maximum at 876 nm and the LH1/RC “core” peak at 908-909 nm. Both of these maxima are of a lower intensity relative to the B800 peaks. A small shoulder is observed at ~ 822 nm in membranes from SHL30 conditions that may correspond to another “B850-like” population implying a mix of LH2 complex types. The NIR absorption spectrum of membranes produced under SHL40 (Figure

3.3 dotted line) conditions show the 797 nm and 808 nm peaks are of a lower intensity relative to the "B850-like" peak at 871 nm and the LH1/RC "Core peak at 909 nm.

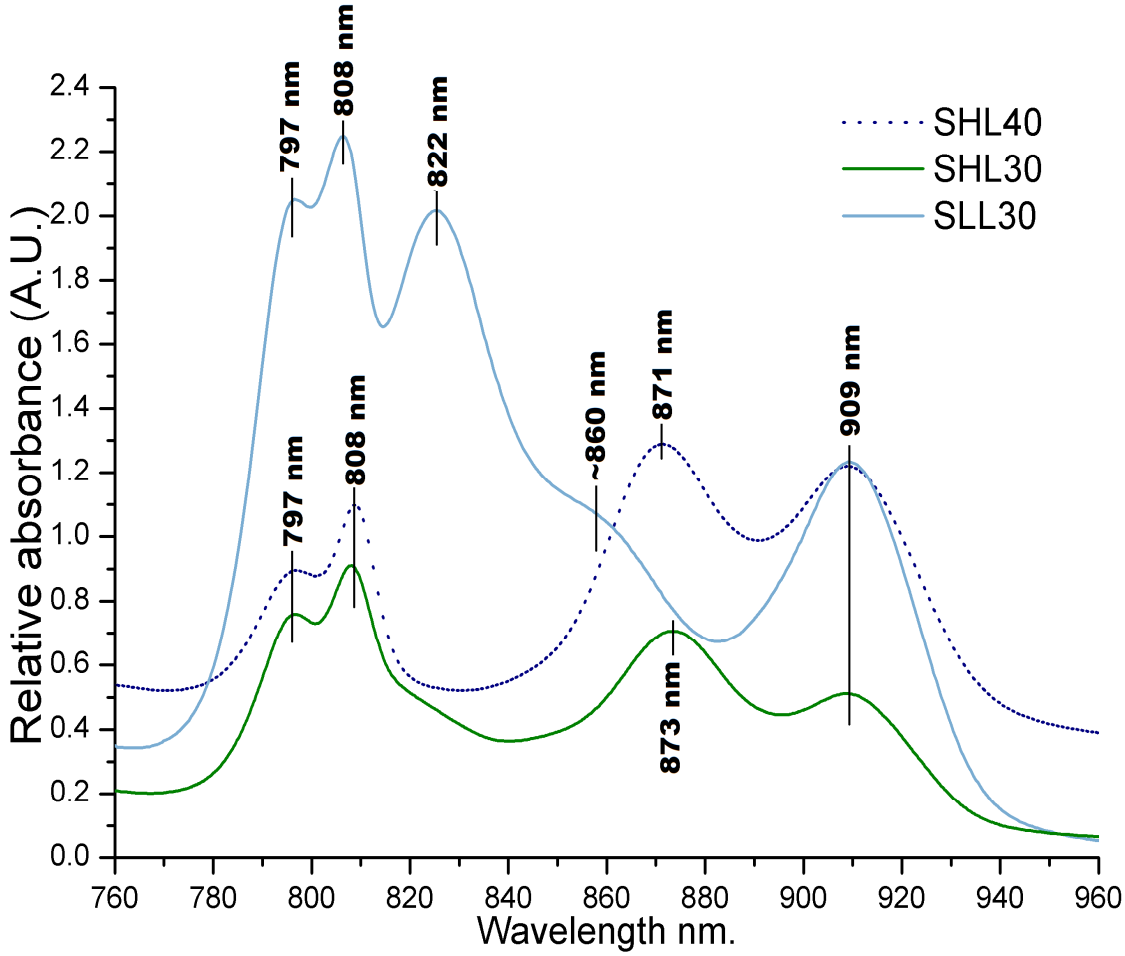

Figure 3.3 Low temperature (77 K) NIR absorption spectra of *Alc. vinosum* membranes from cells grown in the presence of sulphide (S) under different growth conditions (HL: High light, LL: Low light, 30℃ or 40℃).
Membranes from *Alc. vinosum* grown under SHL40 (dotted line) growth conditions produce three peaks in the NIR at 797 nm, 808 nm, 871 nm and 909 nm. The highest intensity peaks are the 871 nm and 909 nm peaks, followed by the 808 nm peak. The 797 nm peak is of the lowest intensity. Membranes from *Alc. vinosum* grown under SHL30 (green) growth conditions produce two peaks in the NIR at 797 nm, 808 nm, 873 nm, and 908 nm. The highest intensity peak is the 808 nm peak, followed by the 797 nm peak. The 873 nm peak and 908 nm peak are of the lowest intensity. Membranes from *Alc. vinosum* grown under SLL30 (cyan) growth conditions produce peaks in the NIR at 797 nm, 808 nm, 822 nm and 909 nm with a shoulder at ~860 nm. The 808 nm peak is the highest intensity followed by the 797 nm and 822 nm peaks. The 909 nm peak is the lowest intensity of all the peaks.

Figure 3.4 shows the low temperature NIR absorption spectra of membranes prepared from *Alc. vinosum* cells grown in the presence of thiosulphate under different growth conditions. As observed in membranes prepared from cells grown in the presence of sulphide, the two absorption bands present at ~ 800 nm are distinguishable from each other at 77 K, and under all conditions the 808 nm

peak is of a higher intensity than the 797 nm peak. In membranes produced under TLL30 (Figure 3.4 pink) growth conditions the split B800 peaks are of a higher intensity than all other peaks present. The “B850-like” peak that presents as a shoulder in room temperature spectra at ~818 nm is observed here as a distinct, red-shifted peak at 823 nm. In TLL30 membranes, the shoulder at 852 nm is more distinct than the one observed in SLL30 membranes. The LH1/RC “core” maximum centres at 908-908 nm. In THL30 growth conditions (Figure 3.4 red) the B800 peaks are of a slightly higher intensity relative to the other peaks present. In HL30 conditions there is a small shoulder at ~ 825 nm, and a distinct peak at 866 nm, potentially relating to two different populations of “B850-like” BChl and thus two LH2 complex types present. The LH1/RC “core” absorption peak centres at 908 nm and relates to the LH1/RC “core”. Under HL40 growth conditions (Figure 3.4 dark red) the “B850-like” peak centres at 870 nm and the LH1/RC “Core” is positioned at 907 nm. These are the are the only conditions to produce higher intensity “B850-like” and LH1/RC “core” peaks relative to the 808 nm peak. Additionally, the 797 nm band produces a shoulder instead of a distinct peak.

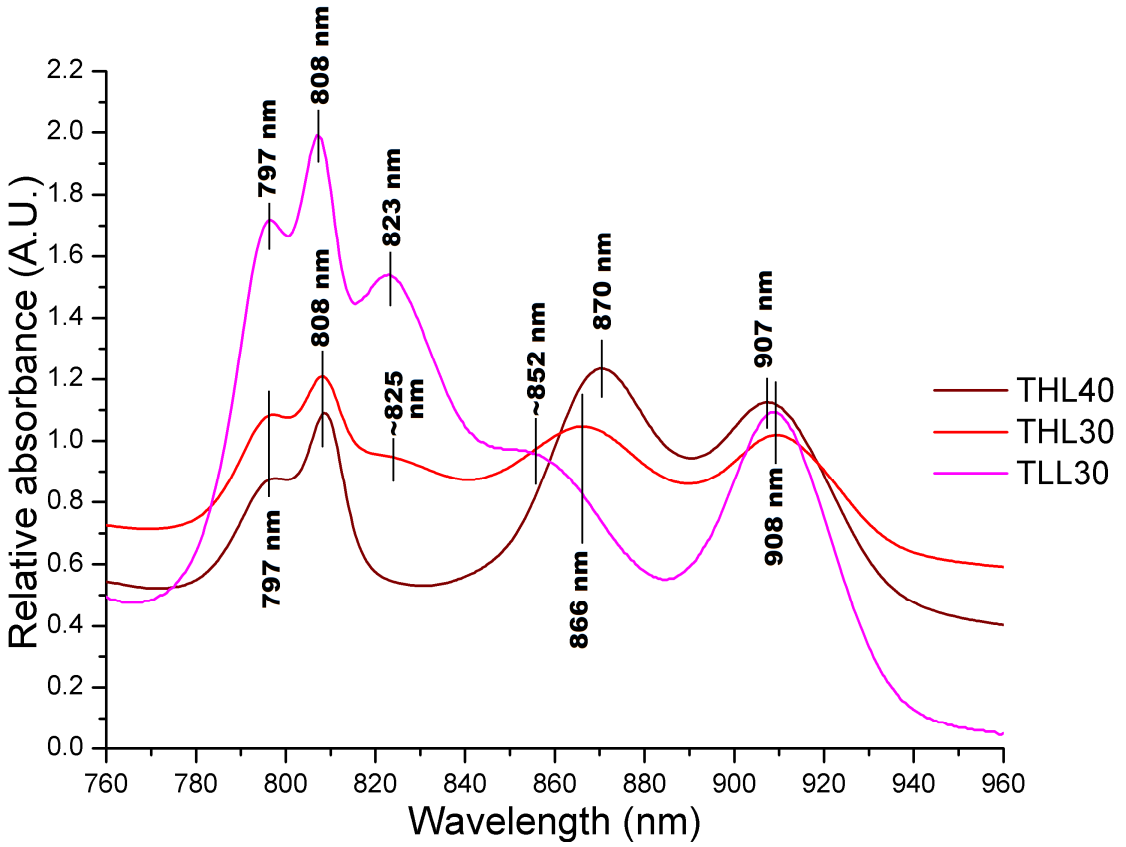

Figure 3.4 Low temperature (77 K) NIR absorption spectra of *Alc. vinosum* membranes from cells grown in the presence of thiosulphate (T) under different growth conditions (HL: High light, LL: Low light, 30 ℃ or 40 ℃).
Membranes from *Alc. vinosum* grown under THL40 (dark red) growth conditions produce three peaks in the NIR at 797 nm, 808 nm, 870 nm and 907 nm. The highest intensity peak is the 870 nm followed closely by the 808 nm and 907 nm peaks. The lowest intensity peak is the 797 nm peak. Membranes from *Alc. vinosum* grown under THL30 (red) growth conditions produce peaks in the NIR at 797nm, 808 nm, 866 nm, 908 nm, with a shoulder at ~825 nm. The highest intensity peak centres at 808 nm followed by the 797 nm peak. The peaks at 866 nm and 908 nm are of nearly equal intensity. Membranes from *Alc. vinosum* grown under TLL30 (pink) growth conditions produce peaks in the NIR at 797 nm, 808 nm, 823 nm, 908 nm, with a shoulder at ~ 852 nm. The highest intensity peak centres at 808 nm followed by the 797 nm and 823 nm peaks. The peak at 908 nm is of the lowest intensity with the exception of the shoulder at ~ 856 nm.

The values of the room temperature and low temperature NIR Qy maxima of the light-harvesting complexes contained within the photosynthetic membranes produced by *Alc. vinosum* under different growth conditions can be found in table 3.1. The values obtained at low temperature are in agreement with previous values observed at 77 K and 80 K of membranes from *Alc. vinosum* (146, 155). While the low temperature absorption spectra of the membranes resolved most peaks present, it did not resolve all peaks. The light-harvesting complexes must be extracted from the membranes and analysed individually to confirm peak identities and begin to identify LH2 complex types.

Table 3.1 Room temperature (RT) and 77 K (LT) wavelength values of Qy maxima produced by the light-harvesting complexes in membranes from *Alc. vinosum* cells cultured under different growth conditions.
Peaks that appear as a shoulder are defined by (sh). The growth conditions are defined as S: sulphide, T: thiosulphate, HL: High light, LL: Low light, 30℃ or 40℃.

	SLL30	SLL40	SHL30	SHL40	TLL30	TLL40	THL30	THL40
RT								
B800 peak (nm)	807	807	807	807	807	807	807	807
"B850-like"peak	822	853	853	856	818(sh)	846	849	857
LH1/RC "core" peak (nm)	890	888-890(sh)	888(sh)	888	890	888	889	890
LT								
B800 peaks (nm)	797 808		796 808	797 808	796-797 808		799 808	799(sh) 808
"B850-like" peaks (nm)	825 ~860(sh)		873	871	823 852(sh)		825(sh) 866	870
LH1/RC "Core" peak (nm)	909		908-909	909	908-909		908-909	907

3.2.3 **Detergent trials**

Typically, purple photosynthetic bacterial membranes have been solubilised in detergent to extract the light-harvesting machinery, LH1/RC "core" complex and LH2 complex types, which are then separated using sucrose density centrifugation gradients (SDCG) (113, 156). Sucrose density gradients are created through the layering of decreasing concentrations of sucrose solutions, in 20 mM Tris-HCl (pH 8.0), in the presence of the CMC of the chosen detergent, into a centrifugation tube onto which the solubilised complexes are aliquoted (as outlined in Methods and Materials section 2.4.1). As different detergents form different sized micelles, the overall density of the micelle-complex structure and therefore the separation of the complexes will vary depending on the detergent present.

Previous work on the light-harvesting machinery from purple photosynthetic bacteria has used detergents such as lauryldimethylamine oxide (LDAO) (101, 115, 140, 141), decyl maltoside (DM)(81) and ß-dodecyl maltoside (DDM) (113, 115). These detergents have different levels of efficacy when solubilising

complexes from membranes. Additionally, some detergents are harsher than others, e.g. LDAO is very effective solubilising agent however can cause degradation of complexes, while DM and DDM are less effective at solubilising membranes however they are less detrimental to the complexes.

Membranes from cells cultured in thiosulphate high light 40℃ growth conditions (as outlined in Methods and Materials sections 2.2 and 2.3) were used for solubilisation experiments. Membranes were solubilised and the absorption spectra of the solubilised material were recorded prior to loading on SDCG (as outlined in Methods and Materials section 2.4.1). Membranes solubilised with DM and LDAO produce slightly blue shifted peaks relative to the values observed in the membranes (Figure 3.5). After solubilisation in DM, the apex of the B800 peak blue-shifts from 807 nm to 804 nm, and the second peak of the split B800 becomes more prominent at 801 nm. The "B850-like" BChl peak, centred at 857 nm in the membranes, blue-shifts to 847 nm, while the LH1/RC "core" complex blue-shifts from 890 nm to 888 nm after DM solubilisation. The intensities of the 847 nm and the 888 nm peaks relative to the 804 nm peak are reduced moderately however both peaks are still of a higher intensity than the 804 nm peak after DM solubilisation. After LDAO solubilisation of the membranes, the wavelength shift of the split B800 peaks are the same as observed after DM solubilisation although the height of the split B800 peaks to each other is reversed as the 801 nm peak changes to a higher intensity than the 804 nm. The "B850-like" peak is reduced and blue-shifted from 857 nm to 840 nm and is of a lower intensity relative to the B800 peaks. The LH1/RC "core" peak is reduced, nearly completely, to a shoulder. This reduction of the "B850-like" peak in addition to the change in ratio between the 804 and 801 nm peaks implies some degradation of the LH2 complexes during LDAO solubilisation. Additionally, the near total loss of the LH1/RC "core" associated peak would indicate a dramatic loss of the LH1/RC "core" complex.

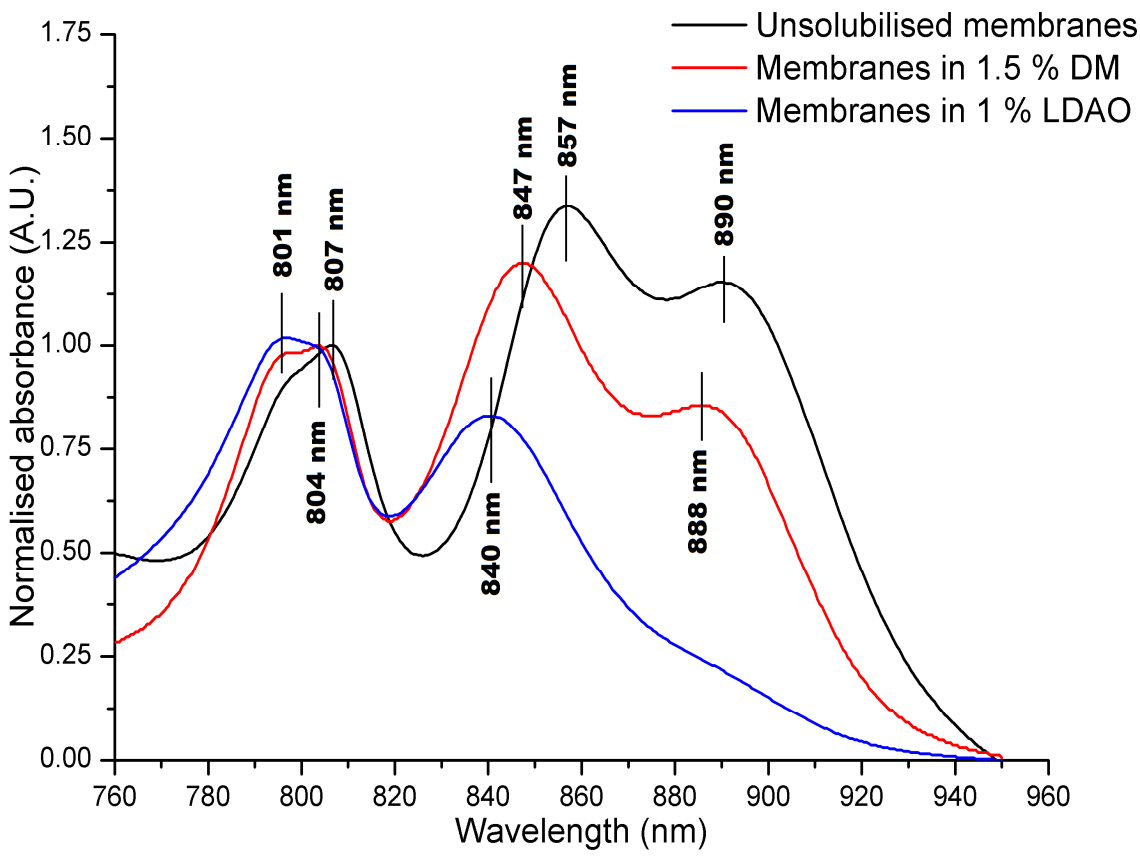

Figure 3.5 NIR absorption spectra of membranes from *Alc. vinosum* solubilised in 1.5 % DM (w/v) or 1 % LDAO (v/v).
The absorption peaks produced by the unsolubilised membranes in the NIR centre at 807 nm, 857 nm, and 890 nm. After solubilisation in LDAO for 30 min the absorption peaks in the NIR centre at 801 nm, 804 nm, and 840 nm. After solubilisation in DM for 30 min the absorption peaks in the NIR centre at 801 nm, 804 nm, 847 nm, and 888 nm. The absorption peaks observed after DM solubilisation are blue shifted from their position in the membranes however the relative intensities of the peaks are unchanged. There is a reduction in the 890 nm peak after LDAO solubilisation and the 857 nm peak in the membranes blue shifts to 840 nm and is reduced in intensity to a lower level than the B800 peak.

Light-harvesting complexes from the solubilised membranes were then separated using SDCG in the presence of the CMC of the appropriate detergent (0.1 % LDAO (v/v) or 0.15 % DM (w/v)) (as outlined in Methods and Materials section 2.4.1). The top band on the SDCG consists of free pigment, and the second band is that of the crude LH2 fraction (Figure 3.6). The bottom band, which equilibrates into the highest density layer, is the LH1/RC "core" complex. Both bands of the LH1/RC "Core" complex and the LH2 complex types are visibly present in the SDCG after DM solubilisation, albeit with poor separation, while the LDAO trial shows a strong LH2 band with a negligible LH1/RC "core" band. This concurs with the observations from the post-solubilisation absorption spectra that the LH1/RC "core" complex is degraded during solubilisation with LDAO.

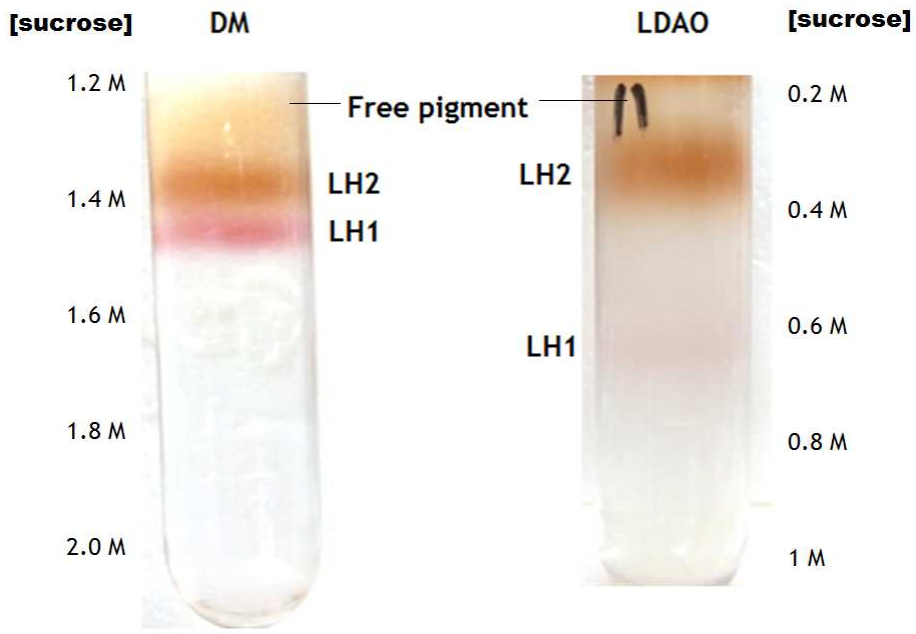

Figure 3.6 The LH1/RC "core" and LH2 complexes from *Alc. vinosum* solubilised in either LDAO or DM and separated by sucrose density centrifugation.
After solubilisation in DM and separation by SDCG the pink LH1/RC "core" band equilibrated to ~ 1.6 M sucrose and the red LH2 complex band equilibrated to ~ 1.4 M sucrose. The level of separation was very poor however both bands were clearly observable. After solubilisation in LDAO and separation by SDCG the faint pink LH1/RC "core" band equilibrated to ~ 0.6 M sucrose and the red LH2 complex band equilibrated to 0.4 M sucrose. The level of separation was very good although the LH1/RC "core" band was very faint, suggesting the LH1/RC "core" complex had degraded in the presence of LDAO.

The deleterious effects of LDAO on the peaks of both the LH2 and LH1/RC "core" complexes rule it out as a detergent for solubilisation. Solubilisation with DM changes the position of the LH2 and LH1/RC "core" maxima and the ratio of the B800:B850 becomes closer to 1:1 than observed in the membranes. To further examine the changes in spectra due to DM, a longer solubilisation (1 hour) (as outlined in Methods and materials section 2.5.2) was repeated on fresh membranes using DM and the spectra of the SDCG crude fractions recorded and compared to unsolubilised membranes (Figure 3.7). The peak position recorded of the LH1/RC "core" complex was unchanged at 890 nm (Figure 3.7 red) however the NIR absorption maxima of the crude LH2 complex fraction (Figure 3.7 blue) was blue-shifted from the values seen in the membrane bound complexes and the solubilised chromatophores to 804 nm and 842 nm. This difference in the maxima between the post-solubilisation and post-SDCG fractions may be due the presence of a mix of both detergent-micelles and mixed phospholipid-detergent micelles straight after solubilisation.

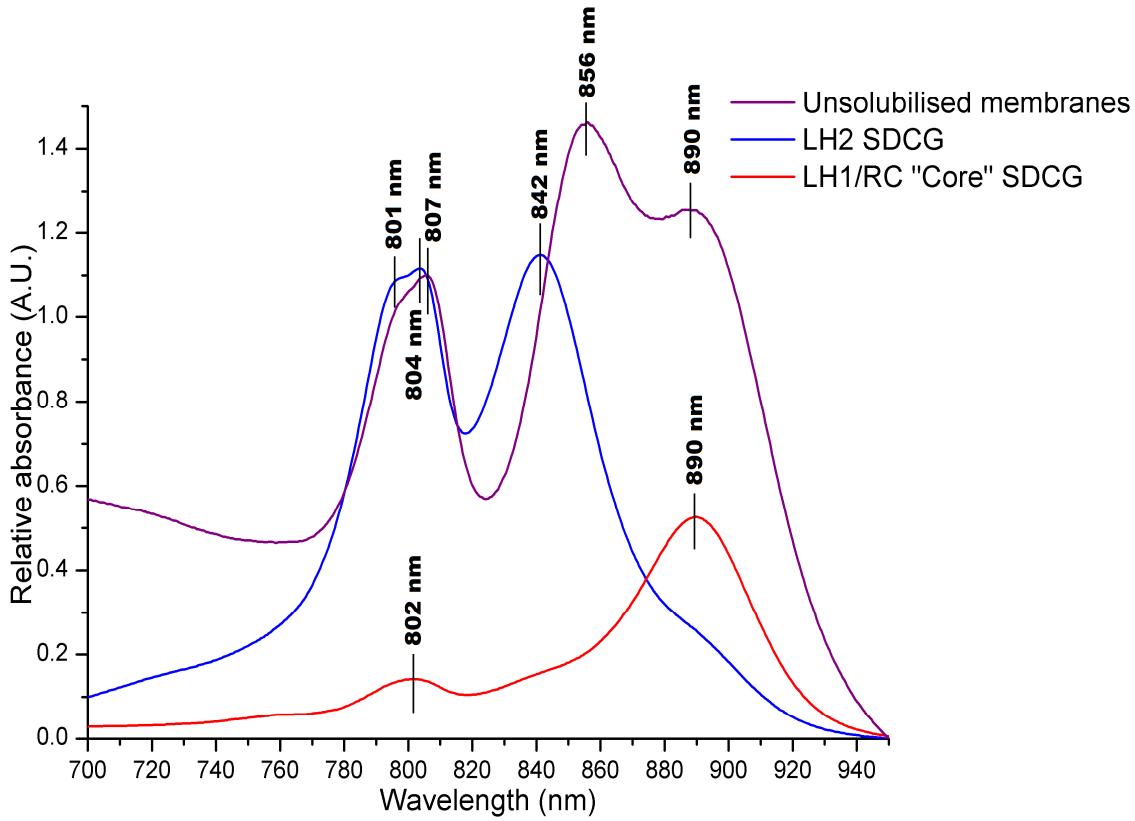

Figure 3.7 NIR absorption spectra of *Alc. vinosum* membranes and sucrose density centrifugation gradient fractions of LH2 and LH1/RC "Core" complexes solubilised in 1.5 % DM (w/v).
The Qy maxima observed from the unsolubilised membranes (purple) centre at 807 nm, 856 nm, and 890 nm. The Qy maxima observed from the crude LH2 fraction (blue) centre at 804 nm, 842 nm and 890 nm. The Qy peaks from the LH2 fraction are of nearly equal intensities. The Qy maxima from the LH1/RC "core" complex fraction (red) centre at 890 nm and 802 nm.

DDM was tested as an alternative to DM as it is a similar detergent but contains a longer hydrocarbon chain. Membranes prepared from cells grown in thiosulphate at 40 °C in high light (as described in methods and materials section 2.2 and 2.3) were solubilised in a concentration of ten times the CMC of DDM (2 % (w/v)) and loaded onto SDCGs in the presence of DDM at the CMC (0.02 % (w/v)) gradients (as described in methods and materials section 2.5.1). DDM solubilisation was sufficient to extract the light-harvesting machinery from the membranes, and the separation observed in the SDCG of the LH1/RC "core" complex and the LH2 complexes types was more pronounced than that of the SDCG in DM. The Qy maxima observed after separation show a blue-shift of the peaks associated with the LH2 complex types present in the membranes (Figure 3.8 blue). The 808 nm peak blue-shifts to 803 nm and the other B800 peak presents at 796 nm, while the B850 peak blue-shifts to 848 nm from the membrane bound position of 856 nm. The LH1/RC "core" peak at 890 nm does not change at all in DDM (Figure

3.8 red). The ratio of the intensity of the B800 peaks to the “B850-like” in 0.02 % (w/v) DDM is more representative of the peaks seen in the membranes than LH2 complexes in the presence of DM (0.15 % (w/v)). The improved separation of the fractions of the LH1/RC “core” and LH2 complexes, reduced blue-shift and the good B800:B850 peak ratio makes DDM a preferable detergent for characterisation of the LH2 complex types. A draw back to the use of DDM is that it cannot be dialysed out or detergent exchanged, therefore DM should be used if a downstream process requires the subsequent removal of a detergent.

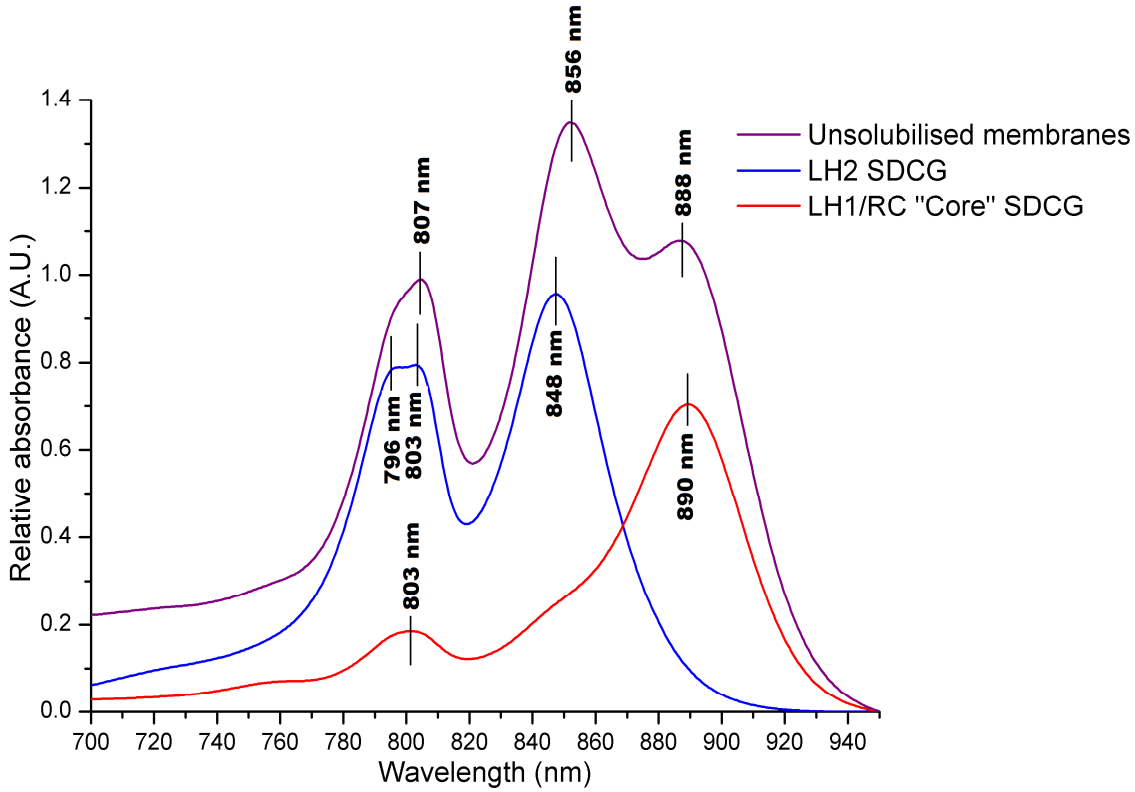

Figure 3.8 NIR absorption spectra of *Alc. vinosum* membranes and sucrose density centrifugation gradient fractions of LH2 and LH1/RC “Core” complexes solubilised in 2 % DDM (w/v).
The Qy maxima observed from the unsolubilised membranes (purple) centred at 807 nm, 856 nm, and 890 nm. The Qy maxima observed from the crude LH2 fraction (blue) centre at 803 nm, 796 nm and 848 nm. The Qy maxima from the LH1/RC “core” complex fraction (red) centre at 890 nm and 803 nm. The longest wavelength Qy absorption peak in the LH2 fraction is of a higher intensity than the B800 peak.

3.2.4 **Sucrose Density Centrifugation Step Gradient optimisation**

After membrane solubilisation, the light-harvesting complexes are separated from each other using SDCG (as described in methods and materials section 2.4.2). The sucrose density gradient used to separate the LH1/RC “Core” complex from the LH2 complex types solubilised in DDM required optimisation to

attain the best separation possible for this detergent. Membranes from *Alc. vinosum* cells grown under thiosulphate, high light 40 ºC growth conditions and prepared as per Methods and Materials sections 2.2 and 2.3 were used to optimize the SDC gradients used. The initial protocol was for sucrose concentration steps of 0.6 M, 0.8 M, 1.0 M and 1.2 M at volumes of 5.5 ml, 6 ml, 6 ml, and 5.5 ml respectively (113), with 2 ml solubilised membranes layered on top of this gradient at an OD_{856} of 50. The LH1/RC "Core" complex reached equilibrium at approximately ~ 1.0 M sucrose, while the LH2 equilibrated in the concentration directly above it at ~ 0.8 M sucrose. The standard protocol produced overloaded gradients with poor separation of the LH1/RC "Core" band from the LH2 complex band, so these were repeated with the lower volume of 1 ml solubilised light-harvesting complexes at OD_{856} of 25 added (Figure 3.9 A). Further adaptations were to increase the volume of the sucrose concentrations that the complexes equilibrated into to improve the separation. Volumes were changed to 3 ml, 8 ml, 8 ml, and 3 ml of 0.6 M, 0.8 M, 1.0 M and 1.2 M respectively. These changes improved separation (Figure 3.9 B) however an additional band of 0.9 M sucrose was added to the step gradient to explore the possibility of improving the separation further. The new volumes used were 3 ml, 6 ml, 6 ml, 6 ml, and 3 ml of 1.2 M, 1.0 M, 0.9 M, 0.8 M, and 0.6 M respectively. The addition of 0.9 M sucrose did not affect the separation of the LH2 and LH1/RC "Core" as much as expected as the LH2 equilibrated to 0.9 M (Figure 3.9 C).

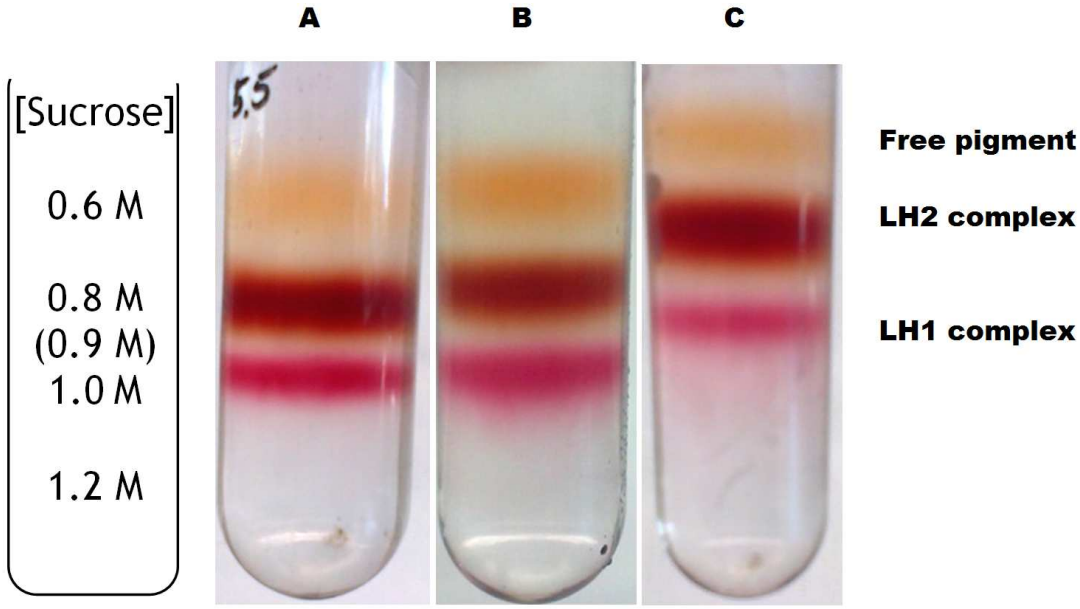

Figure 3.9 LH1/RC "core" and LH2 complexes from *Alc. vinosum* separated by sucrose density centrifugation.
Different volumes of each sucrose concentration were used to optimise the level of separation between the LH1/RC "core" and the LH2 complex types. Tube A consisted of 5.5 ml, 6 ml, 6 ml, and 5.5 ml of 1.2 M, 1.0 M, 0.8 M and 0.6 M, respectively, as had been used in previous work (113). Tube B consisted of 3 ml, 8 ml, 8 ml, and 3 ml of 1.2 M, 1.0 M, 0.8 M and 0.6 M, respectively. Tube C consisted of 2 ml, 6 ml, 6 ml, 6 ml, and 2 ml of 1.2 M, 1.0 M, 0.9 M, 0.8 M and 0.6 M, respectively. All sucrose density gradients resulted in two distinct bands with a diffuse band of free pigment. The LH1/RC "core" band consistently equilibrated to ~ 0.9-1.0 M sucrose, while the LH2 complex equilibrated to ~ 0.8 M sucrose. The separation between the LH1/RC "core" and LH2 band improved when the volumes of 0.8 M and 1.0 M sucrose were increased and was best when 0.9 M sucrose was used in the gradient.

3.3 Composition of LH2 crude extracts from cells grown under different growth conditions

Once the LH1/RC "core" complex and LH2 complexes were extracted from the membranes and separated from each other (As outlined in Methods and Materials section 2.5.1), the Qy peaks of the crude LH2 fractions were examined using room temperature absorption spectroscopy. The removal of the membranes reduced the level of light scattering, allowing the second set of pigments present, the carotenoids, to be observed (see Introduction section 2.2.1). The apparent mixed composition of carotenoids throughout all LH2 fractions makes spectroscopic analysis of the carotenoids impossible without extraction and individual isolation and analysis. For this reason, carotenoid peaks will be examined however analysis of the composition of the carotenoids will be carried out in Chapter four.

3.3.1 Room temperature absorption spectroscopy studies of crude LH2 fractions

As postulated from spectroscopic analysis of the membranes, under different growth conditions *Alc. vinosum* seems to produce a mix of LH2 complex types. It is observable in the crude LH2 extract from SDCG that under high light 40℃ growth conditions *Alc. vinosum* produces a near identical LH2 mix regardless of the sulphur source provided during growth (Figure 3.10). The maxima of which is observed at 798 nm, 803 nm and 848 ±1 nm for THL40 (Figure 3.10 dark red) and 849 ±1 nm for SHL40 (Figure 3.10 dark blue) growth conditions. The absorption bands of the carotenoids present can be observed and the complement of carotenoids present in the LH2 fractions from both thiosulphate and sulphide HL40 seem to be very similar. There is a single peak at 487.5 ±0.5 nm in the absorption spectrum of the extract from THL40 growth conditions, and 488 ±0.5 nm in the absorption spectrum of the extract from SHL40 growth conditions. The two absorption shoulders observed on either side of the main peak centre at ~ 461 ±1 nm and ~ 522 ±1 nm in SDCG from cells grown under high light at 40℃.

The LH1/RC "core" and LH2 from *Alc. vinosum* grown under both SHL40 and THL40 growth conditions equilibrate to the same concentrations in SDCG (Figure 3.10 inset). The LH1/RC "core" complex equilibrates to ~ 1.0 M sucrose and the LH2 equilibrates to ~ 0.8 M sucrose. There are similar levels of LH1/RC "core" to LH2 produced under both SHL40 and THL40 growth conditions. The LH1/RC "core" complex produced under SHL40 growth conditions appears to be deeper pink in colour but this is most probably a variation in the concentration of solubilised light-harvesting complexes loaded onto the sucrose gradient.

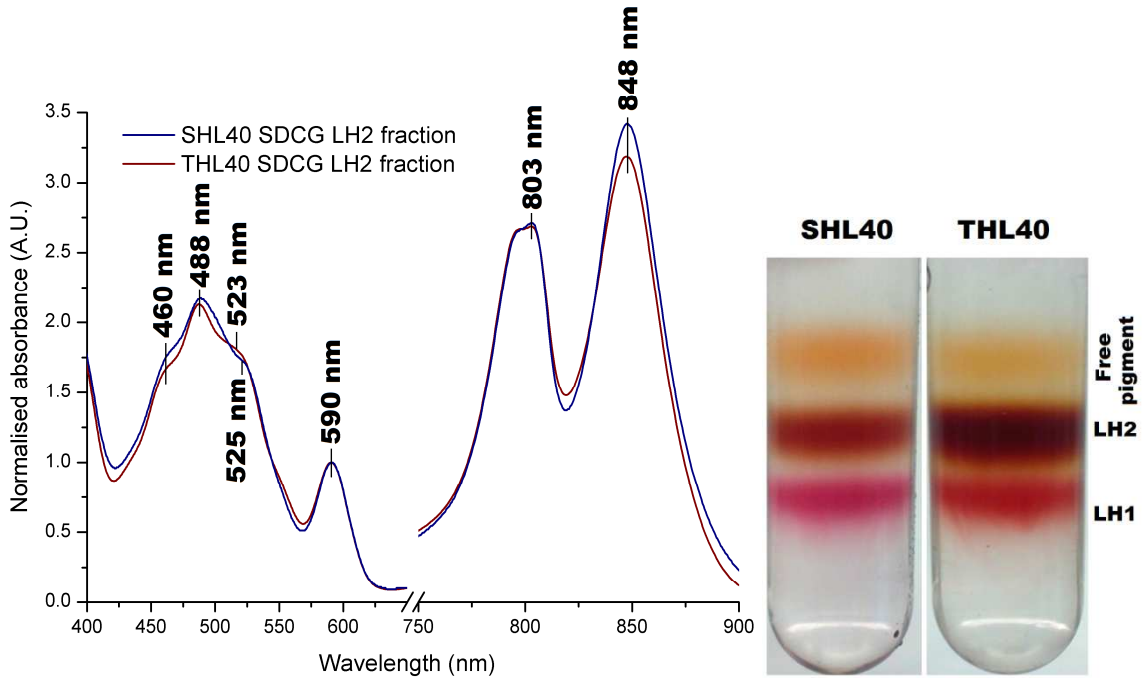

Figure 3.10 Absorption spectra of the crude LH2 fraction in 0.02 % DDM from sucrose density centrifugation (SDC), extracted from *Alc. vinosum* grown in the presence of thiosulphate (T) or sulphide (S), under high light (HL), 40 ℃ growth conditions.
The LH2 fraction produced under SHL40 (Blue) growth conditions produces peaks at 488 ± 0.5 nm, 590 nm, 798 nm, 803 nm, and 849 ± 1 nm with two shoulders at ~460 ± 1 nm and ~525 ± 1 nm. The LH2 fraction produced under THL40 (red) growth conditions produces peaks at 487 ± 0.5 nm, 590 nm, 798 nm, 803 nm, and 848 ± 1 nm with two shoulders at ~460 ± 1 nm and ~523 ± 1 nm. Insert shows LH1/RC "core" and LH2 complexes produced under SHL40 and THL40 growth conditions separated on a sucrose density centrifugation gradient consisting of 0.6 M, 0.8 M, 1.0 M, and 1.2 M sucrose, in 20 mM Tris-HCl, pH 8.0, in volumes of 3 ml, 8 ml, 8 ml, and 3 ml respectively. The LH1/RC "core" complex equilibrated to ~ 1.0 M and the LH2 complex equilibrated to ~ 0.8 M sucrose. Free pigment present in the sucrose density gradient equilibrated aboved the LH2 band at ~ 0.6 M sucrose.

The sulphur source produces a negligible effect on the mix of LH2 complex types produced under low light 30 ℃ growth conditions (Figure 3.11) showing a single broad, maximum at 802 nm with a shoulder at ~ 820 nm in the absorption spectra. Interestingly the Qx peaks seem to be broader in these fractions than the Qx peaks observed in the absorption spectra from the LH2 fraction extracted from HL40 growth conditions. The carotenoid peaks present in low light LH2 fractions produced in the presence of thiosulphate produce an absorption peak at 488.5 ±1 nm, with a shoulder at ~ 460 ±1 nm and a higher intensity, broader shoulder at ~ 518 ±3 nm than that observed in the HL40 fractions. This possibly relates to a larger fraction of carotenoids with longer conjugated double bond systems. In cells grown is the presence of sulphide small differences are observed in the carotenoid peaks as they centre at 489 ±1, ~462 ±1 nm, and ~ 525 ±1 nm.

The LH1/RC "core" and LH2 from *Alc. vinosum* grown under both SLL30 and TLL30 growth conditions equilibrate to the same concentrations in SDCG (Figure 3.11 inset). The LH1/RC "core" complex equilibrates to ~ 1.0 M sucrose and the LH2 equilibrates to ~ 0.8 M sucrose. There are similar levels of LH1/RC "core" to LH2 produced under both SLL30 and TLL30 growth conditions.

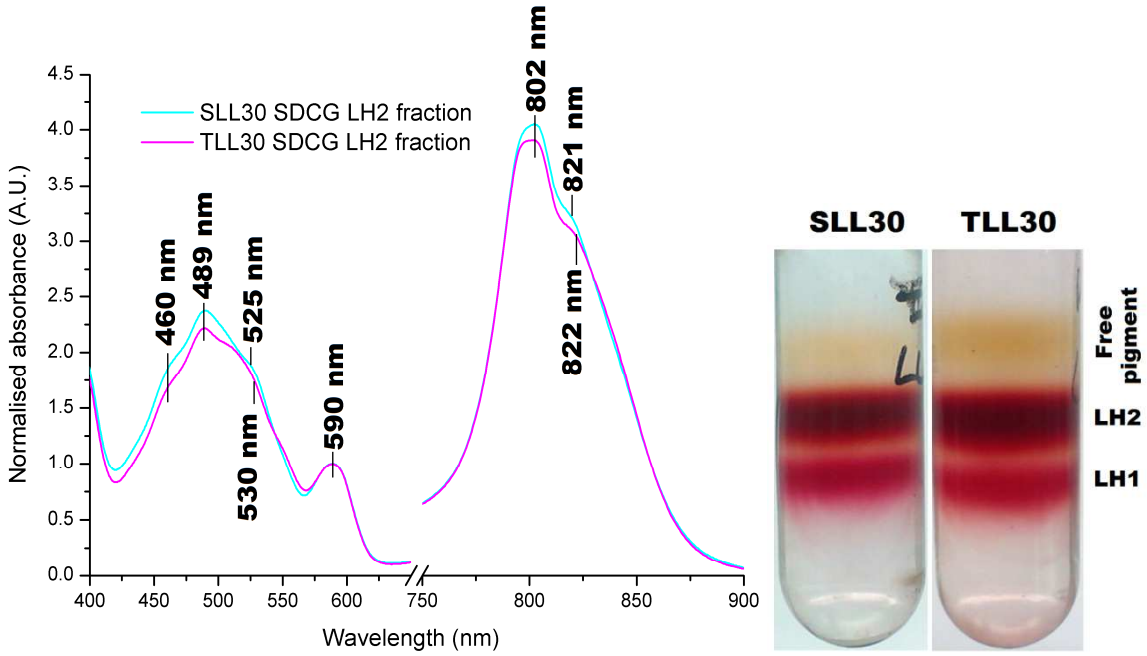

Figure 3.11 Absorption spectra of the crude LH2 fraction in 0.02 % DDM from sucrose density centrifugation (SDC), extracted from *Alc. vinosum* grown in the presence of thiosulphate (T) or sulphide (S), under low light (LL), 30℃ growth conditions.
The LH2 fraction produced under SLL30(cyan) growth conditions produces peaks at 489 ± 1 nm, 590 nm, 802 nm, and three shoulders at ~ 822 nm, ~460 ± 1 nm, and ~525 ± 1 nm. The LH2 fraction produced under TLL30 (pink) growth conditions produces peaks at 489 ± 1 nm, 590 nm, 802 nm, and three shoulders at ~821 nm, ~460 ± 1 nm and ~530 ± 1 nm. Insert shows LH1/RC "core" and LH2 complexes produced under SLL30 and TLL30 growth conditions separated on a sucrose density centrifugation gradient consisting of 0.6 M, 0.8 M, 1.0 M, and 1.2 M sucrose, in 20 mM Tris-HCl, pH 8.0, in volumes of 3 ml, 8 ml, 8 ml, and 3 ml respectively. The LH1/RC "core" complex equilibrated to ~ 1.0 M and the LH2 complex equilibrated to ~ 0.8 M sucrose. Free pigment present in the sucrose density gradient equilibrated aboved the LH2 band at ~ 0.6 M sucrose.

There is variation observed in the absorption spectra of the LH2 fractions produced by *Alc. vinosum* grown under high light 30℃ growth conditions in the presence of different sulphur sources. The B800 peaks appear as a plateau between 798 nm and 803 nm when cells have been cultured in the presence of both sulphide or thiosulphate however there is a ~ 7 nm difference between the "B850-like" peaks produced (Figure 3.12). The "B850-like" maximum observed after culturing cells in sulphide centres at 848 ± 1 nm (Figure 3.12 red) while cells cultured in thiosulphate produce a crude LH2 fraction with a maximum at

841 ± 2 nm (Figure 3.12 green). The carotenoid peaks centre at 487.5 ±0.5 nm (THL30) or 488 (SHL30), ~460 ±1 nm (THL30) or 461 ±1 nm (SHL30), and ~ 521 ±1 nm (THL30) or ~ 520.5 ±0.5 nm (SHL30) with the LH2 fraction from sulphide grown cells producing a slightly more distinct absorption shoulder at ~ 520 nm.

The LH1/RC "core" and LH2 from *Alc. vinosum* grown under both SHL30 and THL30 growth conditions equilibrate to the same concentrations in SDCG (Figure 3.12 inset). The LH1/RC "core" complex equilibrates to ~ 1.0 M sucrose and the LH2 equilibrates to ~ 0.8 M sucrose. There are similar levels of LH1/RC "core" to LH2 produced under both SHL30 and THL30 growth conditions.

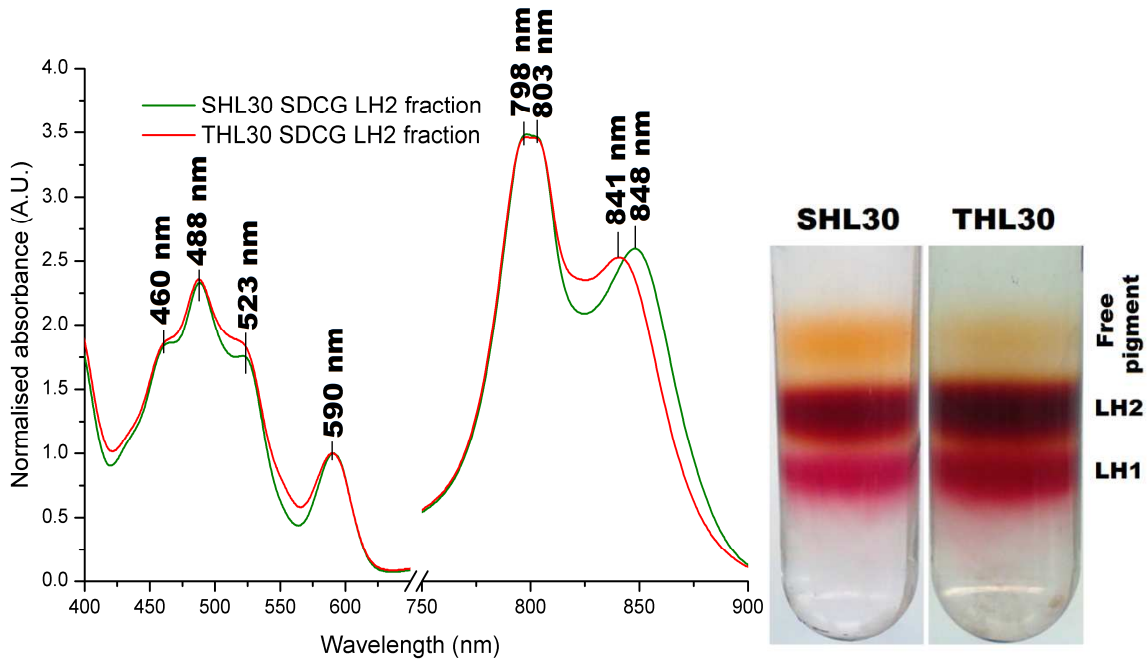

Figure 3.12 Absorption spectra of the crude LH2 fraction in 0.02 % DDM from sucrose density centrifugation (SDC), extracted from *Alc. vinosum* grown in the presence of thiosulphate (T) or sulphide (S), under high light (HL), 30 ℃ growth conditions.
The LH2 fraction produced under SHL30 (green) growth conditions produces peaks at 488 ± 0.5 nm, 590 nm, 798 nm, 803 nm, and 848 ± 1 nm, and two shoulders at ~460 ± 1 nm, and ~523 ± 1 nm. The LH2 fraction produced under THL30 (red) growth conditions produces peaks at 488 ± 0.5 nm, 590 nm, 798 nm, 803 nm, and 841 ± 1 nm, with two shoulders at ~460 ± 1 nm and ~523 ± 1 nm. Insert shows LH1/RC "core" and LH2 complexes produced under SLL30 and TLL30 growth conditions separated on a sucrose density centrifugation gradient consisting of 0.6 M, 0.8 M, 1.0 M, and 1.2 M sucrose, in 20 mM Tris-HCl, pH 8.0, in volumes of 3 ml, 8 ml, 8 ml, and 3 ml respectively. The LH1/RC "core" complex equilibrated to ~ 1.0 M and the LH2 complex equilibrated to ~ 0.8 M sucrose. Free pigment present in the sucrose density gradient equilibrated aboved the LH2 band at ~ 0.6 M sucrose.

A difference in LH2 complement is observed when *Alc. vinosum* is cultured under low light 40 ℃ growth conditions depending on the sulphur source present during growth (Figure 3.13). When grown in the presence of sulphide the Qy maxima

are positioned at 797 nm, 802 nm, and 847.5 ± 0.5 nm (Figure 3.13 blue), while cells grown in the presence of thiosulphate only produce distinct peaks for the split B800 BChl and a large shoulder at ~ 844 nm (Figure 3.13 dark red). The carotenoid peaks observed are similar between fractions produced in the presence of thiosulphate or sulphide, with the primary peak centring at 489.5 ±0.5 nm (SLL40) or 488.5 (TLL40). The absorbance shoulders produced by the SDCG produced under these growth conditions centre at approximately ~ 462 ±1 nm (SLL40) or 460 (TLL40) and 524.5 ±1 nm (SLL40) or ~510 nm (TLL40). The ~ 510 nm absorption shoulder is broader and of a higher intensity from the LH2 fraction produced under TLL40 conditions than the 524.5 nm peak observed from the SLL40 growth conditions fraction.

The LH1/RC "core" and LH2 from *Alc. vinosum* grown under both SLL40 and TLL40 growth conditions equilibrate to the same concentrations in SDCG (Figure 3.13 inset). The LH1/RC "core" complex equilibrates to ~ 1.0 M sucrose and the LH2 equilibrates to ~ 0.8 M sucrose. There are similar levels of LH1/RC "core" to LH2 produced under both SLL40 and TLL40 growth conditions.

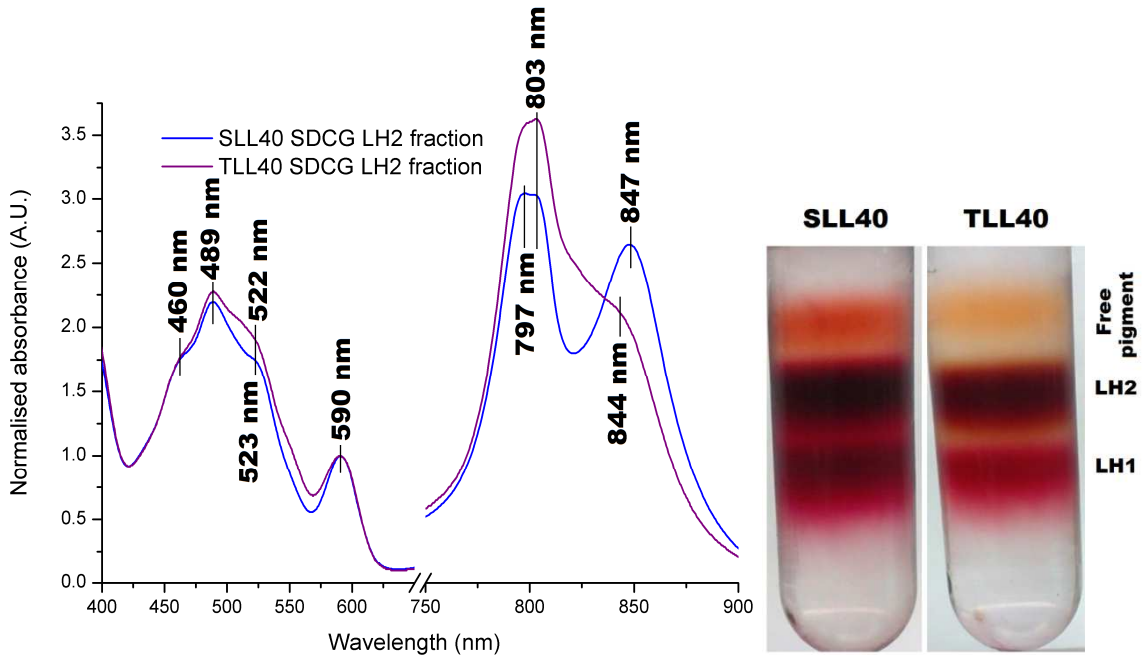

Figure 3.13 Absorption spectra of the crude LH2 fraction in 0.02 % DDM from sucrose density centrifugation (SDC), extracted from *Alc. vinosum* grown in the presence of thiosulphate (T) or sulphide (S), under low light (LL), 40℃ growth conditions.
The LH2 fraction produced under SLL40 (blue) growth conditions produces peaks at 489 ± 0.5 nm, 590 nm, 797 nm, 802 nm, and 847.5 ± 0.5 nm, and two shoulders at ~460 ± 1 nm, and ~523 ± 1 nm. The LH2 fraction produced under TLL40 (purple) growth conditions produces peaks at 489 ± 0.5 nm, 590 nm, 798 nm, 803 nm, and three shoulders at ~ 844 ± 0.5 nm, ~460 ± 1 nm and ~522 ± 1 nm. Insert shows LH1/RC "core" and LH2 complexes produced under SLL30 and TLL30 growth conditions separated on a sucrose density centrifugation gradient consisting of 0.6 M, 0.8 M, 1.0 M, and 1.2 M sucrose, in 20 mM Tris-HCl, pH 8.0, in volumes of 3 ml, 8 ml, 8 ml, and 3 ml respectively. The LH1/RC "core" complex equilibrated to ~ 1.0 M and the LH2 complex equilibrated to ~ 0.8 M sucrose. Free pigment present in the sucrose density gradient equilibrated aboved the LH2 band at ~ 0.6 M sucrose.

The absorption spectra observed for the LH2 extract from *Alc. vinosum* grown under sulphide LL40 growth conditions has more similarities to the LH2 extract from sulphide high light 30℃ growth conditions (Figure 3.14) than to the thiosulphate low light 40℃. The Qy peaks centre at the same wavelengths in both SDCG from SLL40 (847.5) and SHL30 (848) growth conditions. This may indicate the LH2 mix present is similar.

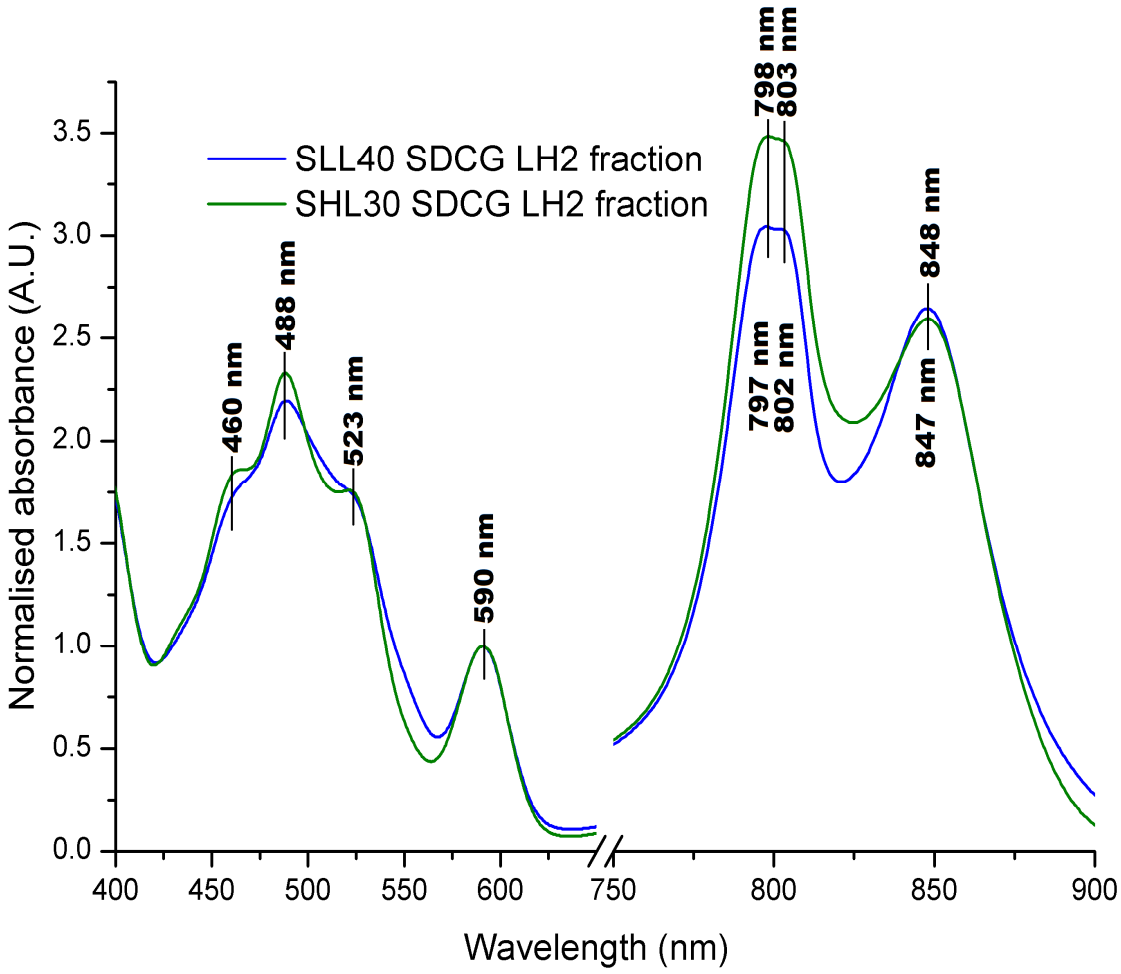

Figure 3.14 Absorption spectra of the crude LH2 fraction in 0.02 % DDM from sucrose density centrifugation (SDC), extracted from *Alc. vinosum* grown in the presence of thiosulphate (T) or sulphide (S), under low light (LL), 40 ℃ growth conditions.
The LH2 fraction produced under SLL40 (blue) growth conditions produces peaks at 489 ± 0.5 nm, 590 nm, 797 nm, 802 nm, and 847.5 ± 0.5 nm, and two shoulders at ~460 ± 1 nm, and ~523 ± 1 nm. The LH2 fraction produced under SHL30 (green) growth conditions produces peaks at 488 ± 0.5 nm, 590 nm, 798 nm, 803 nm, and 848 ± 0.5 nm, and two shoulders at ~460 ± 1 nm, and ~523 ± 1 nm. The LH2 fraction from cells grown under SHL30 growth conditions produce higher intensity B800 peaks than the LH2 fraction produced under SLL40 growth conditions. There is a small level of variation in the carotenoid peaks between the LH2 fractions produced under SLL40 and SHL30 growth conditions. The carotenoid peaks in the LH2 absorption spectrum from SLL40 growth conditions are less distinct but at the same wavelengths.

Cells grown under thiosulphate low light 40 ℃ growth conditions produced an LH2 fraction with an absorption spectrum more similar to cells cultured with thiosulphate at high light 30 ℃ (Figure 3.15) however with a lower peak at 840 nm.

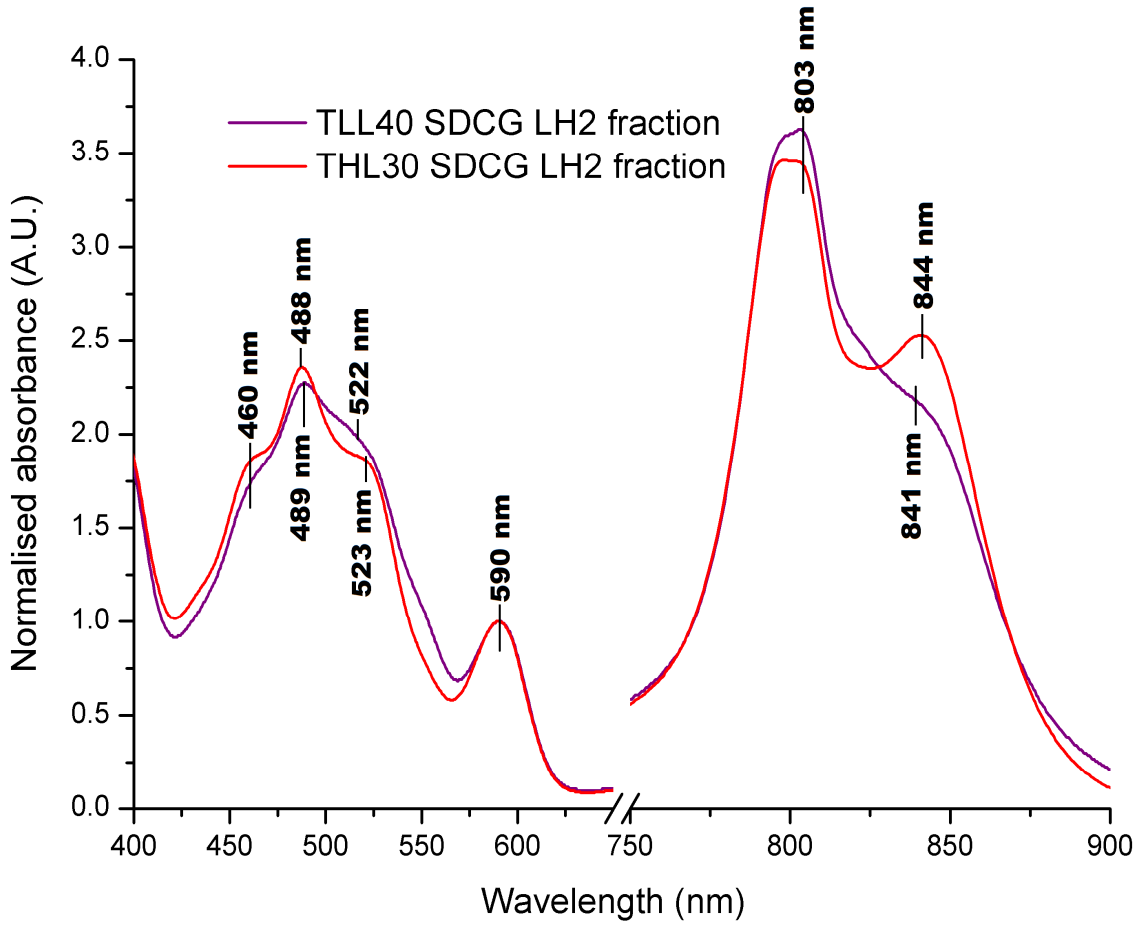

Figure 3.15 Absorption spectra of the crude LH2 fraction in 0.02 % DDM from sucrose density centrifugation (SDC), extracted from *Alc. vinosum* grown in the presence of thiosulphate (T) or sulphide (S), under low light (LL), 40 ℃ growth conditions.
The LH2 fraction produced under TLL40 (purple) growth conditions produces peaks at 489 ± 0.5 nm, 590 nm, 798 nm, 803 nm, and three shoulders at ~ 844 ± 0.5 nm, ~460 ± 1 nm and ~522 ± 1 nm. The LH2 fraction produced under THL30 (red) growth conditions produces peaks at 488 ± 0.5 nm, 590 nm, 798 nm, 803 nm, and 841 ± 0.5 nm, with two shoulders at ~460 ± 1 nm and ~523 ± 1 nm. The LH2 fractions from both TLL40 and THL30 growth conditions produce B800 peaks of similar intensity. While the 841 nm peak is a defined peak in the LH2 fraction from THL30 growth conditions it is an absorption shoulder in the LH2 fraction from TLL40 growth conditions.

3.3.2 Low temperature absorption spectroscopy studies of crude LH2 fractions

The room temperature absorption spectra produced from the crude extracts imply a mix of several different peaks producing a cumulative spectrum. With the assistance of Darek Niedzwiedzki, absorbance at 77 K was measured for sucrose gradient crude fractions, narrowing all the absorption peaks and blue-shifting peaks produced by the excitonically coupled BChl. This narrowing of the Qy absorption bands increases the resolution of the Qy peaks present, uncovering any obscured “B850-like” peaks. As observed in the absorbance spectra from the membranes (section 3.2.2), the split B800 bands are present in all the crude extracts, centring at 804 (Qy_R) nm and 792 nm (Qy_B). Low

temperature absorption spectra were recorded from SDCG from THL40, SHL40, THL30, SHL30, TLL30, and SLL30 growth conditions. Low temperature absorption spectra were recorded before the development of the low light 40℃ set up and so there is no data for these growth conditions.

There is very little variation between the B800 and “B850-like” absorption peaks observed from the LH2 fraction produced under SHL40 and THL40 growth conditions (Figure 3.16). The Qy absorption peaks centre at 867 nm, 792 nm and 805 nm in the LH2 fraction produced in THL40 growth conditions (Figure 3.16 red) and 868 nm, 793 nm and 805 nm when thiosulphate is substituted for sulphide (Figure 3.16 blue). The carotenoid peaks are also narrowed, allowing visualisation of the vibronic peaks of the carotenoids that are at the highest concentrations. A total of five carotenoid peaks are observed in all samples at 467 nm ±1 nm, 489 nm, 502 nm ±1-2 nm, 527 nm and 547 nm although not all bands are fully resolved.

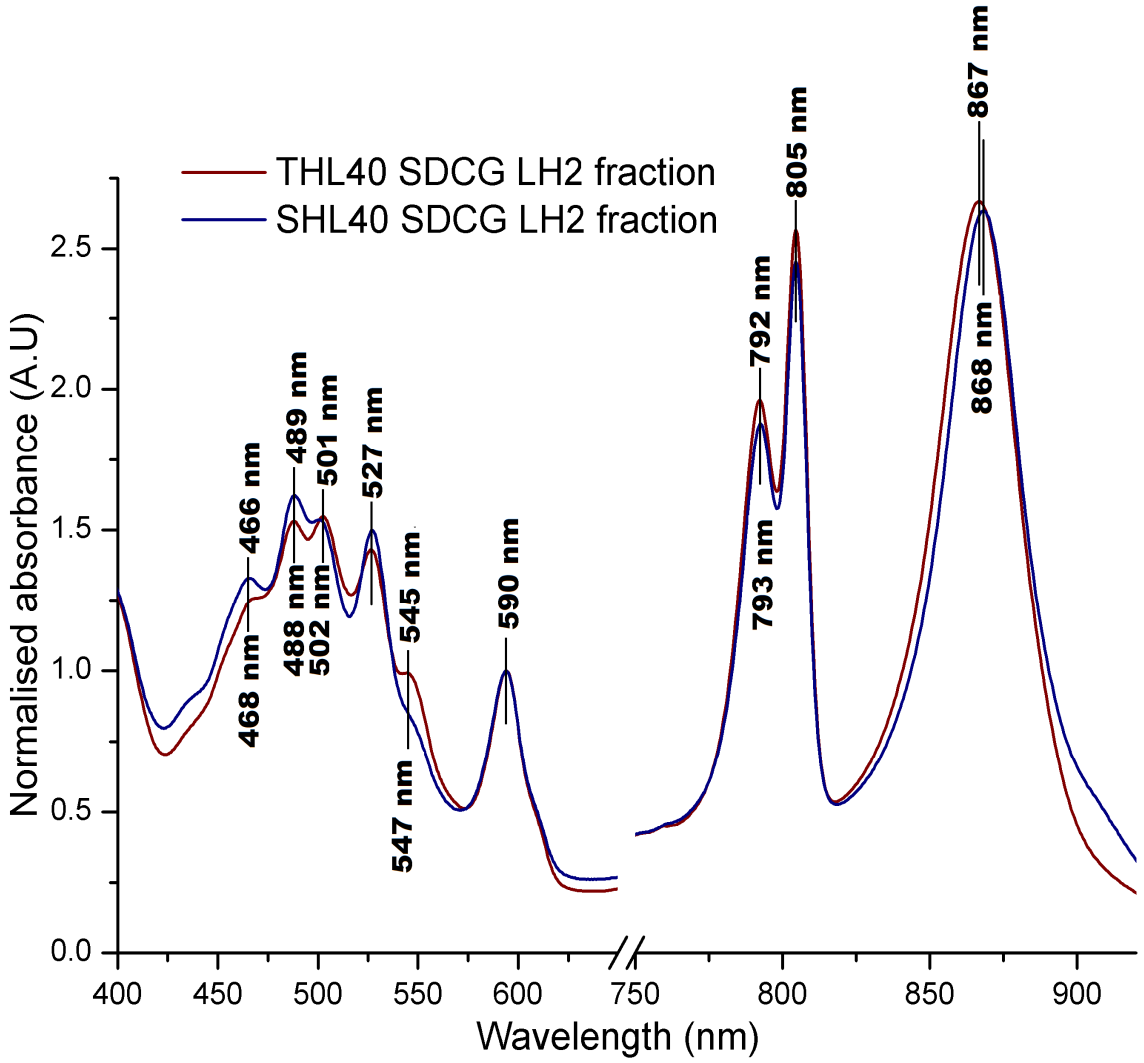

Figure 3.16 Low temperature (77 K) absorption spectra of the crude LH2 fraction in 0.02 % DDM from sucrose density centrifugation (SDC), extracted from *Alc. vinosum* grown in the presence of thiosulphate (T) or sulphide (S), under high light (HL), 40℃ growth conditions. The LH2 fraction produced under SHL40 (blue) growth conditions produces peaks at 466 nm, 489 nm, 501 nm, 527 nm, 590 nm, 793 nm, 805 nm, and 868 nm with a shoulder at ~547 nm. The LH2 fraction produced under THL40 (red) growth conditions produces peaks at 468 nm, 488 nm, 502 nm, 527 nm, 590 nm, 792 nm, 805 nm, and 867 nm with a shoulder at ~545 nm. The absorption spectra of the crude LH2 fraction produced under SHL40 and THL40 varies only slightly in the intensity of the carotenoid peaks but are otherwise identical.

The TLL30 and SLL30 crude extracts both produce Qy peaks at 819 nm and a shoulder at ~852 nm, with B800 peaks at 792 nm (T), 793 nm(S) and 804 nm (Figure 3.17). The carotenoid peaks observed centre at 489 nm, 503 nm (S), 504 nm (T), 528 nm (S), 527 nm (T) with two shoulders at ~ 470 nm (S), ~ 468 nm (T), and ~ 547 nm.

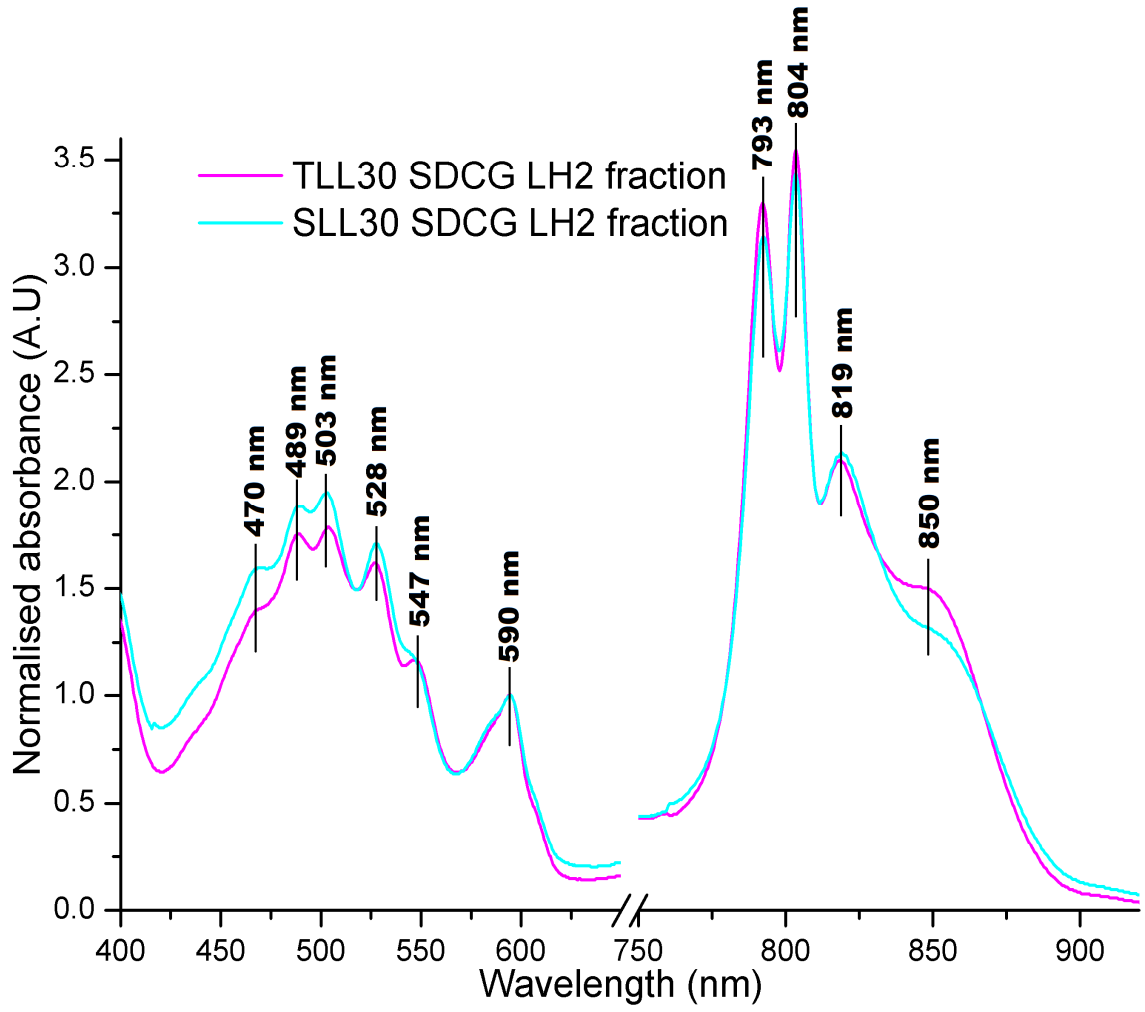

Figure 3.17 Low temperature (77 K) absorption spectra of the crude LH2 fraction in 0.02 % DDM from sucrose density centrifugation (SDC), extracted from *Alc. vinosum* grown in the presence of thiosulphate (T) or sulphide (S), under low light (LL), 30 ℃ growth conditions. The LH2 fraction produced under SLL30 (cyan) growth conditions produces peaks at 489nm, 503 nm, 528 nm, 590 nm, 793 nm, 804 nm, and 819 nm with shoulders at ~470 nm, ~547 nm, and ~ 850 nm. The LH2 fraction produced under TLL30 (pink) growth conditions produces peaks at 489 nm, 504 nm, 527 nm, 547 nm, 590 nm, 792 nm, 804 nm, and 819 nm, with shoulders at ~468 nm and ~ 850 nm. The absorption spectra of the crude LH2 fraction produced under SLL30 and TLL30 varies only slightly in the intensity of the absorption shoulder at ~ 850.

Figure 3.18 shows the differences in the absorption spectra between the LH2 fractions produced under THL30 and SHL30 growth conditions. The “B850-like” maximum from the THL30 growth conditions is centred at 861 nm (Figure 3.18 red) while the SHL30 maximum is positioned at 867 nm (Figure 3.18 green). The NIR absorbance of both fractions show a shoulder at 818 nm that is more prominent in the fraction produced from THL30 conditions. While the “B850-like” Qy peaks are different, the carotenoid peaks observed in these fractions produce similar absorption peaks that centre at 489 nm, 502 nm, 527 nm (S), 528 nm (T) and two shoulders at ~ 547 nm and ~ 467 nm. This data is summarised in table 3.2.

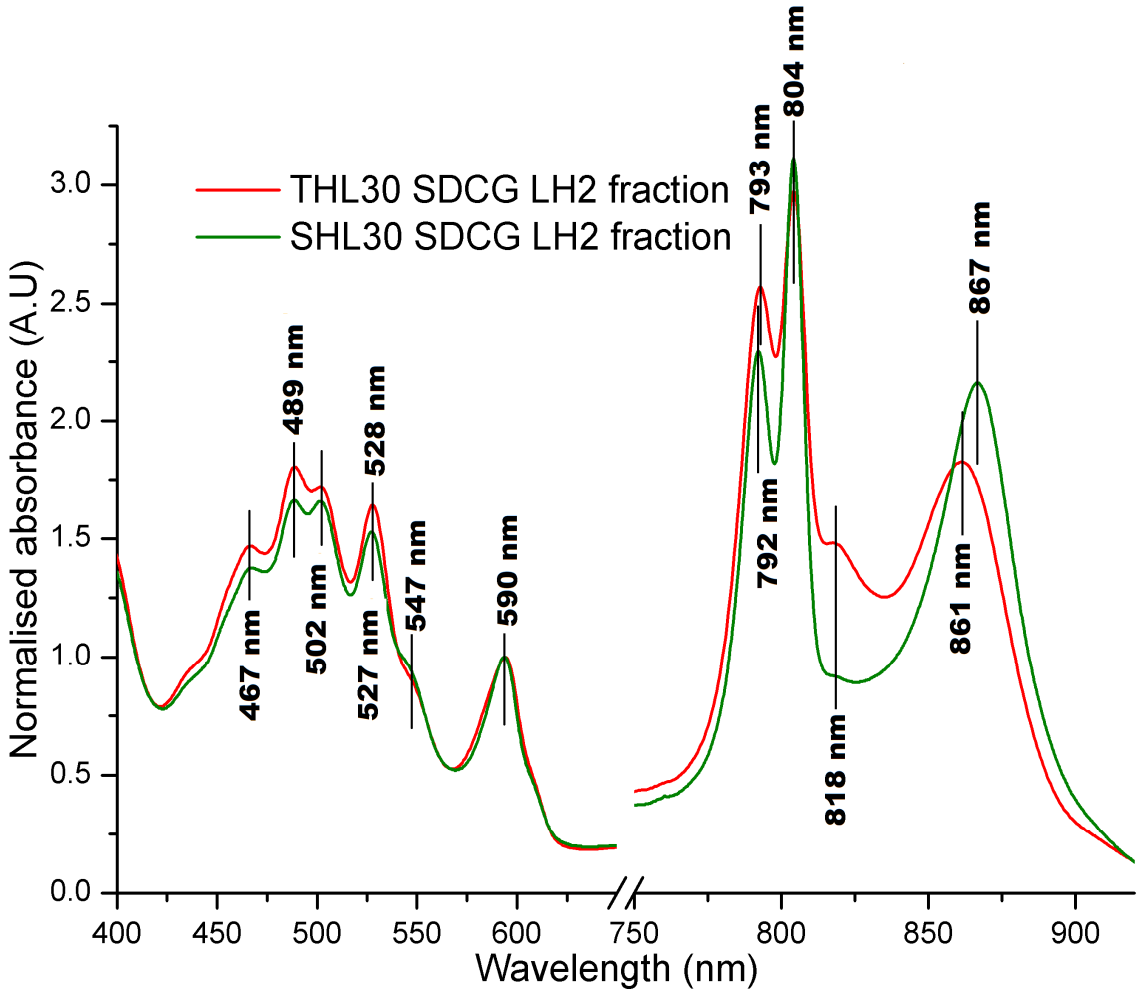

Figure 3.18 Low temperature (77 K) absorption spectra of the crude LH2 fraction in 0.02 % DDM from sucrose density centrifugation (SDC), extracted from *Alc. vinosum* grown in the presence of thiosulphate (T) or sulphide (S), under high light (HL), 30 ℃ growth conditions. The LH2 fraction produced under SHL30 (green) growth conditions produces peaks at 467 nm, 489 nm, 502 nm, 527 nm, 590 nm, 792 nm, 804 nm, and 867 nm with shoulders at ~547 nm, and ~818 nm. The LH2 fraction produced under THL30 (red) growth conditions produces peaks at 467 nm, 489 nm, 502 nm, 528 nm, 590 nm, 793 nm, 804 nm, 818 nm, and 861 nm with a shoulder at ~547 nm. The absorption spectra of the crude LH2 fraction produced under SHL30 and THL30 varies in the position of the longest wavelength Qy peak as well as the THL30 producing a distinct peak at 818 nm.

Table 3.2 Room temperature (RT) and 77 K (LT) wavelength values of Qy maxima produced by the light-harvesting complexes in SDCG in 0.02 % DDM from *Alc. vinosum* cells cultured under different growth conditions.
Peaks that appear as a shoulder are defined by (sh). S: sulphide, T: thiosulphate, HL: High light (60-80 umol m^{-2} s^{-1}), LL: Low light, 30℃ or 40℃.

	SLL30	SLL40	SHL30	SHL40	TLL30	TLL40	THL30	THL40
RT								
Carotenoid peak(s) (nm)	~460(sh) 489 ~530(sh)	~460 489 ~523(sh)	~460(sh) 488 ~523(sh)	~460(sh) 488 ~525(sh)	~460(sh) 489 ~530(sh)	~460 489 ~522(sh)	~460(sh) 488 ~523(sh)	~460(sh) 487 ~523(sh)
B800 peak(s)(nm)	802	797 802	798 803	798 803	802	798 803	798 803	798 803
B850-"like" peak (nm)	~822 ± 2 (sh)	847.5 ± 0.5	848 ± 1	849 ±1	~821 ± 1 (sh)	~844 (sh)	841 ± 2	848 ± 1
LT								
Carotenoid peak(s) (nm)	~470 489 503 528 ~547(sh)		467 489 502 527 ~547(sh)	466 489 501 527 ~547(sh)	~468 489 504 527 547		467 489 502 528 ~547(sh)	468 488 502 527 ~545
B800 peak(s)(nm)	793 804		792 804	793 805	792 804		793 804	792 805
B850-"like" peak (nm)	819 ~850 (sh)		~818(sh) 867	868	819 ~850 (sh)		818 861	867

3.4 Optimisation of Anion Exchange purification protocol

The low temperature absorption spectra of the crude LH2 fractions suggested multiple different LH2 types are produced by *Alc. vinosum*, the production of which is restricted by the growth conditions under which the light-harvesting complexes are produced. It is not clear whether, under these different growth conditions, there are distinct LH2 complex types or a continuum of different complexes constructed with different combinations of polypeptides. To elucidate this, the complexes must be fractionated further to resolve the mix of LH2 complexes. Anion exchange chromatography was used to separate the different LH2 complex types according to their charge.

Gravity flow anion exchange chromatography using Whatman De52 cellulose resin has previously been used to purify the crude LH2 fraction from other purple photosynthetic bacteria (101, 156). This method is sufficient to remove residual

LH1/RC “core” complex and other impurities when the LH2 fraction contains only one LH2 complex type. As *Alc. vinosum* produces several different types of LH2 complex under the same growth conditions, this method is insufficient to separate them. For this reason, protocols using an automated Persceptive Biosystems BioCad 700E perfusion workstation (Applied Biosystems) with a Q20 resin column were developed (as outlined in Methods and Materials section 2.5.3).

The use of the Persceptive Biosystems BioCad 700E perfusion workstation allows the creation of linear/step gradients with small changes in NaCl concentration. The nature of the automated system ensures the concentrations and volumes passed through the column are reproducible. Crude extracts of LH2 complexes isolated by SDCG were loaded onto a Poros Q20 column, attached to a BioCad 700E perfusion workstation and a gradient of 0 M to 1 M NaCl, 20 mM Tris-HCl (pH 8.0), 0.02 % DDM, was used to elute the different LH2 complex types. The absorbance at 280 nm was measured to record the elution of proteins, which was followed by the recording of the 250-950 nm absorption spectrum of each fraction. This allowed the assay of both the separation of the different LH2 complex types and the ratio of the $Qy_{maximum}/A_{280}$ to ascertain purity. Fractions were pooled according to the position of their Qy bands and the level of purity denoted by the Qy/A_{280} ratio. Methods were optimised to ascertain the NaCl concentration required to elute each LH2 complex type present (as outlined in Methods and Materials section 2.5.3).

The presence of an isosbestic point within the absorption spectra of the different LH2 complex types may indicate a relationship between different LH2 complex types. An isosbestic point is formed when the absorption of only two types of complex overlap at the same wavelength. This implies the conversion between the two proceeds without any intermediate other complex types being present. Multiple isosbestic points would be observed if there are several different LH2 complex types present, although this would be difficult to resolve at room temperature.

3.4.1 Anion exchange of LH2 complex types produced under HL 40 growth conditions

The LH2 mix extracted from *Alc. vinosum* grown under SHL40℃ growth conditions was separated using anion exchange chromatography on a Poros Q20 column with the gradient method Alvin-SandThio-HL40-800-850-method-3.met (as outlined in Methods and Materials section 2.5.3.1). The crude LH2 fraction was in the presence of 0.02 % DDM, 20 mM Tris-HCl (pH 8.0) and ~ 0.8 M sucrose after extraction via sucrose density centrifugation.

The crude LH2 fraction from sulphide, high light 40℃ (SHL40) growth conditions produced multiple elution peaks (Figure 3.19, peaks A-E). Peak A eluted at 100 mM NaCl, peak B at 250 mM NaCl, peak C at 310 mM NaCl, peak D at 350 mM NaCl, peak E at 1000 mM NaCl (Figure 3.19). The elution peaks A and B were non-photosynthetic impurities, while peak D was identified as mixed LH2 and LH1/RC "Core" with an increasing concentration of LH1/RC "core" complex as the fractions increased. The final peak is residual impurities that were stripped from the column.

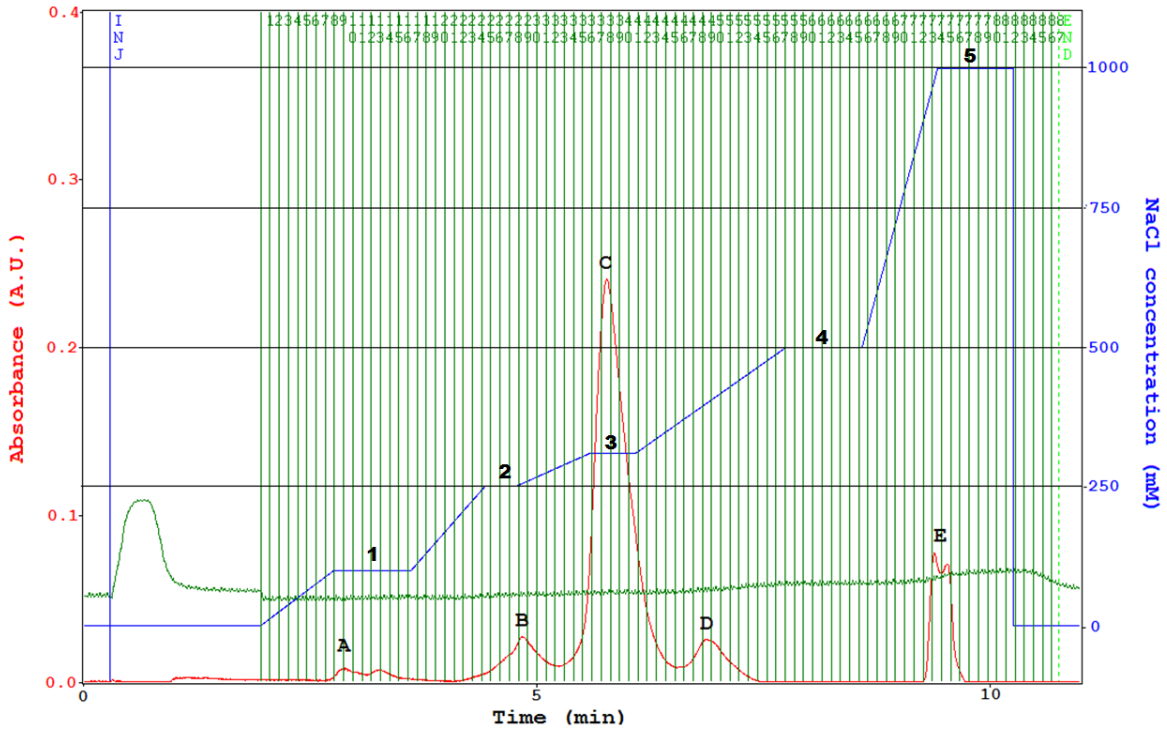

Figure 3.19 Anion exchange chromatogram showing the separation of the crude LH2 fraction from *Alc. vinosum* grown under high light, 40 ℃ in the presence of sulphide. The gradient steps were at 100 mM (1), 250 mM (2), 310 mM (3), 500 mM (4), and 1000 mM (5). Fraction number is shown with green lines, while pressure is the lateral green line. The concentration of NaCl in the elution buffer is shown in blue, and the A_{280} nm in red. After injection there is an increase in pressure due to the sucrose in the sample. At 100 mM NaCl two small peaks (A) were observed eluting from the column. At 250 mM NaCl a single small peak eluted (B). At 310 mM NaCl a substantial peak eluted (C). This was followed by a peak (D) between 310 mM and 500 mM, and a small peak (E) at 1000 mM NaCl. The largest peak that elutes at 310 mM NaCl was identified as the B800-850 LH2 complex type.

The 250-950 nm absorption spectra of the fractions of peak C showed that they corresponded to a B800-850 LH2 complex type with Qy absorption peaks at 796 nm, 802 nm and 848 ± 1 nm (Figure 3.20 purple). The carotenoid peaks observed are the same as those observed in the SDCG, at ~ 460 nm, 488 nm, and ~525 nm. This method was sufficient to purify the B800-850 LH2 complex type at a purity ratio of 1.9-2.0 from both SDCG extracted from cells grown under SHL40 and THL40 growth conditions. The NaCl concentrations at which peaks eluted were unchanged when this gradient was run in the presence of 0.15 % DM instead of 0.02 % DDM.

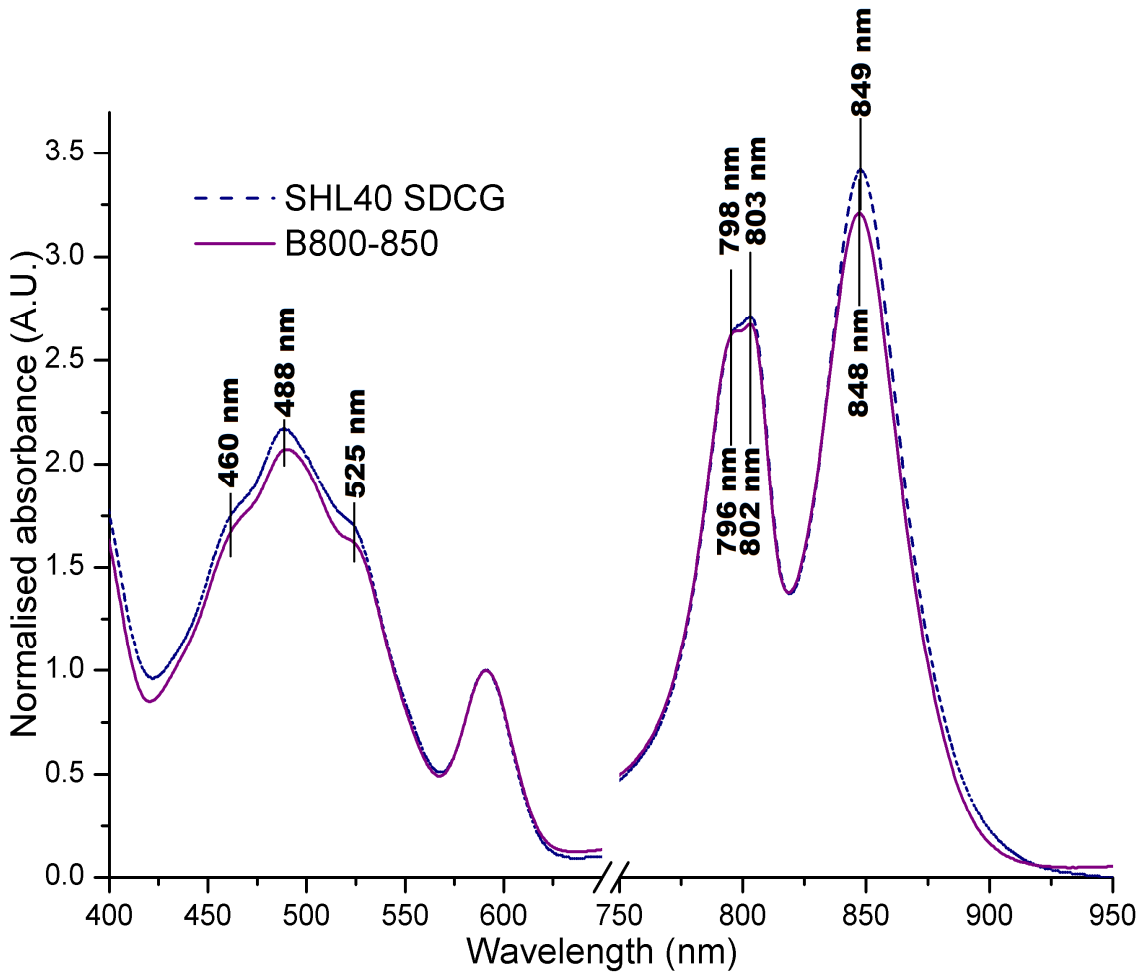

Figure 3.20 Normalised absorption spectra of the original crude LH2 extract from SHL40 growth conditions (dotted line) and the purified B800-850 LH2 complex type (purple) in 0.02 % DDM from fractions pooled after anion exchange chromatography.
The crude LH2 fraction was extracted from *Alc. vinosum* cells grown in the presence of sulphide, under high light, 40℃ growth (SHL40) conditions. The B800-850 LH2 complex type eluted at 310 mM NaCl in a single peak. The crude LH2 fraction from sucrose density centrifugation produced Qy peaks at 798 nm, 803 nm, and 849 ±1 nm while the purified B800-850 LH2 complex produced Qy peaks at 796 nm, 802 nm and 848 nm ±1. There is a small blue shift of the Qy peaks, and no difference in the carotenoid peaks at ~460 nm, 488 nm, and ~ 525 nm.

3.4.2 Anion exchange of LH2 complex types produced under THL30, TLL40 and LL30 growth conditions

The LH2 mix extracted from *Alc. vinosum* grown under thiosulphate, high light 30℃ (THL30) growth conditions was separated using anion exchange chromatography on a Poros Q20 column with the gradient method Alvin-800-820-and800-840-method.met (as outlined in Methods and Materials section 2.5.3.2). The crude LH2 fraction was in the presence of 0.02 % DDM, 20 mM Tris-HCl (pH 8.0) and ~ 0.8 M sucrose. The crude LH2 fraction from THL30 growth conditions produced multiple elution peaks (Figure 3.21, peaks A-G). Peak A eluted at 0 mM

NaCl, peak B at 100 mM NaCl, peak C at 240 mM NaCl, peak D at 260 mM NaCl, peak E at 330 mM NaCl, peak F at 350 mM NaCl and peak G at 1000 mM NaCl.

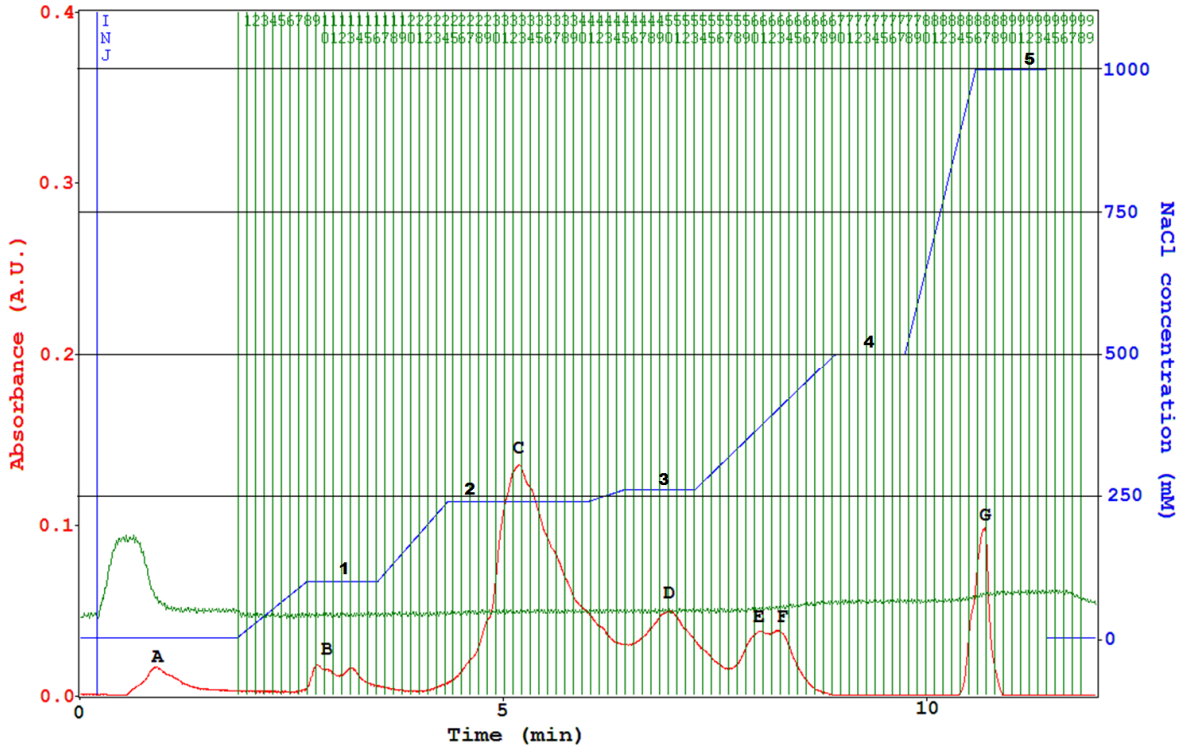

Figure 3.21 Anion exchange chromatogram showing the separation of the crude LH2 fraction from *Alc. vinosum* grown under high light, 30 ℃ in the presence of thiosulphate. The gradient steps were at 100 mM (1), 240 mM (2), 260 mM (3), 500 mM (4), and 1000 mM (5). Fraction number is shown with green lines, while pressure is the lateral green line. The concentration of NaCl in the elution buffer is shown in blue, and the A_{280} nm in red. After injection there is an increase in pressure due to the sucrose in the sample. During the wash step at 0 mM NaCl a small peak eluted (A) after the sucrose was washed from the column. At 100 mM NaCl, two small peaks eluted (B). At 240 mM NaCl a substantial peak eluted (C) that produced a long tail. This was followed by a peak (D) at 260 mM, and two peaks (E and F) in close succession between 260 mM and 500 mM. At 1000 mM NaCl a single peak (G) eluted. The largest peak that elutes at 240 mM NaCl was identified as the B800-820 LH2 complex type, while the peak at D was identified as the B800-840h and B800-840p. Peak E was identified as a potential B800-850a LH2 complex type but was in low abundance. All other peaks were non-photosynthetic contaminants except for peak E and F that was a mix of LH1/RC "core" and LH2 complex types.

Peak C, fractions 30 to 34, was found to constitute the B800-820 LH2 complex type producing absorption maxima at 796 nm, 803 nm, and a shoulder at ~ 818 nm (Figure 3.22 red). In fractions eluted after these, the "B850-like" BChl peak of each fraction became more red-shifted. When the absorption spectra of the fractions from peak D were recorded, they were found to produce a hump in the absorption at ~ 840 nm (Figure 3.22 dark yellow) that red-shifts to an absorbance peak at 840 ± 2 nm (Figure 3.22 black) after the main elution peak. These were both identified as a B800-840 LH2 complex type, but differentiated as B800-840 peak (B800-840p) and B800-840 hump (B800-840h) (Figure 3.23).

Peak E was made up of a LH2 complex that produced a “B850-like” Qy absorption peak centred at 845 nm, implying it may be a B800-850 LH2 complex type. Peak F was identified as a mix of LH1/RC “core”, and LH2 complex types.

The carotenoid peaks show small variations depending on the complex type they are present in. In the B800-820 LH2 complex type the carotenoid peaks centre at ~ 460 ±0.5 nm, 488.5 nm, and ~ 523 ±1 nm. The B800-840h and B800-840p complex types produce carotenoid maxima at ~461 ± 1 nm, 488 ± 0.5 nm, and ~521.5 ± 1 nm. The B800-850 complex type produced under these conditions produces carotenoid peaks at ~461 ±1 nm, 487 nm, and ~ 520.5 ±0.5 nm.

An apparent isosbestic point is observed in NIR absorption of the LH2 complex types. The wavelengths at which the LH2 complex types overlap differ as the B800-820 LH2 complex intercepts the B800-840h LH2 complex at 831.5 nm, and the B800-840p LH2 complex at 832.5 nm, and at 833.5 nm with the B800-850 LH2 complex. The B800-840h LH2 complex absorption intercepts the B800-840p LH2 complex absorption at 833.5 nm, and the B800-850 at 834 nm. The B800-840p LH2 complex produces an isosbestic point at the longest wavelength at 835 nm when intercepting the absorption of the B800-850 LH2 complex.

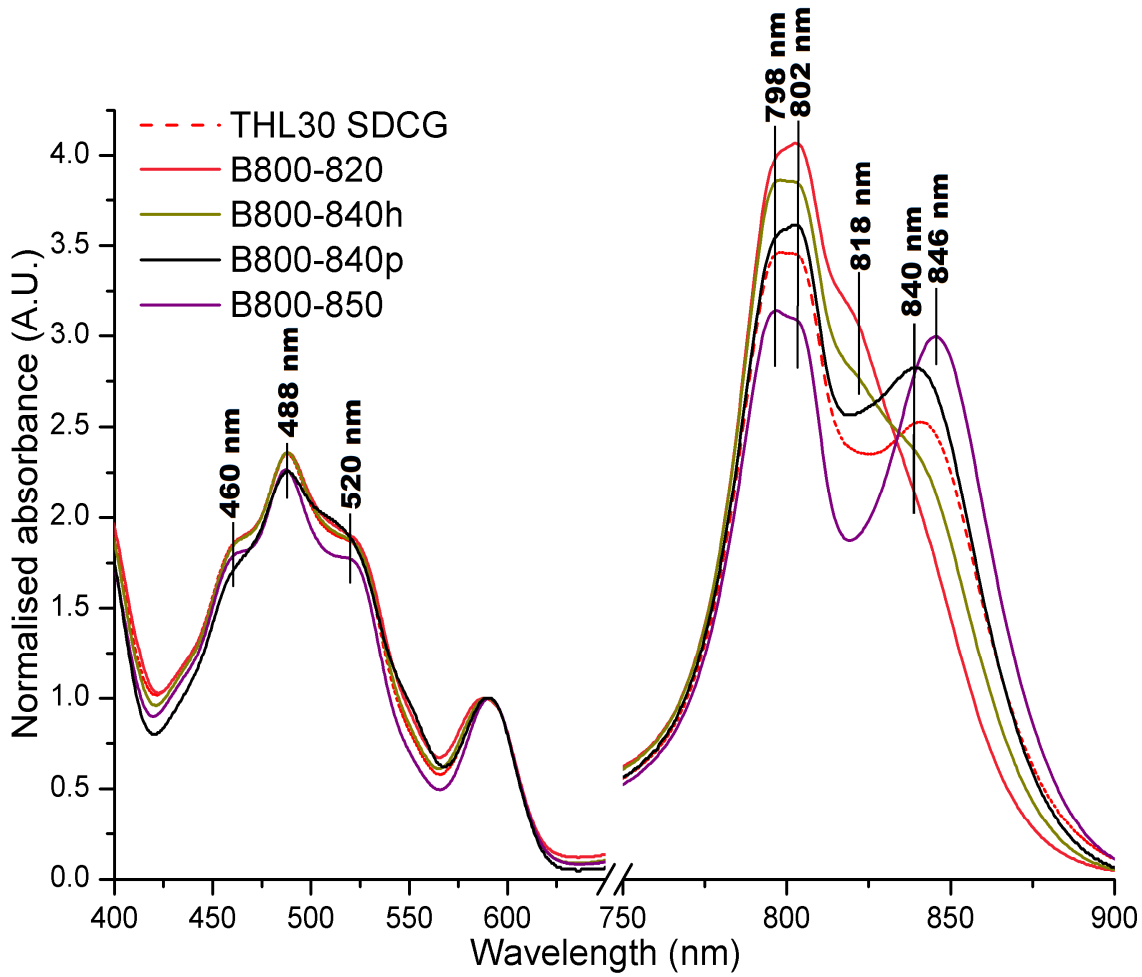

Figure 3.22 Normalised absorption spectra of the original crude LH2 extract from THL30 growth conditions (dotted line) and the purified B800-820 (red), B800-840h (green), B800-840p (blue), and B800-850a (purple) LH2 complex types in 0.02 % DDM from fractions pooled after anion exchange chromatography.
The crude LH2 fraction was extracted from *Alc. vinosum* cells grown in the presence of thiosulphate, under high light, 30℃ growth (THL30) conditions. The B800-820 LH2 complex type eluted at 240 mM NaCl, the B800-840 complex types eluted at 240 mM NaCl, and the B800-850a eluted at 330 mM NaCl. The crude LH2 fraction from sucrose density centrifugation produced Qy peaks at 798 nm, 803 nm, and 841 ±2 nm. The purified B800-820 LH2 complex produces Qy peaks at 798 nm, 802 nm, with a shoulder at ~ 818 nm. The purified B800-840h produces peaks at 798 nm, 802 nm, with a shoulder at ~840 nm. The purified B800-840p produces peaks at 798 nm, 802, and 840 nm ±1. The purified B800-850a produced peaks at 798 nm, 802 nm and 846 nm ±1. There are no substantial changes observed in the carotenoid region of the absorption spectrum at ~460 nm, 488 nm, and ~520 nm. The changes in the Qy peaks appear to produce isosbestic points, as the ~818 nm peak shifts to 845 nm. There are several isosbestic points observed between the B800-820 and the B800-850a (833.5 nm), B800-840p (832.5 nm) and the B800-840h (831.5 nm). There are isosbestic points observed between the B800-840h and the B800-840p (833.5 nm) and the B800-850a (834 nm). The isosbestic point between the B800-840p and the B800-850a centres at 835 nm. These isosbestic points are within 3.5 nm of each other.

The B800-820 LH2 complex type appears to be the origin of the absorption at ~ 818 nm observed in the SDCG and membranes of THL30. Therefore, as this method successfully separates the B800-820 from the B800-840 complex types it was used to purify the crude LH2 extract from THL30, TLL40, SLL30 and TLL30

growth conditions as they produce prominent ~ 818 nm shoulders (as outlined in Methods and Materials section 2.5.3.2).

Anion exchange chromatography of LH2 complexes produced under TLL40 conditions produced elution peaks A, B, C, D, F, and G when separated using the gradient from Alvin-800-820-and800-840-method.met. The method eluted three LH2 complex types similar to those observed from the crude LH2 fraction from THL30 growth conditions. The B800-820 LH2 complex type identified produced absorption peaks centring at ~ 796 nm, 801 nm and a shoulder at ~ 818 nm (Figure 3.23 red). The peaks of the B800-840h complex type centred at 798 nm, ~ 805 nm, and a shoulder at ~ 835 nm (Figure 3.23 dark yellow), while the B800-840p complex type peaks centre at 797 nm, ~ 802 nm, and 840 nm (Figure 3.23 purple).

The carotenoid peaks of the different LH2 complex types produced under TLL40 growth conditions centre at ~ 460 nm and 489 nm. The carotenoid peak at the longest wavelength differs in intensity between the different complex types, centring at ~ 508 nm in the B800-820 LH2 complex type with the highest intensity, shifting to ~ 520 nm in the B800-840p complex type. The isosbestic points observed in the NIR between the complex types produced under these growth conditions centre at 831.5 nm between the B800-820 and the B800-840h, and 832 nm between the B800-820 and the B800-840p. While the B800-840h intercepts the NIR absorption of the B800-840p at 831 nm.

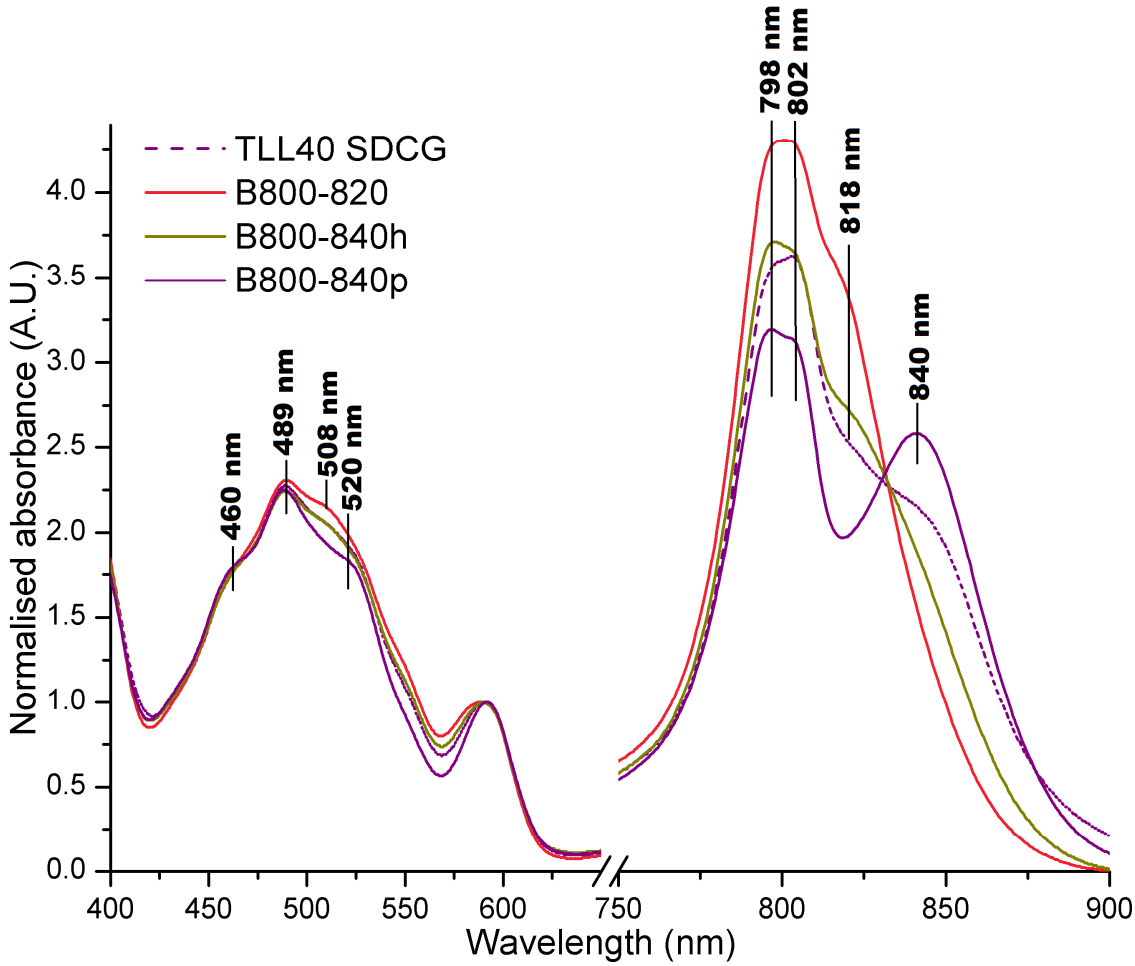

Figure 3.23 Normalised absorption spectra of the original crude LH2 extract from TLL40 growth conditions (dotted line) and the purified B800-820 (red), B800-840h (green), B800-840p (blue), and B800-850a (purple) LH2 complex types in 0.02 % DDM from fractions pooled after anion exchange chromatography.
The crude LH2 fraction was extracted from *Alc. vinosum* cells grown in the presence of thiosulphate, under low light, 40℃ growth (TLL40) conditions. The B800-820 LH2 complex type eluted at 240 mM NaCl and the B800-840 complex type eluted at 240 mM NaCl. The crude LH2 fraction from sucrose density centrifugation produced Qy peaks at 798 nm, 803 nm, and a shoulder at ~ 844 nm. The purified B800-820 LH2 complex produces Qy peaks at 798 nm, 802 nm, with a shoulder at ~ 818 nm. The purified B800-840h produces peaks at 798 nm, 802 nm, with a shoulder at ~840 nm. The purified B800-840p produces peaks at 798 nm, 802, and 840 nm ±1. There is a change in the carotenoid absorption between the three LH2 complex types identified. The red-most shoulder at ~ 520 nm decreases in intensity from the B800-820 LH2 complex type to the B800-840p LH2 complex type. The changes in the Qy peaks appear to produce isosbestic points, as the ~818 nm peak shifts to 840 nm. There are several isosbestic points observed between the B800-820 and the B800-840p (832 nm), and the B800-840h (831.5 nm). There is an isosbestic point observed between the B800-840h and the B800-840p (831 nm). These isosbestic points are within 1 nm of each other.

The LH2 complex types produced under sulphide, low light 30 ℃ (SLL30) conditions are the B800-820 (Figure 3.24 red) and B800-840h (Figure 3.24 dark yellow). The B800-820 complex type absorption peaks were observed at 803 nm, and ~ 819 nm, while the B800-840h complex type centred at 803nm, with a shoulder at ~ 839 ± 1 nm. The B800-840p maxima centre at 839.5 ± 0.5 nm. The carotenoid maxima observed vary only a small amount, centring at 463 nm, 490

nm and 525 nm (B800-820) or 526 (B800-840h). The NIR isosbestic point observed between these two LH2 complex types centres at 834 nm.

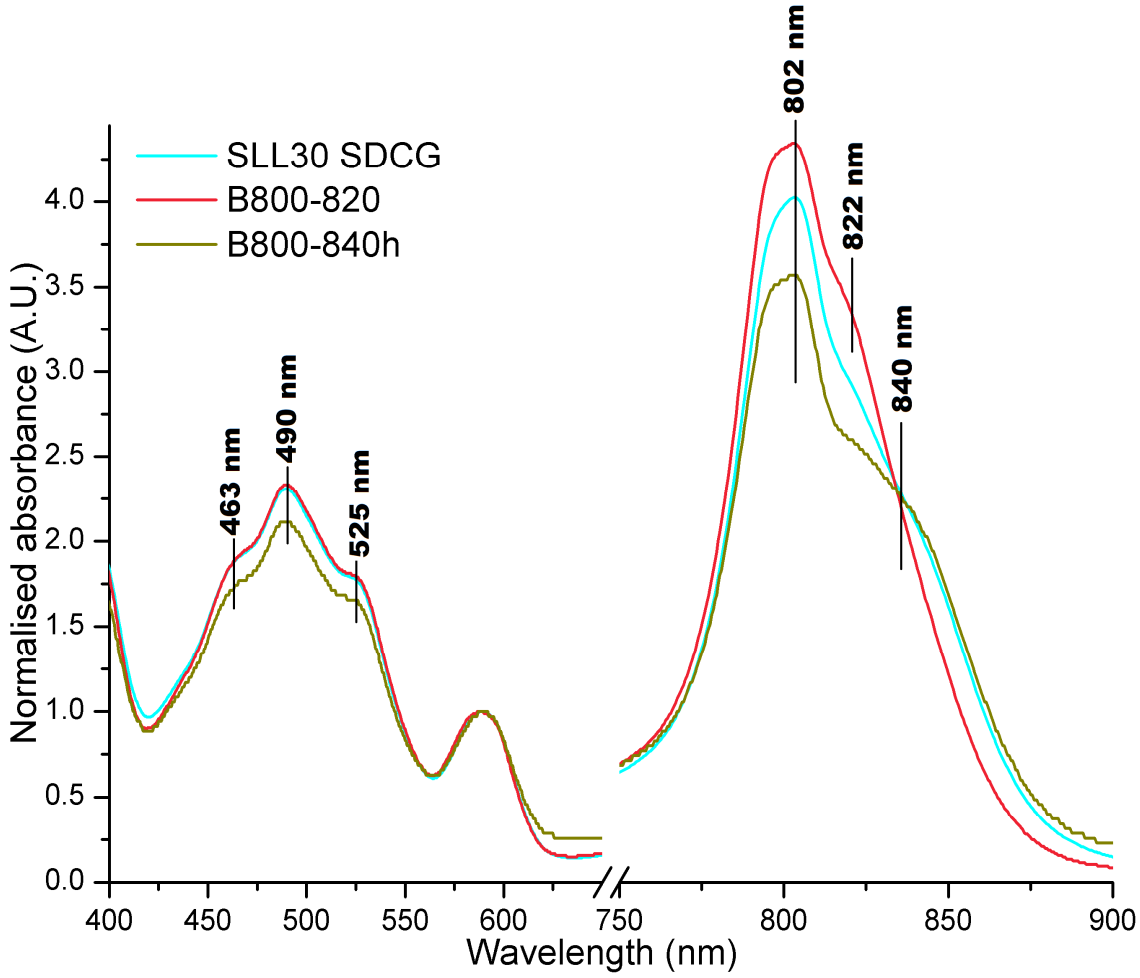

Figure 3.24 Normalised absorption spectra of the original crude LH2 extract from SLL30 growth conditions (cyan) and the purified B800-820 (red) and B800-840h (green) LH2 complex types in 0.02 % DDM from fractions pooled after anion exchange chromatography. The crude LH2 fraction was extracted from *Alc. vinosum* cells grown in the presence of sulphide, under low light, 30℃ growth (SLL30) conditions. The B800-820 LH2 complex type eluted at 240 mM NaCl and the B800-840 complex type eluted at 240 mM NaCl. The crude LH2 fraction from sucrose density centrifugation produced Qy peaks at 802 nm, and a shoulder at ~ 822 nm. The purified B800-820 LH2 complex produces Qy peaks at 798 nm, 802 nm, with a shoulder at ~ 818 nm. The purified B800-840h produces peaks at 798 nm, 802 nm, with a shoulder at ~840 nm. There is no substantial change in the carotenoid absorption between the three LH2 complex types identified at 463 nm, 490 nm, and 525 nm. The changes in the Qy peaks appear to produce an isosbestic point, as the ~818 nm peak shifts to 840 nm (834 nm).

When the crude LH2 fraction, extracted from *Alc. vinosum* cells grown in the presence of thiosulphate, under low light and 30℃ (TLL30), is separated using the same gradient as the SLL30 fraction the same elution peaks are observed however the complexes show some differences (Figure 3.25). The B800-820 complex maxima centre at 803 nm and ~818 nm (Figure 3.25 red). The B800-840h complex type produces a more prominent hump at ~ 830 nm (Figure 3.25

dark yellow), and the B800-840p produces a distinct peak at 839 ±1 nm (Figure 3.25 black). The carotenoid peaks of the B800-820 complex type centre at 489 ±0.5 nm, with shoulders in the absorption at ~ 510 ±2 nm, ~ 460 ±0.5 nm and ~ 550 nm. The carotenoid peaks of the B800-840h are similar to the B800-820 with a slight reduction in the intensity of the ~ 510 nm shoulder. The B800-840p produces the same carotenoid maxima but with a red-shifted shoulder at ~ 519 nm.

There are isosbestic points observed between the complexes produced under TLL30 growth conditions. The B800-820 LH2 complex absorption intersects the absorption of the B800-840p at 831 nm and the B800-840h at 828 nm. The absorption of the B800-840p and B800-840h LH2 complex types intersect at 842 nm.

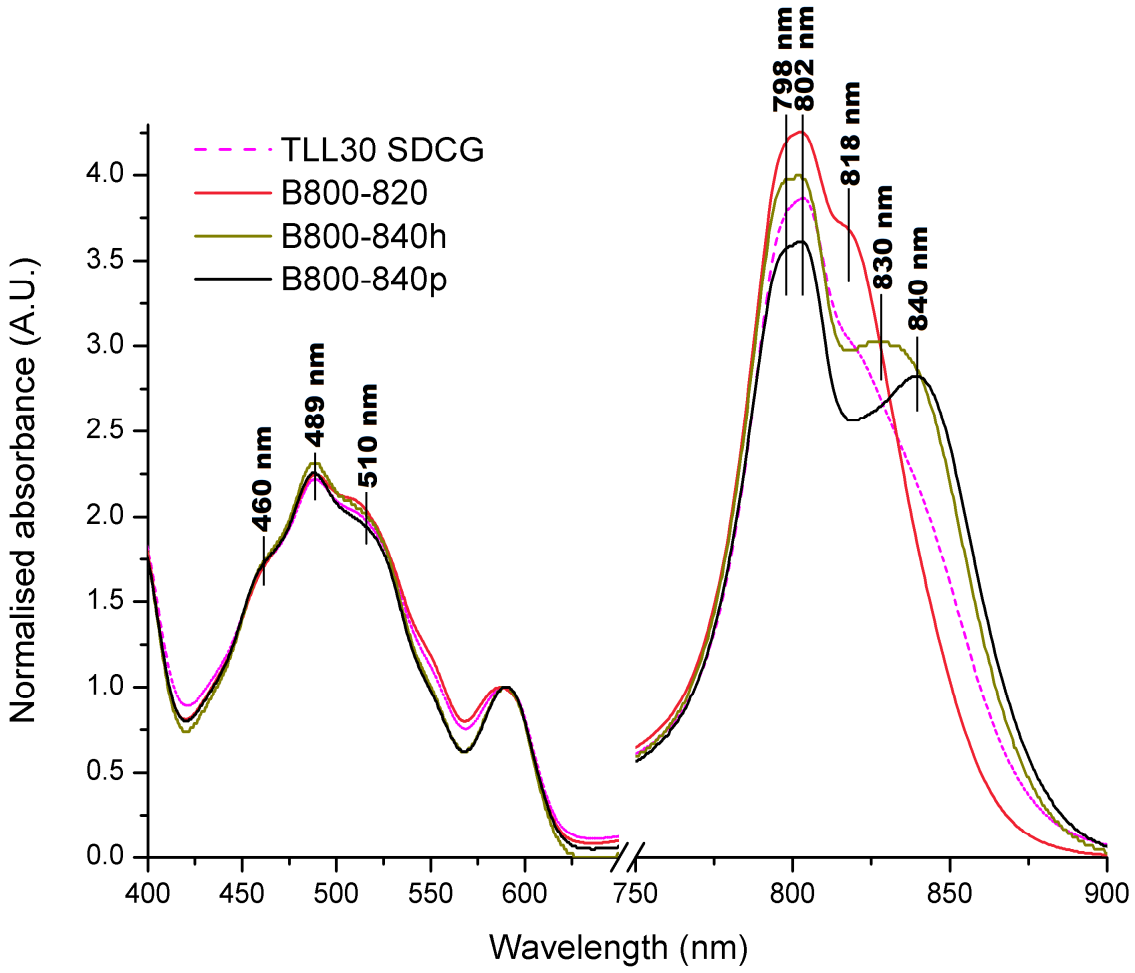

Figure 3.25 Normalised absorption spectra of the original crude LH2 extract from TLL30 growth conditions (dotted line) and the purified B800-820 (red), B800-840h (green), and B800-840p (blue) LH2 complex types in 0.02 % DDM from fractions pooled after anion exchange chromatography.
The crude LH2 fraction was extracted from *Alc. vinosum* cells grown in the presence of thiosulphate, under low light, 30℃ growth (TLL30) conditions. The B800-820 LH2 complex type eluted at 240 mM NaCl and the B800-840 complex types eluted at 240 mM NaCl. The crude LH2 fraction from sucrose density centrifugation produced Qy peaks at 802 nm, and a shoulder at ~ 821 nm. The purified B800-820 LH2 complex produces Qy peaks at 798 nm, 802 nm, with a shoulder at ~ 818 nm. The purified B800-840h produces peaks at 798 nm, 802 nm, with a shoulder at ~830 nm. The purified B800-840p produces peaks at 798 nm, 802 nm, and 840 nm. There is no substantial change in the carotenoid absorption between the three LH2 complex types identified at ~460 nm, 489 nm, and ~510 nm. There is more variation between the intercepts of the Qy absorption spectrum of the different LH2 complexes. There are isosbestic points observed between the B800-820 and the B800-840h (828 nm) and the B800-820 and the B800-840p (831 nm) and between the B800-840h and the B800-840p (842 nm). The difference in the isosbestic points between the different LH2 complex types varies by 11 nm.

3.4.3 Anion exchange of LH2 complex types produced under SHL30 and SLL40 growth conditions

There is a small ~ 818 nm shoulder in the 77 K absorption spectrum of SDCG from SHL30 but the most prominent Qy maximum centres at 867 nm (Figure 3.18). This suggests that the primary LH2 complex type produced under the SHL30 growth conditions is a B800-850 LH2 complex type but that there may be some

B800-820 present. The potential joint production of these two complex types led to the adaption of the Alvin-800-820-and800-840-method.met method to optimise purification of both LH2 complex types. This was achieved via the addition of a step of 310 mM NaCl to elute the B800-850 complex type. This method was named Alvin-SHL 30 - exp03-6-02-13.met (as outlined in Methods and Materials section 2.5.3.3).

As expected, the main elution peaks were observed at 240 mM, and 310 mM NaCl with a small peak at 260 mM. The B800-820 LH2 complex type eluted at 240 mM and produced peaks at 796nm, 802 nm and ~ 818 nm (Figure 3.26 red). A small amount of B800-840h (Figure 3.26 dark yellow) and B800-840p (Figure 3.26 black) eluted at 260 mM NaCl. The B800-840 LH2 complex types produced absorption peaks at 796nm and 802 nm with a distinct peak (B800-840p) or an absorption shoulder (B800-840h) at 846 nm. At 310 mM NaCl the B800-850 LH2 complex type eluted, which produced absorption peaks at 796 nm, 802 nm, and 849 ± 1 nm (Figure 3.26 purple). The carotenoid composition changes slightly between the B800-820 LH2 complex type and the B800-850 LH2 complex type. The main peak centres at 488 ±0.5 nm, with a shoulder at ~ 464 nm and ~ 521 ±1 nm. The shoulders are more distinct as peaks in the B800-850 complex type produced under these growth conditions than the B800-820 or B800-840 LH2 complex types.

The isosbestic point observed between the B800-820 and B800-850 complex types centres at 838 nm and can be observed across all the fractions pooled.

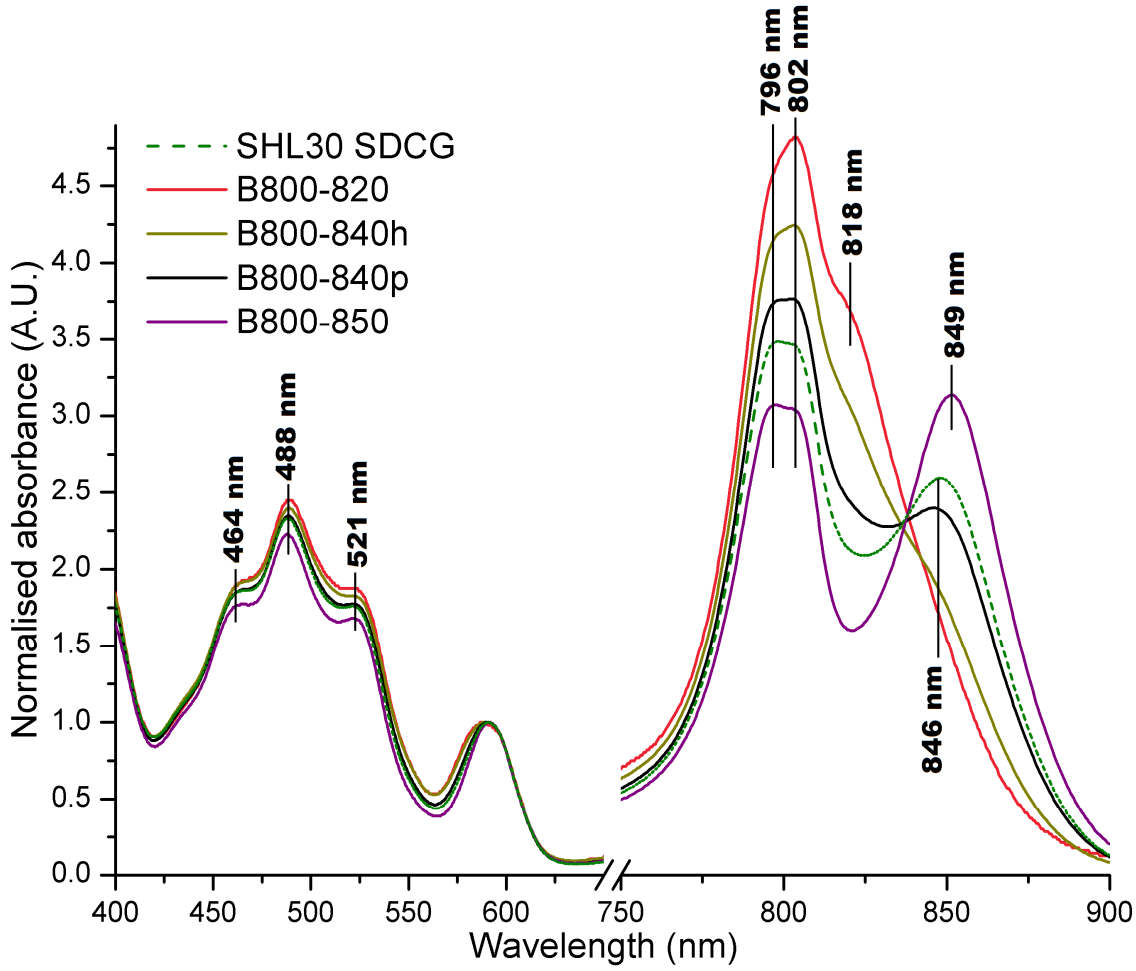

Figure 3.26 Normalised absorption spectra of the original crude LH2 extract from SHL30 growth conditions (dotted line) and the purified B800-820 (red), B800-840h (dark yellow), B800-840p (black), and the B800-850 (purple) LH2 complex types in 0.02 % DDM from fractions pooled after anion exchange chromatography.
The crude LH2 fraction was extracted from *Alc. vinosum* cells grown in the presence of sulphide, under high light, 30℃ growth (SHL30) conditions. The B800-820 LH2 complex type eluted at 240 mM NaCl and the B800-850a complex types eluted at 310 mM NaCl. The crude LH2 fraction from sucrose density centrifugation produced Qy peaks at 798 nm, 803 nm, and 848 ± 0.5 nm. The purified B800-820 LH2 complex produces Qy peaks at 796 nm, 802 m, and a shoulder at ~ 818 nm. The B800-840h produces Qy peaks at 798 nm, 802 nm, and two absorption shoulders at ~818 nm and ~846 nm. The B800-840p produces Qy peaks at 798 nm, 802 nm, and 846 nm.The purified B800-850a LH2 complex produces Qy peaks at 796 nm, 802 nm, and 849 ± 0.5 nm. There is no substantial change in the carotenoid absorption between the two LH2 complex types identified. The isosbestic point between the B800-820 LH2 complex and the B800-850a LH2 complex centres at 838 nm.

When the crude LH2 fraction from cells grown under SLL40 growth conditions was separated using this gradient method, the NaCl concentration at which the complexes eluted was the same as those from the LH2 fraction produced under SHL30 growth conditions. The LH2 complexes eluted at 240 mM and 310 mM NaCl. The LH2 complex types recorded were the B800-820 (Figure 3.27 red) that eluted at 240 mM NaCl with a peak centring at 802 nm, and a shoulder at ~ 818 nm. The B800-850 LH2 complex (Figure 3.27 purple) eluted at 310 mM NaCl and produced Qy absorption peaks at 797nm, 802nm and 848 nm. The carotenoid

complement between the B800-820 LH2 complex type and the B800-850 LH2 complex type produced under these growth conditions varies. The carotenoids of the B800-820 complex produce maxima at ~460 nm, 451 nm, and ~ 510 nm. The B800-850 LH2 complex type carotenoid peaks centres at ~ 462 nm, 488.5 nm, and ~ 521.5 nm. The absorption at ~460 nm and ~510 nm are less distinct in the B800-820 complex type produced under these growth conditions. The isosbestic point observed centres at 833.5 nm between the B800-820 and B800-850 produced under these growth conditions.

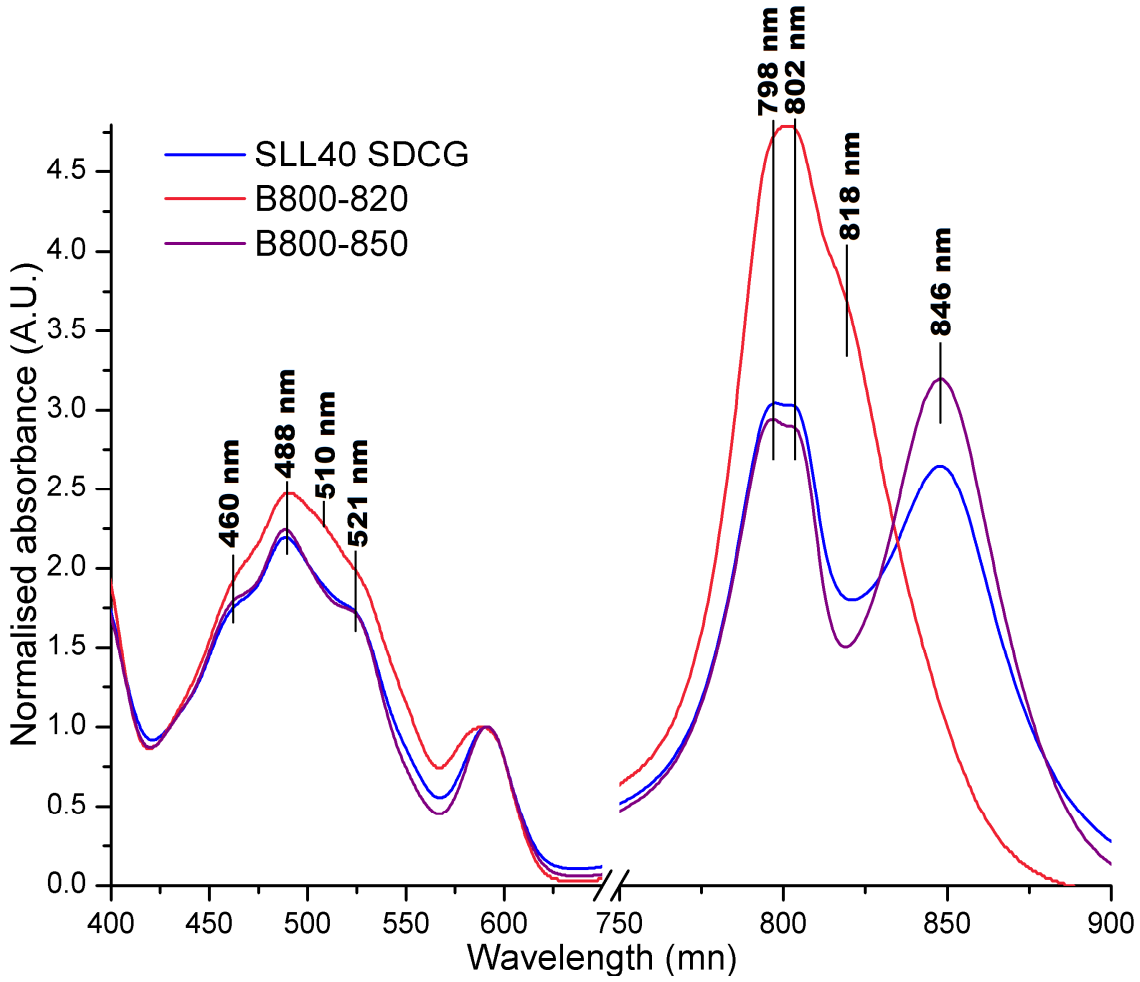

Figure 3.27 Normalised absorption spectra of the original crude LH2 extract from SLL40 growth conditions (blue) and the purified B800-820 (red), and B800-850 (purple) LH2 complex types in 0.02 % DDM from fractions pooled after anion exchange chromatography. The crude LH2 fraction was extracted from *Alc. vinosum* cells grown in the presence of sulphide, under low light, 40 ℃ growth (SLL40) conditions. The B800-820 LH2 complex type eluted at 240 mM NaCl and the B800-850a complex types eluted at 310 mM NaCl. The crude LH2 fraction from sucrose density centrifugation produced Qy peaks at 797 nm, 802 nm, and 847 ± 0.5 nm. The purified B800-820 LH2 complex produces Qy peaks at 798 nm, 802 nm, with a shoulder at ~ 818. The purified B800-850 LH2 complex produces Qy peaks at 798 nm, 802 nm, and 846 ± 0.5 nm. There is a small change in the carotenoid absorption in the red-most carotenoid peak, as it is obscured as a shoulder in the B800-820 LH2 complex but is a more distinct peak in the B800-850a LH2 complex.

In summary, the different LH2 complex types are produced under a variety of growth conditions (Table 3.3). Some growth conditions produced negligible quantities of some of the LH2 complex types. These are classified as LH2 complex types that are 'present' but not 'abundant'. High light 40℃ growth conditions solely produced B800-850, while high light 30℃ in the presence of sulphide produced B800-820, a small amount of B800-840h and a B800-850 LH2 complex type. Cells cultured in high light 30℃ conditions with thiosulphate produced B800-820, B800-840h, B800-840p and a B800-850 LH2 complex type. The primary LH2 complex type was the B800-820, with a small amount of B800-840h and B800-840p under low light 30℃ conditions in the presence of thiosulphate. Growth under low light 40℃ conditions in the presence of sulphide produced small amounts of B800-820 LH2 complex type, and a B800-850 complex. In the presence of thiosulphate cells cultured under low light 40℃ growth conditions produce primarily a B800-820 LH2 complex type with some B800-840h.

It is possible that the B800-840 complex types are intermediates between the B800-820 and B800-850 LH2 complex types. The isosbestic points observed vary between the different LH2 complex types and suggest that there is probably more than one factor changing. This factor is the polypeptide composition and therefore there are probably several different alpha and beta peptides difference between the B800-820 and B800-850.

Table 3.3 Showing the different LH2 complex types produced by *Alc. vinosum* under different growth conditions.
The growth conditions are S: sulphide, T: thiosulphate, HL: High light, LL: Low light, 30℃ or 40℃.

Conditions / Complex	SLL30	SLL40	SHL30	SHL40	TLL30	TLL40	THL30	THL40
B800-820	Abundant	Present	Present	Absent	Abundant	Abundant	Abundant	Absent
B800-840P	Absent	Absent	Present	Absent	Absent	Present	Abundant	Absent
B800-840H	Present	Present	Present	Absent	Abundant	Abundant	Abundant	Absent
Classic B800-850	Absent	Present	Absent	Abundant	Absent	Absent	Absent	Abundant
Alternative B800-850	Absent	Abundant	Abundant	Absent	Absent	Absent	Present	Absent

3.5 The LH2 complex types

Direct comparisons of an LH2 complex type sourced from different growth conditions will determine whether they are spectroscopically identical or whether there is significant variation within an LH2 complex type.

3.5.1 B800-820 LH2 complex type

There is little variation between the B800-820 LH2 complex type produced under TLL30, SLL30, THL30, and TLL40 growth conditions (Figure 3.28). The B800-820 LH2 complex type from these growth conditions produce Qy peaks that centre at 796 nm and 802 nm with a shoulder at ~ 818 nm. The Qx peak observed is broader than those observed in other LH2 complex types. The broadening of the Qx peak observed in the SDCG absorption spectrum in section 3.3.1 relates to the B800-820 LH2 complex type, as it is observed in the absorption spectra of purified complexes.

The shoulder at ~818 nm is most distinct in the B800-820 from TLL30 growth (Figure 3.28 pink) conditions than the B800-820 LH2 complex from SLL30. The B800-820 produced under SLL30 (Figure 3.28 cyan), THL30 (Figure 3.28 red) and TLL40 (Figure 3.28 purple) produce a near negligible shoulder at ~818 nm, and the B800-820 from SLL30 appears to have a more pronounced hump at ~ 840 nm. The intensity of the B800 peak of the B800-820 from TLL40 and THL30 is slightly higher than that of the complexes produced under LL30 conditions.

The carotenoid composition varies to a small degree depending on the growth conditions the B800-820 complex type was produced under. The blue-most carotenoid absorption shoulder varies between ~ 461 nm (THL30), ~ 460 nm (T/SLL30), and ~463 nm (TLL40). The main peak centres at either 488.5 ± 0.5 nm (THL30), 489 ± 0.5 nm (TLL30 and TLL40), and 489.5 ± 0.5 nm (SLL30). The red-most absorption shoulder produces the most variability, producing higher intensity absorption shoulders at ~ 510 ±2 nm from TLL40 and TLL30 growth conditions than the absorption measured from SLL30 and THL30 conditions (522 nm and 525 ±0.5 nm respectively).

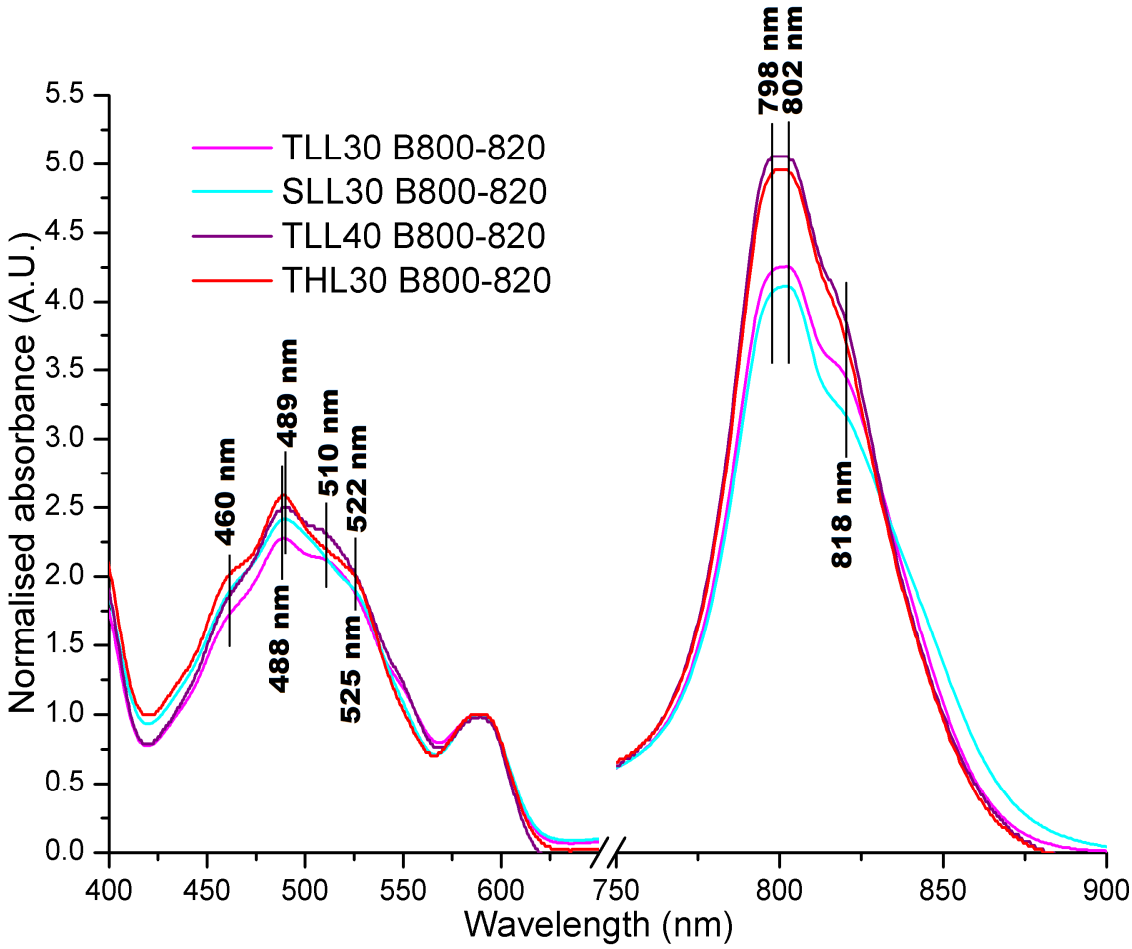

Figure 3.28 Normalised absorption spectra of the purified B800-820 LH2 complex type in 0.02 % DDM produced from four different growth conditions, TLL30 (pink), SLL30 (cyan), THL30 (red), and TLL40 (purple) by *Alc. vinosum*.
The different growth conditions of *Alc. vinosum* were in the presence of thiosulphate (T) or sulphide (S), under low light (LL) or high light (HL), at 30 ℃ or 40 ℃. LH2 complex types were separated from each other using anion exchange chromatography before absorption spectra were recorded. The purified B800-820 LH2 complex produces Qy peaks at 798 nm, 802 nm, with a shoulder at ~ 818. The carotenoid peaks show the largest variation between the different purified B800-820 LH2 complex types. The carotenoid peak of the B800-820 (TLL30) centres at 489 nm with two shoulders at ~ 460 nm and 510 nm. The carotenoid peak of the B800-820 (SLL30) centres at 489 nm with two shoulders at ~ 460 nm and 522 nm. The carotenoid peak of the B800-820 (TLL40) centres at 489 nm with two shoulders at ~ 460 nm and 510 nm. The carotenoid peak of the B800-820 (THL30) centres at 488 nm with two shoulders at ~ 461 nm and ~525 nm. The B800-820 from TLL40 and THL30 growth conditions produce the highest intensity B800 peaks and the least defined ~818 nm shoulder.

3.5.2 **B800-840 LH2 complex types**

The B800-840 LH2 complex type falls into two sub-types, the B800-840 hump and the B800-840 peak distinguished by whether the peak at 840 nm ±2 nm is a distinct peak or a hump. The B800-840 hump is produced in small quantities under low light conditions, and in significant quantities under high light conditions at 30 ℃. The B800-840p is predominantly produced under high light 30 growth conditions in the presence of thiosulphate.

Figure 3.29 shows the absorption spectra of the different B800-840h identified after anion exchange chromatography purification. The amount of B800-840h produced under most growth conditions is not of a sufficient amount to pool for further purification but is adequate for comparison. All the B800-840h produced by cells in the presence of thiosulphate produce B800-840h that has a higher 796 nm peak relative to the 803 (Figure 3.29 pink, purple, and red), while this is reversed in the case of the B800-840h produced by cells grown in the presence of sulphide (Figure 3.29 cyan and green). The B800-840h LH2 complex from all growth conditions produce a hump in the absorbance at ~ 840 nm to different degrees, and a broad Qx peak. This may imply that this complex is a variation on the B800-820 complex type.

There are pronounced differences in the carotenoids present in the B800-840h sourced from *Alc. vinosum* grown under different growth conditions. The absorption peak centres at 489 nm. The carotenoid composition of the B800-840h from TLL30 and TLL40 produce higher intensity shoulders at ~ 510 nm and a shoulder at ~ 550 nm, and the ~ 460 nm shoulder is reduced. This contrasts with the B800-840h produced under THL30, SLL30 and SHL30 growth conditions which produce clear shoulders at ~ 522 nm and ~460 nm.

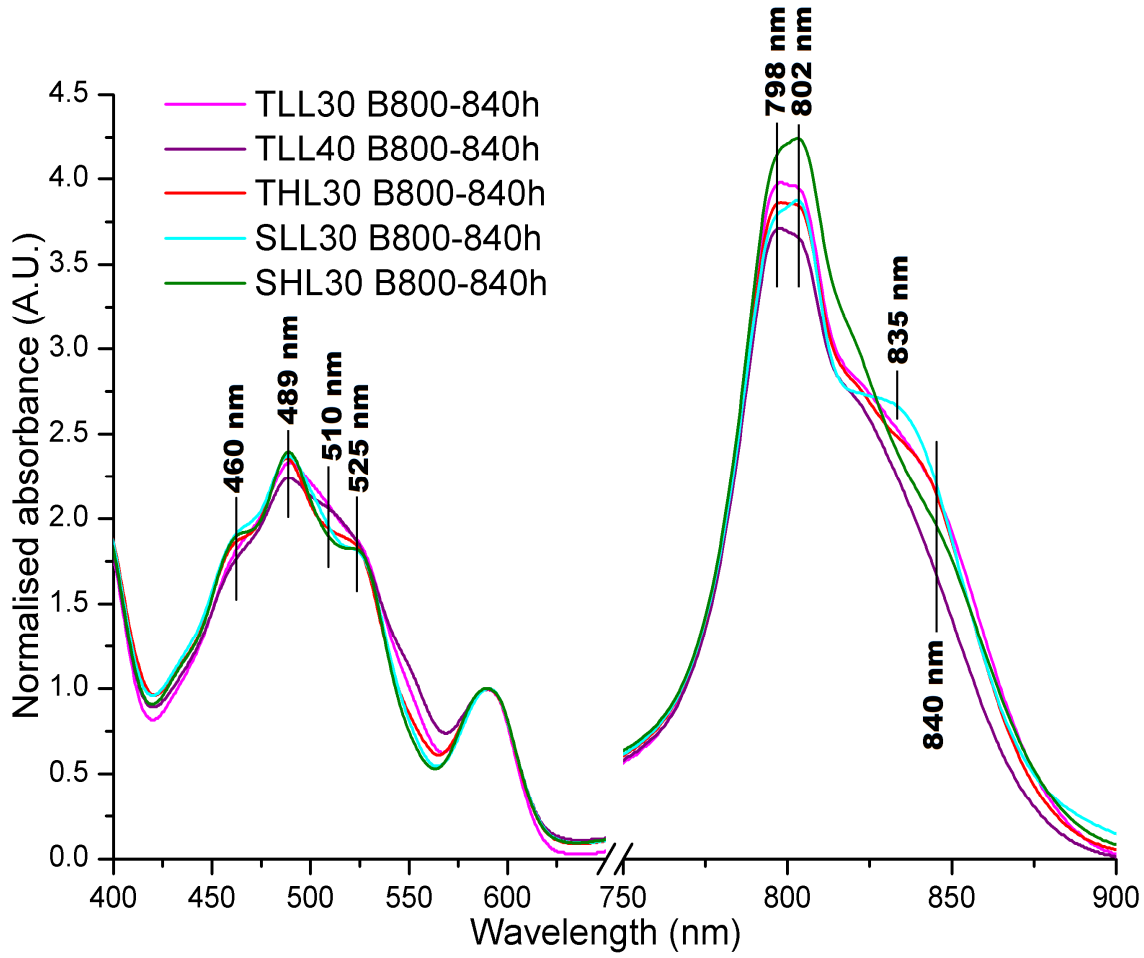

Figure 3.29 Normalised absorption spectra of the purified B800-840h LH2 complex type in 0.02 % DDM produced from four different growth conditions, TLL30 (pink), SLL30 (cyan), THL30 (red), SHL30 (green), and TLL40 (purple) by *Alc. vinosum*.
The different growth conditions of *Alc. vinosum* were in the presence of thiosulphate (T) or sulphide (S), under low light (LL) or high light (HL), at 30 ℃ or 40 ℃. LH2 complex types were separated from each other using anion exchange chromatography before absorption spectra were recorded. The purified B800-840h LH2 complex produces Qy peaks at 798 nm, 802 nm, with a shoulder that varies between 835- 840 nm. The carotenoid peaks show the largest variation between the different purified B800-840h LH2 complex types. The B800-840h carotenoid peaks centre at 489 nm but the intensity of the absorption shoulders varies. The B800-840h (TLL30) produces a low shoulder at ~ 460 nm and higher intensity shoulder at ~ 510 nm. The B800-840h LH2 complex type from TLL40 growth conditions produces a low intensity shoulder at ~ 460 nm and a higher intensity shoulder at ~ 515 nm. The B800-840h LH2 complex type from THL30 conditions produces a shoulder at ~ 460 nm and a shoulder of equal intensity at ~ 525 nm. The B800-840h LH2 complex type from SLL30 produces a shoulder at ~ 460 nm and a shoulder of lower intensity at ~ 525 nm. The B800-840h LH2 complex type from SHL30 produces a shoulder at ~ 460 nm and a shoulder of lower intensity at ~ 525 nm.

The carotenoid composition of the B800-840h from TLL30 and TLL40 growth conditions produce higher intensity shoulders at ~ 510 nm and a shoulder at ~ 550 nm, and the ~ 460 nm shoulder is reduced. This contrasts with the B800-840h produced under THL30, SLL30 and SHL30 growth conditions which produce clear shoulders at ~ 522 nm and ~460 nm.

Few differences are observed between the absorption spectra of the purified B800-840p LH2 complex type and the B800-840h, other than the presence or absence of a defined peak. In the split B800 peaks, as observed in some of the B800-840h complexes, the 796 nm peak is higher relative to the 803 nm absorption. Figure 3.30 contrasts the two types of B800-840 after gel filtration showing the differences in B800 peak intensity and the “B850-like” maxima. Most obviously the B800-840h doesn’t have a dip in absorbance at ~ 820 nm (Figure 3.30 dark yellow) unlike the B800-840p (Figure 3.30 red) and there is a small difference in the breadth of the Qx peaks.

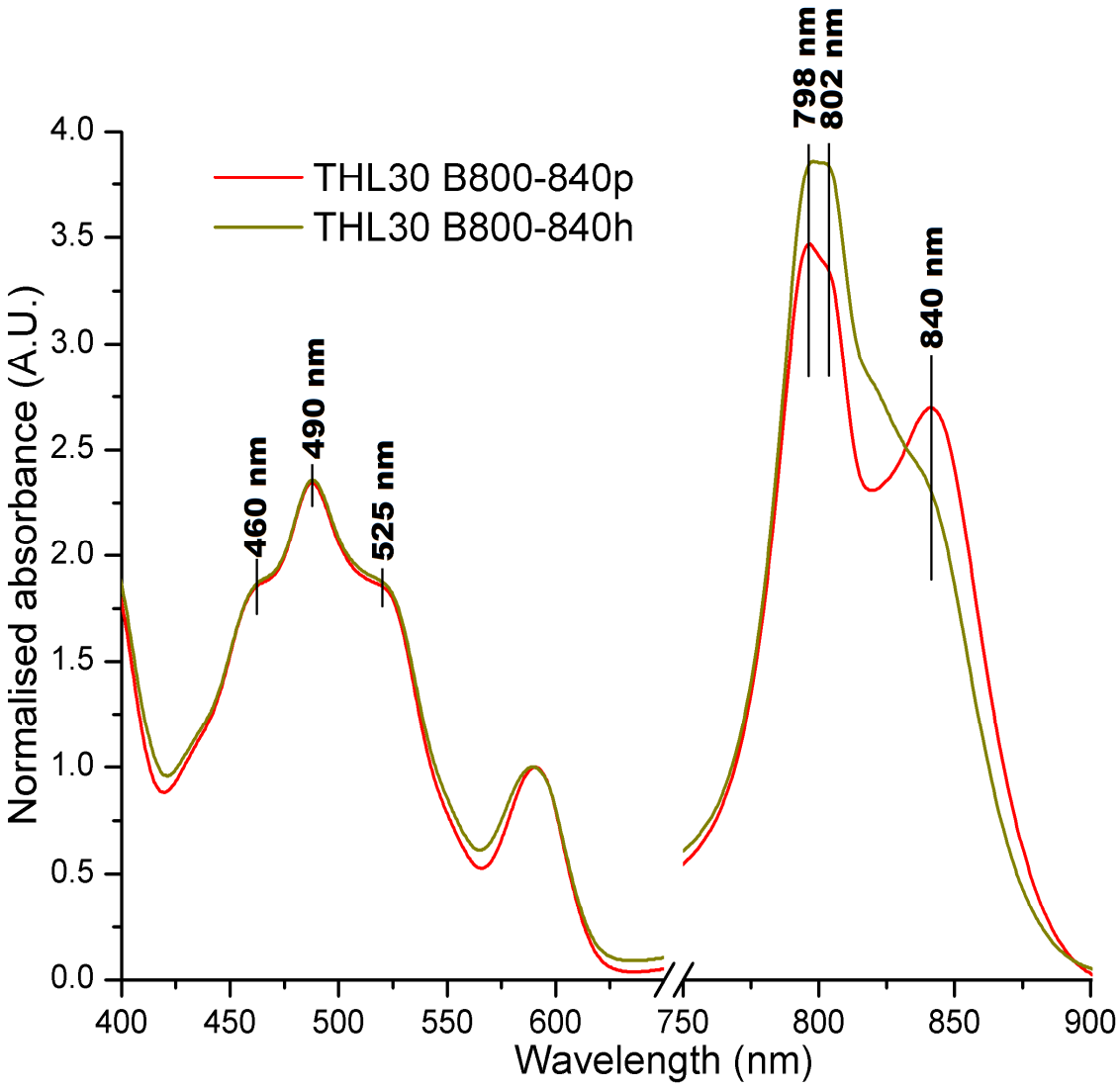

Figure 3.30 Normalised absorption spectra of the purified B800-840h (dark yellow) and B800-840p (red) LH2 complex types in 0.02 % DDM produced under thiosulphate (T), high light (HL), at 30 ℃ (THL30).
LH2 complex types were separated from each other using anion exchange chromatography before absorption spectra were recorded. The purified B800-840h LH2 complex produces Qy peaks at 798 nm, 802 nm, with a shoulder that varies between 835- 840 nm. The purified B800-840p LH2 complex produces Qy peaks at 798 nm, 802 nm, and 840 nm. There is no variation between the carotenoid peaks of the purified B800-840 LH2 complex types. The B800 peak produced by the B800-840h LH2 produces a distinct peak at 798 nm with the 802 nm showing as a shoulder. The B800-840p LH2 produces a flat B800 peak with both the 798 nm and 802 nm peaks of equal intensity.

The B800-840p was used as the standard B800-840 LH2 complex in further characterisation as it was found in highest abundance with the least variation between preparations.

3.5.3 **B800-850 LH2 complex type**

Figure 3.31 shows the comparison of the absorption spectra of the different B800-850 LH2 complex types from *Alc. vinosum* grown under different

conditions. The B800-850 LH2 complexes produced under high light, 40℃ growth conditions seem to be nearly identical regardless of sulphur source, producing maxima at 796 nm, 802 nm and 847 ± 1 nm (Figure 3.31 dark red and black). This LH2 complex type is most similar to the standard B800-850 *Rsp. acidophila* model, bar the split B800 peak. When this complex is contrasted with the B800-850 complexes produced under THL30 and SHL30 there is a variation in the intensity of the "B850-like" BChl Qy peak (Figure 3.31 green and red). The red-most Qy peak is of equal or lower intensity relative to the B800 peaks present in these complexes. For this reason the B800-850 complexes produced under these growth conditions were dubbed the alternative B800-850 (B800-850a), and the more standard-like B800-850 from the high light conditions is the classic B800-850 (B800-850c).

Under SLL40 growth conditions *Alc. vinosum* produces a B800-850 LH2 complex type that produces maxima at 848 nm, 796 nm and 802 nm (Figure 3.31 blue). This B800-850 has a lower intensity "B850-like" Qy peak than the B800-850c complexes produced under high light 40℃ conditions but it is still of a higher intensity than the B800 absorption peaks. The B800-850a LH2 complex type produced under THL30 growth conditions produces a "B850-like" Qy peak at 845 ±1 nm, with a more intense 796 nm peak relative to the 802 nm peak (Figure 3.31 red). It is observed that the "B850-like" Qy peak is of a lower intensity relative to the B800 peaks therefore establishing this as an alternative B800-850. The peak of the B800-850a produced under SHL30 growth conditions centres at 848 ± 1 nm and there is a large difference between the intensity of the B800 and "B850-like" peaks. Between the two B800 peaks, the 796 nm absorption peak is of a much higher intensity relative to the 802 nm. The Qx peak produced by these complex types is a distinct peak at 588 nm.

The carotenoid composition between the complexes produced under the different growth conditions shows small to negligible variation. The main carotenoid peak centres at ~ 460 ± 0.5 nm, 487.5 nm ± 0.5 nm, and ~522 ± 0.5 nm in the B800-850c from THL40 conditions. The B800-850c from SHL40 produces carotenoid peaks at ~ 463 ± 0.5 nm, 488 ± 0.5 nm, and ~523.5 ± 0.5 nm. The B800-850a complex type from THL30 produces carotenoid peaks at ~461 ± 1 nm, 487 ± 0.5 nm, and ~520 ± 0.5 nm. The B800-850a produced under SHL30 growth

conditions produce carotenoid peaks at ~463 ± 1 nm, 488 ± 0.5 nm, and ~521 ± 1 nm. The carotenoid peaks produced by the B800-850 from SLL40 condition centre at ~ 463 nm, 488.5, and ~ 521.5 ± 0.5 nm.

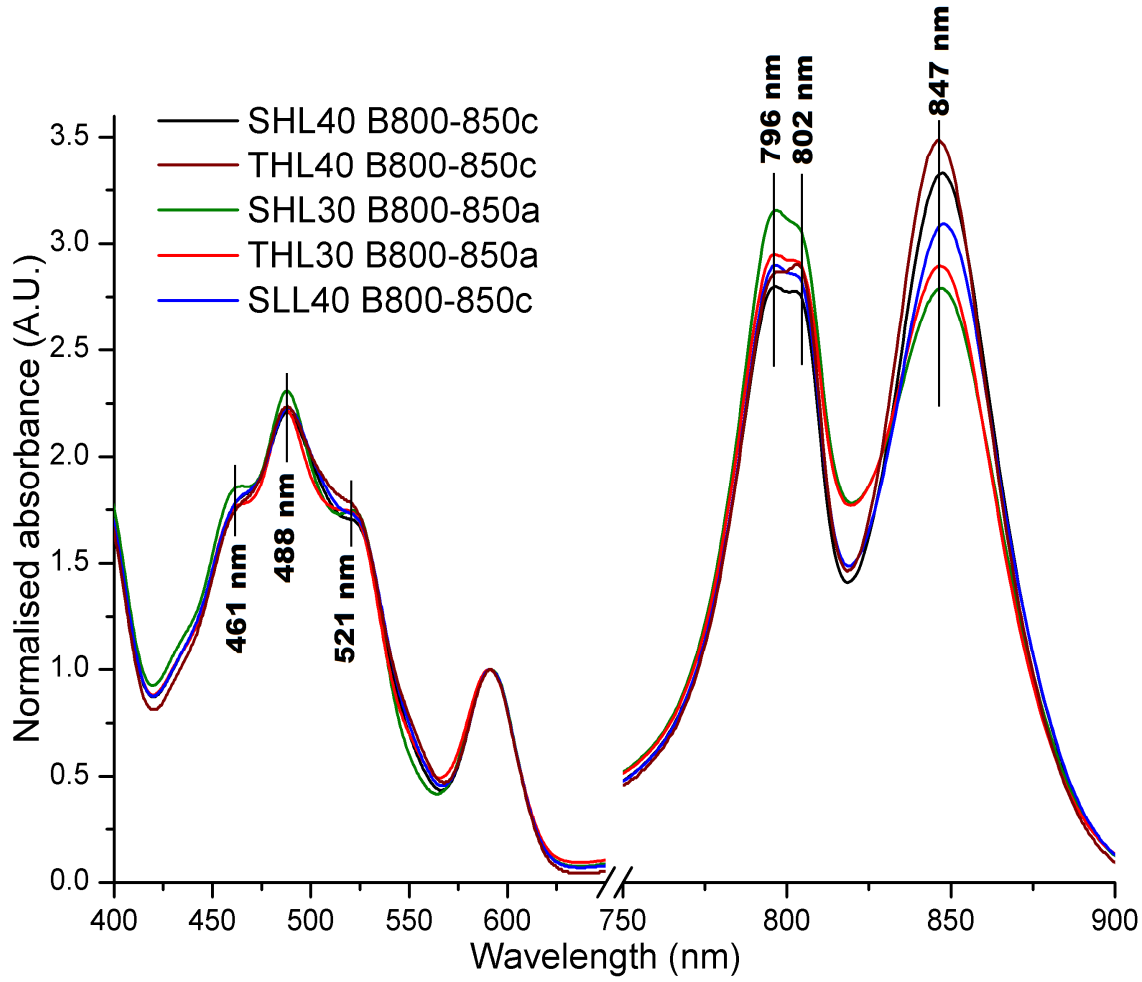

Figure 3.31 Normalised absorption spectra of the purified B800-850 LH2 complex type in 0.02 % DDM produced from five different growth conditions, SHL40 (black), THL40 (dark red), SHL30 (green), THL30 (red), and SLL40 (blue) by *Alc. vinosum*.
The different growth conditions of *Alc. vinosum* were in the presence of thiosulphate (T) or sulphide (S), under low light (LL) or high light (HL), at 30 ℃ or 40 ℃. LH2 complex types were separated from each other using anion exchange chromatography before absorption spectra were recorded. The NIR Qy absorption peaks of the B800-850 produced under all growth conditions centre at 796 nm, 802 nm, and 847 ± 1 nm. Two types of B800-850 LH2 complex were identified, the classic B800-850 (B800-850c) and the alternative B800-850 (B800-850a). The distinction between the two B800-850 LH2 complex types derives from the ratio of the B800 peak to the B850 peak. If the B800 peak is higher than the B850 peak the LH2 complex is identified as a B800-850a and if the B850 peak is higher than the B800 peak, as observed in most other well characterised B800-850 LH2 complex types, it is identified as a B800-850c LH2 complex type. There is variation in the B800 peaks as to which is of a higher intensity, in the B800-850 LH2 complexes from SLL40, SHL30 and THL30 growth conditions the 796 nm peak is the highest intensity. In the B800-850 from THL40 and SHL40 growth conditions the peaks are of similar intensities. The carotenoid peaks centre at 488 nm with two absorption shoulders at ~ 461 nm ± 1 nm and ~ 521 ± 1 nm. There is only a small level of variation in the carotenoid peaks between the different B800-850 LH2 complexes.

As the carotenoid composition within the different complex types varies it is clear that while there may be biases towards the incorporation of certain

carotenoids into LH2 complex types, this is not the only factor affecting the carotenoid complement. This will probably be due to what carotenoids are most abundant during LH2 formation, which will be regulated by different factors within the growth conditions.

3.6 Gel filtration

Molecular sieve chromatography was used after complexes were purified via anion exchange chromatography to desalt the sample and remove any residual impurities according to their size (as outlined in Methods and Materials section 2.5.4). All LH2 complex types eluted between 92 ± 1 ml. As there was only small variation (± 0.5 ml) between the elution of the LH2 complex types the hypothesis is that the different complex types are approximately the same ring size (Figure 3.32).

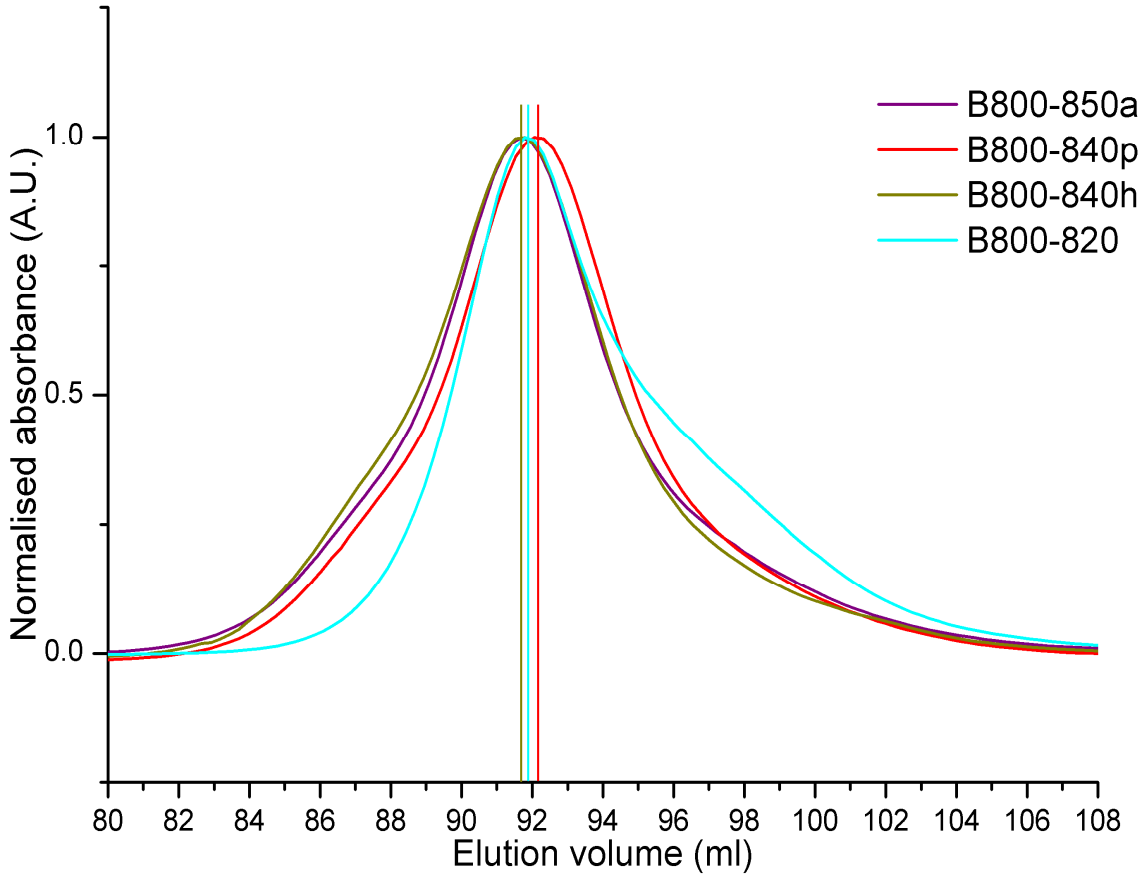

Figure 3.32 Normalised size exclusion chromatogram of the B800-820, B800-840h, B800-840p, B800-850a, and B800-850c LH2 complex types from *Alc. vinosum*.
Elution was monitored using the A_{280} and all complexes eluted at 92 ± 1 ml as shown by the red (B800-840p elution), cyan (B800-820 elution), and dark yellow lines (B800-840h and B800-850a elution).

3.6.1 **Comparison of the room, and low temperature, absorption spectra of the purified LH2 complex types of *Alc. vinosum*.**

The differences in the Qy absorption bands are most pronounced when the different LH2 complex types are directly compared (Figure 3.33). The B800 absorption band is at the highest intensity in the B800-820 complex (Figure 3.33 red), being approximately four times larger than the Qx peak. The intensity of the B800 band is lower in the B800-840p (Figure 3.33 dark yellow) and B800-850a (Figure 3.33 green) until it is at the lowest intensity in the B800-850c LH2 complex type (Figure 3.33 purple) where it is only approximately three times the intensity of the Qx peak. The broad nature of the Qx peak observed in the B800-820 complex types is more obvious in comparison to the other complexes and may be a product of increased or different heterogeneity of the B800-820 complex type.

From the absorption spectra, the carotenoid composition of the B800-850 and B800-840 complex types appears to be similar while the B800-820 has a more pronounced ~ 510 nm absorption shoulder and the main peak is red shifted to 491 nm. This variation in the carotenoid content may be due to both growth conditions and the LH2 complex type the carotenoid is incorporated into.

There are several isosbestic points observed between these LH2 complex types. The B800-820 intercepts the B800-850c absorption at 832 nm, the B800-850a at 832.5 nm and the B800-840p at 830 nm. The B800-850c intercepts the B800-850a at 831 nm and the B800-840p at 836 nm. The B800-850a intercepts the B800-840p at 842 nm.

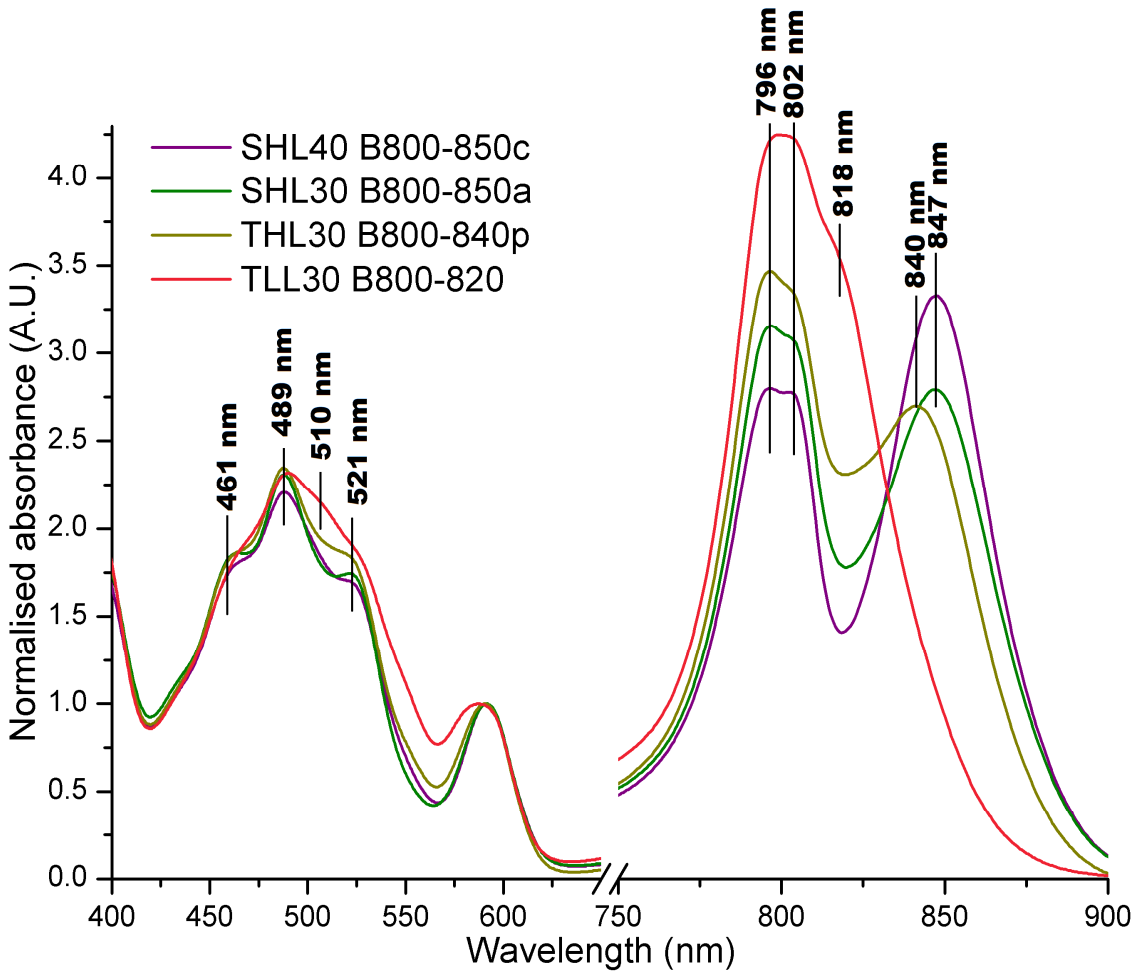

Figure 3.33 Normalised absorption spectra of the purified B800-850c (purple), B800-850a (green), B800-840p (dark yellow), and the B800-820 (red) LH2 complex types from *Alc. vinosum*.
LH2 complex types were sourced from *Alc. vinosum* grown under different growth conditions, in the presence of thiosulphate (T) or sulphide (S), under low light (LL) or high light (HL), at 30 ℃ or 40 ℃. The NIR Qy absorption peaks of the B800-850c and B800-850a centres at 796 nm, 802 nm, and 847 ± 1 nm. The NIR Qy absorption peaks of the B800-840p centres at 796 nm, 802 nm, and 840 ± 2 nm. The NIR Qy absorption peaks of the B800-820 centres at 796 nm, 802 nm, and shoulder at ~ 818 ± 1 nm. The B800-850c and B800-850a carotenoid peaks centre at 488 nm with two absorption shoulders at ~ 461 nm ± 1 nm and ~ 521 ± 1 nm. The B800-820 LH2 carotenoid peaks centre at 489 nm and two shoulders at ~460 and ~510 nm. The B800-840p LH2 carotenoid peaks centre at 489 nm and two shoulders at ~460 and ~520 nm. Some variation is observed in the carotenoid content between the different complex types. There are isosbestic points between the B800-820 LH2 complex and the B800-840 LH2 complex (830 nm), and the B800-850a (832.5 nm), and the B800-850c (832 nm). There are isosbestic points between the B800-840p and the B800-850a (842 nm) and the B800-850c (836 nm). The isosbestic point between the B800-850a and B800-850c centres at 831 nm. There is 1-2 nm difference in the isosbestic points between the B800-820 and B800-850 LH2 complex types, but the difference between the B800-840p and the other complex types are most substantial (up to 10 nm).

Absorption spectra were recorded at 77 K (Figure 3.34), with the help of Darek Niedzwiedzki, to aid in the analysis of the isolated complexes. As observed in the SDCG and membranes, the B800 BChl produce a split peak at 792 nm and 804 nm in the B800-850a LH2 complex type (Figure 3.34 purple) from SHL30 conditions and the B800-840p LH2 complex type (Figure 3.34 dark yellow) from

THL30 growth conditions. The split B800 peak centres at 794 nm and 803 nm in the B800-820 LH2 complex type (Figure 3.34 red) from TLL30 growth conditions. The split peaks of the B800-820 produce less of a dip at ~ 800 nm than observed in the B800-840p and B800-850a complex types. The Qy peak of the B800-820 LH2 complex type sourced from TLL30 growth conditions produces a Qy peak that red-shifts to 820-821 nm with a shoulder at ~ 850 nm. The Qx peak produced varies from the other LH2 complex types as it produces a broad peak with an apex at 590 nm. The absorption peaks of the carotenoids observed at low temperature centre at 469-470 nm, 489-490 nm, 503 nm, 528 nm, and 545 nm.

The "B850-like" Qy peak of the B800-840p is observed at 861-862 nm with a small peak at 818 nm. These peaks correspond closely to the absorption bands observed in the SDCG, supporting the findings that the B800-840p is the primary LH2 complex type produced under THL30 growth conditions. The decrease in absorbance of the peak at 818 nm and the increase of absorbance at 861 nm in the purified sample illustrates the removal of the B800-820 LH2 complex type and enrichment for the B800-840p LH2 complex type. The 818 nm peak is still present in the purified sample of B800-840p, which may mean there is residual B800-820 complex present or that some of the peptides that comprise the B800-840p complex are the same as those found in the B800-820. The Qx peak narrows in the purification from SDCG supporting the concept that the broad Qx peak is attributed to the B800-820 LH2 complex type. The carotenoid bands present in the B800-840p complex centre at 466 nm, 488 nm, 501-502 nm, 527 nm, and 546 nm.

In the low temperature absorption of the B800-850a, the "B850-like" Qy maximum centres at 867 in the SDCG and is red-shifted to 869 nm in the purified B800-850a LH2 complex type. The shoulder at ~ 818 nm and the 804 nm split peak are reduced in intensity after purification as these shifts are due to the removal of the B800-820 LH2 complex type. There is a possible shoulder still present at ~818 nm, which may imply B800-820 contamination or the presence of peptides typically found in the B800-820 LH2 complex type in the B800-850a LH2 complex. The carotenoid maxima present in the B800-850a from SHL30 growth

conditions centre at 485 nm, 489 nm, ~ 502 nm, and 528 nm. All data are summarised in table 3.4.

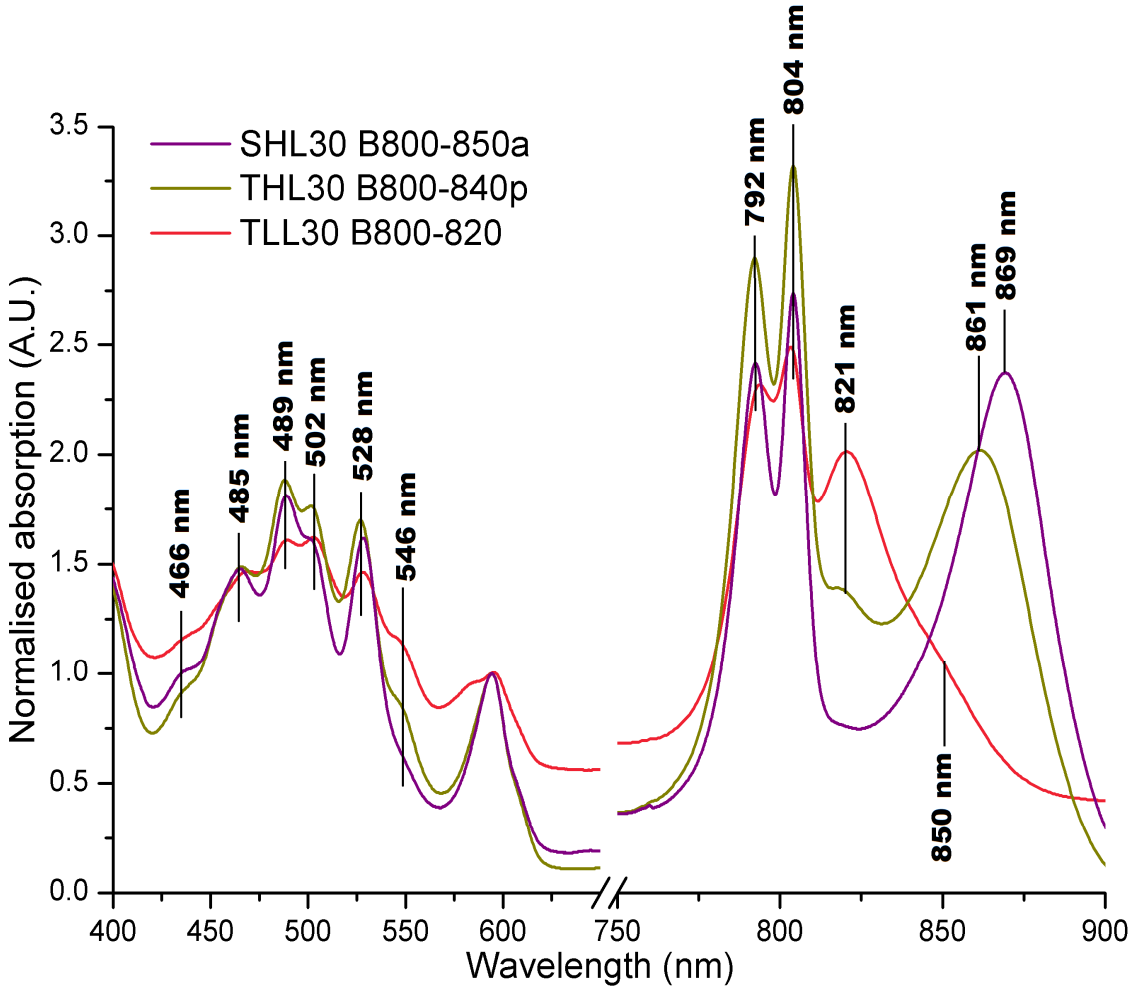

Figure 3.34 Normalised low temperature (77 K) absorption spectra of the purified B800-850a (purple), B800-840p (dark yellow), and the B800-820 (red) LH2 complex types in 0.02 % DDM from *Alc. vinosum*.
LH2 complex types were sourced from *Alc. vinosum* grown under different growth conditions, in the presence of thiosulphate (T) or sulphide (S), under low light (LL) or high light (HL), at 30 ℃. The NIR Qy absorption peaks of the B800-850a centres at 792 nm, 804 nm, and 869 nm. The NIR Qy absorption peaks of the B800-840p centres at 792 nm, 804 nm, 818 nm and 861 nm. The NIR Qy absorption peaks of the B800-820 centres at 794 nm, 803 nm, 821 nm, and shoulder at ~ 850 nm. The B800-850a carotenoid peaks centre at 485 nm, 489 nm, 528 nm with an absorption shoulder at ~ 502 nm. The B800-840p LH2 carotenoid peaks centre at 466 nm, 488 nm, 501 nm, 527 nm and 546 nm. The B800-820 LH2 carotenoid peaks centre at 470 nm, 490 nm, 503 nm, 528 nm, and 545 nm. The B800-840p produces the highest intensity B800 peaks while the B800-820 LH2 complex produces the lowest intensity B800 peaks. As the red-most Qy peak shifts to the blue through the B800-840p and B800-820 LH2 complexes there is an increase in the intensity of the 818 nm peak. The carotenoid peaks observed are in similar positions but vary in intensity, which may indicate differences in carotenoid composition.

Table 3.4 Showing the Qy peaks of LH2 complex types produced by *Alc. vinosum* under different growth conditions at room temperature (RT) and the 77K absorption spectra (LT) of the B800-850a, B800-840p and B800-820 from SHL30, THL30 and TLL30 respectively.
Alc. vinosum growth conditions are S: sulphide, T: thiosulphate, HL: High light, LL: Low light, 30℃ or 40℃.

	Qy maxima (RT)	B800-850	B800-840p	B800-840h	B800-820	LT
SHL40	B800 Qy_B(nm)	798	NA	NA	NA	NA
	Qy_R (nm)	802				
	B850 Qy (nm)	847 ±1				
	Carotenoid peaks	~463 ±0.5 488 ±0.5 ~523.5 ±0.5				
THL40	B800 Qy_B(nm)	798	NA	NA	NA	NA
	Qy_R (nm)	802				
	B850 Qy (nm)	846.5 ±1				
	Carotenoid peaks	~460.7 ±0.5 487.5 ±0.5 ~522.5 ±0.5				
SHL30	B800 Qy_B(nm)	798	NA	NA	798	792
	Qy_R (nm)	802			802	804
	B850 Qy (nm)	848 ± 1			~ 818	869
	Carotenoid peaks	~463.5 ±1 488 ~521	NA	NA	~463 488 ~521	485 489 ~502 528
THL30	B800 Qy_B(nm)	798	798	798	798	792
	Qy_R (nm)	802	802	802	802	804
	B850 Qy (nm)	846 ±1	840 ±1	~ 840	~ 818	861-862/818
	Carotenoid peaks	~461 ±1 487 ~520 ±0.5	~461 ±1 487 ±0.5 ~521 ±1	~461 ±1 487 ±0.5 ~521 ±1	~461 ±0.5 488.5 ~522	466 488 501-502 527 546
SLL40	B800 Qy_B(nm)	798	NA	NA	798	NA
	Qy_R (nm)	802			802	
	B850 Qy (nm)	848 ±1			~ 818	
	Carotenoid peaks	~463 488.5 ~522			~460 489 ~510 ~520	
TLL40	B800 Qy_B(nm)	NA	798	798	798	NA
	Qy_R (nm)		802	802	802	
	B850 Qy (nm)		840 ±1	~ 840	818-819	
	Carotenoid peaks		~461 488.5 ~520	~460 489 ~508 ~525	~460 489 ~510 525	
SLL30	B800 Qy_B(nm)	NA	NA	798	798	NA
	Qy_R (nm)			802	802	
	B850 Qy (nm)				818-819	
	Carotenoid peaks			~463 488.5 ~525	~ 463 ±1 490 ~525 ±0.5	
TLL30	B800 Qy_B(nm)	NA	798	798	798	794
	Qy_R (nm)		802	802	802	803
	B850 Qy (nm)		840 ±1	~ 840	818-819	820-821
	Carotenoid peaks		~460 488 ~519	~460 488 ~520	~460.5 ±1 489±0.5 ~510±2 ~550	469-470 489-490 503 528 545

3.7 Summary

Alc. vinosum is able to limit the LH2 complex types it produces depending on the growth and nutrient conditions it is grown under. The LH2 complex types were separated from the LH1/RC "core" complex via sucrose density centrifugation, and anion exchange chromatography was used to partially fractionate the LH2 complex mix and enrich for certain LH2 complex types. The LH2 complex types identified were the B800-820, B800-840, and the B800-850 LH2 complex types. The B800-840 and B800-850 LH2 complex types were identified as having LH2 complex subtypes; the B800-840h and B800-840p LH2 complex subtypes, and the B800-850a and B800-850c LH2 complex subtypes. Both B800-850 LH2 subtypes eluted at the same salt concentration, as do both B800-840 LH2 subtypes, indicating similar levels of anionic interaction with the resin. This suggests small changes in the peptide composition between these different LH2 complex subtypes that affects the NIR absorption peaks without dramatically changing the anionic interactions. In cases such as the B800-840 LH2 complex type, a lack of resolution of the LH2 complex type mix makes it difficult to make any definite analyses.

Absorption spectra of the fractions collected between the main elution peaks during anion exchange chromatography indicate that there are intermediate LH2 complexes formed between the different LH2 complex types. This suggests that the LH2 complexes of *Alc. vinosum* form a continuum however there are preferential LH2 complex types that are created in larger quantities, identified as the B800-820, B800-840, and the B800-850 LH2 complex types.

Isosbestic points in the NIR absorption spectra of the different LH2 complex types indicate that there are several elements that change across the different LH2 complex types. This indicates that there are multiple polypeptides different between the different LH2 complex types however this requires further analysis to identify the different polypeptides present within all of the LH2 complex types (see Chapter 4).

Low temperature spectroscopy successfully identified peaks that were hidden at room temperature. This was useful in elucidating the potential mix of LH2

complexes during purification as well as the purity of the LH2 complex mix after purification.

The observations on the carotenoid mix imply that there are several factors at play as to the carotenoid composition of an LH2 complex type. In the case of the differences observed in the carotenoid mix present in the LH2 complexes produced under the low light, 40℃ growth conditions it appears unlikely that carotenoid incorporation is solely due to the carotenoids present during LH2 formation. This may indicate that certain complex types preferentially incorporate certain carotenoids. However, in complexes such as the B800-820 from THL30 growth conditions the carotenoid complement appears to be closer to that observed in the B800-840 and B800-850 LH2 complex types. This suggests that the different complex types are not entirely restricted in the carotenoids they can incorporate, although there may be a bias under some growth conditions. The carotenoid complement requires more in depth study that will be covered in chapter four.

Chapter 4- Characterisation of the purified LH2 complex types of *Allochromatium (Alc.) vinosum.*

4.1 Introduction

The aim of the following work was to characterise the LH2 complexes in light of the current structural (62, 63, 99) and genomic understanding (10, 157) to start to explore the basis of the differences between the LH2 complex types produced by *Alc. vinosum*. This will help in illuminating whether these complexes are distinct from each other or form a continuum.

Questions surrounding the basis of the variation between the different LH2 complex types produced by *Alc. vinosum* can be answered now that they can be separated effectively, as outlined in Chapter three. From observations made in Chapter three, the basis of the variation between the NIR absorption of the different LH2 complex types is due to differences in the peptides that 'tune' the spectra of the pigments rather than dramatic changes in the composition of the pigments themselves. The different LH2 complex types of *Alc. vinosum* are most probably heterogeneous, meaning they contain non-identical heterodimer subunits, like those identified from other species such as *Rps. palustris* (101, 103, 104). This highlights the need to identify which of the *puc* genes of *Alc. vinosum* (10) contribute to each LH2 complex type. The changes in the carotenoid composition between the different LH2 complex types was analysed to determine the basis of the variation in the green region of the absorption spectra.

Unlike the LH2 complex types of most other purple photosynthetic bacteria, the LH2 complexes from *Alc. vinosum* produce a split B800 peak (72, 141). Earlier work (113) found that both peaks of the split B800 are produced from within the same LH2 complex. How two different B800 populations exist within the same ring is part of the investigation covered in the following chapter.

4.2 Polypeptide analysis of the different LH2 complexes of *Alc. vinosum*

As outlined in the Introduction section 1.2.3.2, the structural determination of the LH2 complex (62, 72, 80, 99, 154) confirmed that the LH2 complex is formed from oligomerised heterodimer subunits consisting of alpha and beta polypeptides that hold the pigments in position. The position of the NIR absorption peak, the Qy band, of the BChl was determined to be due to a combination of the site energy and pigment-pigment interactions. The site energy is the protein-pigment interactions and binding, through the direct binding of the central Mg^{2+} ion and H bonding on the rest of the chlorin ring. Further 'tuning' occurs if the BChl are excitonically coupled, as this red-shifts the Qy peak (34).

The importance of the polypeptides in 'tuning' the BChl absorption necessitates a thorough analysis of the protein complement of the different LH2 complex types of *Alc. vinosum*. The annotation of the genome of *Alc. vinosum* (10) identified six possible *puc* gene pairs (Figure 4.1), which can code for the alpha and beta peptides. It is unknown whether all or only some of these genes are transcribed, and if so, under what growth conditions they contribute to the LH2 complexes.

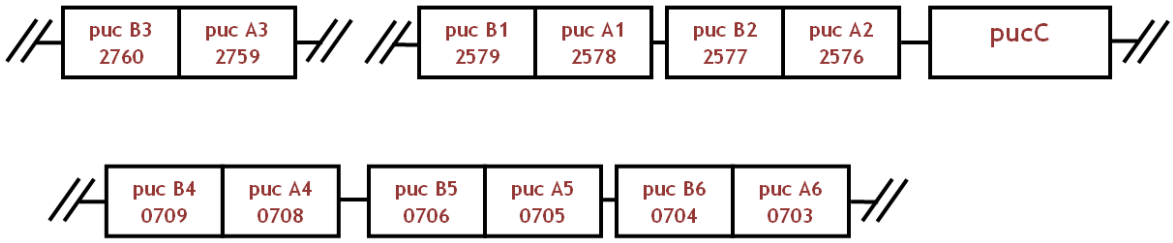

Figure 4.1Schematic diagram showing the *puc* operons of the purple photosynthetic bacterium *Alc. vinosum.*
A total of six *puc* operons have been identified (10) that code for the alpha and beta polypeptides that form the LH2. The *puc* genes are named A1, B1, A2, B2, A3, B3, A4, B4, A5, B5, A6, and B6. There are three clusters of *puc* operons that sit in proximity to each other, the 4, 5 and 6 operons and the 1 and 2 operons. Operon 3 sits separately from the other *puc* operons.

4.2.1 Sequence alignments and preliminary peptide allocations to different LH2 complex types

The protein sequences of the potential different peptides from *Alc. vinosum* can be extrapolated from the identified *puc* genes (10) and then compared to peptides from well characterised LH2 complexes. The shift in the absorption band of the LH2 complex is due to a change in the site energy of the BChl due to differences in H bond donor residues on the alpha peptide. On the basis of changes in these key H bonding residues it may be possible to predict the peptides that are present in the different complex types from *Alc. vinosum*.

The structures of both the B800-850 and B800-820 from *Rps. acidophila* have been determined, and the basis of the shift from 850 nm to 820 nm is understood (Introduction section 1.2.3.3). Some strains of *Phs. molischianum* are also able to produce a B800-820 LH2 complex type (94, 95). The structure of the B800-850 LH2 from *Phs. molischianum* (80) is known to differ in the binding of the B800 from the B800-850 from *Rps. acidophila*. Even without a B800-820 LH2 complex structure from *Phs. molischianum*, a comparison between the alpha peptides of the two LH2 complex types from *Phs. molischianum* may indicate the structural basis of the shift from B850 to B820, if it is similar to that observed in the LH2 from *Rps. acidophila*.

Figure 4.2 shows the twelve potential alpha and beta peptides from *Alc. vinosum* aligned to the BChl coordinating histidine of the B800-850 and B800-820 alpha and betas from *Rps. acidophila* 10050 (B800-850), *Rps. acidophila* 7050 (B800-820), and *Phs. molischianum* DSM 120. The LH2 complexes from both *Rps. acidophila* and *Phs. molischianum* bind the B800 BChl with different residues on the alpha peptide. The LH2 complex from *Phs. molischianum* binds the B800 BChl via an aspartic acid residue at position 6 while *Rps. acidophila* binds using a formyl-methionine residue at position 1 (Figure 4.2 red). Analysis of the alpha peptides of *Alc. vinosum* found there are two aspartic acid residues at the position of the B800 BChl binding site in peptides A2, A3, and A6, and one aspartic residue on the A1, A4 and A5 peptides. This suggests that the B800 binding may be is akin to that observed in the LH2 of *Phs. molischianum* but there is variation in the B800 binding site between the peptides. The conserved

histidine on both the alpha and beta that coordinates with the central ion of the dimerised BChl is observed in all the residues aligned (Figure 4.2 red H).

The residues known to 'tune' the position of the Qy absorption peak of the excitonically coupled BChl in the B800-850 and B800-820 LH2 complex types from *Rps. acidophila* are highlighted blue in figure 4.2. These residues are the αTrp45 (position +14 relative to the conserved αHis) and αTyr44 (position +14) that form H bonds with the B850 BChl, and the αTyr41 (position +10) that forms an H bond with the B820 BChl. In the B800-850 LH2 complex from *Phs. molischianum* it is the αTrp45 (position +11) and ßTrp44 (position + 27) residues that bind the B850 BChl in the (Figure 4.2 purple). The basis for the difference between the B800-850 and B800-820 LH2 complex types from *Phs. molischianum* is the same as the complexes from *Rps. acidophila* (80), as the tryptophan is replaced by a phenylalanine on the alpha peptide of the B800-820 LH2 complex. Analysis of the beta peptides from *Alc. vinosum* shows the ßTrp is present at position + 27 relative to the conserved ßHis, indicating that all of the beta peptides are able to form an H bond with the B850 BChl. The LH2 beta peptides of *Alc. vinosum* show high conservation showing the highest homology between the peptides of *Alc. vinosum* and the beta peptides of *Phs. molischianum* (Figure 4.2).

Analysis of the alpha peptides from *Alc. vinosum* identified the αTrp at the position + 11 relative to the conserved αHis in peptides A1 and A6, and at position + 10 in peptides A2 and A3. This indicates that these peptides are all able form H bonds to BChl and are potential B800-850 peptides. Peptides A2, A3, and A6 all contain amino acids that could be alternative H bond donors; peptides A2 and A3 contain a Gln at position +11, and the A6 peptide contains a Thr at position + 10. This suggests that there may be competition for H bond formation with the BChl.

The A5 peptide has a substitution of the tryptophan to phenylalanine at position + 11, which is observed in the B800-820 alpha peptides of both *Phs. molischianum* and *Rps. acidophila*. This suggests that the A5 peptide may be found in the B800-820 LH2 complex type. The A4 peptide contains an αTrp at position + 8 that indicates it may be unable to form an H bond to the B850 BChl, which suggests that the A4 peptide may also be found in the B800-820 LH2

complex type. However, there doesn't appear to be a suitable tyrosine present on either the A5 or A4 peptides that may form an H bond with the BChl in place of the tryptophan. At the equivalent position +10 relative to the αHis there are glycine residues on all of the alpha peptide of *Alc. vinosum* bar the A6 alpha peptide, which contains a threonine. This may indicate that, assuming all of the peptides are expressed and incorporated into LH2 complexes, the B850 binding by the A1, A2, A3, A4, and A5 peptides require the flexibility or lack of steric hindrance facilitated by a glycine residue.

Without a B800-840 LH2 complex structure to compare with, it is difficult to preliminarily determine which peptides are expressed in this complex. The B800-840 may be a mix of B800-850 and B800-820 peptides or may include other peptides that can form different H bonds than those from the known structures.

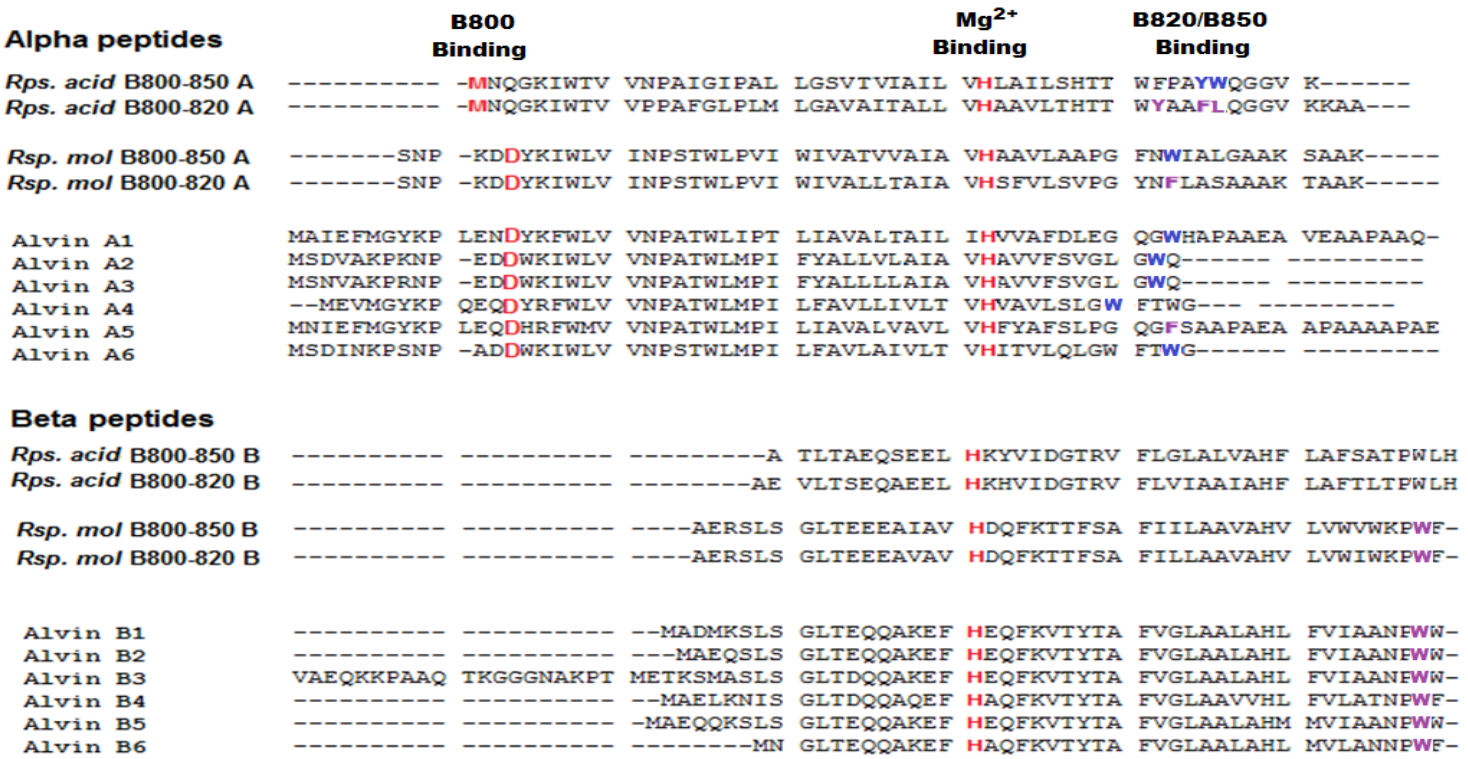

Figure 4.2 Alignments of the alpha and beta peptides from *Rps. acidophila* 7050 B800-820 LH2 complex type, *Rps. acidophila* 10050 B800-850 LH2 complex type, *Rsp. molischianum* DSM120 B800-850 LH2 complex type, *Rsp. molischianum* DSM 120 mutant B800-820 (94), and *Alc. vinosum* stain D identified by (10).

The alignments were made to the conserved B850 coordinating histidine on both the alpha and beta peptides (red H). The B800 BChl binding of the *Rps. acidophila* peptides is the methionine at position 1 of the alpha peptide (red M) however the B800 BChl binding of the *Rsp. molischianum* peptides is an aspartic acid residue (red D). In the alpha peptides of *Alc. vinosum* there are two aspartic acid residues present in A2, A3, and A6. In peptides A1, A4, and A5 there is only one aspartic acid residue. The B850 BChl binding site of the *Rps. acidophila* alpha peptide is a αTyr44 and αTrp45 (blue Y and W). However, the B820 BChl binding site of the *Rps. acidophila* alpha peptide is a αTyr41 (blue Y). The B850 BChl binding site of the *Rsp. molischianum* is a αTrp45 and βTrp44 (purple W). However, the B820 BChl binding site of the *Rsp. molischianum* alpha peptide is a substitution of the αTrp45 to αPhe45 (purple F). The αTrp45 is conserved across the A1, A2, A3, A4, and A6 alpha peptides of *Alc. vinosum.* The α45 is substituted for a phenylalanine in the A5 peptide. The βTrp44 residue is conserved throughout all the beta peptides aligned. Alignments were performed using the ClustelW, in BioEdit (158).

4.2.2 SDS PAGE of membranes, crude LH2 extracts and purified LH2 complexes from *Alc .vinosum*

SDS PAGE is able to separate the different alpha and beta peptides present in the different LH2 complex types of *Alc. vinosum*, and potentially differentiate between the different types of alpha and beta. The separated peptides can then be analysed by mass spectroscopy to confirm the identities of the peptides and determine the composition of the different LH2 complexes. An AnykD (Biorad) gel was used to effectively separate small molecular weight proteins, although the exact percentage of the gels is an industry secret.

The proteins present within the membranes from *Alc. vinosum* grown under different growth conditions were separated by SDS PAGE (as described in Methods and Materials section 2.8). The growth conditions tested were *Alc. vinosum* grown in the presence of thiosulphate or sulphide under high light (HL) or low light (LL) intensity, at 30℃ or 40℃. The membrane samples were heated to 70℃ for 20 min with additional 2 % SDS to better denature the complexes present. SimplyBlue Safestain (Life Technologies) was found to bind the light-harvesting peptides sufficiently to visualise them on the finished gel. The resulting gel (Figure 4.3) showed multiple bands of different molecular weights due to the large amount of proteins present within the membranes. There appeared several resolved bands <10 kDa that could be the alpha and beta peptides from both the LH1 and LH2 light-harvesting complexes. The RC peptides, L, M, and H, are also present but due to their hydrophobic nature the molecular weights observed are not correct. The bands that correspond to the RC peptides are found at ~ 20 kDa (L subunit), ~ 25 kDa (M subunit), and <37 kDa (H subunit) as observed in previous work (159).

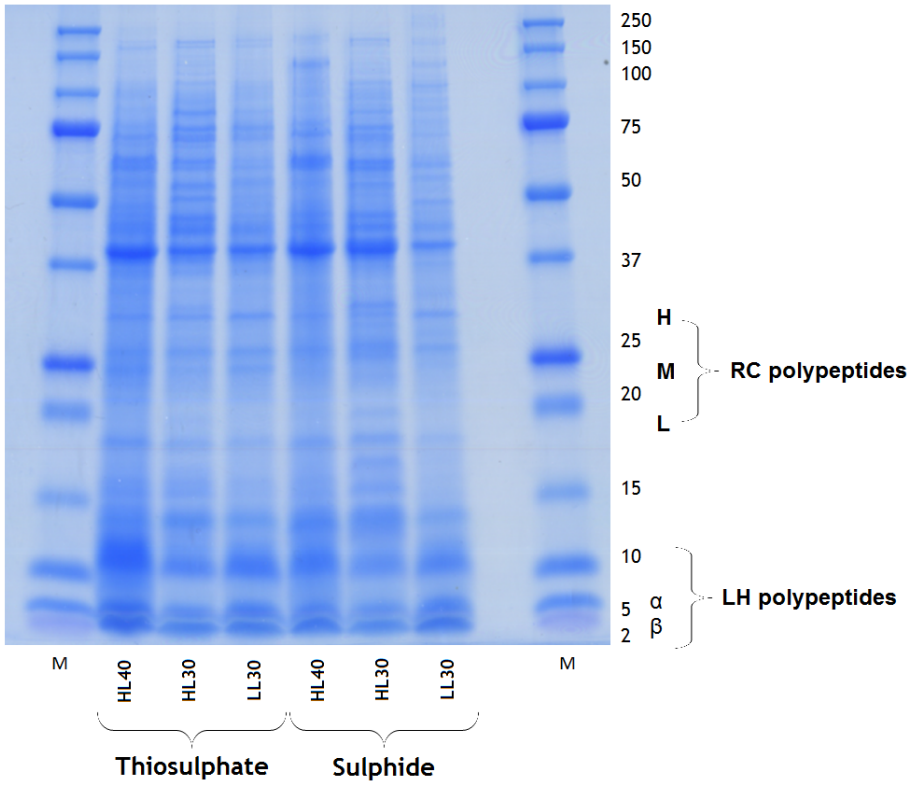

Figure 4.3 SDS PAGE of membranes prepared from *Alc. vinosum* cells grown under different growth and nutrient conditions.
Alc. vinosum cells were grown in the presence of thiosulphate (T) or sulphide (S), under high light (HL) or low light (LL) intensity, at 30 ℃. There are multiple protein bands were observed on the gel due to the abundance of proteins present within the membranes. The three bands under 10 kDa are the alpha and beta light-harvesting peptides of the LH2 and LH1 complex types. The RC peptides are expected to be the bands in the range between 20-37 kDa found in each sample, these were observed at 20 kDa (L subunit), ~ 25 kDa (M subunit), and <37 kDa (H subunit) as observed previously (159).

The crude LH2 fraction was extracted from the different membrane samples, using sucrose density centrifugation, and analysed by SDS PAGE (as outlined in Methods and Materials section 2.8) (Figure 4.4). Sucrose density centrifugation separates the LH2 from the proteins and complexes of different density. Figure 4.4 shows the reduction in non-light-harvesting proteins present after sucrose density centrifugation, although there are still residual impurities present in the sample observed in the gel. There are bands at ~ 10 kDa in fractions produced under all growth conditions and a ~15 kDa band in the HL40 and HL30 samples not observed in the fractions grown under low light. There are low levels of proteins between 37 – 50 kDa in all fractions that don't appear to be linked to a light-harvesting complex. The two bands below 10 kDa previously observed in the SDS PAGE of separated membrane proteins are the most abundant proteins present in the crude LH2 fraction. This suggests that these are the alpha and beta proteins from the LH2 complex types; the heavier band is the larger alphas

and the lighter band is the betas. The presence of only two bands shows that the separation of the different alpha types and beta types has not been achieved.

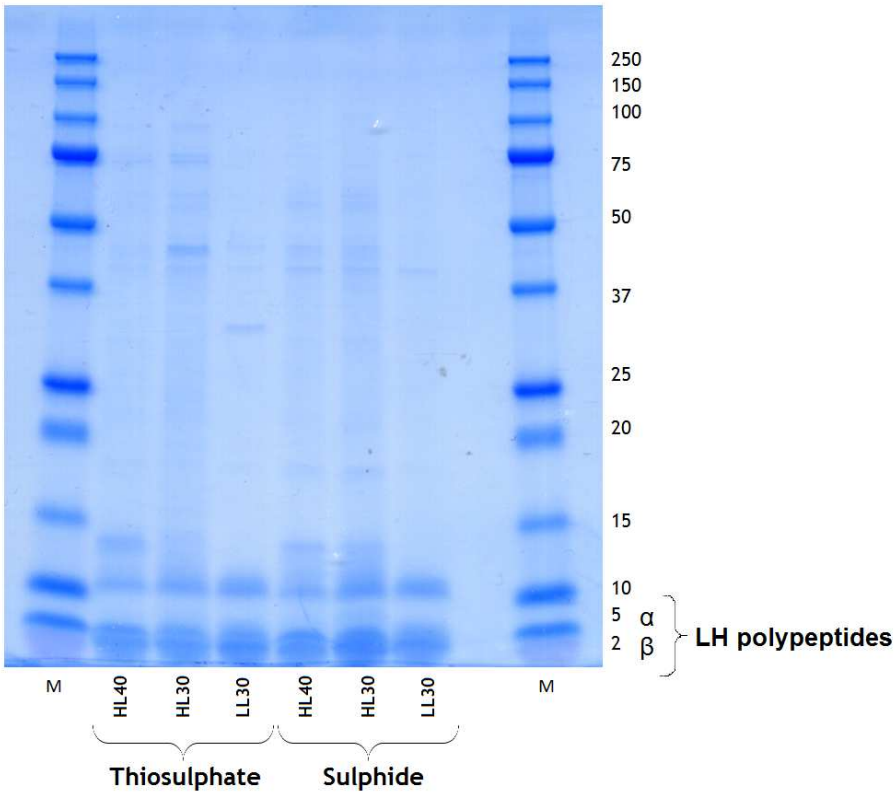

Figure 4.4 SDS PAGE of the crude LH2 fraction prepared from *Alc. vinosum* grown under different growth and nutrient conditions.
Growth conditions for *Alc. vinosum* cells were the presence of thiosulphate (T) or sulphide (S), under high light (HL) or low light (LL) intensity, at 30℃. Bands observed between 15 – 100 kDa are residual impurities. The bands at 2 and 5 kDa are postulated as the alpha and beta peptides from the LH2 complex.

The LH2 complex types were further purified via anion exchange and size exclusion chromatographies before they were analysed using an AnykD SDS PAGE and stained with SimplyBlue SafeStain (Figure 4.5). The three bands <10 kDa were well resolved but without any further separation of alpha and beta bands, suggesting that SDS PAGE is not effective at separating the different alpha and betas from each other. The band at 2 kDa has faded strongly after purification, and the band at ~ 10 kDa is still present. The band at ~ 10 kDa may be a SDS induced dimer, but only mass spec of this band would confirm this.

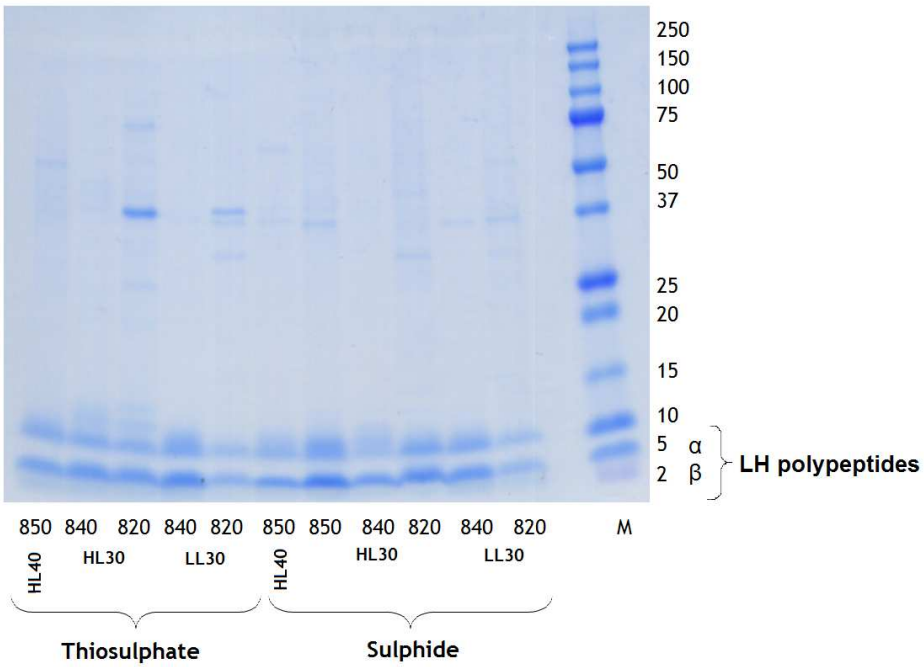

Figure 4.5 SDS PAGE of purified LH2 complexes prepared from *Alc. vinosum* grown under different growth and nutrient conditions.
Growth conditions for *Alc. vinosum* cells were the presence of thiosulphate (T) or sulphide (S), under high light (HL) or low light (LL) intensity, at 30℃. Bands <10 kDa are postulated the light-harvesting peptides. The band at ~ 2 kDa, most probably the beta peptides, is highly faded in comparison with previous gels. The 5 kDa band is still observed and is most probably the alpha peptides. The band at 10 kDa is still present potentially indicating a SDS induced dimer or contamination.

4.2.3 Polypeptide composition analysis using HPLC and MALDI-TOF of THL40 B800-850c, THL30 B800-840p, and TLL30 B800-820

SDS PAGE was insufficient in resolving the different peptides and so techniques with higher accuracy and sensitivity such as high pressure liquid chromatography (HPLC) and Matrix-assisted laser desorption/ionisation time of flight mass spectroscopy (MALDI-TOF) were implemented. Our team, headed by Dr Anne-Marie Carey, collaborated with Dr Zheng-Yu Wang-Otomo to separate the peptides from the three main complex types of *Alc. vinosum* using reverse phase HPLC. This was followed by MALDI-TOF mass spectroscopy as described by (160). The B800-820, B800-840p, and B800-850c LH2 complex types from *Alc. vinosum* were purified in 0.02 % DDM (as outlined in Methods and Materials section 2.5.1) and sent to Dr Wang-Otomo to determine the peptides present and the percentage composition within the different LH2 complex types. Peptides from the LH1 from *Rsp. rubrum* and LH2 from *Tch. tepidum* were used as standards to allow the percentage composition to be determined. Composition was calculated

from peak areas and extinction coefficients deduced from the tryptophan and tyrosine residues present in each peptide. In the case of some of the peptides that could not be separated by HPLC due to similarities in their hydrophobicity, the TOF/MS spectral counts were used to find relative abundance.

The peptides present in the B800-820, B800-840p and B800-850c were identified (Figure 4.6) and quantified as shown in table 4.1. The HPLC elution profiles of the LH2 complex types from *Alc. vinosum* showed the first peptides to elute were the beta peptides followed by the alpha peptides, as observed with LH1 and LH2 complexes from other bacteria (120, 160-163). The ß2 and ß3 peptides were not able to be separated using this technique due to close homology between them, and they presented as a single peak on chromatograms.

The α4 and ß4 peptides were not observed in any of the complexes measured. The A1 peptides observed tended to be one of six truncated versions, dubbed A1-1, A1-2, A1-3, A1-4, A1-5, and A1-6. The A5 also was observed in two truncated versions.

It was found that the B800-850c complex shows the lowest level of heterogeneity and is made up of three types of alpha and beta; α1, α2, α3, ß1, ß2, and ß3. The different types of beta seem to be in similar amounts with the ß1 and ß2 at 37 and 39 % respectively and the ß3 with 24 %, while the primary alpha present by far is the α1, making up 56 % of the alpha peptide composition. The α2 and α3 make up the rest of the B800-850 α composition at 27 and 17 % respectively. The peptides of the B800-850 LH2 complex type eluted as follows ß1, followed jointly by the ß2 and ß3. The α 1 peptide and the different modifications of alpha1, A1-1, A1-2, A1-3, A1-4, A1-5, and A1-5, eluted before the other alphas present, which were the α2 and α3 in this case.

The B800-840p contains the same peptides as the B800-850c but with the addition of the α6 and ß5. The α1 and α2 peptides are in similar quantities (35 % and 32 %) followed by the α6 at 23 % and the α3 was at the lowest amount at 10 %. Not all truncations of α1 were observed. The ß5 makes up half of all the ß peptides present, followed by the ß2 (21 %), ß1 (18 %) and ß3 (11 %). The peptides eluted in the following order ß5, ß1, ß2+3 followed by α1-1, α1-5, and α1-6. The α2 and α6 peptides eluted closely together followed by the α3.

In the B800-820 the highest level of heterogeneity is observed with four α peptides, and five ß peptides expressed. Unlike in the B800-850 and B800-840p no α1 peptide was observed, but α5 and ß6 were found to be present when they were not found in either of the two other complex types. The primary αlpha peptide present is the α6 (39 %) followed by the α5 (30 %), α3 (16 %) and finally the α2 (15 %). The primary ß peptide is the ß5 (49 %) followed by the ß6 (16 %), ß1 (12 %), ß2 (12 %), and the ß3 (11 %). The peptides eluted as follows ß6, ß5, ß1, ß2+3, α5, α6, α2 and then α3. Percent composition of the peptides in the different LH2 complexes is summarised in table 4.1.

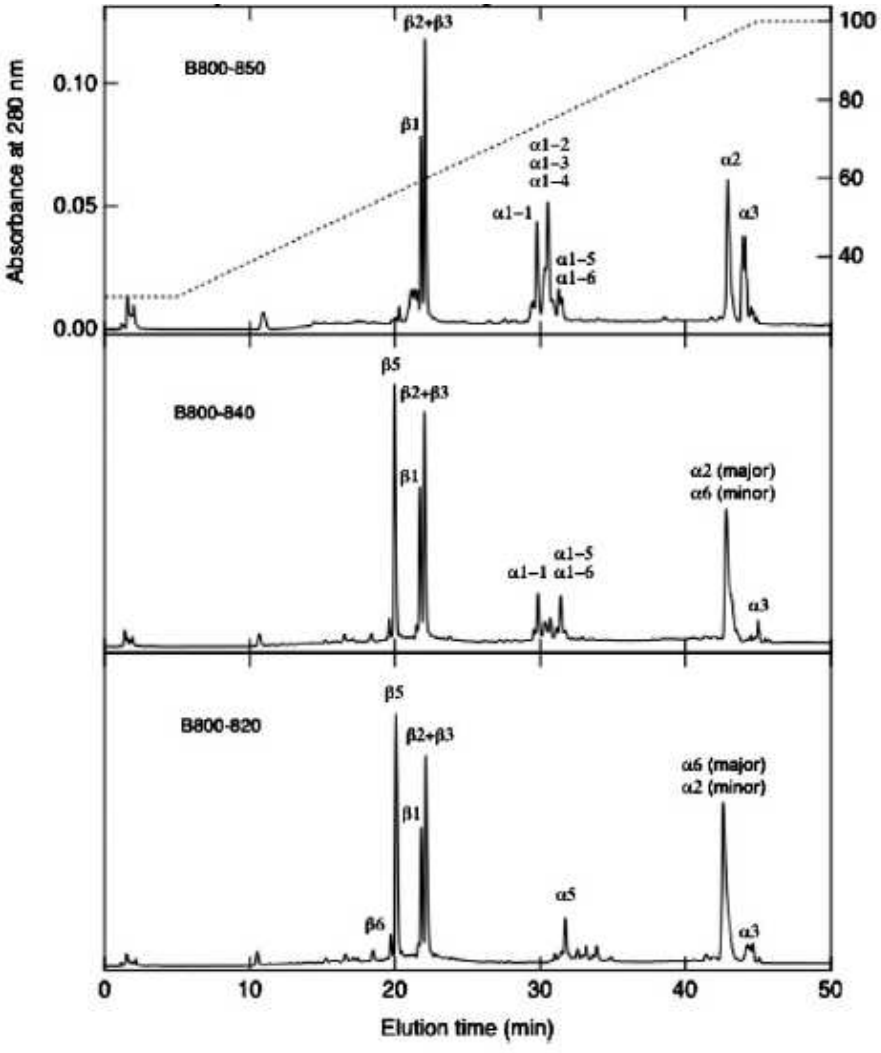

Figure 4.6 HPLC chromatograms of the peptide complement from the B800-850c, B800-840p, and B800-820 LH2 complex types from *Alc. vinosum* as published in Carey et al, 2014 (164). The B800-850c LH2 complex consisted of truncated A1 peptides (A1-1, A1-2, A1-3, A1-4, A1-5, and A1-6), and the A2, A3, B1, B2, and B3 peptides. The B2 and B3 peptides elute as a single peak due to high sequence identity. The B800-840p LH2 complex consisted of truncated A1 peptides (A1-1, A1-5, and A1-6), and the A2, A3, A6, B1, B2, B3, and B5 peptides. The A2 and A6 peptides eluted together as do the B2 and B3 peptides due to high sequence identity. The B800-820 LH2 complex consisted of A2, A3, A6, B1, B2, B3, B5 and B6 peptides. The A2 and A6 peptides eluted together as do the B2 and B3 peptides due to high sequence identity.

Table 4.1 The α and β peptide percentage composition with ± 5 % error of the B800-850c, B800-840p, and B800-820 complex types produced by *Alc. vinosum*.
As published in (164).

	α 1	α 2	α 3	α 5	α 6	β 1	β 2	β 3	β 5	β 6
B800-850c	56	27	17	-	-	37	39	24	-	-
B800-840p	35	32	10	-	23	18	21	11	50	-
B800-820	-	15	16	30	39	12	12	11	49	16

Some of the structural elements highlighted previously as corresponding to the B800-820 or B800-850 like complexes can now be compared with the actual peptide complement. The A1 and A6 peptides both contain a Trp at position + 11 relative to the conserved αHis however only the A1 was found in the B800-850 LH2 complex, while the A6 is found in both the B800-820 and B800-840 LH2 complex types. This suggests that the presence of a threonine in place of a glycine affects the ability of the Trp to H bond either through steric hindrance or competition for H bond formation. This would mean an H bond from the Threonine, or a complete lack of H bond, changes the orientation of the C3-acetyl and blue shift the wavelength at which the Qy band absorbs. The A2 and A3 peptides were found in all of the LH2 complex types and contain a Trp at position +10 indicating that amino acids at this position are still able to form H bonds with the B850 BChl, however they do not convey a specific spectral shift. The A4 was not observed within any of the LH2 complex types. The A5 peptide was found exclusively within the B800-820 LH2 complex type, confirming that the substitution of the phenylalanine for the tryptophan at the position +11 creates a blue shift as observed in other species. The convoluted peptide composition of the different LH2 complex types suggests that residues at position +10/+11 are important in the 'tuning' of LH2 complex absorption spectra in *Alc. vinosum* but are not the only factor.

There is high conservation between the different beta peptides however the different LH2 complex types contain different beta compositions. Full operons

are not translated together as the B800-840 LH2 complex contains the A6 peptide and not the B6, which are contained within the same operon.

The peptides of the LH2 of *Alc. vinosum* had several modifications identified. All of the alpha peptides bar α5 had the N terminal methionine removed and the α1 and α5 peptides had several versions due to truncation of the C terminus. This indicates that the methionine cannot be involved in the binding of the B800 BChl as observed in *Rps. acidophila*. Thus supporting the hypothesis that it is an aspartic acid residue that coordinates to the Mg^{2+} of the BChl as observed in *Phs. molischianum*. The presence of multiple truncations of the C terminus of the α1 peptide may indicate post-translational modification (160) or alternatively may be due to degradation or cleavage during the purification process. The C terminal residues are predominantly hydrophilic and most probably exist outside of the membrane structure. Structural modelling of the α1 peptides against the alpha peptides from both *Phs. molischianum* and *Rps. acidophila* using the modelling software Phyre suggests these residues are indeed external to the membrane and will be suspetible to cleavage.

The post-translational modifications of the beta peptides are N terminal methionine removal and methylation. The removal of the methionine is observed in all but the β6 peptide, and has been observed in other bacterial species (165). The beta peptides that are methylated at the N terminus are the β1, β2, and β5.

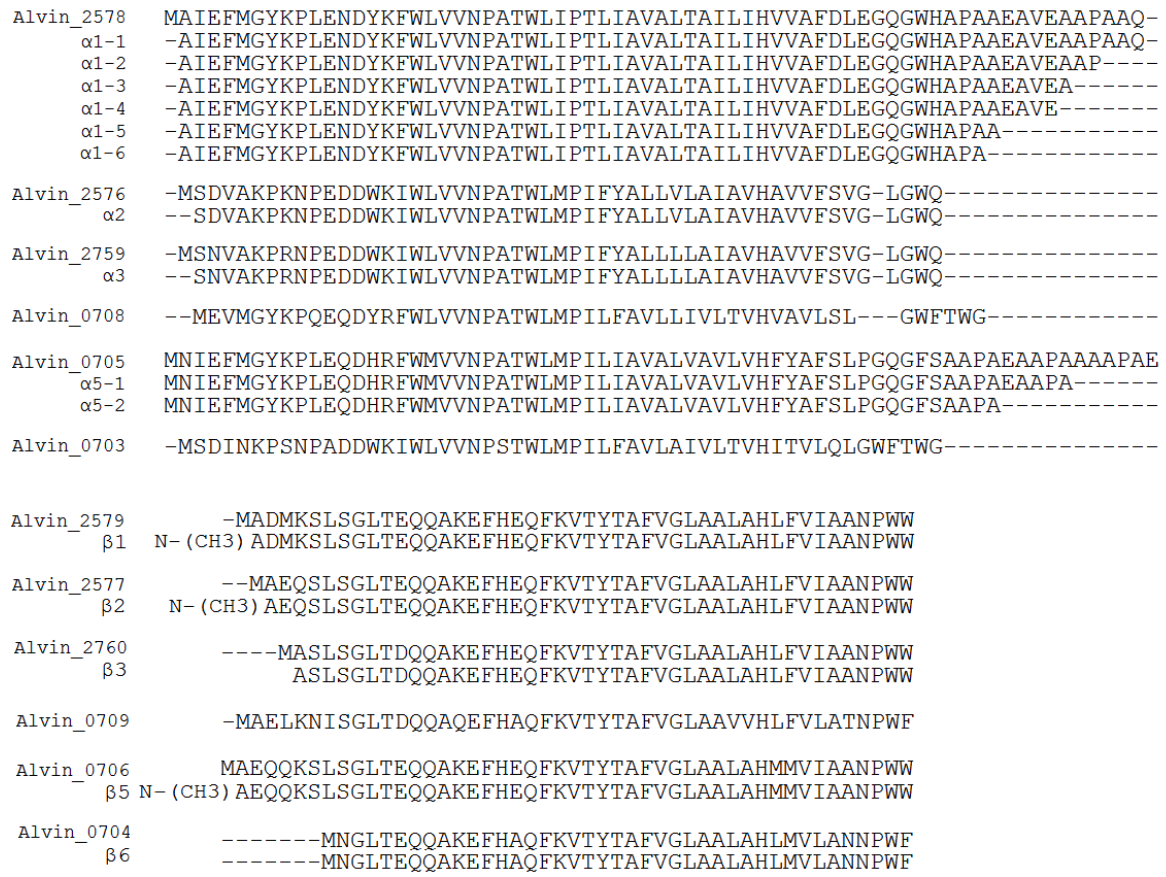

Figure 4.7 Alignments of the expected gene products of each of the *puc* genes and the peptides and their modifications identified by HPLC and MALDI-TOF.
The A1 peptide is a product of the Alvin_2578 *puc* gene and was observed as multiple c-terminal truncated versions named A1-1, A1-2, A1-3, A1-4, A1-5, and A1-6. The A2 peptide is a product of the Alvin_2576 *puc* gene and was observed with the n-terminal methionine removed. The A3 peptide is a product of the Alvin_2759 *puc* gene and was observed with the n-terminal methionine removed. The A4 peptide was not observed in any of the LH2 complexes analysed. The A5 peptide is a product of the Alvin_0705 *puc* gene and two versions were observed (A5-1 and A5-2) with the c-terminal truncations. The A6 peptide is a product of the Alvin_0703 *puc* gene and no modifications were observed. The B1 peptide is a product of the Alvin_2579 *puc* gene and was observed with the n-terminal methionine removed and methylation of the n terminus. The B2 peptide is a product of the Alvin_2577 *puc* gene and was observed with the n-terminal methionine removed and methylation of the n terminus. The B3 peptide is a product of the Alvin_2760 *puc* gene and was observed with the n-terminal methionine removed and methylation of the n terminus. The B4 peptide was not observed in any of the LH2 complexes analysed. The B5 peptide is a product of the Alvin_0706 *puc* gene and was observed with the n-terminal methionine removed and methylation of the n terminus. The B6 peptide is a product of the Alvin_0704 *puc* gene and was observed with the n-terminal methionine removed and is the only beta peptide observed that did not contain methylation of the n terminus.

4.2.4 **Polypeptide composition analysis of the B800-850a LH2 complex type**

After the work covering the main LH2 complex types was published, it was seen as prudent to further elucidate the basis of the difference between the B800-850c and the B800-850a. The B800-850a was purified and peptides extracted and

sent to Dr Bill Mullen for Tandem MS-MS (as outlined in Methods and Materials section 2.9).

The peptides identified from the B800-850a were the α1, α2, ß1, ß2, ß3, ß5 and the ß6 (Table 4.2). The ß5 peptide did not fragment well and was not identified until the threshold for peaks was lowered. The α3 peptide was not observed at all although it is present in all of the other complexes currently analysed. The absence of the α3 peptide may be due to low concentrations or loss during the extraction procedure. The use of the molecular sieve chromatography using LH60 resin could mean that any smaller molecular weight peptides could be lost if they elute simultaneously with the carotenoid and BChl pigments. The molecular weight of the α3 peptide (5760 kDa) is close to that observed for the α2 peptide (5719 kDa) (164), indicating that as the α2 peptide is observed it is unlikedly that the α3 was lost during the purification procedure. The ß6 and the ß5 peptides observed are not found in the B800-850c complex type. The ß6 peptide is only found in the B800-820 complex type and ß5 is found in both the B800-840 and B800-820 LH2 complex types. This may indicate that the differences in the absorption spectrum between the B800-850 LH2 complex types is due to differences in the binding by the beta peptides, not the just the alpha peptides. The lack of the α3 peptide may indicate that not all peptides from the B800-850a LH2 complex type were extracted or that the peptide did not fragment well.

Table 4.2 The peptides identified by tandem MS-MS mass spectroscopy from the B800-850a complex and their modifications.
* are peptides observed in some form in other LH2 complex types but with or without the modifications observed in the B800-850a LH2 complex type.

Peptide	Sequence	MH + [Da]	Modification	Observed in
A1	MAIEFMGYKPLENDYKFWLVVNPATWLIPTLIAVALTAILIHVVAFDLEGQGWHAPAAEAVEAAPAAQ	7402	none	B800-850 and B800-840p
A1-1	AIEFMGYKPLENDYKFWLVVNPATWLIPTLIAVALTAILIHVVAFDLEGQGWHAPAAEAVEAAPAAQ	7271	N/C term trunc	B800-850 and B800-840p
A1-4	AIEFMGYKPLENDYKFWLVVNPATWLIPTLIAVALTAILIHVVAFDLEGQGWHAPAAEAVE	6762	N/C term trunc	B800-850
A1-4.2	AIEFMGYKPLENDYKFWLVVNPATWLIPTLIAVALTAILIHVVAFDLEGQGWHAPAAEAV	6633	N/C term trunc	None
A1-5	AIEFMGYKPLENDYKFWLVVNPATWLIPTLIAVALTAILIHVVAFDLEGQGWHAPAA	6333	N/C term trunc	B800-850 and B800-840p
A1-6	AIEFMGYKPLENDYKFWLVVNPATWLIPTLIAVALTAILIHVVAFDLEGQGWHAPA	6262	N/C term trunc	B800-850 and B800-840p
A2	MSDVAKPKNPEDDWKIWLVVNPATWLMPIFYALLVLAIAVHAVVFSVGLGWQ	5848	N term trunc	All LH2 complexes*
	SDVAKPKNPEDDWKIWLVVNPATWLMPIFYALLVLAIAVHAVVFSVGLGWQ	5717	N/C term trunc	All LH2 complexes
B1	MADMKSLSGLTEQQAKEFHEQFKVTYTAFVGLAALAHLFVIAANPWW	5296	none	All LH2 complexes*
B2	MAEQSLSGLTEQQAKEFHEQFKVTYTAFVGLAALAHLFVIAANPWW	5179	none	All LH2 complexes*
B3	METKSMASLSGLTDQQAKEFHEQFKVTYTAFVGLAALAHLFVIAANPWW	5484	none	All LH2 complexes*
	SMASLSGLTDQQAKEFHEQFKVTYTAFVGLAALAHLFVIAANPWW	4995	N term trunc	All LH2 complexes*
	MASLSGLTDQQAKEFHEQFKVTYTAFVGLAALAHLFVIAANPWW	4907	N term trunc	All LH2 complexes*
	ASLSGLTDQQAKEFHEQFKVTYTAFVGLAALAHLFVIAANPWW	4776	N term trunc	All LH2 complexes
B5	MAEQQKSLSGLTEQQAKEFHEQFKVTYTAFVGLAALAHMMVIAANPWW	5436	none	B800-820 and B800-840p
B6	MNGLTEQQAKEFHAQFKVTYTAFVGLAALAHLMVLANNPWF	4607	none	B800-820 LH2 complex

The modifications observed for the previous peptides were not all observed in the peptides from the B800-850a. Several truncation products of the A1 peptide were observed including one not seen before. This previously unseen A1 peptide was between the A1-4 and A1-5 and so was dubbed the A1.4.2. The A1-1, A1-4, A1-4.2, and A1-6 were all observed.

4.3 Carotenoid composition

The pigment other than BChl bound within the protein scaffold, in the light-harvesting machinery of purple photosynthetic bacteria, is the carotenoid (as outlined in Introduction section 2.2.1). Previous work (11, 166) and genomic analysis (10) has established that the carotenoids that *Alc. vinosum* can synthesise are those of the spirilloxanthin pathway i.e. lycopene, rhodovibrin, anhydrorhodovibrin, spirilloxanthin, and rhodopin. Like BChl, the absorbance of the carotenoids is affected by their binding environment within the LH2 complex. The established heterogeneity of the LH2 complexes means that the carotenoids are bound within multiple different binding sites and that the absorption spectrum observed is an average of these.

The diversity of the carotenoids that *Alc. vinosum* can produce, in addition to the heterogeneity of the LH2 complex types makes deducing the carotenoid complement impossible without extracting the carotenoids.

Between the LH2 complexes of *Alc. vinosum* there is a slight colour difference between the B800-820 and B800-850 that can be observed by the human eye, wherein the B800-820 is more pink than the B800-850 LH2 complex. In room temperature absorption spectra the most pronounced difference observed between 400-600 nm is the red-most absorption shoulder at ~520 nm (Figure 4.8). The B800-820 LH2 complex produces a higher intensity peak at ~520 nm than the other LH2 complex types. Room temperature absorption spectroscopy doesn’t sufficiently resolve the absorption bands of all the carotenoids present therefore low temperature absorption spectra were acquired.

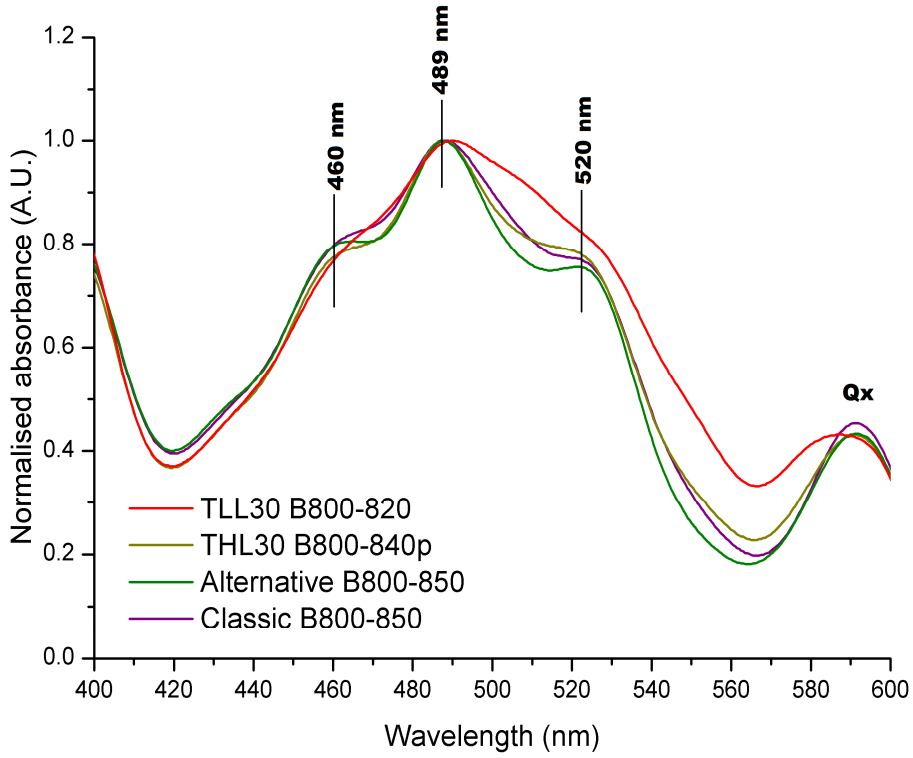

Figure 4.8 Normalised absorption spectra of carotenoid peaks of the B800-820, B800-840p, B800-850a, and B800-850c LH2 complex types from *Alc. vinosum*.
The B800-820 (red) produces the main carotenoid peak at 490 nm with a broad shoulder between 490 nm – 525 nm. The shoulder at ~ 463 nm is not well defined and appears red shifted relative to the carotenoid peaks from the other complexes. The B800-840p (dark yellow) produces the main carotenoid peak at 489 nm with a shoulder at ~ 520 nm and ~ 460 nm. The B800-850a (green) produces the main carotenoid peak at 488 nm with a shoulder at ~ 520 nm and ~ 460 nm. The B800-850c (purple) produces the main carotenoid peak at 488 nm with a shoulder at ~ 520 nm and ~ 460 nm. The B800-850a produces the lowest intensity ~ 520 nm shoulder. Both the B800-850c and B800-850a produce higher intensity ~460 nm absorption shoulders than the B800-820 and B800-840p complexes.

At 77 K the absorption bands are narrowed, improving the resolution of the peaks observed and distinguishing between the several peaks that cumulate in the room temperature spectrum. This improved resolution shows the complexity of the carotenoid complement present. The low temperature absorption spectra of the LH2 complex types shows the absorption peaks of the carotenoid molecules that are at a high enough concentration to be visualised (Figure 4.9). The peaks observed in the absorption spectra of the B800-850 and B800-840p LH2 complex types are well resolved showing several discrete peaks but the B800-820 complex type produces less distinct peaks. Regardless of this variation in resolution between the complex types, there are a total of four distinct absorption bands (Figure 4.9 absorption peaks at ~ 470 nm, ~ 489 nm, ~ 503 nm, ~528 nm) and two shoulders observed (Figure 4.9, ~ 440 nm and ~ 545 nm).

In the B800-850 LH2 complex type (Figure 4.9 purple), the peaks in order of decreasing intensity are 488 nm, 528 nm, 503 nm, 470 nm, and 440 nm while the sixth absorption shoulder is negligible to non-existent. The B800-840p complex type (Figure 4.9 dark yellow) peaks in order of decreasing intensity are 489 nm, 503 nm, 528 nm, 470 nm, and 440 nm and it produces an absorption shoulder for the absorption band at ~ 545 nm. In the B800-820 complex type (Figure 4.9 red), peaks 490 nm and 503 nm are of highest intensity, followed by peaks 470 nm and 528 nm, and lastly peaks 440 nm and 545 nm. The highest intensity carotenoid peak in the B800-850 and B800-840p complex types is the peak at 489 and 488 nm respectively, while this peak is of equal intensity to the peak at 503 nm, in the B800-820 complex type. These data suggest that while the type of carotenoids found in the LH2 complexes are the same, the relative amounts of each carotenoid vary, most significantly between the B800-820 and the other complex types.

When the spectra are normalised to the distinct peak at ~528 nm, the peaks at ~489 nm and 528 nm appear to be at the same relative intensity in all LH2 complex types and therefore are most probably produced by the same carotenoid. The shared trend between the peaks at 503 nm and ~ 545 nm that are at their highest intensity in the B800-820 complex type and the lowest in the B800-850 complex type indicates that they are produced by the same carotenoid. The peaks at ~440 nm and ~470 nm are of highest intensity in the B800-850 and the lowest intensity relative to the other peaks in the B800-820. This implies the B800-850 has proportionally more carotenoids with shorter conjugation lengths that absorb in the blue end of the carotenoid region (peaks at 440 nm and 470 nm) while the B800-820 contains more carotenoids with longer conjugation lengths that absorb towards the red-end of the carotenoid region (Peaks 503 nm and ~545 nm). This would indicate that the B800-820 LH2 complex type contains a higher amount of spirilloxanthin (n=13) and the B800-850c LH2 complex type contains shorter conjugation length carotenoids such as Rhodopin (n=11) and lycopene (n=11).

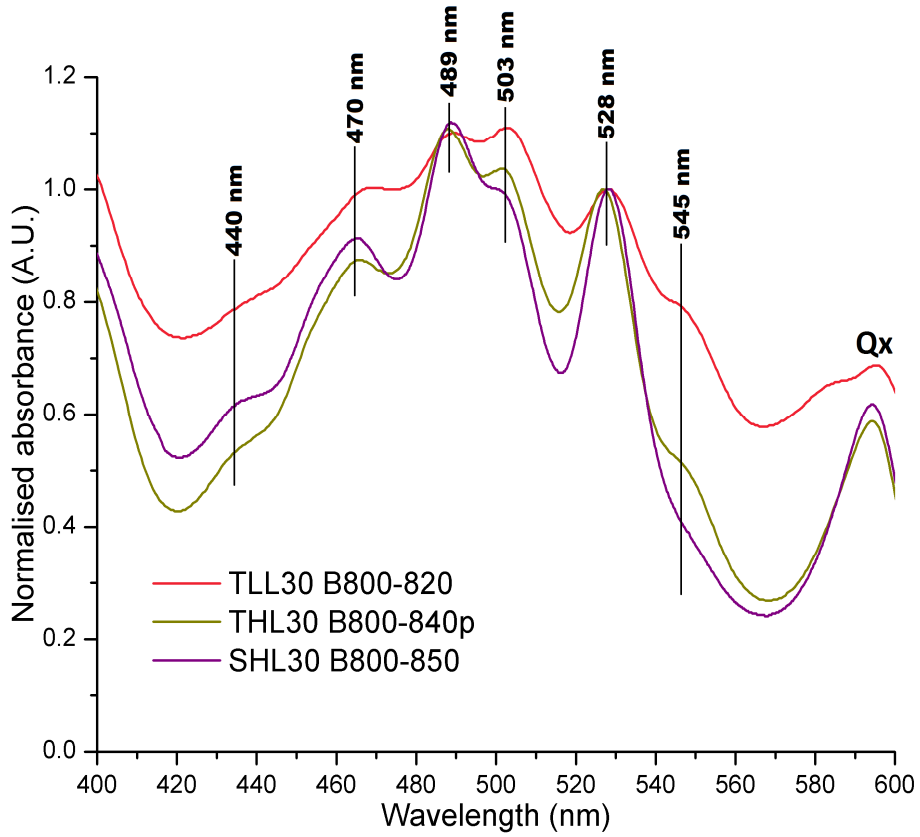

Figure 4.9 Normalised low temperature (77 K) absorption spectra of carotenoid peaks of the B800-820, B800-840p, and B800-850a LH2 complex types produced by *Alc. vinosum*.
All LH2 complexes produced four peaks with two shoulders. The absorption peaks centre at ~470 nm, 489 nm, 503 nm, 528 nm, and two absorption shoulders at ~ 440 nm and ~ 545 nm. The peaks at ~489 nm and 528 nm have the same intensity relative to each other across all LH2 complex types, suggesting that these are produced by the same carotenoid. Additionally, peaks 503 nm and 545 nm increase in intensity from the B800-850, to the B800-840, and are at their highest in the B800-820. This may indicate that the peaks are produced by the same carotenoid and that this carotenoid is increasing in abundance through these LH2 complex types.

4.3.1 Thin layer chromatography of the carotenoids from different LH2 complex types.

The differences in carotenoid complement can only be determined if the carotenoids are extracted and identified independently. Thin layer chromatography (TLC) is a classic biochemical technique that separates molecules according to their hydrophobicity, and has previously been used successfully with carotenoids. TLC plates were performed on the extracted carotenoids from the different LH2 complex types as a preliminary analysis of the carotenoids present and to visualise any large differences between the complexes (as described in Methods and Materials section 2.10).

Separation of the carotenoid complement on the TLC plate (Figure 4.10) showed four distinct carotenoid bands present in all the LH2 complex types. Band 1 is

the most abundant carotenoid as well as being the most polar, having moved the shortest distance in the solvent. Band 2 is a pink band that moved the same distance as the spirilloxanthin band from the LH1/RC control. The third band was rather faint and orange in colour. The final band was yellow and travelled just behind the solvent front showing the most hydrophobic carotenoid present in the carotenoid composition of *Alc. vinosum*. The relative amounts of the different carotenoids to each other seem similar across the different LH2 complex types, this indicates that TLC is not sensitive enough to visualise any differences.

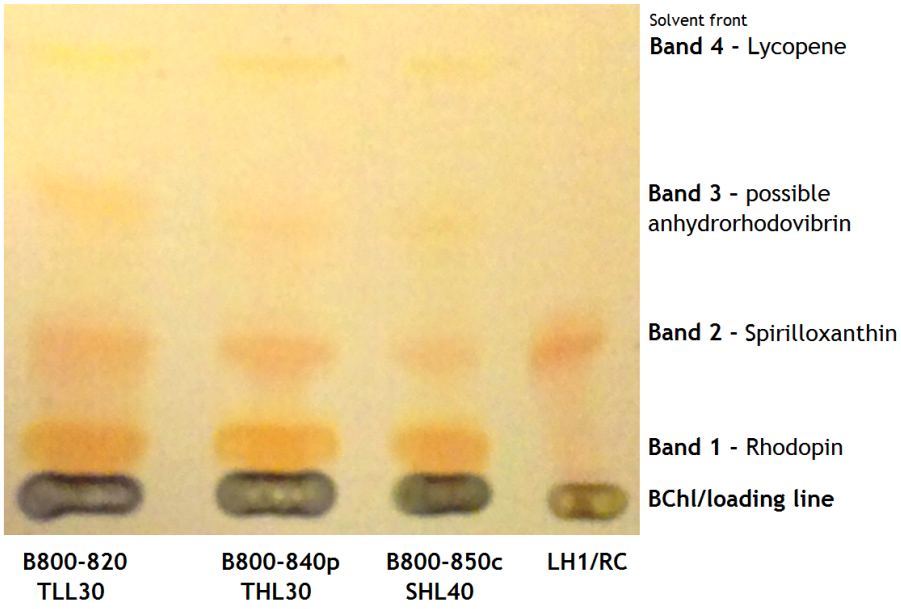

Figure 4.10 The carotenoids of the B800-820, B800-840p, and B800-850c LH2 complexes from *Alc. vinosum* separated by thin-layer chromatography.
Four bands were observed in all LH2 complex types, presenting as an orange band (band 1), pink band (band 2), a faint orange band (band 3) and a yellow band (band 4). The LH1/RC "core" complex was run as a control as spirilloxanthin is its primary carotenoid (60). Band 4 is the most hydrophobic carotenoid as it moved the furthest up the TLC plate, while band 1 is the least hydrophobic carotenoid as it travelled the least distance.

The bands were scraped from the TLC plate and re-suspended in acetone in order to extract the carotenoids and record the absorption spectra (Figure 4.11, the lycopene absorption spectrum was omitted as it is identical to rhodopin). Carotenoids were identified through the comparison of their absorption spectrum and their hydrophobic character from the TLC plate. Rhodopin and lycopene contain the same chromaphore and so produce the same absorption spectrum, however rhodopin contains a hydroxyl group. As bands 1 and 4 both produced absorption peaks at 448 nm, 474 nm, and 505 nm (Figure 4.11 blue)

this indicated that they are rhodopin and lycopene. The hydrophobic character of these two carotenoids enables them to be differentiated as band 4 is highly hydrophobic this would indicate that it is lycopene, and therefore band 1 is the more polar rhodopin. Band 2 ran parallel to the control, indicating that that it was spirilloxanthin. The absorption spectrum of band 2 (Figure 4.11 green) produced peaks at 465 nm, 492 nm, and 525 nm confirming the carotenoid as spirilloxanthin. The absorption spectrum of band 3 (Figure 4.11 red) was recorded and the absorption peaks centred at 459 nm, 488 nm, and 522 nm indicating it is either rhodovibrin or anhydrorhodovibrin. Due to the hydrophobicity of the carotenoid it is most probably anhydrorhodovibrin. Rhodovibrin was not observed but would be expected to be present in small quantities and produce an absorption spectrum identical to anhydrorhodovibrin as it contains the same chromaphore.

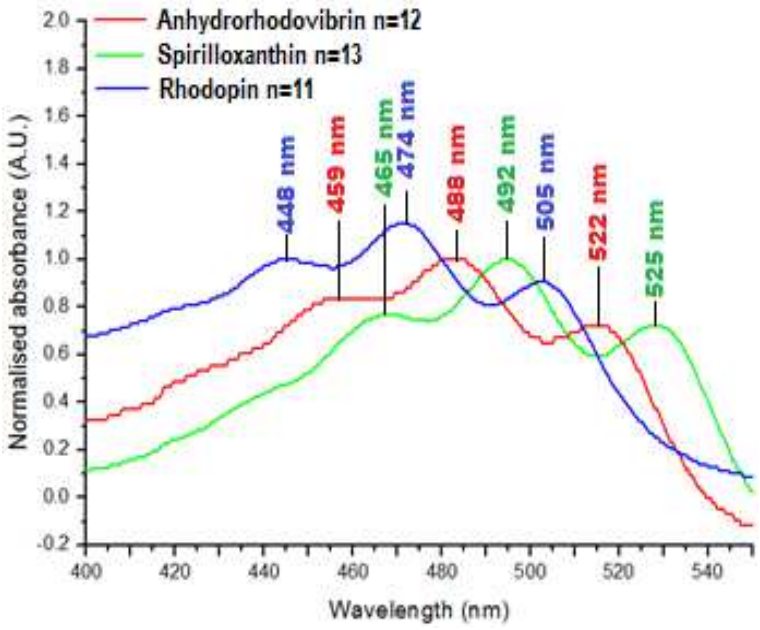

Figure 4.11 Normalised absorption spectra of the carotenoids extracted from the LH2 complex types of *Alc. vinosum* by TLC plate.
Spirilloxanthin was identified (green) from the TLC producing peaks at 465 nm, 492 nm, and 525 nm. Rhodopin (blue) and lycopene share the same chromophore and produced peaks at 448 nm, 474 nm, and 505 nm. Anhydrorhodovibrin (red) was identified from the peaks observed in the absorption spectrum at 459 nm, 488 nm, and 522 nm. The difference in peak position observed between the different carotenoids is indicative of the π-conjugation length of their chromophore, as chromophore length increases the positions of the peaks red shift. The conjugation lengths of the different carotenoids are Rhodopin n = 11, anhydrorhodovibrin = 12, and spirilloxanthin n = 13.

The carotenoids identified were confirmed by individually extracting and purifying the carotenoids from known sources and running a TLC plate for a direct comparison (Figure 4.12). All carotenoids were extracted as previously described in Methods and Materials section 2.10. Lycopene was extracted from

tomato paste, anhydrorhodovibrin and spirilloxanthin were extracted from *Rsp. rubrum* S1, and rhodopin was extracted from *Alc. vinosum* Strain D. Figure 4.12 shows these four carotenoids run in parallel to the carotenoid complement extracted from the B800-850c LH2 complex type. Each of the individually sourced carotenoids ran parallel to the carotenoids extracted from the B800-850 LH2 complex type. This would support the identifications made from the hydrophobic character and absorption spectra.

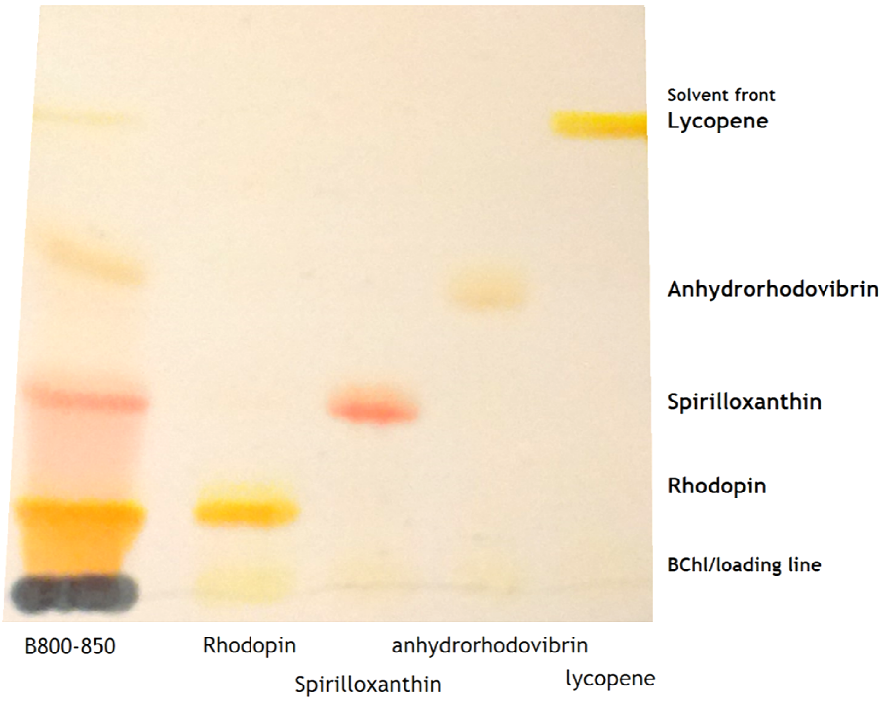

Figure 4.12 The carotenoids of the B800-850 LH2 complex from *Alc. vinosum* and individually purified carotenoids separated by thin-layer chromatography.
Four bands were observed in the B800-850 LH2 complex, presenting as an orange band (band 1), pink band (band 2), a faint orange band (band 3) and a yellow band (band 4). These were preliminarily identified as rhodopin, spirilloxanthin, anhydrorhodovibrin, and lycopene. To confirm this identification carotenoids were extracted from known sources; lycopene (tomato paste), anhydrorhodovirbin (*Rsp. rubrum* S1), Spirilloxanthin (*Rsp. rubrum* S1), and Rhodopin (*Alc. vinosum* strain D). The four bands observed in the B800-850 LH2 complex ran parallel to the individually purified carotenoids suggesting they were the same carotenoids.

4.3.2 Determining the carotenoid composition of the B800-820, B800-840p and B800-850c LH2 complex types by HPLC

Thin layer chromatography was effective in separating the carotenoids but the percentage composition of the carotenoids could not be determined using this technique. Additionally, photobleaching of the carotenoids on the plate impeded the identification of any carotenoids present at very low concentrations. The technique of HPLC has the capacity to quantitatively determine the carotenoid

differences between complexes as well as the sensitivity to identify all the carotenoids present.

The preliminary studies on the carotenoid complement of the LH2 complex types of *Alc. vinosum* were taken on for further analysis by post doctorial researcher Dr Anne-Marie Carey. This work was published as part of the Carey, et al 2014 publication. Carotenoids from the B800-820, B800-840 and B800-850c LH2 complex types were extracted and separated using reverse phase HPLC (RP HPLC) in a method adapted from (135). The peak area of each carotenoid for absorption at a known wavelength (470 nm for lycopene and rhodopin, 475 nm for spirilloxanthin, 482 nm for anhydrorhodovibrin) was used with the relevant extinction coefficient (37) to determine the percentage composition of the carotenoid observed.

Five peaks were observed in the HPLC chromatogram from in each of the LH2 complex types (Figures 4.13-4.16). The identity of the pigments was determined via absorption spectroscopy and their relative hydrophobicity, as with the TLC plates. The first pigments to elute from the column during reverse phase HPLC are those with the highest polarity, followed by pigments with increasing hydrophobicity. The elution order of the pigments was identical for the pigment mix from all three LH2 complex types but the intensity of the peaks and the retention times varied. As the most polar of the pigments, BChl eluted first (Figures 4.13-4.16 peak a) followed by rhodopin (Figures 4.13-4.16 peak b), spirilloxanthin (Figures 4.13-4.16 peak c), anhydrorhodovibrin (Figures 4.13-4.16 peak d), and finally the most hydrophobic carotenoid, lycopene (Figures 4.13-4.16 peak e). Variations in retention times are most probably due to temperature differences between runs.

During RP HPLC of the B800-820 LH2 complex (Figure 4.13) BChl eluted at 16 min (Figure 4.13, peak a) followed by rhodopin at 22:30 min (Figure 4.13, peak b), spirilloxanthin at 24:30 min (Figure 4.13, peak c), anhydrorhodovibrin at 26 min (Figure 4.13, peak d), and then lycopene at 27 min (Figure 4.13, peak e). Rhodopin produced the highest intensity peak (0.7 A.U.) followed by spirilloxanthin (0.3 A.U.), and then anhydrorhodovibrin (0.2 A.U.). Lycopene produced the lowest intensity peak (>0.1 A.U.).

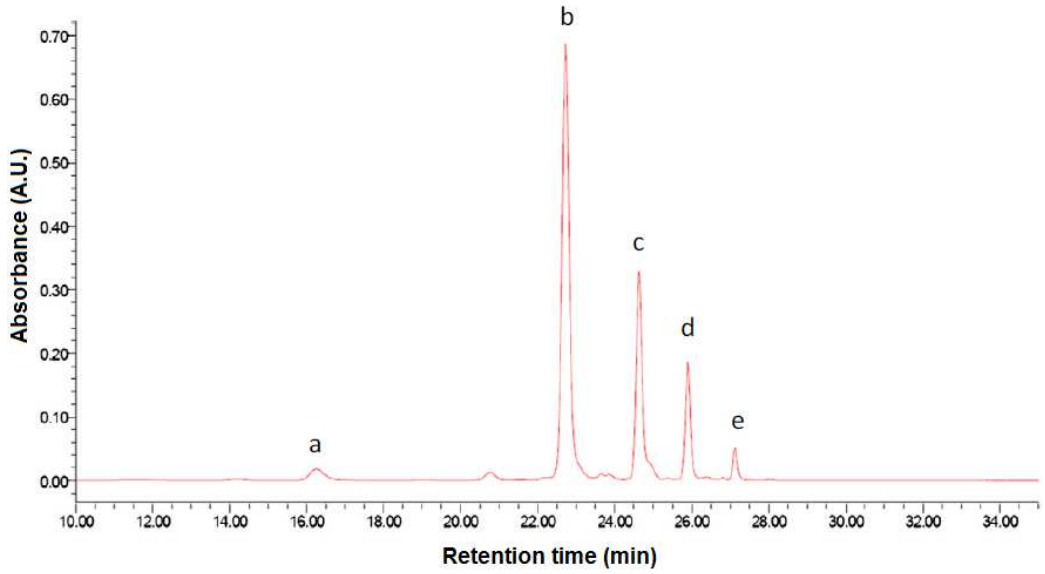

Figure 4.13 The A_{470} of the carotenoids of the B800-820 LH2 complex from *Alc. vinosum* separated by reverse phase HPLC.
Five peaks eluted at 16 min (peak a), 22:30 min (peak b), 24:30 min (peak c), 26 min (peak d) and 27 min (peak e). The fractions were collected and identified by their absorption spectra and their relative hydrophobicity. Peak a is BChl, peak b is rhodopin, peak c is spirilloxanthin, peak d is anhydrorhodovibrin, and peak e is lycopene. The highest intensity peak is produced by rhodopin (peak b) and is the most abundant carotenoid in the B800-820 LH2 complex type, closely followed by spirilloxanthin (peak c). As published in Carey et at,. 2014 (164).

The retention times of the carotenoids from the B800-840 LH2 complex (Figure 4.14) was similar to those observed in the carotenoids from the B800-820 LH2 complex but the pigments eluted slightly quicker. Once again rhodopin (Figure 4.14, peak b) produces the highest intensity peak (0.7 A.U.), followed by spirilloxanthin (Figure 4.14, peak b, 0.2 A.U.), anhydrorhodovibrin (Figure 4.14, peak b, 0.1 A.U.), and finally lycopene (Figure 4.14, peak b, >0.1 A.U.). The level of spirilloxanthin and anhydrorhodovibrin is lower than that observed in the B800-820 LH2 complex type.

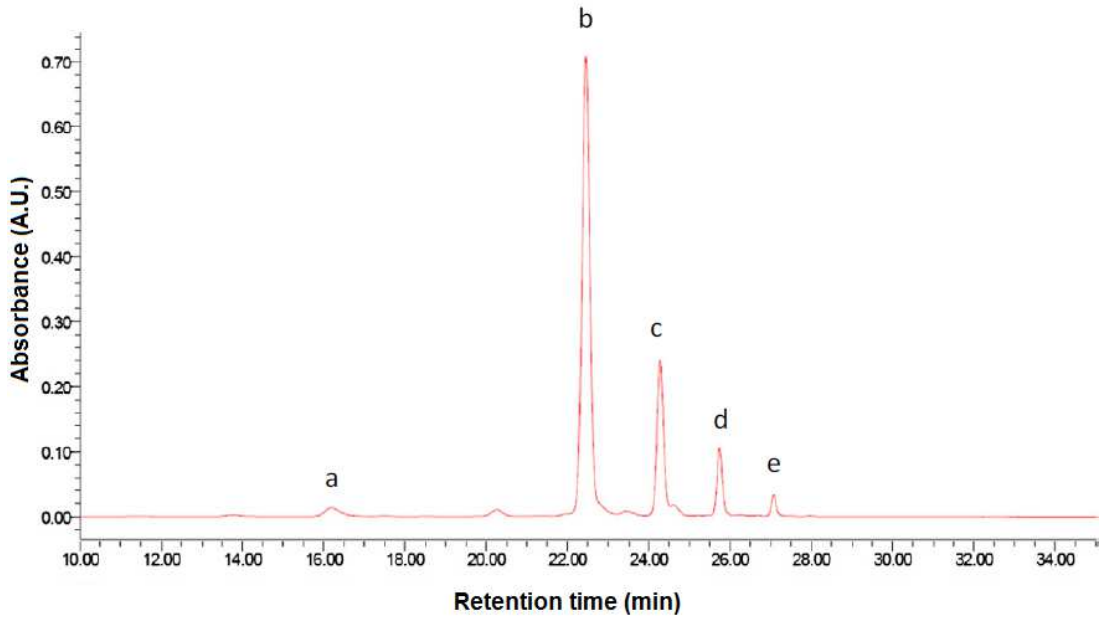

Figure 4.14 The A_{470} of the carotenoids of the B800-840 LH2 complex from *Alc. vinosum* separated by reverse phase HPLC.
Five peaks eluted at 16 min (peak a), 22:30 min (peak b), 24:30 min (peak c), 25:30 min (peak d) and 27 min (peak e). The fractions were collected and identified by their absorption spectra and their relative hydrophobicity. Peak a is BChl, peak b is rhodopin, peak c is spirilloxanthin, peak d is anhydrorhodovibrin, and peak e is lycopene. The highest intensity peak is produced by rhodopin (peak b) and is the most abundant carotenoid in the B800-840 LH2 complex type, closely followed by spirilloxanthin (peak c). As published in Carey et at,. 2014 (164).

The retention times of the carotenoids from the B800-850 LH2 complex (Figure 4.15) were similar to those observed in the carotenoids from the B800-840 LH2 complex type. Once again rhodopin (Figure 4.15, peak b) produces the highest intensity peak (0.95 A.U.), but the intensity of both the spirilloxanthin (Figure 4.15, peak b, 0.15 A.U.) and anhydrorhodovibrin peaks are the same (Figure 4.15, peak b, 0.15 A.U.). Lycopene was the final carotenoid to elute (Figure 4.15, peak b, >0.1 A.U.) and was of a similar intensity to that observed in the HPLC chromatograms from all the LH2 complex types. The level of spirilloxanthin and anhydrorhodovibrin is lower than that observed in the B800-820 LH2 complex type.

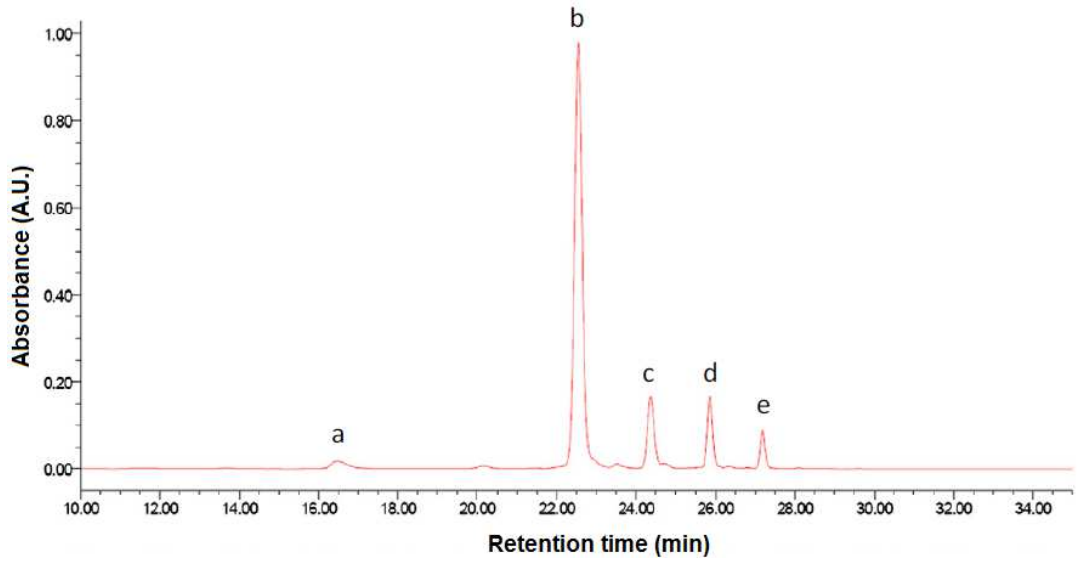

Figure 4.15 The A_{470} of the carotenoids of the B800-850 LH2 complex from *Alc. vinosum* separated by reverse phase HPLC.
Five peaks eluted at 16:30 min (peak a), 22:30 min (peak b), 24:30 min (peak c), 26 min (peak d) and 27 min (peak e). The fractions were collected and identified by their absorption spectra and their relative hydrophobicity. Peak a is BChl, peak b is rhodopin, peak c is spirilloxanthin, peak d is anhydrorhodovibrin, and peak e is lycopene. The highest intensity peak is produced by rhodopin (peak b) and is the most abundant carotenoid in the B800-820 LH2 complex type, closely followed by spirilloxanthin (peak c) and anhydrorhodovibrin (peak d). As published in Carey et at,. 2014 (164).

The spirilloxanthin peak (peak c) varies most between the different LH2 complex types, which is highest in the B800-820 and lowest in the B800-850c LH2 complex type. The concentration of anhydrorhodovibrin changes slightly between the different LH2 complex types, as show in variations on peak d, highest in the B800-820 and lowest in the B800-840p and B800-850c LH2 complex types.

The percentage composition of the different carotenoids was determined using the extinction coefficients and the peak area from the chromatogram. The most abundant carotenoid in all LH2 complex types is rhodopin, followed by spirilloxanthin, anhydrorhodovibrin, and then lycopene. The relative amounts of these carotenoids vary across the different LH2 complex types, most prominently between spirilloxanthin and rhodopin. The level of spirilloxanthin was at its highest in the B800-820 LH2 complex, followed by the B800-840p, and then the B800-850c had the lowest levels.

This data was repeated as part of collaborative work with the Frank lab as part of the Magdaong et al, (2016) publication (167). The LH2 complex types were purified (as outlined in Methods and Materials section 2.5.1) and sent to Dr Nikki

Magdaong for analysis by normal phase HPLC. Rhodovibrin was identified in addition to the four carotenoids identified in the Carey paper. Rhodovibrin contains the same chromophore as anhydrorhodovibrin but with an additional hydroxyl group, so has the same absorption spectrum but has a different hydrophobic character.

The relative abundances of the carotenoids in the B800-850 LH2 complex type were rhodopin (70 % ± 2 (Carey), 59 % ± 7 (Magdaong)), spirilloxanthin (19 % ±1 (Carey), 6.0 % ± 0.7 (Magdaong)), anhydrorhodovibrin (7 % ± 3 (Carey), 9 % ± 1 (Magdaong)), rhodovibrin (not observed (Carey), 22 %± 3 (Magdaong)), and lycopene (4 % ± 0.4 (Carey), 3.8 % ± 0.4 (Magdaong)). The B800-840 LH2 complex type contained rhodopin (66 % ± 4 (Carey), 62 % ± 7 (Magdaong)), spirilloxanthin (22 % ±4 (Carey), 15 % ± 2 (Magdaong)), anhydrorhodovibrin (8 % ± 1 (Carey), 9 % ± 1 (Magdaong)), rhodovibrin (not observed (Carey), 11 % ± 1 (Magdaong)), and lycopene (4 % ± 1 (Carey), 4.1 % ± 0.5 (Magdaong)). In the B800-820 LH2 complex type the relative abundances of carotenoids were rhodopin (47 % ± 1(Carey), 44 % ± 5 (Magdaong)), spirilloxanthin (40 % ± 2 (Carey), 23 % ± 3 (Magdaong)), anhydrorhodovibrin (12 % ± 1 (Carey), 17 % ± 2 (Magdaong)), rhodovibrin (not observed (Carey), 14 % ± 2 (Magdaong)), and lycopene (2 % ± 0.1 (Carey), 2.3 % ± 0.3 (Magdaong)). These data are outlined in table 4.2.

The relative abundances observed between the Cogdell lab for the Carey paper and the Frank lab for the Magdaong paper were similar but varied most due to the identification of rhodovibrin by the Magdaong group. The higher levels of rhodovibrin corresponded predominantly to a reduction in the level of spirilloxanthin and, to a lesser degree, rhodopin. This may indicate that the spirilloxanthin peak observed by Carey (2015) was insufficiently separated spirilloxanthin and rhodovibrin. The relative amounts of anhydrorhodovibrin and lycopene do not change very much across the different complex types in either the data from Magdaong et al,(2016)(167) or Carey et al, (2014) (164).

Carey et al determined that the differences in the LH2 complex types' spectra within the carotenoid region are due to changes in the ratio of spirilloxanthin to rhodopin. The data from Carey et al (2014) and Magdaong et al (2016) generally agreed that there is an increase of longer conjugation length carotenoids (n=12

and n=13) in the B800-820 produced under low light, 30℃ growth conditions in comparison to the B800-850 and B800-840 produced under high light growth conditions. This concurs with the speculation made that the variations observed in the low temperature absorption spectra are due to changes in the levels of spirilloxanthin between the different LH2 complex types. This supports the evidence put forward in section 3.3 and previous work (113) that there is a larger amount of carotenoids that contain longer chromophores in the B800-820 LH2 complex type.

Table 4.3 The percentage composition of the different carotenoids identified in the B800-820, B800-840p and B800-850c LH2 complex types produced by *Alc. vinosum* identified by Carey et al,. (2014) (164)and Magdaong et al,. (2016) (167).

LH2 complex type/carotenoid	B800-820	B800-840p	B800-850c	*n* =
Rhodopin				11
Carey et al	47 ± 1	66 ± 4	70 ± 2	
Magdaong et al	44 ± 5	62 ± 7	59 ± 7	
Lycopene				11
Carey et al	2 ± 0.1	4 ± 1	4 ± 0.4	
Magdaong et al	2.3 ± 0.3	4.1 ± 0.5	3.8 ± 0.4	
Anhydrorhodovibrin				12
Carey et al	12 ± 1	8 ± 1	7 ± 3	
Magdaong et al	17 ± 2	9 ± 1	9 ± 1	
Rhodovibrin				12
Carey et al	-	-	-	
Magdaong et al	14 ± 2	11 ± 1	22 ± 3	
Spirilloxanthin				13
Carey et al	40 ± 2	22 ±4	19 ±1	
Magdaong et al	23 ± 3	15 ± 2	6.0 ± 0.7	

4.4 Fluorescence of the different LH2 complex types of *Alc. vinosum*

The B800-820, B800-840p, and B800-850 LH2 complex types were purified (as described in Methods and Materials section 2.5.1) and the fluorescence emission spectra were recorded. The B800-850 LH2 complex produces an emission peak at 853 nm with a small shoulder at ~ 810 nm (Figure 4.16 red). The emission at ~ 810 nm is from the B800 BChl whereas the emission at 852 nm is produced by the B850 BChl. There is energy transfer from the B800 BChl to the B850 BChl

resulting in only a small amount of fluorescence from the B800 BChl. The B800-840p LH2 complex produces an emission peak at 850 nm with a shoulder at ~ 820 nm (Figure 4.16 green). There is no emission peak observed for the B800 BChl as it is obscured by the fluorescence from the dimeric BChl. The B800-820 LH2 complex type produces an emission peak at 827 nm (Figure 4.16 blue) regardless of the growth conditions it is produced under. There is a single emission peak observed from the B820 BChl, as the emission from the B800 BChl is obscured beneath the B820 emission.

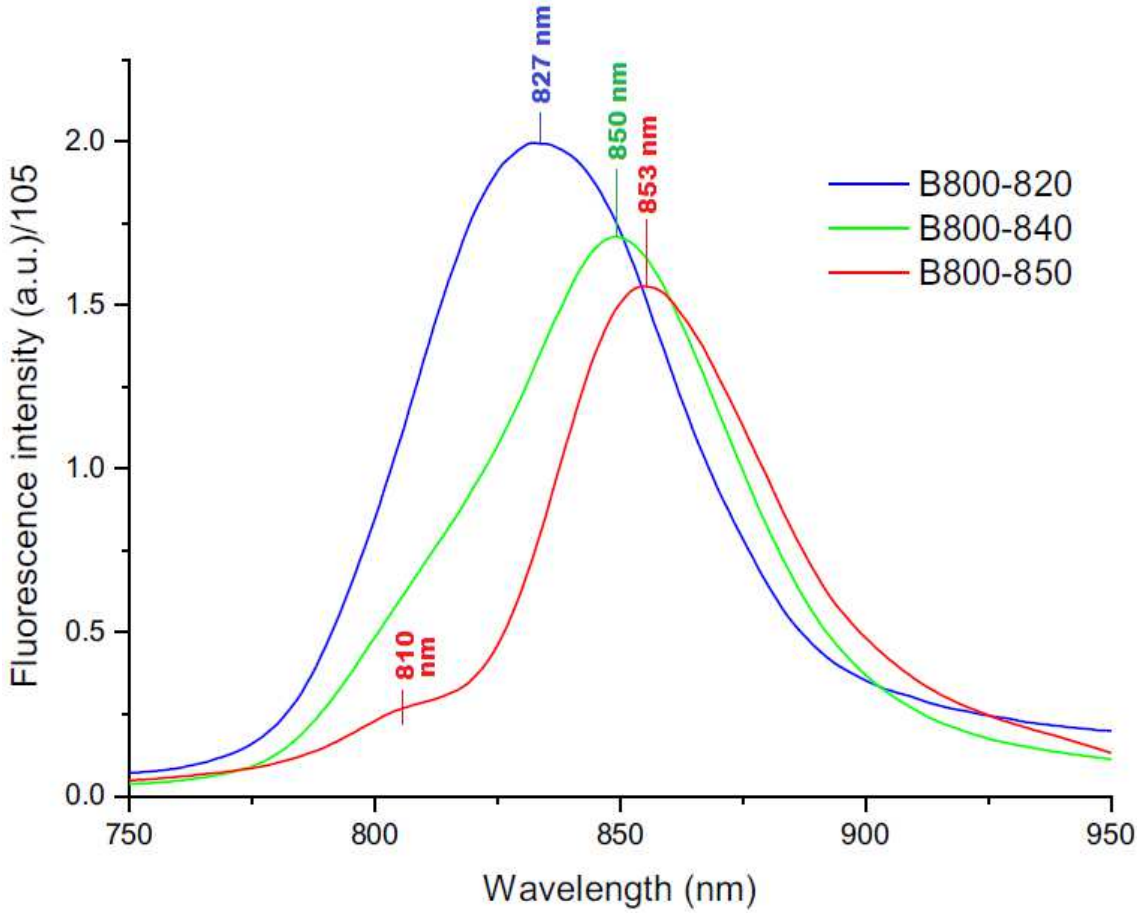

Figure 4.16 Fluorescence emission spectra of the B800-820, B800-840p and the B800-850c LH2 complex types from *Alc. vinosum*.
The B800-820 complex type (blue) produces a single emission peak at 827 nm. The B800-840p LH2 complex type (green) and produces an emission peak at 850 nm with a slight shoulder at ~ 820 nm. The B800-850c LH2 complex type produces an emission peak at 853 nm with a small shoulder at ~ 810 nm. Emission spectra were divided by 105 at the Qy maxima to normalise the data. The emission at ~ 810 nm relates to the B800 BChl while the main emission peaks relate to the dimeric BChl. The B800-850c LH2 complex produces the most red-shifted emission spectra and the B800-820 produces the most blue-shifted emission spectra.

The emission peaks of both the B800-850a LH2 complex (Figure 4.17 green) and B800-850c LH2 complex (Figure 4.17 blue) centre at the same wavelength, 853 nm. Unlike the B800-850c LH2 complex, the B800-850a LH2 complex produces a

pronounced shoulder at ~810 nm. This appears to be similar to the B800-840p LH2 complex type but the shoulder is more distinct and the main emission peak is more red-shifted in the B800-850a LH2 complex.

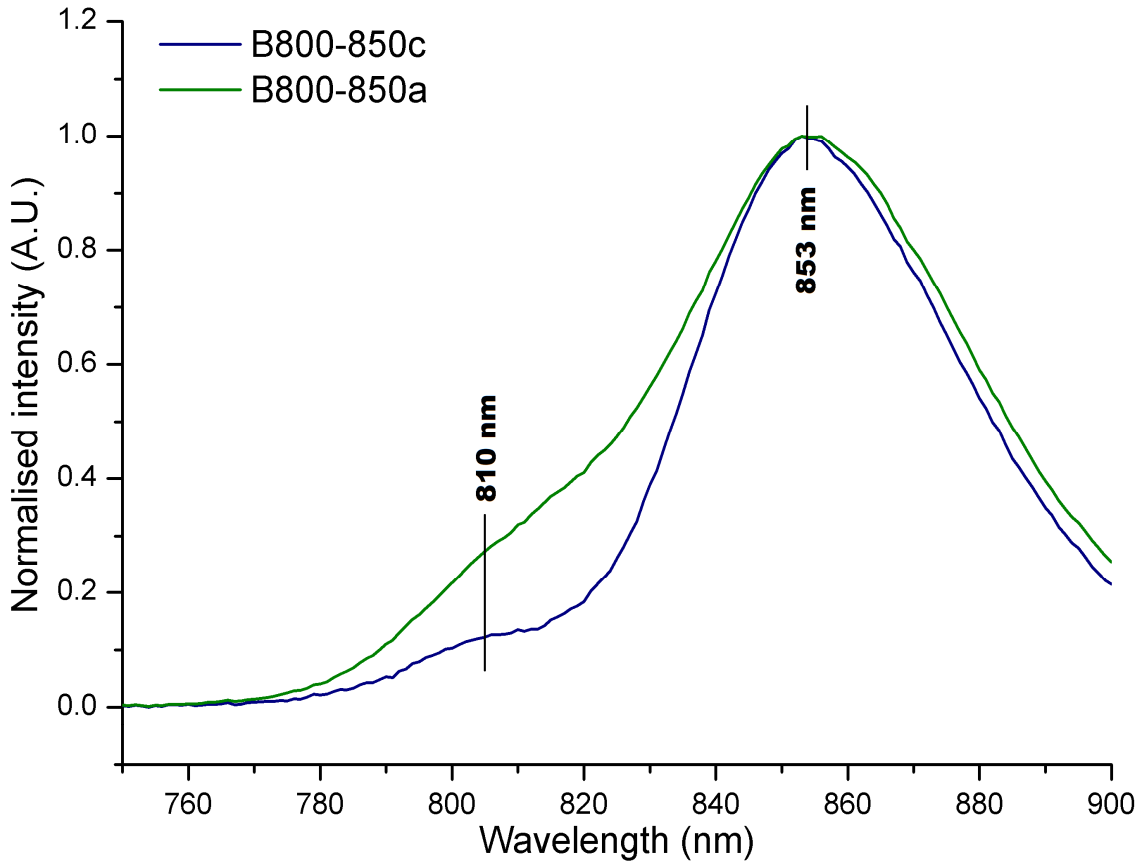

Figure 4.17 Fluorescence emission spectra of the B800-850a and the B800-850c LH2 complex types from *Alc. vinosum*.
The B800-850c complex type (blue) produces a single emission peak at 853 nm. The B800-850a LH2 complex type (green) and produces an emission peak at 853 nm with a shoulder at ~ 810 nm. The emission at ~ 810 nm relates to the B800 BChl while the main emission peaks relate to the dimeric BChl.

Fluorescence excitation spectra provides the means to determining the efficiency of the intra-complex energy transfer from the carotenoids to the BChl by comparing the total energy absorbed by the carotenoids (1-Transmittance) to the energy that contributes to emission at a specific wavelength (Excitation fluorescence). As fluorescence is in a linear mode the absorption measurement is measured as percent transmittance. A comparison of these values gives the excitation energy transfer efficiency (EET).

Work published (167) from the collaboration with the Frank lab (section 4.3.2) used a more up-to-date Fluorolog-3 FL3-22 fluorimeter (Horiba Jobin Yvon) with

better calibration into the red end of the spectrum that corrected our emission values. Percent transmittance and excitation fluorescence spectra were recorded and the excitation energy transfer for the different complex types was determined.

The emission peak of the B800-820 LH2 complex centred at 830 nm (Figure 4.18 blue), red-shifted by 3 nm compared to previous data. The 1-T (Figure 4.18 black) and fluorescence excitation (Figure 4.18 red) spectra were near identical when overlaid, with the exception of the carotenoid peaks. The Qx dipole at ~ 590 nm, Soret peak at ~ 370 nm, and the BChl Qy absorption peaks were observed and overlaid well in both spectra, and this was the case for all the LH2 complex types measured. Comparison of the carotenoid region of the 1-T and the fluorescence excitation found the EET from the carotenoids to the BChl is 38 %.

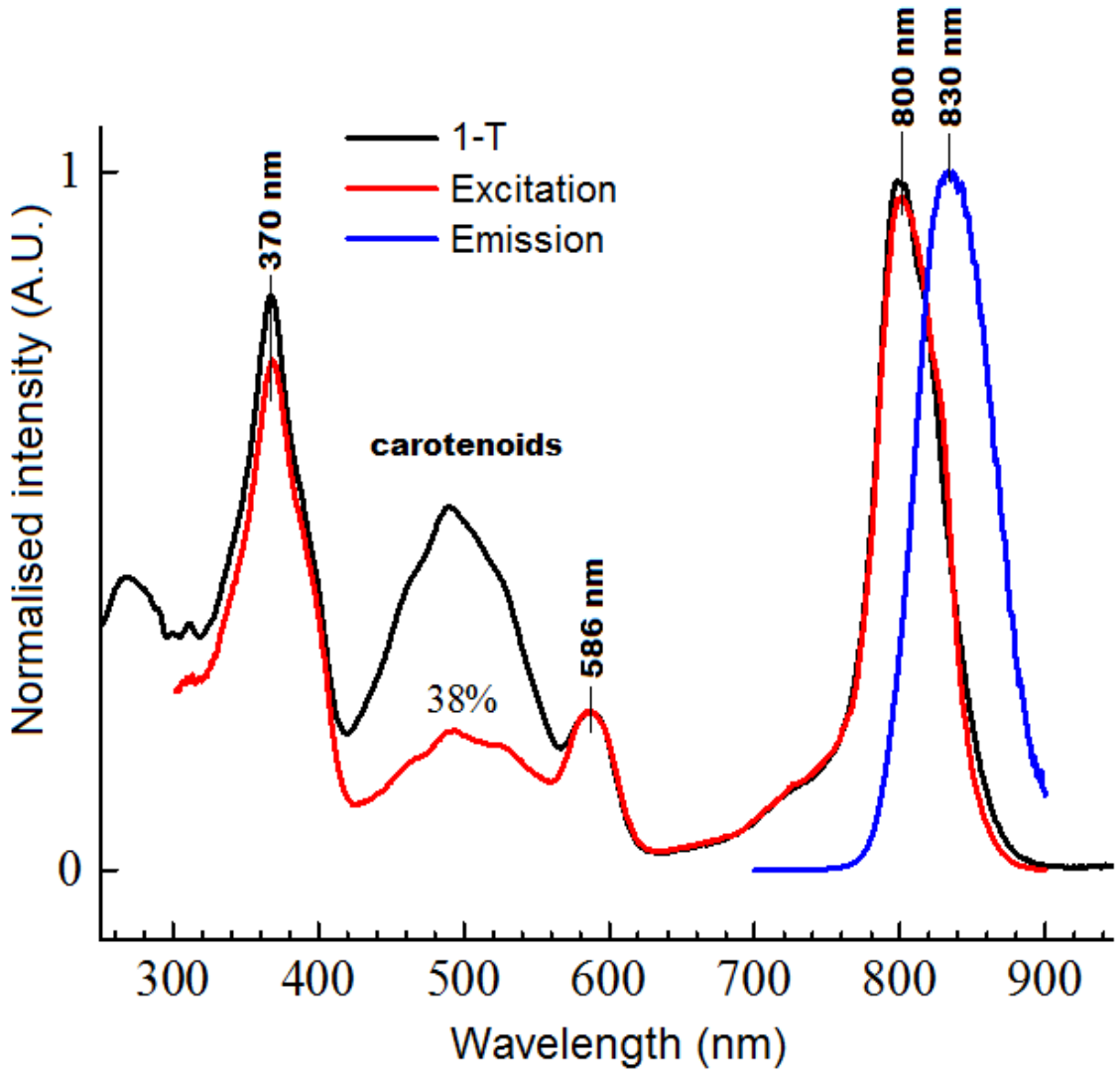

Figure 4.18 Normalised 1-T, fluorescence excitation and emission spectra of the B800-820 LH2 complex type from *Alc. vinosum*.
A single fluorescence emission peak (blue) was observed at 830 nm. The Qx dipole at 586 nm, the soret peak at ~370 nm, BChl Qy absorption at ~ 800 nm in the 1-T (black) and fluorescence excitation (red) spectra overlapped almost perfectly. The carotenoid region varies due to only some of the energy absorbed by the carotenoids (1-T) transferring on the BChl. The percentage EET is the difference between the 1-T and fluorescence excitation and was found as 38 %. The emission spectra were recorded after excitation at 588 nm in the Qx band. Fluorescence excitation spectra were recorded for emission at 830 nm. As published as part of Magdaong et al,. (2016) (167).

The emission peak of the B800-840p LH2 complex centred at 855 nm (Figure 4.19 blue), red-shifted by 5 nm compared to previous data. The fluorescence emission spectra still showed a slight asymmetry of the emission peak with a shoulder at ~810 nm. Comparison between the 1-T (Figure 4.19 black) and the fluorescence excitation (Figure 4.19 red) found the EET from the carotenoids to the BChl is 33 %.

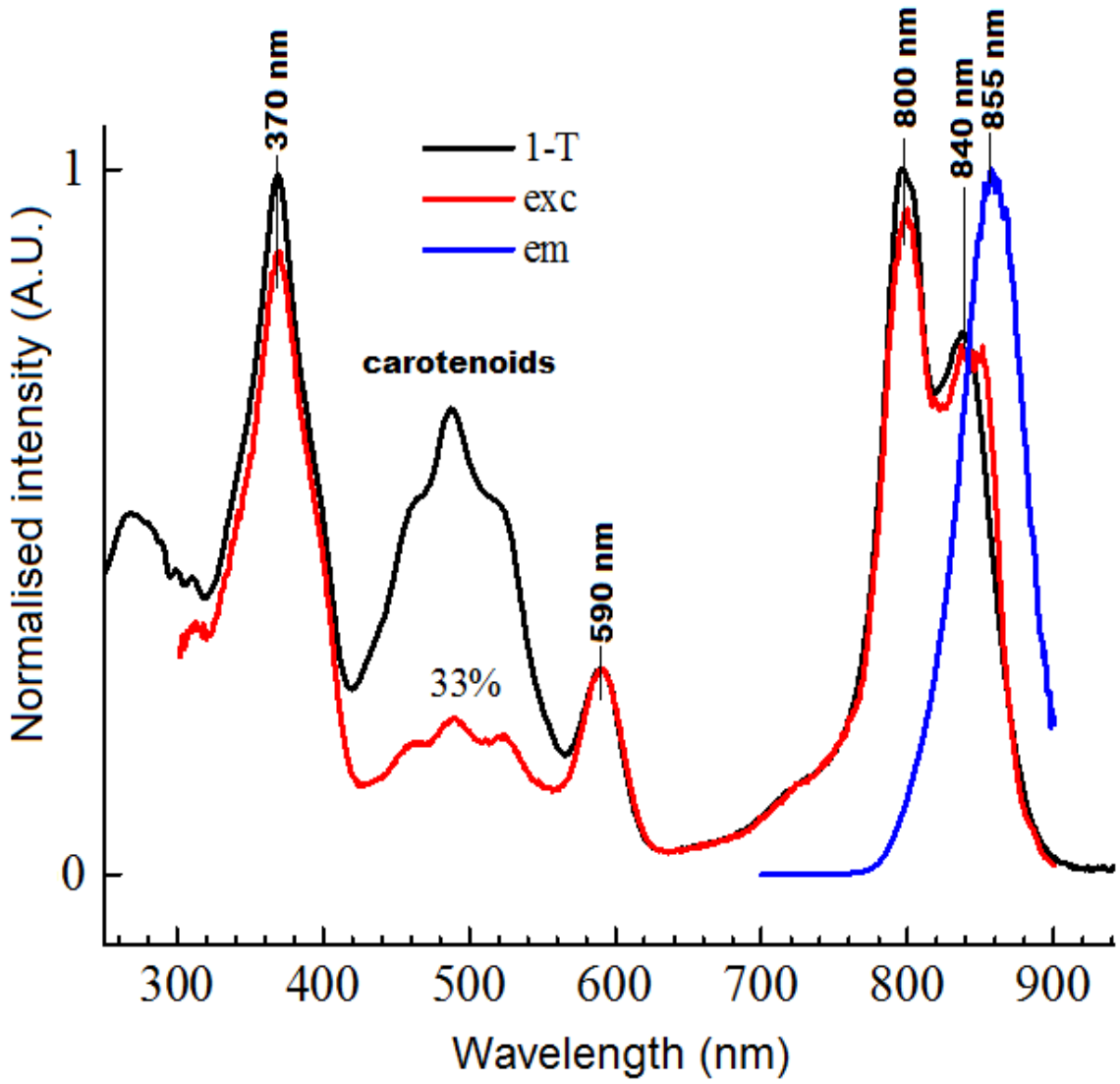

Figure 4.19 Normalised 1-T, fluorescence excitation and emission spectra of the B800-840p LH2 complex type from *Alc. vinosum*.
A single fluorescence emission peak (blue) was observed at 855 nm. The Qx dipole at 590 nm, the soret peak at ~370 nm, BChl Qy absorption at ~ 800 nm and 840 nm in the 1-T (black) and fluorescence excitation (red) spectra overlapped almost perfectly. The carotenoid region varies due to only some of the energy absorbed by the carotenoids (1-T) transferring on the BChl. The percentage EET is the difference between the 1-T and fluorescence excitation and was found as 33 %. The emission spectra were recorded after excitation at 588 nm in the Qx band. Fluorescence excitation spectra were recorded for emission at 855 nm. As published as part of Magdaong et al,. (2016)(167).

The emission peak of the B800-850c LH2 complex centred at 867 nm (Figure 4.20 blue), red-shifted by 14 nm compared to previous data. The fluorescence emission spectra shows the small peak at ~ 810 nm that relates to emission from the B800 BChl. Comparison between the 1-T (Figure 4.20 black) and the fluorescence excitation (Figure 4.20 red) found the EET from the carotenoids to the BChl is 38 %.

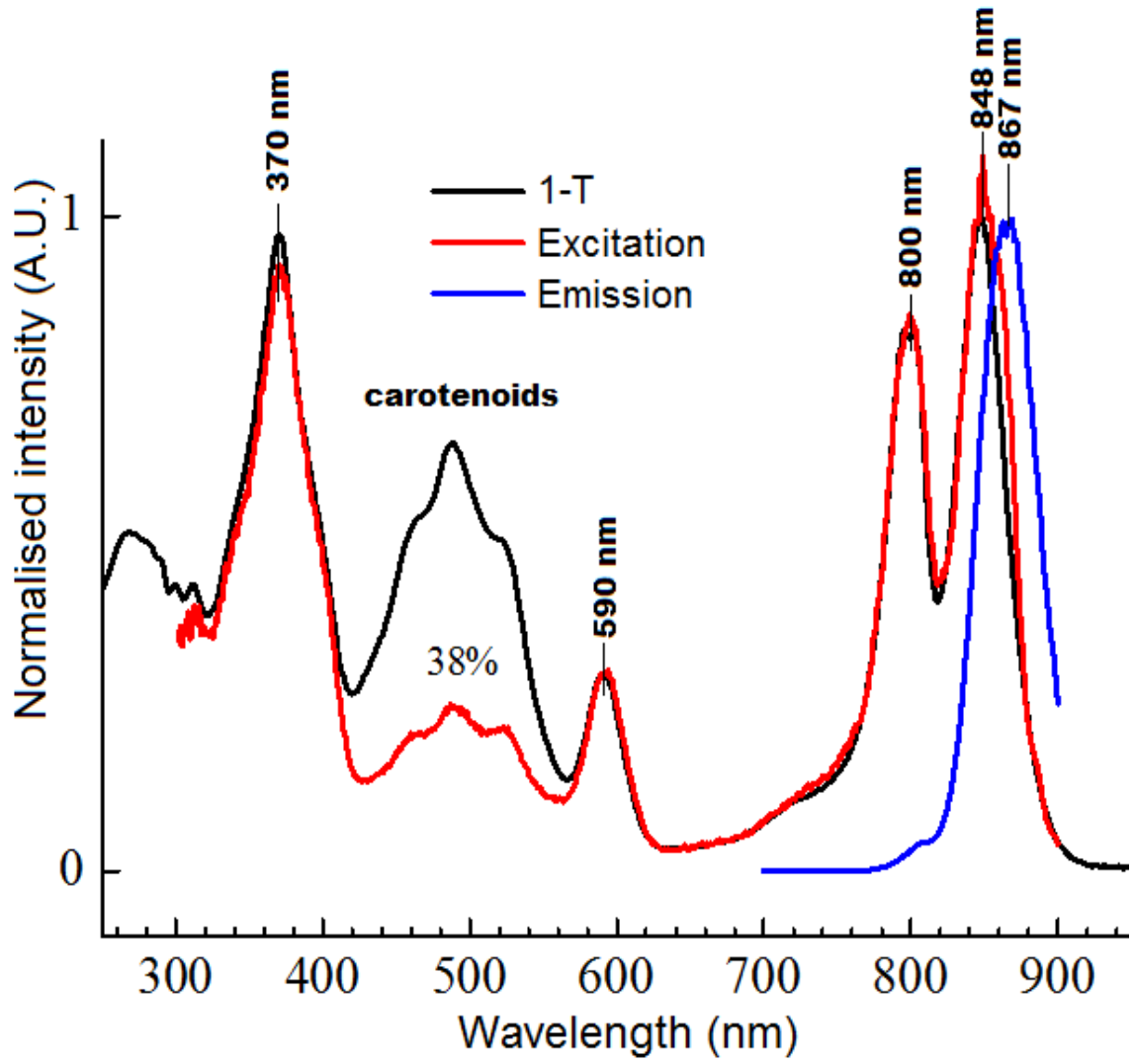

Figure 4.20 Normalised 1-T, fluorescence excitation and emission spectra of the B800-850c LH2 complex type from *Alc. vinosum*.
A single fluorescence emission peak (blue) was observed at 867 nm. The Qx dipole at 590 nm, the soret peak at ~370 nm, BChl Qy absorption at ~ 800 nm and 848 nm in the 1-T (black) and fluorescence excitation (red) spectra overlapped almost perfectly. The carotenoid region varies due to only some of the energy absorbed by the carotenoids (1-T) transferring on the BChl. The percentage EET is the difference between the 1-T and fluorescence excitation and was found as 38 %. The emission spectra were recorded after excitation at 588 nm in the Qx band. Fluorescence excitation spectra were recorded for emission at 867 nm. As published as part of Magdaong et al,. (2016) (167).

4.5 The origin of the split B800 peak

The split B800 peak that is observed in the LH2 complex types of *Alc. vinosum* is fairly unusual in the LH2 complexes of purple photosynthetic bacteria with the exception of *Thr. tepidum* (160). The basis of the split peak is unknown but previous work (113) discovered that both B800 peaks originate from within the same complex. This result could be due to a second pool of BChl within the LH2 complex types produced by *Alc. vinosum*. From the structure of the B800-850 from *Rps. acidophila* the ratio of BChl/carotenoids is known as 3:1, which would

change to 4:1 if additional BChl were present. Dr Anne-Marie Carey extracted the BChl and carotenoids from the B800-850 complex from *Alc. vinosum* and compared the absorption spectra to the B800-850 LH2 from *Rsp. acidophila* (168). The mean ratio of the BChl/carotenoid was 1:1.2 ± 0.02 for the B800-850 LH2 complex from *Alc. vinosum* and 1:1.10 ± 0.01 for the B800-850 LH2 from *Rps. acidophila* (Figure 4.21). The similar ratios suggest the LH2 from *Alc. vinosum* doesn't contain an extra BChl per heterodimer subunit. Small differences observed in the intensity of the carotenoid peaks will be due to the different extinction coefficients of the different carotenoids present between the LH2 complexes of *Rps. acidophila* and *Alc. vinosum*.

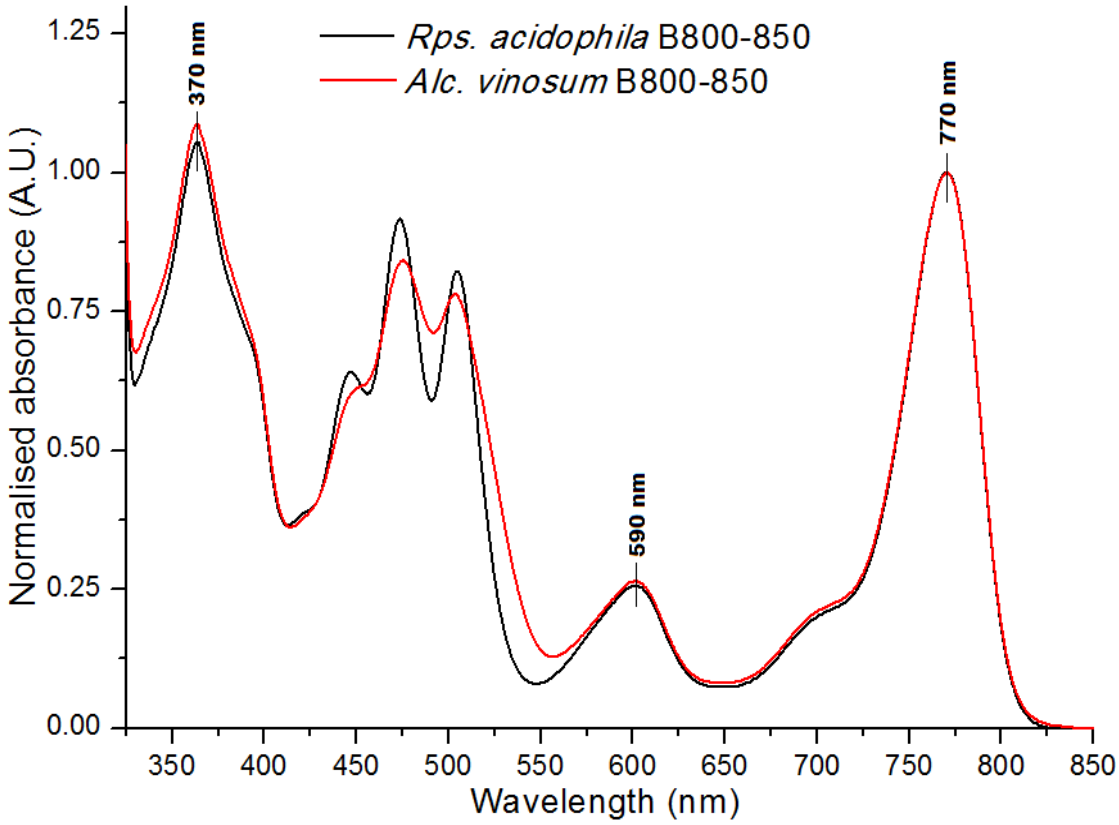

Figure 4.21 Normalised absorption spectra of the pigment mix extracted from the B800-850 LH2 complex from *Rps. acidophila* the B800-850 LH2 complex from *Alc. vinosum*. Absorption spectrum of the pigments extracted from the B800-850 LH2 from *Alc. vinosum* (red) and *Rps. acidophila* showed peaks at relating to the free BChl at 770 nm (Qy), 600 nm (Qx), and 370 nm (Soret) and carotenoids between 450 nm- 550 nm. The ratio of the Qy peak to the highest intensity carotenoid peak was 1:1.2 ± 0.02 for the B800-850 LH2 complex from *Alc. vinosum* and 1:1.10 ± 0.01 for the B800-850 LH2 from *Rps. acidophila*. This suggests there isn't an additional BChl molecule per heterodimer subunit in the LH2 of *Alc. vinosum*. This data were published in Löhner et al, 2015 (168).

Differences in the B800 BChl binding within an individual LH2 complex can be further elucidated through the use of single molecule spectroscopy, to

determine the level of variation between the different B800 BChl. Low temperature, single molecule fluorescence excitation spectroscopy of the B800-850c LH2 complex type from *Alc. vinosum* was acquired by Prof Alexander Löhner and Jurgen Kohler working closely with Dr Anne-Marie Carey as part of this work (168). Recording the fluorescence-excitation spectrum for single LH2 complexes allows the resolution of some of the absorption bands of individual B800 BChl bound within the LH2 complex that are not observable in the ensemble fluorescence-excitation spectrum. Variations observed in the B800 BChl absorption bands relate to the differences in site energy between the B800 BChl. However, there may not be absorption bands for all the BChl in each spectrum due to the level of delocalisation that occurs over several of the BChl present in the ring (169). As in absorption spectroscopy, the low temperature narrows the emission and excitation bands observed and improves the resolution of them.

The B800-850c LH2 complex was purified (as described in Methods and Materials section 2.5.1) and diluted to either 20 pM for the single complex spectra or 6 nM for ensemble spectra. The absorption lines observed were compared to the standard models of the B800-850 LH2 complexes from *Rps. acidophila* and *Phs. molischianum*.

The study (168) found that the number of B800 BChl absorption bands observed for the B800-850 LH2 from *Rps. acidophila* averaged between 2 and 5, with a mean of 3.1 ± 0.2 absorption bands (Figure 4.22). For the B800-850 LH2 from *Phs. molischianum* the number of B800 BChl bands observed ranged from 2 to 6, with an average of 3.4 ± 0.3 absorption bands. Multiple absorption bands were observed for the LH2 from *Alc. vinosum* with a range of between three and nine absorption bands observed with a mean of 6.8 ± 0.15 bands. This indicated that the B800-850c LH2 complex from *Alc. vinosum* has more than double the average number of B800 BChl absorption bands recorded in comparison with B800-850 from Phs. *molischianum* and *Rps. acidophila*.

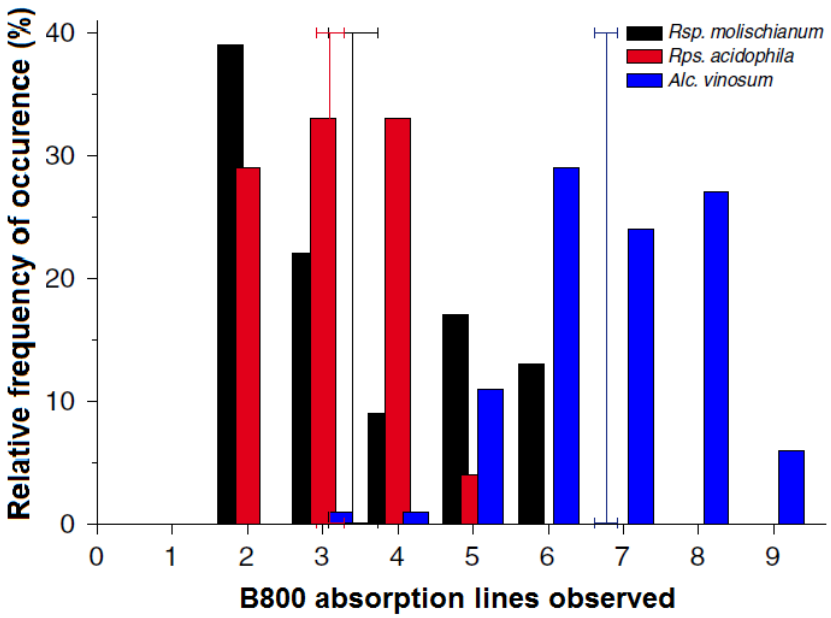

Figure 4.22 Number of absorption bands observed from the B800 BChl in the B800-850 LH2 complex from *Rps. acidophila*, *Phs. molischianum*, and *Alc. vinosum* using single molecule fluorescence spectroscopy.
The range of the number of B800 BChl absorption bands observed for the B800-850 LH2 from *Rps. acidophila* averaged between 2 and 5 (red), with a mean of 3.1 ± 0.2. The range of the number of absorption bands observed for the B800-850 LH2 from *Phs. molischianum* (black) was from 2 to 6, with a mean of 3.4 ± 0.3. The range in the number of absorption bands observed for the B800-850 LH2 from *Alc. vinosum* (blue) was between 3 and 9 absorption bands observed with an average 6.8 ± 0.15. The average number of absorptions recorded for the B800-850 LH2 from *Alc. vinosum* is higher than that observed for the B800-850 LH2 complex from both *Phs. molischianum* and *Rps. acidophila*. This data were published in Löhner et al, 2015 (168).

The bigger the range of B800 absorption bands, the larger number of different site energies and angles present in the LH2 complex. Being that the range was more than double that observed in that of either *Phs. molischianum* or *Rps. acidophila* this would imply more than double the number of site energies for the B800 from *Alc. vinosum*. This would concur with the heterogeneity of the LH2 complexes and the fact that there are two differently bound populations of B800 BChl.

The fluorescence excitation spectra were modelled through several Monte Carlo simulations to re-create the ensemble spectrum and ultimately test the understanding of the system. Deductions from earlier in this work were incorporated into the simulations such as similarities of the peptide binding of the B800 BChl to the B800-850 of *Phs. molischianum* (section 4.2.1) and the implication of a larger ring size than that of either the two known model LH2s that is probably a 12-mer (115, 119). The final simulation was created on the basis that the B800 BChl are excitonically coupled, rotated at 10 ° with respect

to the B850 BChl, as in *Phs. molischianum* (80), within a 12-mer ring. It was found that these considerations suitably recreated the native B800-850 LH2 fluorescence ensemble spectrum from *Alc. vinosum* (168).

4.5.1 Circular dichroism of the different LH2 complex types from *Alc. vinosum*

Circular dichroism (CD) can be used to measure the conformational integrity of the light-harvesting system and can be used to yield information on the excitonic coupling state of the BChl. This technique was used to investigate whether the B800 BChl are excitonically coupled as indicated by the Monte Carlo simulations (section 4.5.1). Previous CD studies have shown that monomeric BChl are observed as a single peak (170) whileas excitonic coupling exhibits a doublet (positive and negative Cotton effects) in the NIR region of the spectrum (171).

The NIR CD spectra were recorded for the different LH2 complex types of *Alc. vinosum* and the B800-850 LH2 from *Rps. acidophila*. The B800-820, B800-840p, and B800-850c LH2 complexes were prepared as outlined in Methods and Materials section 2.5.1. The CD spectrum of the B800-850 LH2 from *Rps. acidophila* was acquired (as outlined in Methods and Materials section 2.7) and the spectrum observed (Figures 4.22-4.26 black) matched previously published data (72, 141). There was a negative singlet at ~795 nm, and a doublet consisting of a positive maximum at 850 nm followed by a negative minimum at 872 nm in the CD spectrum.

The CD spectra of all the complex types of *Alc. vinosum* show a doublet consisting of a positive maximum at ~ 786 nm followed by a zero crossing at 796 nm and a negative minimum at ~ 807 nm or ~ 810 nm. This doublet relates to the B800 BChl. The spectral characteristics and the magnitude of the peaks observed at longer wavelengths were found to differ for each LH2 complex type.

The B800-850c LH2 complex type produces a doublet with a maximum at ~786 followed by a minimum at ~807 nm, with intensities of 5 mdeg and -10 mdeg respectively (Figure 4.23 blue and red). Only the B800-850 from SHL40 growth conditions (Figure 4.23 blue) produce a zero crossing at 838 nm while the B800-850 from THL40 (Figure 4.23 red) dips towards a zero crossing. In both B800-850c

LH2 complexes, there is a second doublet observed that relates to the B850 BChl. The B800-850c produces a minimum at 864 nm of – 14 mdeg (THL40) or – 16 mdeg (SHL40). The B800-850a LH2 complex (Figure 4.23 green) produces a double at ~786 and ~807 nm but with larger peak magnitudes. The dip towards a zero crossing is present at 838 nm but it is further from zero than in the B800-850c complexes. The peaks furthest into the NIR form a doublet as in the B800-850c LH2 complex and the magnitude is the same as the B800-850c produced under THL40 growth conditions.

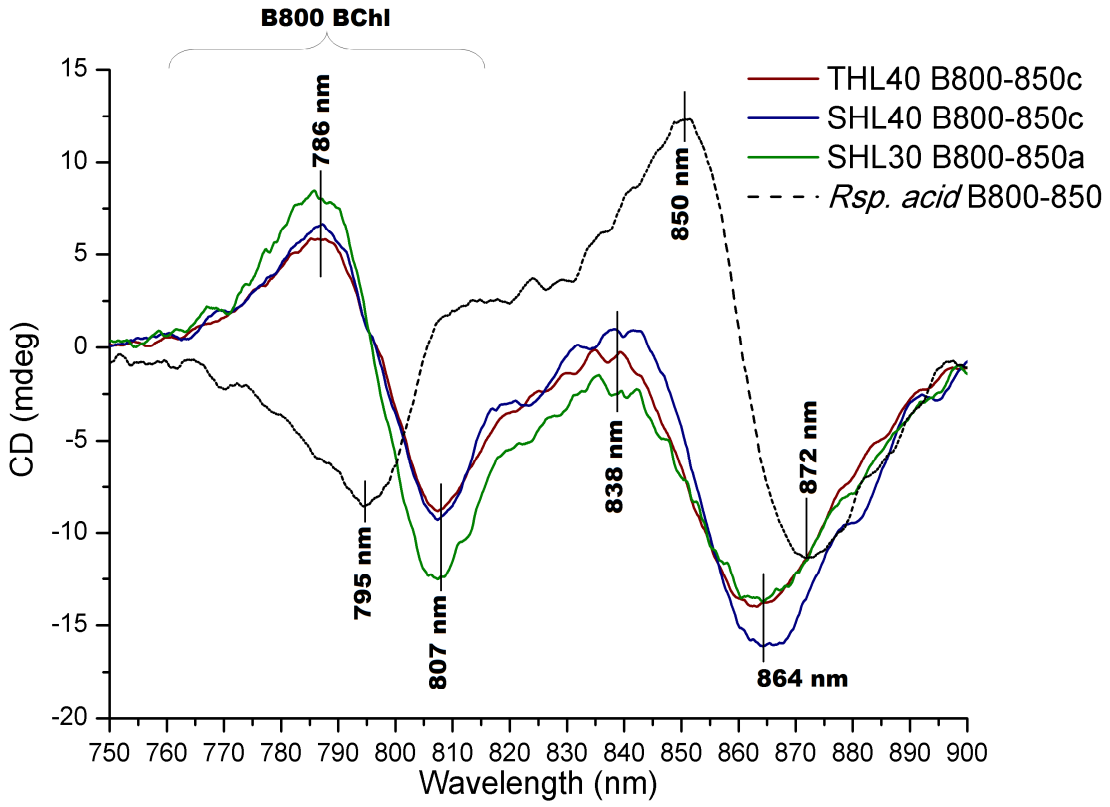

Figure 4.23 NIR room temperature circular dichroism spectra of the B800-850 LH2 complex types produced by *Alc. vinosum* under different growth and nutrient conditions compared to the B800-850 LH2 from *Rps. acidophila*.
The B800-850 LH2 complex from *Rps. acidophila* (black) produces a singlet at 795 nm, followed by a doublet with a maximum at 850 nm followed by a minimum at 872 nm. The B800-850c LH2 complex from THL40 growth conditions (dark red) produces two doublets in the spectrum with a maximum at ~786 followed by a minimum at ~807 nm, and the second doublet with a maximum at 838 nm and minimum at 864 nm. The B800-850c from THL40 growth conditions does not produce a zero crossing. The B800-850c LH2 complex from SHL40 growth conditions (blue) produces two doublets at the same wavelengths as the B800-850c LH2 complex from THL40 growth conditions but it produces a brief zero crossing at 838 nm. The B800-850a LH2 complex from SHL30 growth conditions (green) produces two doublets at the same wavelengths as the B800-850c LH2 complex without a zero crossing. Additionally, the 786 nm and 807 nm peaks are of a higher intensity than those observed in the B800-850c LH2 complex types. Data were published in Carey, et al 2014 (164).

The CD spectra of both the B800-840h (Figure 4.24 cyan) and B800-840p (Figure 4.24 red) LH2 complex types exhibits doublets relating to the B800 BChl that are

centred at the same wavelengths observed in the B800-850 LH2 complex types (786 nm and 807 nm). The intensities of these peaks are identical in the B800-840h and B800-840p LH2 complex types, at 9 mdeg and -12.5 mdeg respectively. The 807 nm minimum of both B800-840 LH2 complex types is a distinct peak followed by a dip towards zero. After a small increase in intensity there is a further negative minimum at ~850 nm in the B800-840h from cells grown in SLL30 growth conditions and at ~ 855 nm in the B800-840p from cells grown in THL30 growth conditions. The intensity of the second negative peak is -10 mdeg for the B800-840p and -8 mdeg for the B800-840h.

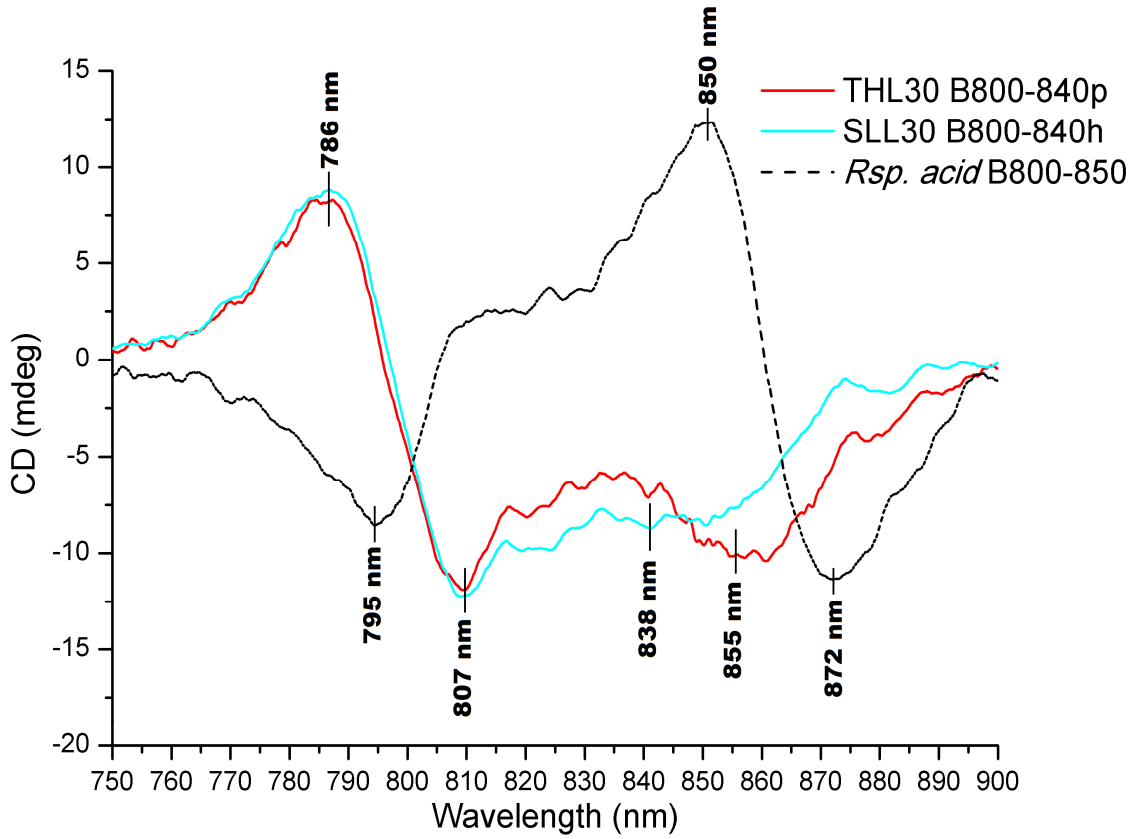

Figure 4.24 NIR room temperature circular dichroism spectra of the B800-840 LH2 complex types produced by *Alc. vinosum* under different growth and nutrient conditions compared to the B800-850 LH2 from *Rps. acidophila*.
The B800-850 LH2 complex from *Rps. acidophila* (black) produces a singlet at 795 nm, followed by a doublet with a maximum at 850 nm followed by a minimum at 872 nm. The B800-840p LH2 complex from THL30 growth conditions (red) produces two doublets in the spectrum with a

maximum at ~786 followed by a minimum at ~807 nm, and the second doublet with a maximum at 838 nm and minimum at ~ 855 nm. The B800-840h LH2 complex from SLL30 growth conditions (cyan) produces the first doublet at the same wavelengths as the B800-840p LH2 complex but the second doublet centres at ~ 838 nm with a minimum at ~ 850 nm. The first doublet is of the same intensity in both the B800-840h and B800-840p LH2 complexes, however the minimum of the second doublet is red-shifted and of a more negative intensity in the B800-840p LH2 complex. Data were published in Carey, et al 2014 (164).

The NIR CD spectra produced by the B800-820 complex type (Figure 4.25 pink) shows the ~786 nm maximum at an amplitude of 10 mdeg followed by a broad (from ~ 810 nm to ~830 nm) negative minimum of -15 mdeg that centres at 820 nm.

When comparing all of the LH2 complex types from *Alc. vinosum* with the B800-850 LH2 from *Rsp. acidophila* (Figure 4.25 black) consistent differences are observed in the CD spectra. The B800 associated maxima and minima produced by the LH2 complex types of *Alc. vinosum* (Figure 4.25 dark red, green, red, pink) form a doublet unlike the singlet observed from the B800-850 from *Rsp. acidophila*. Additionally, the B800 BChl associated minimum at 806 nm in the LH2 complexes of *Alc. vinosum* is more red-shifted than the B800-850 from *Rsp. acidophila* at 795 nm. None of the LH2 complex types of *Alc. vinosum* cross the origin between the B800 and dimeric BChl associated peaks. The LH2 complex types of *Alc. vinosum* produce more blue-shifted doublets associated with the dimeric BChl than the standard B800-850 LH2 model from *Rsp. acidophila* 10050.

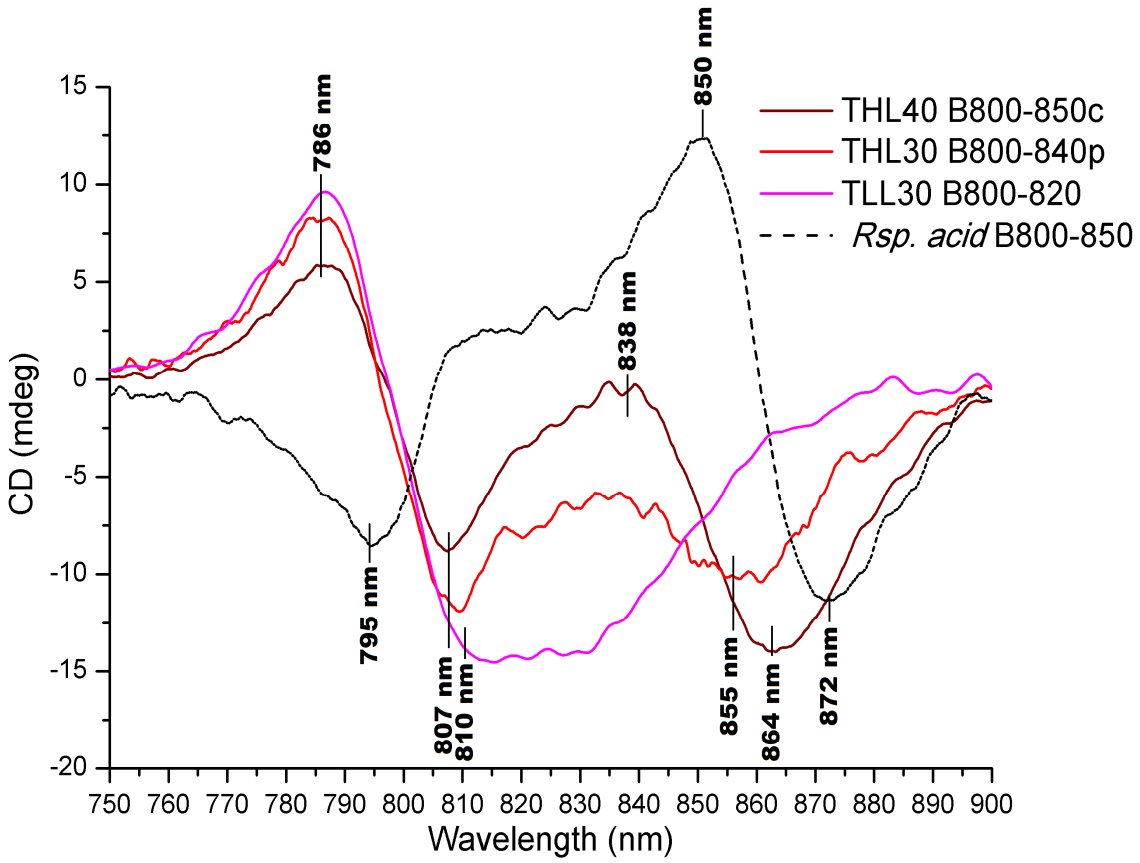

Figure 4.25 NIR room temperature circular dichroism spectra of the LH2 complex types produced by *Alc. vinosum* compared to the B800-850 LH2 from *Rps. acidophila*.
The B800-850 LH2 complex from *Rps. acidophila* (black) produces a singlet at 795 nm, followed by a doublet with a maximum at 850 nm followed by a minimum at 872 nm. The B800-850c LH2 complex (dark red) produces two doublets in the spectrum with a maximum at ~786 followed by a minimum at ~807 nm, and the second doublet with a maximum at 838 nm and minimum at 864 nm. The B800-840p LH2 complex (red) from produces two doublets in the spectrum with a maximum at ~786 followed by a minimum at ~807 nm, and the second doublet with a maximum at 838 nm and minimum at ~ 855 nm. The B800-820 LH2 complex produces a one doublet with a maximum at ~786 followed by a minimum at ~810 nm. The minimum produces a plateau between 807 nm and 830 nm. Data were published in Carey, et al 2014.

These differences observed in the CD spectra imply that the organisation of the BChl in all the LH2 complex types of *Alc. vinosum* is different from those in the B800-850 LH2 complex from *Rps. acidophila*. The presence of the doublet peaks for the B800 BChl is indicative of excitonic coupling and may mean that the B800 split peak is produced from a population of excitonically coupled BChl.

4.6 Resonance Raman spectroscopy

Resonance Raman spectroscopy has been used previously to determine information on the structures of pigments and hydrogen bonding of chemical groups within the light-harvesting complexes of purple photosynthetic bacteria (87, 89, 172-174).

It was hoped that resonance Raman spectroscopy would illuminate the H bonding involved in the B800 BChl and "B850"-like binding sites to identify the changes that form the basis for the spectral changes. The peak frequencies of interest relate to the C3-acetyl and keto carbonyl groups of the BChl ring that are known to be hydrogen bonded in LH2 complex structures. The peaks relating to the keto carbonyl groups and unbound C3 acetyl groups are observed in the higher frequencies. The peaks that relate to unbound C3-acetyls and keto carbonyl groups shift to lower frequencies upon H-bonding; the amount of shift depends on the strength of the H bond formed. In the LH1 there are peaks at 1645 cm^{-1} that have been assigned to the bound C3 acetyl, and at 1667 and 1676 cm^{-1} that relate either to a H bound 13^1 keto carbonyl or unbound C3. Unbound 13^1 keto carbonyls centre at about 1700 cm^{-1}.

The B800-850 and B800-820 LH2 complex types were purified (as described in Materials and Methods section 2.5.1) and sent to collaborators Prof. David Bocian and Qun Tang. Samples were excited in the soret peak of the BChl at 371 nm and the Raman spectra recorded. The peak relating to the carbon-carbon double bond of the carotenoids was observed at 1520 cm^{-1} and 1526 cm^{-1} in the B800-850c LH2 complex (Figure 4.26 bottom spectrum) and B800-820 LH2 complex (Figure 4.26 top spectrum), respectively. The methine bridge of BChl a (172) was observed at 1608/1609 cm^{-1} in both the B800-850 and B800-820 LH2 complex. In the higher frequencies, there is too much background noise to be able to distinguish individual peaks. In the B800-820 LH2 Raman spectrum small peaks were observed at 1691 cm^{-1} and 1817 cm^{-1}. In the B800-850c LH2 Raman spectrum a small peak at 1674 cm^{-1} was observed. This could potentially relate to a H bound 13^1 keto carbonyl or unbound C3 acetyl group although there is very poor resolution in this area of the spectra due to fluorescence.

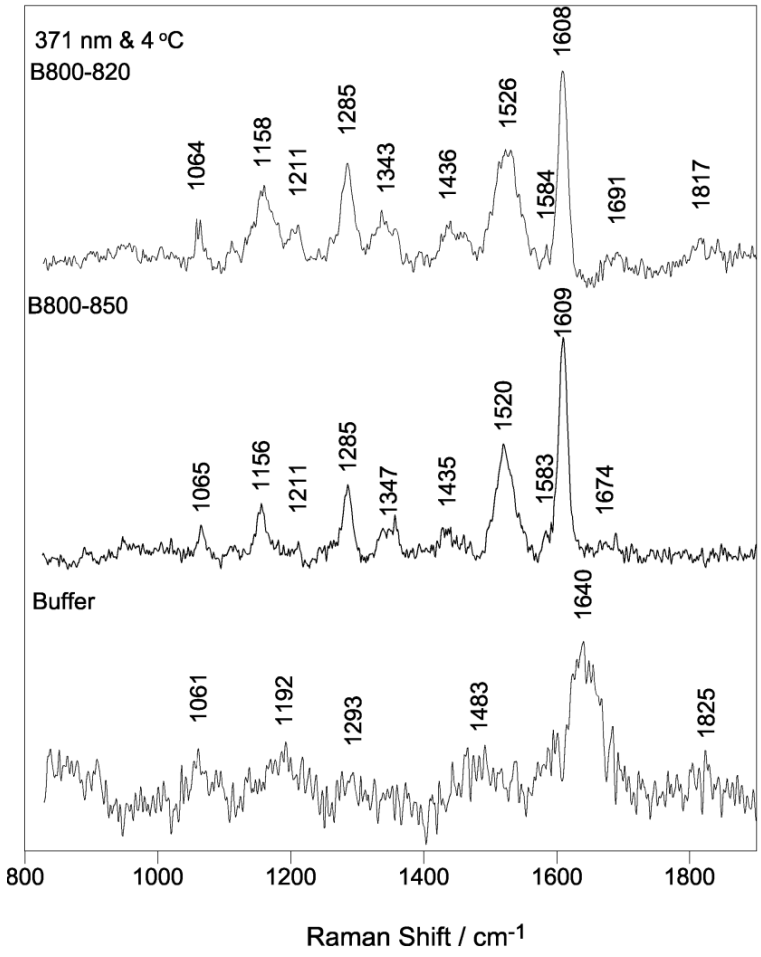

Figure 4.26 Resonance Raman spectra of the B800-820 and B800-850c LH2 complex types from *Alc. vinosum* excited at 371 nm.
The B800-820 LH2 complex (top spectrum) produced peaks in the Raman spectrum at 1064 cm^{-1}, 1158 cm^{-1}, 1211 cm^{-1}, 1285 cm^{-1}, 1343 cm^{-1}, 1436 cm^{-1}, 1526 cm^{-1}, 1584 cm^{-1}, 1608 cm^{-1}, 1691 cm^{-1}, and 1817 cm^{-1}. The B800-850c LH2 complex (middle spectrum) produced peaks in the Raman spectrum at 1065 cm^{-1}, 1156 cm^{-1}, 1211 cm^{-1}, 1285 cm^{-1}, 1347 cm^{-1}, 1435 cm^{-1}, 1520 cm^{-1}, 1583 cm^{-1}, 1609 cm^{-1}, and 1674 cm^{-1}. The peaks at ~ 1520 cm^{-1} is known to be associated with the carbon carbon double bond within the carotenoids, while the peak at 1608 cm^{-1} relates to the methine bridge of the BChl. The higher frequency peaks in the spectrum relate to the C3-acetyl and keto carbonyl chemical groups. There is very poor resolution of the peaks above 1609 cm^{-1}.

Resonance Raman spectra were repeated in the presence of 70 % glycerol (v/v) in preparation for low temperature Raman studies to confirm there were no changes in the spectra due to the addition of glycerol. The presence of 70 % glycerol caused shifts in some of the peaks of both the B800-820 (Figure 4.27 top spectrum) and B800-850 (Figure 4.27 bottom spectrum) LH2 complex types. The shifts observed of the high frequency peaks of the B800-820 LH2 complex is from 1691 cm^{-1} without glycerol to 1665 cm^{-1} and a loss of the potential 1817 cm^{-1} peak in the presence of glycerol. In the B800-850 LH2 complex the 1674 cm^{-1} shifts to 1659 cm^{-1} when in the presence of glycerol. These shifts to lower frequencies suggest that the presence glycerol induces H bonding in the B800-

820 and may enhance the H bonding in the B800-850. Experiments were repeated with fresh samples in 70 % sucrose and the same result was observed. This suggests that both glycerol and sucrose interact with the complexes and alter H bonding meaning that low temperature Resonance Raman cannot be conducted with either of these standard cryoprotectants.

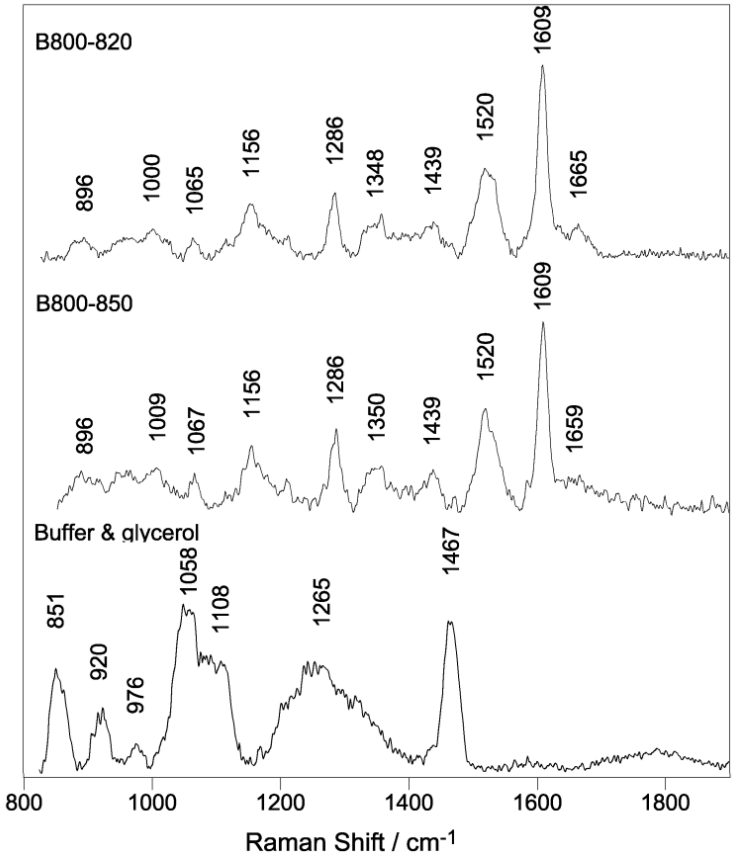

Figure 4.27 Resonance Raman spectra of the B800-820 and B800-850c LH2 complex types from *Alc. vinosum* excited at 371 nm in 70 % glycerol (v/v).
The B800-820 LH2 complex (top spectrum) produced peaks in the Raman spectrum at 1064 cm^{-1}, 1158 cm^{-1}, 1211 cm^{-1}, 1285 cm^{-1}, 1343 cm^{-1}, 1436 cm^{-1}, 1526 cm^{-1}, 1584 cm^{-1}, 1608 cm^{-1}, 1691 cm^{-1}, and 1817 cm^{-1}. The B800-850c LH2 complex (middle spectrum) produced peaks in the Raman spectrum at 1065 cm^{-1}, 1156 cm^{-1}, 1211 cm^{-1}, 1285 cm^{-1}, 1347 cm^{-1}, 1435 cm^{-1}, 1520 cm^{-1}, 1583 cm^{-1}, 1609 cm^{-1}, and 1674 cm^{-1}. The peaks at ~ 1520 cm^{-1} is known to be associated with the carbon carbon double bond within the carotenoids, while the peak at 1608 cm^{-1} relates to the methine bridge of the BChl. The higher frequency peaks in the spectrum relate to the C3-acetyl and keto carbonyl chemical groups. There is very poor resolution of the peaks above 1609 cm^{-1}.

Additional experiments were conducted using other excitation wavelengths to try and explore the BChl binding further. These experiments were hampered by the intense fluorescence signals in the high frequency region of the spectrum due to the BChl soret peak, which prevented the measurement of Raman signals. Ultimately, the issues with high fluorescence from the BChl could not be remedied and the resolution of the red region of spectrum was not forthcoming.

The poor resolution of the high frequency peaks could very well be due to heterogeneous complexes producing multiple site energies within a single complex.

4.7 Summary

The peptides incorporated into the B800-820, B800-840p, B800-850a, and B800-850c LH2 complex types of *Alc. vinosum* were identified using a mix of reverse phase HPLC, MALDI-TOF and tandem MS-MS. This confirmed the heterogeneity of these LH2 complex types and explains some of the trends in data observed using other techniques. The peptides from the puc B4/A4 operon were not identified in any of the LH2 complexes analysed. Of the LH2 complex types, the B800-820 has the most heterogeneity, consisting of four alphas and five betas, while the B800-850c has the least heterogeneity consisting only three alphas and betas. The B800-850a LH2 complex appears to have a similar peptide content to the B800-850c LH2 complex with the exception that the A3 and B2 peptides were not observed. Additionally, the B6 peptide, exclusively found in the B800-820 LH2 complex, and the B5 peptide were observed in the B800-850a LH2 complex.

The modifications of the alpha peptides included the removal of the N terminal methionine. The presence of either an Asp-Asp or Asn-Asp motif indicate the B800 BChl binding site is most probably akin to the *Phs. molischianum* as opposed to that of *Rps. acidophila*. The conservation throughout the beta peptides of *Alc. vinosum* of the ßTrp at position + 26, indicate the beta peptides are probably involved in H bonding the BChl as observed in the LH2 complexes of *Phs. molischianum*.

The ‘tuning’ of the Qy absorption band of the dimeric BChl by the alpha peptides in the case of the A5 peptide appears to be the same as that observed in the B800-820 LH2 complexes of both *Phs. molischianum* and *Rps. acidophila*. For all other peptides identified within the LH2 complexes of *Alc. vinosum*, the basis of the variation in the Qy absorption is more convoluted. Amino acids in positions +10 and +11 are potentially able to form H bonds with the BChl C3-acetyl groups however in the cases of peptides A2, A3, and A6 there are H bond donors in both of these positions. This indicates there may be competition for H bonding and

this will affect the angle of the C3-acetyl group and ultimately the wavelength shift.

The B800-840 LH2 complex type shares peptide in common with both the B800-820 and the B800-850 LH2 complex types, however it lacks the A5 peptide and has a high abundance of B5. This indicates that the LH2 complexes of *Alc. vinosum* are not necessarily descrete complexes but that there may be a range of peptide compositions.

The range of carotenoids observed in the different LH2 complex types didn't change. It was found that the amount of spirilloxanthin was higher in the B800-820 than the B800-850 LH2 complex type and that the level observed in the B800-840p was intermediate between the two LH2 complex types. The EET identified from the different complex types showed little variation in overall efficiency regardless of the LH2 complex type or the variations in carotenoid content. This suggests that the change in carotenoid content is not in order to increase the efficiency of energy transfer between the carotenoid and BChl under different growth conditions. It also suggests that the primary role of the carotenoid in the LH2 complex types from *Alc. vinosum* may not be light-harvesting due to the low efficiency of energy transfer.

Single molecule data and Monte Carlo simulations published in conjuction with this work (113) supported previous findings that both B800 absorption peaks in the LH2 complexes from *Alc. vinosum* are produced from within the same complex. The range of the B800 absorption bands observed confirmed the heterogeneity of the LH2 complexes observed from the peptide analysis. Examination of the potential B800 BChl binding region of the different peptides identified by MALDI-TOF implied there are two different B800 BChl binding sites within the different LH2 complex types, either a double aspartic acid or an asparagine followed by an aspartic acid. This suggested the basis for the difference between the two B800 peaks may lie partially in the binding of the B800 BChl. CD spectra supported the hypothesis from the Monte Carlo simulations that the B800 are excitonically coupled.

Resonance Raman spectroscopy was unsuccessful at illuminating the H bonding on the BChl due to high fluorescence and the inability to perform data

acquisition at low temperatures as both cryo-protectants used, sucrose and glycerol, appeared to cause changes in the hydrogen bonding of the BChl.

Data from this chapter was published in

Carey, A. Hacking, K. Picken, N. Honkanen, S. Kelly, S. Niedzwiedski, D.M. Blankenship, R.E. Shimizu, Y. Wang-Otomo, Z. Cogdell, R.J. "Characterisation of the LH2 spectral variants produced by the photosynthetic purple sulphur bacterium *Allochromatium vinosum*". 2014. Biochimica et Biophysica Akta. (1837). 1849-1860.

Löhner, A. Carey, A. Hacking, K. Picken, N. Kelly, S. Cogdell, R. Köhler, J. "The origin of the split B800 absorption peak in the LH2 complexes from *Allochromatium vinosum*". 2015. Photosyn. Res. (123) 23-31

And the accepted manuscript

Magdaong, N.M. LaFountain, A.M. Hacking, K. Niedzwiedzki, D.M., Gibson, G.N., Cogdell, R.J. Frank, H.A. "Spectral heterogeneity and carotenoid-to-bacteriochlorophyll energy transfer in LH2 light-harvesting complexes from *Allochromatium vinosum*". 2016. Photosyn. Res. (127). 171-187

Chapter 5 - Creation of a carotenoidless LH2 from *Alc. vinosum*

5.1 Introduction

The aims of this chapter were to create a carotenoidless LH2 complex from *Alc. vinosum* for reversible dissociation trails. This will take a multi-pronged approach to create carotenoid-depleted LH2 complexes either through inhibition, genetic 'knock-out', or extraction of the carotenoid after the complex has formed.

Reconstitution has been used effectively in past research to examine the relationships between different structural elements within the LH1 (121-123, 127, 175). The process of reconstitution involves taking the complex apart and putting it back together (reversible dissociation) or creating a complex from component parts. Dissociation of LH1 is best achieved in the absence of carotenoids, as this increases the yield of reconstituted complex (122). Carotenoidless mutants are therefore useful for reconstitution studies. A carotenoidless LH2 complex from *Alc. vinosum* must be developed as a reconstitution candidate to prepare for reversible dissociation studies.

Previous work has used carotenoidless mutants (121), light-harvesting complexes produced under carotenoid biosynthesis inhibition conditions (128), or alternatively the carotenoids were from the light-harvesting complexes using a benzene wash (68).

5.2 Inhibition studies

One method of creating carotenoid depleted light-harvesting complexes has been to use carotenoid biosynthesis inhibitors. Diphenylamine (DPA) inhibits the carotenoid biosynthesis pathway (as outlined in Introduction section 1.4) through the inhibition of the phytoene desaturase enzyme (CrtI) (83, 133, 135, 137, 176-178). DPA has been found to be effective at inhibiting the carotenoid biosynthesis in *Alc. vinosum* previously (134) but the correct concentration range of DPA to create carotenoidless LH2 complexes needs to be established.

5.2.1 **Confirming effective DPA concentration range**

Previous studies identified concentrations above ~ 70 µM DPA to be effective in inhibiting the carotenoid biosynthesis pathway without preventing cell growth in *Alc. vinosum* (134), *Rps. palustris* (83), and *Alc. minuitissimum* (135).

Alc. vinosum was grown under a range of DPA concentrations from 0 µM to 100 µM DPA (as described in Materials and Methods section 2.11.1). There was no observable change in colour of the cells in concentrations of DPA beneath 40 µM (Figure 5.1 control, 10 µM, 20 µM, and 30 µM bottles), after which there is a shift from red/orange to yellow/green (Figure 5.1 40 µM). At 50 µM the colour is pronouncedly more green (Figure 5.1), but there are still carotenoids produced under these conditions.

Figure 5.1*Alc. vinosum* cultured in the presence of DPA between 0 µM and 50 µM under sulphide, high light, 40 ºC growth conditions.
The control culture grew and produced pigmented cells that were red/pink in colour. In the presence of 10 µM, 20 µM, and 30 µM DPA there are no visible changes in growth or carotenoid content. In the presence of 40 µM DPA the culture produced is yellow in colour indicating an abundance of carotenoids with shorter chromophores, a by-product of the inhibition of phytoene desaturase. At 50 µM DPA the culture appears green, indicating that there may be some carotenoids still present but they have much shorter chromophores and so their absorbance is further towards the blue part of the absorption spectrum.

Alc. vinosum cultures grown at 65 µM DPA were a grey-green colour, while cultures grown at 70 µM DPA were a grey-blue colour (Figure 5.2). At 100 µM DPA, growth of *Alc. vinosum* cells was completely inhibited due to the toxic effects of DPA.

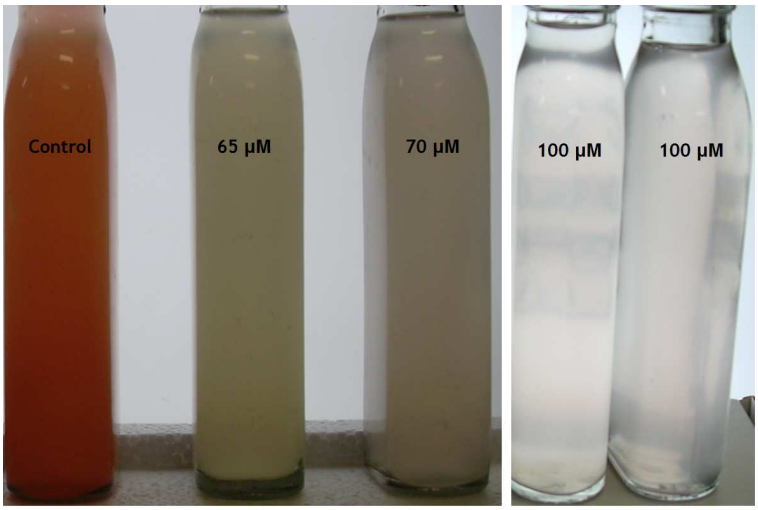

Figure 5.2 *Alc. vinosum* cultured in the presence of DPA between 65 µM and 100 µM under sulphide, high light, 40 ºC growth conditions.
The control culture grew and produced pigmented cells that were red/pink in colour. In the presence of 65 µM DPA the colour of the culture appears to be somewhat green-grey colour indicating a reduction in the carotenoid content and that the carotenoids present have shorter chromophores. At 70 µM DPA the culture appears blue-grey, indicating that there is a negligible level of carotenoids. In the presence of 100 µM DPA no growth of the cultures was observed, suggesting this is a toxic concentration for the *Alc. vinosum* cells.

Production of the carotenoidless LH2 complex was up-scaled to larger culture volumes for DPA concentrations between 65 µM and 80 µM (as described in Methods and Materials section 2.11.2). Cultures grown in the presence of DPA between 65 µM to 75 µM grew well and were blue in colour (Figure 5.3). The blue colour is due the fact that level of carotenoid is too low to absorb any of the blue-green light indicating that there is little to no carotenoid present in the cultures.

Figure 5.3 *Alc. vinosum* cultured in the presence of DPA at 65 µM, 70 µM and 75 µM under sulphide, high light, 30 ºC growth conditions.
The control culture grew and produced pigmented cells that were red/pink in colour. In the presence of 65 µM DPA the colour of the culture appears to be somewhat blue-grey colour indicating a reduction in the carotenoid content and that the carotenoids present have shorter chromophores. At 70 µM and 75 µM DPA the culture appears blue, indicating that there is a negligible level of carotenoids. In the range of DPA concentrations between 65-75 µM the level of inhibition that could be assayed by eye was similar, suggesting this is definitely an effective concentration range to use to create carotenoid depleted light-harvesting complexes.

5.2.2 Carotenoid biosynthesis inhibition under different growth conditions using DPA

Having confirmed the effective concentration range of DPA for inhibiting carotenoid biosynthesis, further work required testing the effect of carotenoid depletion on the different LH2 complex types, by growth under different growth conditions. *Alc. vinosum* was grown in the presence of DPA under different growth conditions (as described in Methods and Materials section 2.11.2) as different LH2 complex types are produced depending on the growth and nutritional conditions as outlined in chapter 3. It was unknown whether all or only some of the LH2 complex types are able to be carotenoid depleted.

Absorption spectra of DPA treated and untreated whole cells were recorded to preliminarily confirm the presence of the light-harvesting complexes and carotenoids. As ascertained in chapter 3 section 3.3 of this work, in whole cells and membranes the peak at ~ 890 nm is associated with the LH1/RC “core” complex while the other two peaks in the NIR, such as the broad peak at 807 nm

and the variable second peak between 820 – 850 nm correspond to the LH2 complex types present.

Cells grown under thiosulphate, high light, 40 ºC growth conditions produce absorption peaks at 807 nm, 856 nm (LH2), and 890 nm (LH1) in the NIR (Figure 5.4 black). In cells grown under the same growth conditions but in the presence of DPA (Figure 5.4 red) produce the 807 nm and 856 nm peaks but the 890 nm absorption peak is reduced in intensity to a shoulder. The peaks associated with the carotenoids at ~460 nm, ~ 490 nm, ~ 525 nm, and ~ 550 nm are present in the cells treated with DPA but the level of light scattering is higher than that observed in untreated cells.

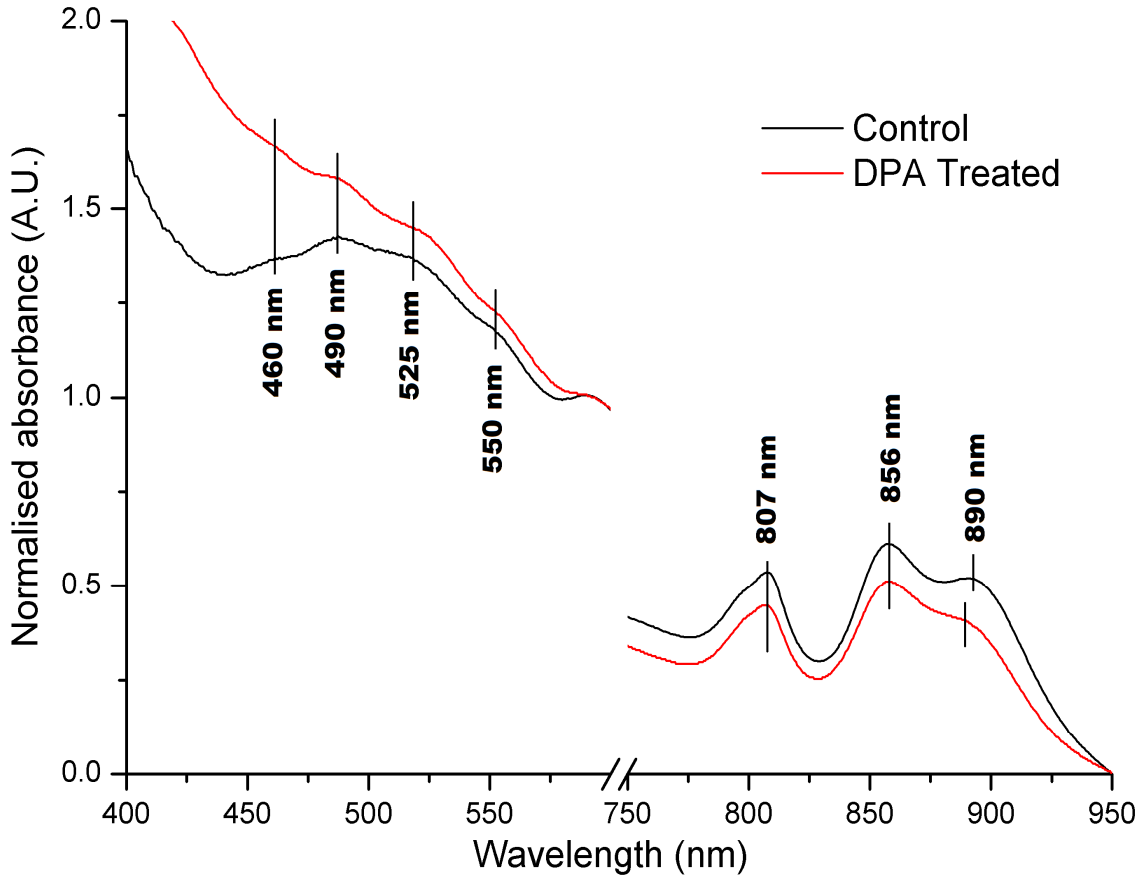

Figure 5.4 Normalised absorption spectra of *Alc. vinosum* cells grown under thiosulphate, high light, 40 ºC growth conditions in the presence of 75 µM DPA contrasted with untreated cells.
Cells grown without DPA treatment (black) produce absorption peaks at 807 nm, 857 nm (LH2) and 890 nm (LH1). The carotenoid peaks in the region between 450 nm and 550nm produce humps at ~460 nm, ~490 nm, 525 nm, and 550 nm. Cells grown in the presence of DPA (red) produce absorption maxima at the same positions in the NIR as untreated cells although the 890 nm peak is reduced to a shoulder. In the carotenoid region there is an increase in light scattering but the carotenoid peaks are still observed. The carotenoid peaks present appear to be in similar positions to those from untreated cells.

Alc. vinosum cells grown in the presence of sulphide under high light at 40 ºC growth conditions (Figure 5.5 black) produce absorption peaks at the same wavelengths as cells cultured under thiosulphate, high light, 40 ºC growth conditions. When cells were grown in the presence of DPA (Figure 5.5 red), the 856 nm peak red-shifted by 1-2 nm and the 890 nm peak blue-shifted by 4-5 nm, from their positions in the absorption spectrum of untreated cells. The absorption peaks observed in the carotenoid region are completely levelled out in cells grown in the presence of DPA. The increase in scattering observed under THL40 growth conditions was also observed under SHL40 growth conditions. There was change in intensity of the Qy peaks associated with the LH2 complex however the peak at ~ 890 nm associated with the LH1 complex shows a slight decrease in intensity relative to the 856 nm peak associated with the LH2.

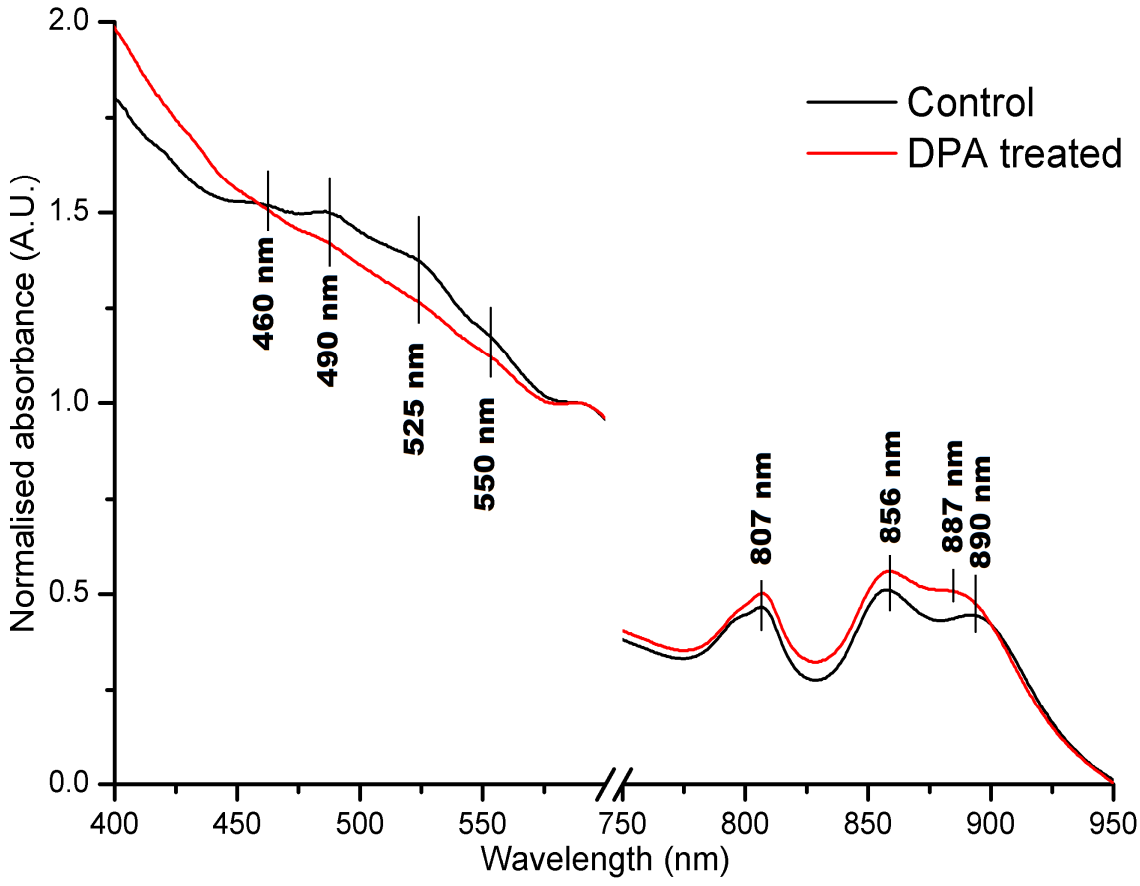

Figure 5.5 Normalised absorption spectra of *Alc. vinosum* cells grown under sulphide, high light, 40 ºC growth conditions in the presence of 75 µM DPA contrasted with untreated cells. Cells grown without DPA treatment (black) produce absorption peaks at 807 nm, 856 nm (LH2) and 890 nm (LH1). The carotenoid peaks in the region between 450 nm and 550 nm produce humps at ~460 nm, ~490 nm, 525 nm, and 550 nm. Cells grown in the presence of DPA (red) produce absorption maxima at 807 nm, 858 nm, and 887 nm. The carotenoid peaks are reduced in intensity after DPA treatment and are not well resolved due to the light-scattering from the membranes. The carotenoid peaks present appear to be in similar positions to those from untreated cells.

When cells were grown under sulphide in high light at 30 °C growth conditions (Figure 5.6 black) the absorption peaks centred at 807 nm, 853 nm, with a shoulder at ~ 890 nm. The carotenoid peaks observed centred at ~ 460 nm, 486 nm, and 525 nm. Cells grown under the same growth conditions but in the presence of DPA produced a red shift of the peak at 853 nm to 856 nm and the shoulder at ~890 nm blue shifted to ~ 885 nm. There was no increase in light scattering in the carotenoid region of the spectra. There were little to no carotenoid peaks observed between 450 – 550 nm over the light-scattering.

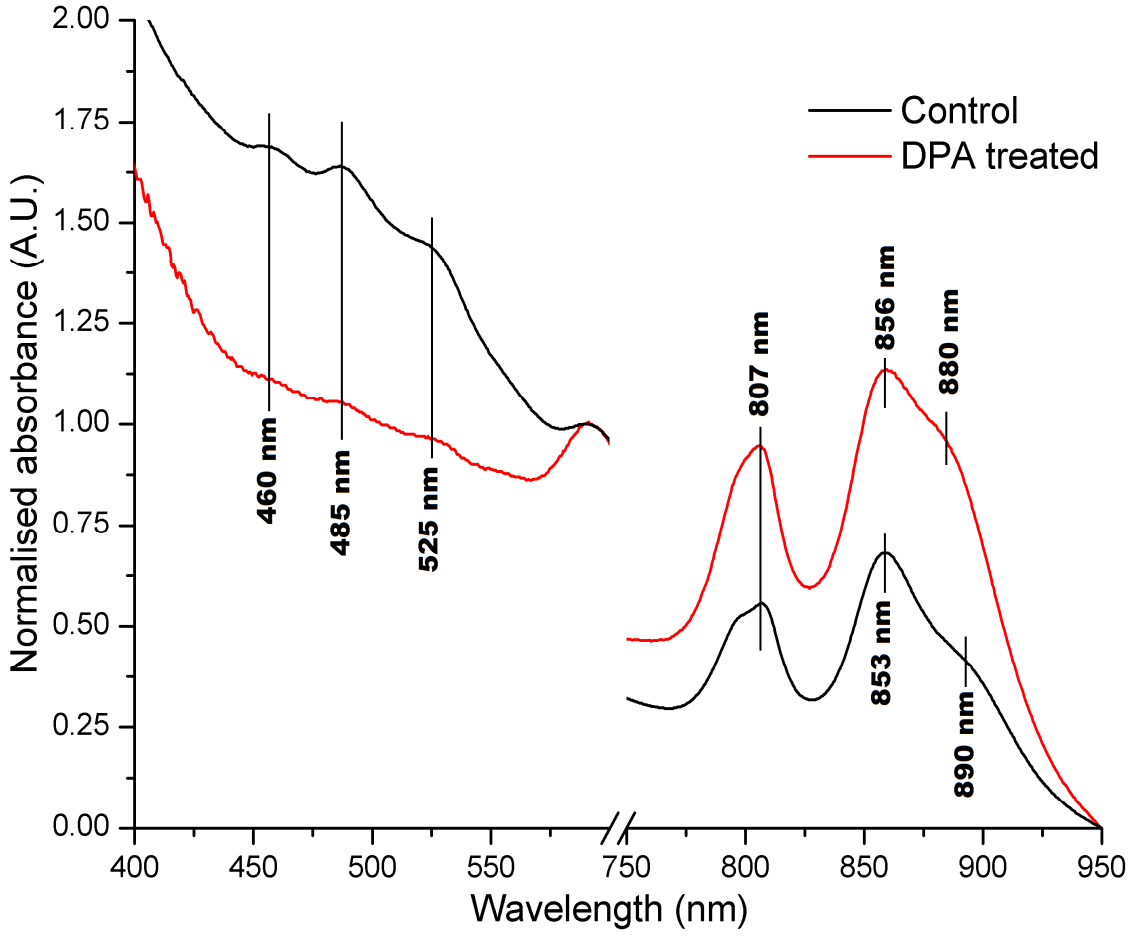

Figure 5.6 Normalised absorption spectra of *Alc. vinosum* cells grown under sulphide, high light, 30 °C growth conditions in the presence of 75 µM DPA contrasted with untreated cells. Cells grown without DPA treatment (black) produce absorption peaks at 807 nm, 853 nm (LH2) and 890 nm (LH1). The carotenoid peaks in the region between 450 nm and 550 nm produce humps at ~460 nm, 485 nm, and 525 nm. Cells grown in the presence of DPA (red) produce absorption maxima at 807 nm, 856 nm, and a shoulder at ~ 880 nm. The carotenoid peaks are reduced in intensity after DPA treatment and are not well resolved due to the light-scattering from the membranes. The overall level of light-scattering is far lower than that observed when *Alc. vinosum* is grown under other growth conditions.

The peaks observed in the absorption spectrum of cells grown under high light at 30 °C in the presence of thiosulphate centre at ~ 460 nm, 490 nm, ~ 525 nm, ~

550 nm, 807 nm, 849 nm, and 889 nm (Figure 5.7 black). The absorption spectrum of cells grown in the presence of DPA (Figure 5.7 red) shows a red-shift of the 849 nm peak to 856 nm. In addition to this, the 807 nm peak is reduced in intensity in whole treated whole cells relative to the untreated cells.

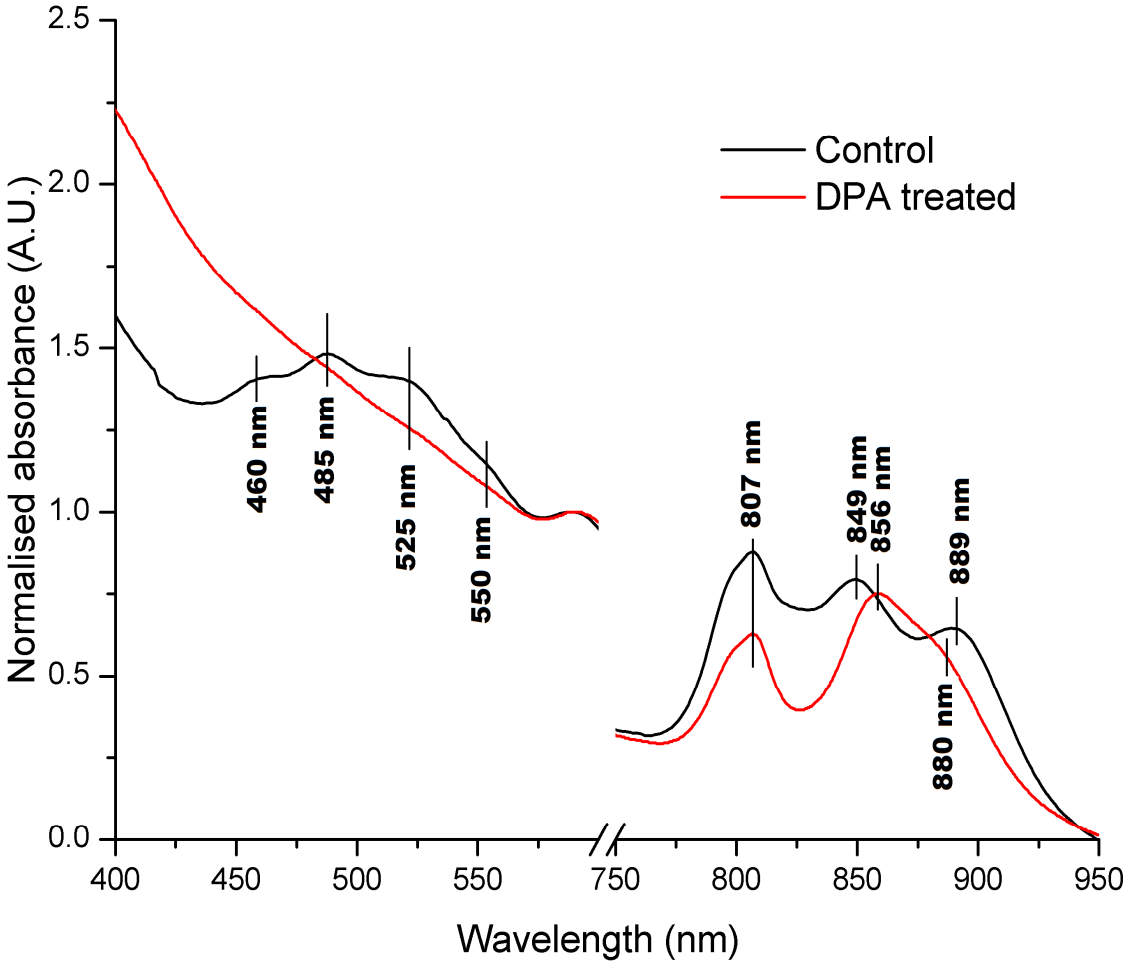

Figure 5.7Normalised absorption spectra of *Alc. vinosum* cells grown under thiosulphate, high light, 30 ºC growth conditions in the presence of 75 µM DPA contrasted with untreated cells.
Cells grown without DPA treatment (black) produce absorption peaks at 807 nm, 849 nm (LH2) and 889 nm (LH1). The carotenoid peaks in the region between 450 nm and 550 nm produce humps at ~460 nm, 485 nm, ~ 525 nm, and ~ 550 nm. Cells grown in the presence of DPA (red) produce absorption maxima at 807 nm, 856 nm, and a shoulder at ~ 880 nm. The carotenoid peaks are reduced in intensity after DPA treatment and are not well resolved due to the light-scattering from the membranes. The overall level of light-scattering is lower than that observed when *Alc. vinosum* is grown under other growth conditions.

As an adaption to low light conditions, *Alc. vinosum* increases the amount of membranes it produces (as outlined in Introduction section 1.2.3). This results in higher light scattering in the absorption spectra of cells cultured under low light conditions. To be able to visualise the carotenoid region, low light cells were lysed and the membranes analysed (as outlined in Methods and Materials section

2.11.2). Membranes from *Alc. vinosum* cells grown in the presence of sulphide, under low light at 30℃ (Figure 5.8 black) produce absorption peaks at 807 nm, 822 nm, 890 nm, with the main carotenoid peak at 485 nm with two shoulders at ~ 460nm and ~ 525 nm. Membranes produced by cells grown in the presence of DPA (Figure 5.8 red) produced NIR absorption peaks at 807 with a shoulder at ~ 818 nm. The 890 nm peak is blue shifted to 885 nm in membranes from DPA treated cells. The carotenoid peaks are still present but are blue-shifted with a larger shoulder at ~ 460 nm than that observed in membranes from untreated cells.

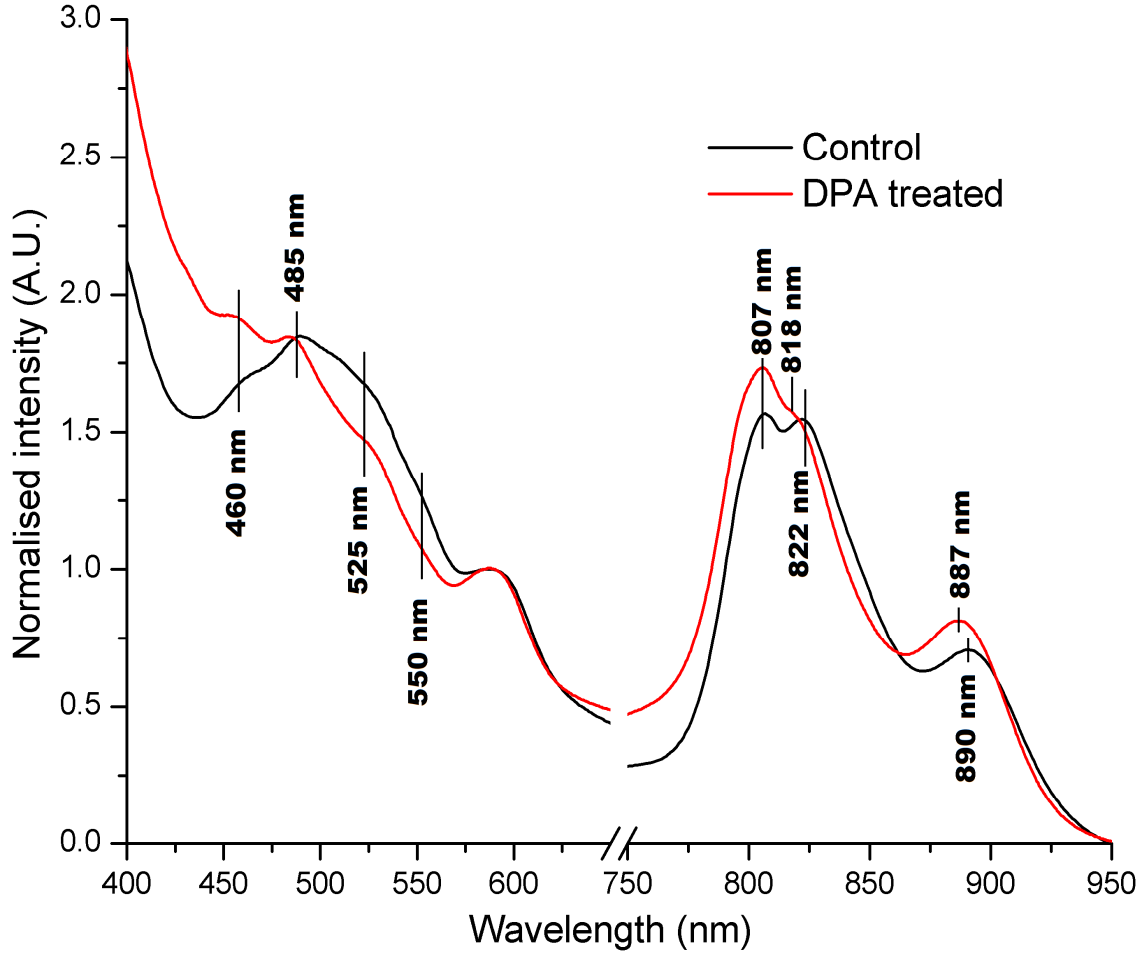

Figure 5.8 Normalised absorption spectra of membranes from *Alc. vinosum* cells grown under sulphide, low light, 30 ºC growth conditions in the presence of 70 µM DPA contrasted with untreated cells.
Membranes from cells grown without DPA treatment (black) produce absorption peaks at 807 nm, 822 nm (LH2) and 890 nm (LH1). The carotenoid peaks in the region between 450 nm and 550 nm produce humps at ~460 nm, 485 nm, ~ 525 nm, and ~ 550 nm. Membranes from cells grown in the presence of DPA (red) produce absorption maxima at 807 nm, 887 nm, and a shoulder at ~ 818 nm. The main carotenoid peak still centres at 485 but the shoulder at 525 nm is blue shifted and reduced in intensity. The shoulder at ~ 460 nm is increased in intensity this indicates an increase in the number of shorter chromophore length carotenoids.

Membranes produced by *Alc. vinosum* grown under low light at 30 °C in the presence of thiosulphate (Figure 5.9 black) produce absorption peaks at 807 nm, 822 nm, and 890 nm in the NIR and at 485 nm, 520 nm, with two absorption shoulders at ~ 460 nm and ~ 550 nm in the carotenoid region. The absorption spectrum of membranes from cells treated with DPA (Figure 5.9 red) shows 820 nm peak is red-shifted to 853 nm and the 890 nm is reduced in intensity to a shoulder. The main absorption peak from the carotenoids is still at 485 nm but peak at 520 nm is reduced in intensity to a shoulder and the shoulder at ~ 460 nm is increased in intensity. The Qx peak is also narrower in the membranes from DPA treated cells.

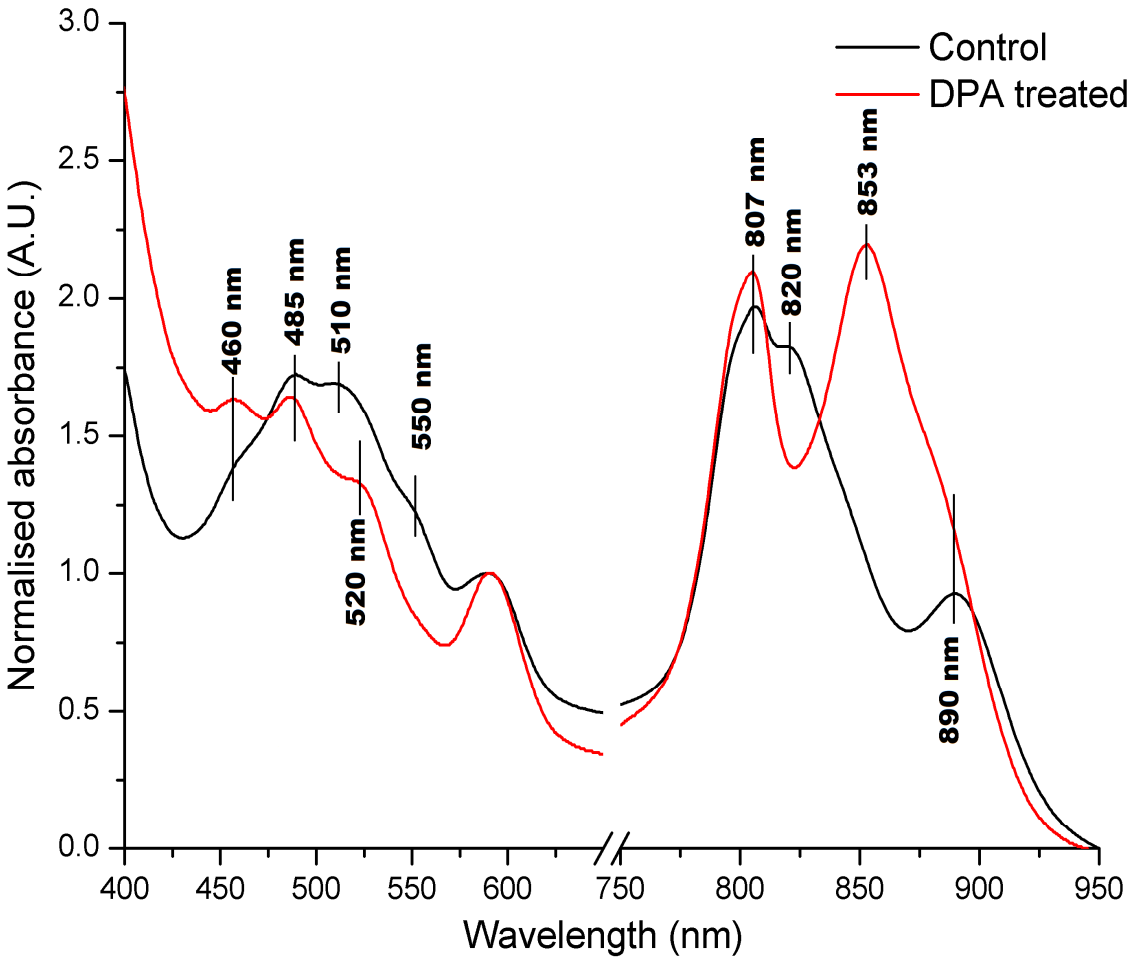

Figure 5.9 Normalised absorption spectra of membranes from *Alc. vinosum* cells grown under thiosulphate, low light, 30 ºC growth conditions in the presence of 75 µM DPA contrasted with untreated cells.
Membranes from cells grown without DPA treatment (black) produce absorption peaks at 807 nm, 820 nm (LH2) and 890 nm (LH1). The carotenoid peaks in the region between 450 nm and 550 nm produce humps at ~460 nm, 485 nm, 510 nm, and ~ 550 nm. Membranes from cells grown in the presence of DPA (red) produce absorption maxima at 807 nm with the 820 nm peak red-shifted to 853 nm and the 890 peak obscured as a shoulder. The main carotenoid peak still centres at 485 but the absorption at 510 nm is red shifted to a shoulder at ~ 520 nm and reduced in intensity. The shoulder at ~ 460 nm is increased in intensity this indicates an increase in the number of shorter chromophore length carotenoids.

Of the carotenoid biosynthesis inhibition observed under all the growth conditions, SHL30 growth conditions showed the lowest levels of carotenoid with the least change to the NIR absorption spectra. This suggests SHL30 growth conditions are the optimum for DPA inhibition studies to create carotenoid depleted LH2 complexes. The absorbance spectra of whole cells from high light conditions and from membranes from low light conditions suggest that the level of carotenoid biosynthesis inhibition is far higher under high light growth conditions.

The 30℃ thiosulphate growth conditions produce large shifts in the NIR absorption spectra after DPA treatment. The LH2 peak associated with the dimeric BChl red-shifts and the LH1 peak blue-shifts. The 807 nm peak associated with the monomeric BChl is of a lower intensity after cells were treated with DPA. The red-shift of the dimeric BChl and the reduction in the 807 nm peak suggests that the carotenoid inhibition is affecting the LH2 complexes produced. This may be either directly through unknown effects on the polypeptide production or due to stability differences between the LH2 complex types meaning that certain LH2 complex types are not stable enough to exist without carotenoids present.

5.2.3 Carotenoid incorporation into the different light-harvesting complexes of *Alc. vinosum* under carotenoid inhibition by DPA.

Spectra of whole cells and membranes cannot show whether the carotenoids present are equally distributed between the LH1/RC "core" and LH2 complexes or whether there is a preferential incorporation into one complex type over another. To determine how the limited carotenoid content is incorporated into the complex types present the light-harvesting complexes must be separated using sucrose density centrifugation. Membranes were prepared and solubilised (as per Methods and Materials sections 2.3 and 2.5.1) to determine the whether the level of carotenoid in the different light-harvesting complex types.

Sucrose density centrifugation gradients (SDCG) separated the LH1/RC and LH2 complex types (Figure 5.10). The top most band of observed in the SDCG are free pigments, followed by the LH2 complex band, and the bottom most band is the LH1/RC "core" complex band. The strong difference in carotenoid content between the light-harvesting complexes produced under low light and high light can be assayed by eye. Across all growth conditions the carotenoid content appears to be higher in the LH2 than the LH1/RC band. This concurs with previous work that found that the carotenoids that were present under carotenoid biosynthesis inhibition with DPA were preferentially incorporated into the LH2 complexes present (83). The LH2 and LH1/RC "core" complexes produced under HL 30 ℃ growth conditions both show high levels of carotenoid depletion. There is very little free pigment observed in the SDCG produced from

SHL30 growth conditions and only a small amount in the THL30 SDCG. The LH2 and LH1/RC complexes from low light conditions show a reduced amount of carotenoid present but are still red pigmented. The LH1/RC and the LH2 bands from cells grown under TLL30 growth conditions show a higher level of carotenoid depletion than the bands from cultures grown under SLL30 growth conditions. The LH1/RC "core" band in the SDCG from TLL30 shows a large reduction in the level of carotenoid present.

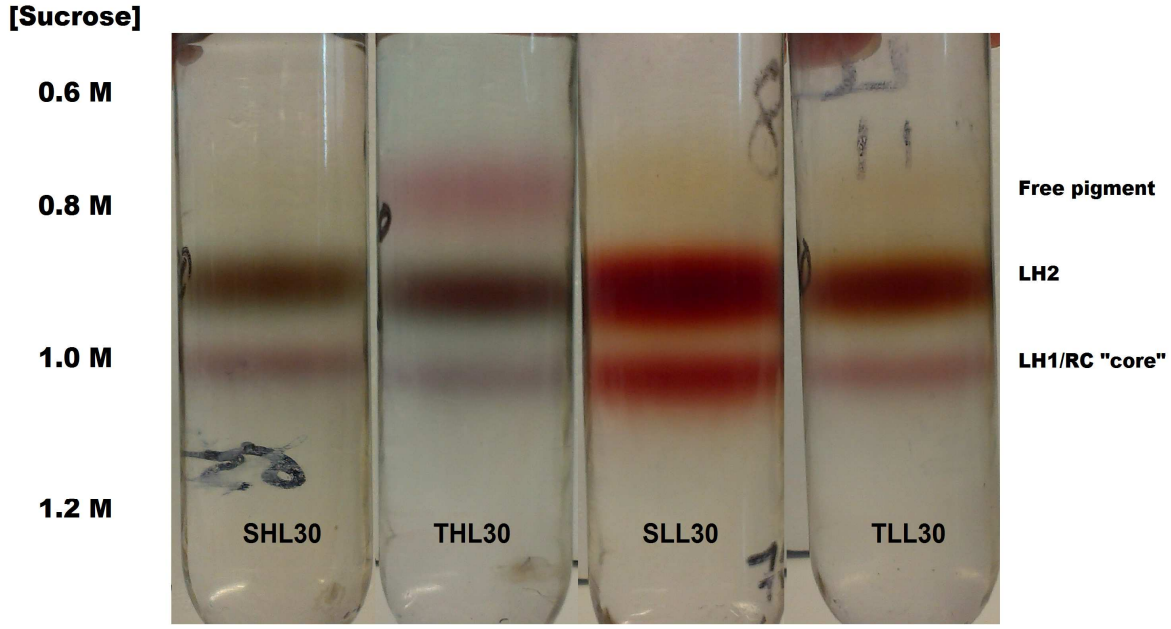

Figure 5.10 LH2 and LH1/RC "core" complexes from *Alc. vinosum* grown in the presence of 70-75 µM DPA under different growth conditions separated by sucrose density centrifugation.
Growth conditions for *Alc. vinosum* cells were thiosulphate (T) or sulphide (S), under high light (HL) or low light (LL) intensity, at 30℃. The top band that equilibrates to ~ 0.8 M sucrose is the LH2 complex, while the band that equilibrates to ~ 1.0 M sucrose is the larger LH1/RC "core" complex. Unbound carotenoid pigments equilibrate in a band above the LH2 complex. Of the light-harvesting complexes produced under SHL30 growth conditions, the LH2 band is dark green and is larger than the LH1/RC "core" band, which is blue-purple. There is a small amount of free pigment that is yellow in colour in a band above the LH2 band. In the SDCG of light-harvesting complexes produced under THL30 growth conditions, the LH2 band is dark green and is larger than the LH1/RC "core" band, which is blue-purple. The free pigment band present is pink in colour. In the SDCG of light-harvesting complexes produced under SLL30 growth conditions, the LH2 band is dark red and is larger than the LH1/RC "core" band, which is red. The free pigment present above the LH2 complex band is orange in colour. In the SDCG of light-harvesting complexes produced under TLL30 growth conditions, the LH2 band is dark red-brown and is larger than the LH1/RC "core" band, which is pale pink. The free pigment present is orange in colour. The carotenoid content is higher in the LH2 complexes than the LH1/RC "core" complex produced under all growth conditions.

Absorption spectra of the crude LH1/RC "core" complex fraction from SDCG produced by *Alc. vinosum* grown under different nutritional and growth conditions show a high level of carotenoid inhibition (Figure 5.11). The HL30

growth conditions have the least carotenoid present in the LH1/RC “core” complexes (Figure 5.11 green and red), while the LH1/RC “core” from SLL30 growth conditions (Figure 5.11 cyan) has the highest amount of carotenoid. LH1/RC “core” produced under TLL30 growth conditions (Figure 5.11 purple) has a low level of carotenoid but still produces peaks at 485 nm, with shoulders at ~ 460 nm, and ~ 525 nm. All the carotenoid peaks present are blue-shifted from those observed in the untreated LH1/RC “core” complex indicating an increase in shorter length chromophores in the carotenoids present. The Qy peaks show a small blue shift of 5 nm in LH1/RC complexes from all growth conditions except those produced under SLL30 growth conditions. This blue shift in the absence of carotenoids was observed in previous studies on the LH1/RC “core” (121).

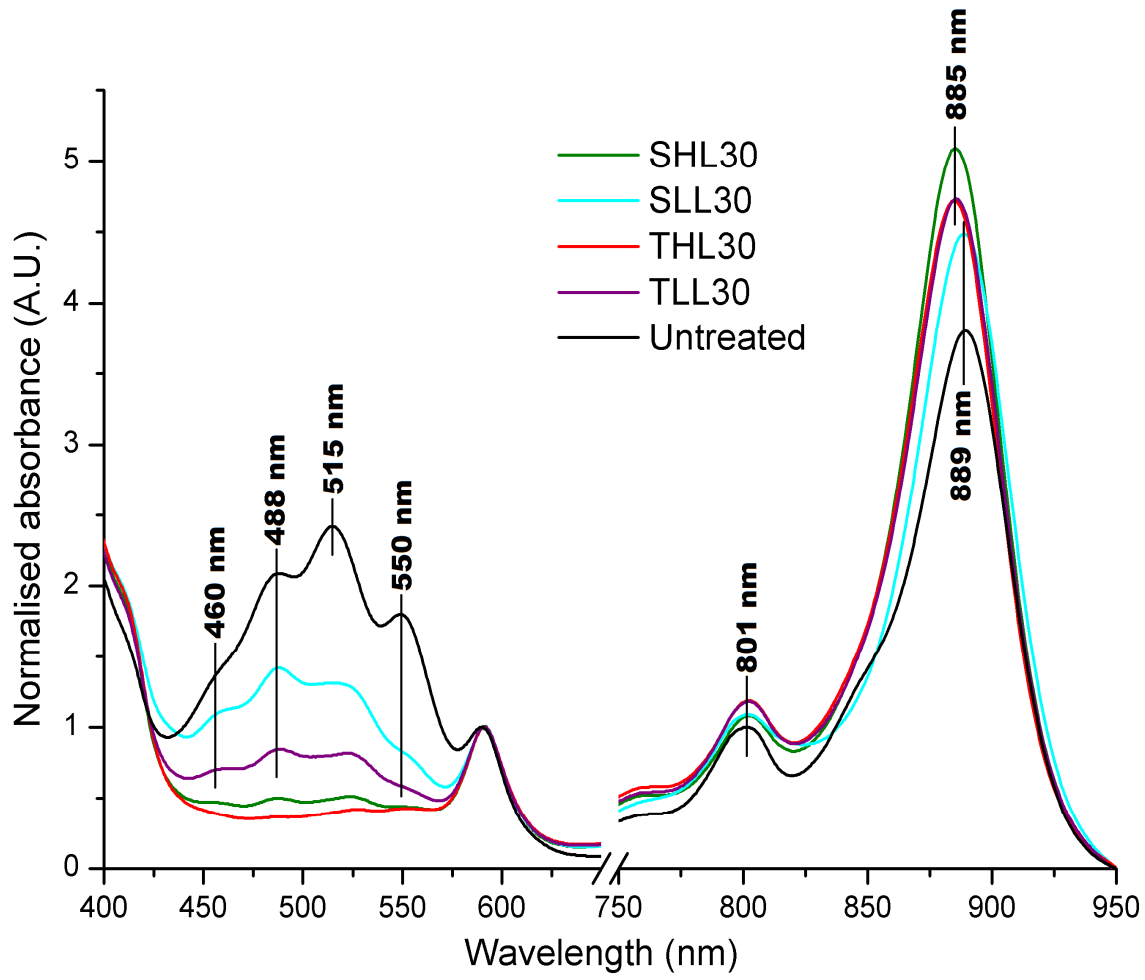

Figure 5.11 Normalised absorption spectra of the LH1/RC complexes from *Alc. vinosum* grown under different growth and nutritional conditions in the presence of 70 µM - 75 µM DPA and separated by sucrose density centrifugation.
Growth conditions for *Alc. vinosum* cells were thiosulphate (T) or sulphide (S), under high light (HL) or low light (LL) intensity, at 30℃. The LH1/RC "core" complex produced by untreated *Alc. vinosum* (black) produces a peak at 889 nm and 801 nm in the NIR, and 488 nm, 515 nm, and 550 nm in the carotenoid region. The LH1/RC "core" complex produced under SHL30 growth conditions (green) in the presence of DPA produces a peak at 885 nm and 802 nm. The LH1/RC "core" complex produced under THL30 growth conditions (red) in the presence of DPA produces a peak at 885 nm and 802 nm. The LH1/RC "core" complex produced under carotenoid biosynthesis conditions under SHL30 and THL30 growth conditions produce small to negligible peaks in the 450-550 region of the spectrum. The LH1/RC "core" complex produced under TLL30 growth conditions (violet) in the presence of DPA produces peaks at 886 nm and 802 nm, 488 nm, and 514 nm with a shoulder at ~460 nm in the carotenoid region. The LH1/RC "core" complex produced under SLL30 growth conditions (cyan) in the presence of DPA produces a peak at 889 nm, 802 nm, 488 nm and 514 nm with a shoulder at ~ 460 nm. The LH1/RC "core" complex produced under SLL30 growth conditions in the presence of DPA has the largest amount of coloured carotenoids of all the LH1/RC "core" complexes produced under carotenoid biosynthesis inhibitive conditions.

The absorption spectra of the crude LH2 complex fraction extracted from *Alc. vinosum* under carotenoid biosynthesis inhibiting conditions show different levels of carotenoid depletion depending on the growth conditions (Figure 5.12). There is a large depletion in the carotenoid content of the crude LH2 fraction from cells grown in the presence of DPA under SHL30 growth conditions (Figure 5.12

green). In the NIR region, the maxima observed centre at 798 nm, and 845 nm. The red-most maximum of the “B850”-like BChl is blue-shifted relative to the crude LH2 fraction from untreated cells.

Under THL30 growth conditions, a similar level of carotenoid inhibition is observed in the LH2 crude fraction (Figure 5.12 red). The level of carotenoid is negligible and far below the intensity of the Qx peak. The differences in the NIR region of the spectrum suggest that the LH2 is the basis of the differences observed in the whole cell spectrum. The “B850”-like peak is red-shifted to 844 nm from 841 nm in the LH2 fraction from untreated cells. This confirms the observations from the whole cell spectra, that the LH2 complex type produced under these conditions is changed due to the presence of DPA.

The crude fraction LH2 spectrum from cells cultured under TLL30 growth conditions (Figure 5.12 purple) have an observable but reduced level of carotenoid present. The largest difference in the crude LH2 spectrum is in the NIR region of the spectrum where the “B850”-like peak red shifts to 847 nm after DPA treatment while the “B850”-like peak from LH2 from untreated cells centres at ~ 821 nm. The level of carotenoid still present in the LH2 from SLL30 growth conditions (Figure 5.12 cyan) is the highest observed from all the LH2 complex types and is the only crude LH2 fraction that produces only one peak, at ~800 nm with a shoulder at ~818 nm, as observed in untreated cells.

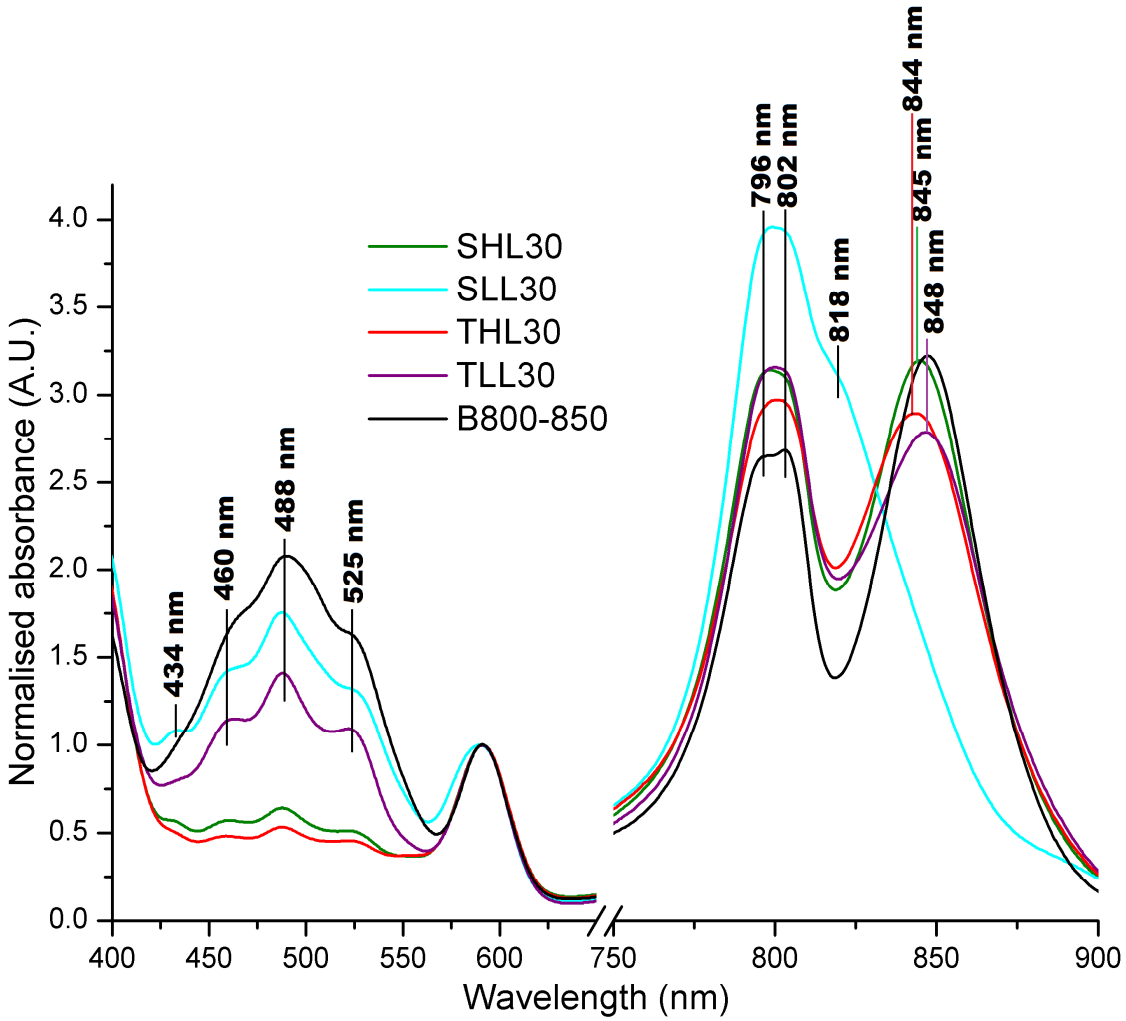

Figure 5.12 Normalised absorption spectra of LH2 complexes produced by *Alc. vinosum* grown under different growth and nutritional conditions in the presence of DPA separated by sucrose density centrifugation.
Growth conditions for *Alc. vinosum* cells were thiosulphate (T) or sulphide (S), under high light (HL) or low light (LL) intensity, at 30℃. The B800-850 LH2 complex produced by untreated *Alc. vinosum* (black) produces a split peak at ~ 800 nm between 796 nm and 802 nm, and a peak at 848 ± 1 nm in the NIR. In the carotenoid region, the LH2 complex produced by untreated cells produces peaks at 590 nm (Qx peak) and 488 nm with two shoulders at ~ 525 nm and ~ 460 nm (carotenoid peaks).. The LH2 complex produced under SHL30 growth conditions (green) in the presence of DPA produces a peak at 845 nm and 800 nm. The LH2 complex produced under THL30 growth conditions (red) in the presence of DPA produces a peak at 844 nm and 800 nm. The LH2 complexes produced under carotenoid biosynthesis conditions under SHL30 and THL30 growth conditions produce small carotenoid peaks at the same wavelengths as the LH2 complex from untreated cultures. This suggests the LH2 complexes produced under these conditions are carotenoid depleted but the complement of carotenoids they do contain appears to be similar to that of the standard LH2 complex.The LH2 complex produced under TLL30 growth conditions (violet) in the presence of DPA produces a peak at 847 nm and 800 nm,464 nm, 488 nm, and 522 nm. The LH2 complex produced under SLL30 growth conditions (cyan) in the presence of DPA produces at 802 nm, 488 nm, with shoulders at ~ 460 nm, ~ 525 nm, ~434 nm and ~ 818 nm. The LH2 complex produced under SLL30 growth conditions in the presence of DPA has the largest amount of coloured carotenoids of all the LH2 complexes produced under carotenoid biosynthesis inhibitive conditions. .

Previous work on other bacteria observed a blue shift of the “B850”-like peak in the B800-850 LH2 complexes in the absence of carotenoid (135). This was observed in the crude LH2 fraction from the SHL30 growth conditions but not

under other conditions where a red-shift was observed. This may be due to other factors than the absence of carotenoid such as the change of which LH2 complex is being produced.

5.2.4 Carotenoid incorporation into the different LH2 complex types of *Alc. vinosum* under carotenoid inhibition by DPA.

The crude LH2 extract from *Alc. vinosum* grown under SHL30 growth conditions was separated using anion exchange chromatography (as outline in Methods and Materials section 2.5.3.3). As was determined earlier in this work (Chapter 3 section 3.4.3), SHL30 growth conditions produce both the B800-850 and B800-820 LH2 complex types. Anion exchange chromatography can be used to determine whether the B800-820 LH2 complex type is still produced under carotenoid biosynthesis inhibitive conditions. If the B800-820 LH2 complex is still present, the level of carotenoid incorporation into the different LH2 complex types can be examined spectroscopically. This could indicate whether the change in LH2 complex is due to unknown non-carotenoid inhibitive effects of the DPA on the polypeptides produced/incorporated into LH2 complexes or whether the B800-820 requires the presence of carotenoid to form.

When the crude LH2 extract from cells treated with DPA and grown under SHL30 was separated on a Biocad anion exchange column both the B800-820 and B800-850a LH2 complex types as well as the B800-850c were observed. The LH2 complex types eluted at the same salt concentration as those in crude extracts from untreated cells. There was not a lot of B800-820 present but enough to record an absorption spectrum (Figure 5.13 red). There was a higher amount of carotenoid incorporated into the B800-820 than the B800-850 fractions, which was also visible to the human eye. The absorption spectra reflected this showing carotenoid peaks higher than the Qx peak of the BChl in the fractions of the B800-820 LH2 complex type. The level of carotenoid present in the B800-850a LH2 complex type (Figure 5.13 green) was greatly reduced from that in the B800-820 LH2 complex type showing peaks of half the intensity of the Qx. The fractions that B800-850c LH2 complex type (Figure 5.13 blue) showed the lowest level of carotenoid incorporation observed with negligible absorption peaks between 450-550 nm.

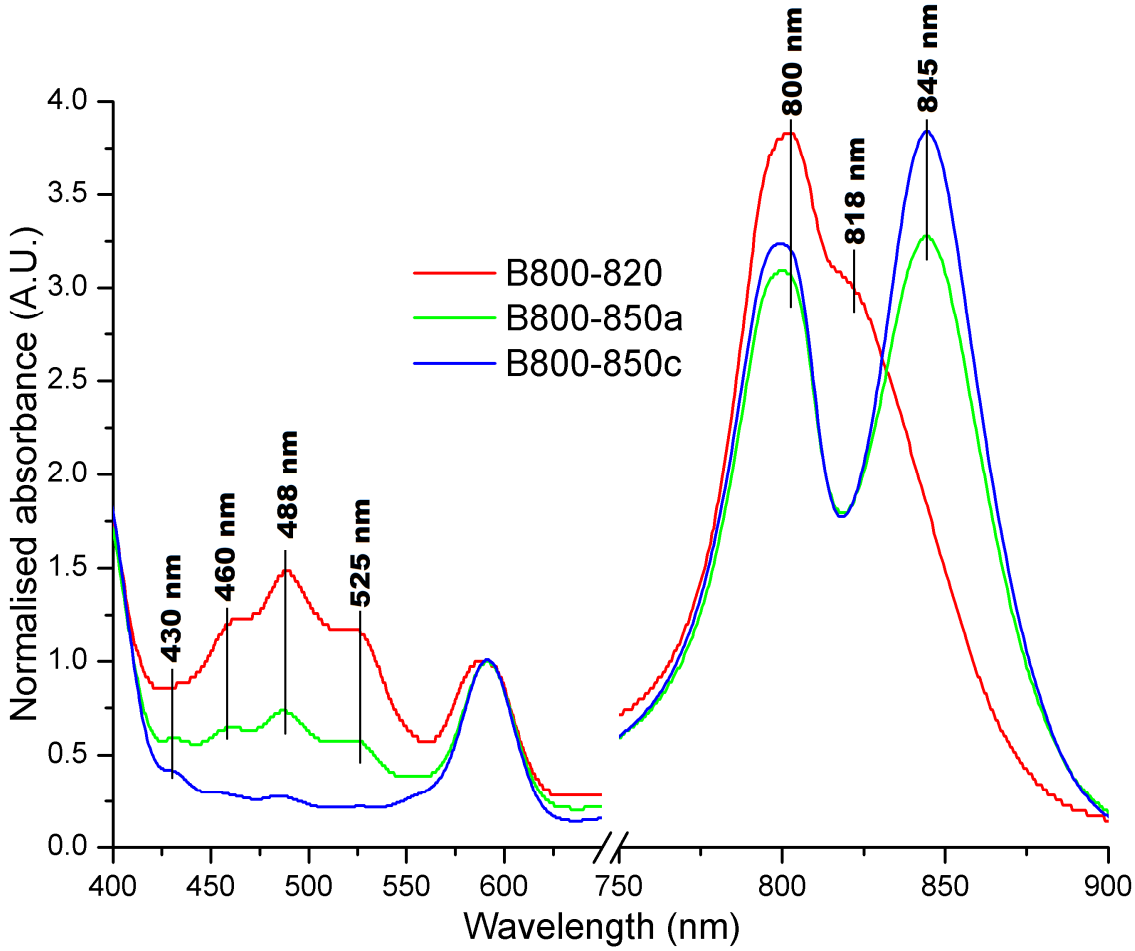

Figure 5.13 Normalised absorbance spectra the fractions eluted after anion exchange chromatography of the crude LH2 SDCG fraction from *Alc. vinosum* grown in the presence of sulphide, under high light, 30℃ growth conditions in the presence of 75 μM DPA. The B800-820 LH2 complex eluted at 240 mM NaCl, while the B800-850a eluted at 310 mM NaCl followed by the B800-850c after several fractions. The B800-820 LH2 complex produced under SHL30 growth conditions (red) in the presence of DPA produced the split B800 peak with a shoulder at ~ 818 nm in the NIR, with carotenoid peaks at 488 and two shoulders at ~525 nm and ~ 460 nm. The carotenoid peaks observed were higher than the Qx peak (590 nm). The B800-850a LH2 produced under SHL30 growth conditions (green) produced peaks at 845 nm and 800 nm in the NIR and 487 nm, 461 nm, 430 nm, and a shoulder at ~ 525 nm. The level of the carotenoid peaks was far lower than the intensity of the Qx peak, indicating a reduction in the level of carotenoid as opposed to just a change in the carotenoid content. The B800-850c LH2 complex type produced under SHL30 growth conditions (blue) in the presence of DPA produces peaks at 845 nm and 800 nm in the NIR and had negligible peaks present in the region of the spectrum between 425-550 nm.

The B800-850c from SHL30 growth conditions had the highest level of carotenoid depletion and so was pooled and then further purified using SEC (as outlined in Methods and Materials section 2.5.4) to desalt and assess whether there were any large changes to the ring size. The carotenoid depleted B800-850a LH2 complex type eluted at the same point at the LH2 from untreated cells, eluting at ~92 ± 0.5 ml suggesting that there was no change in ring size.

When comparing the absorption spectra of the purified carotenoidless B800-850a (Figure 5.14 blue) LH2 complex and the standard B800-850a LH2 complex (Figure 5.14 red) there was a blue-shift of the B850 peak by ~3 nm. This was observed in previous work on carotenoid depleted LH2 complexes from *Alc. minutissimum* (135). Additionally, the red-most Qy peak is no longer at a lower intensity relative to the B800 BChl peak, suggesting a more B800-850c like LH2 complex. The B800 BChl peaks still show a higher 797 nm peak relative to the 803 nm peak, as observed in the standard B800-850a LH2 complex type. The region between 400 nm to 550 nm, where the carotenoids absorb, shows the most pronounced differences. The absorption peaks of the carotenoid molecules are no longer present in the DPA treated B800-850a, indicating an absence of coloured carotenoids within the LH2 complex. Comparison between the B800-850c LH2 complex type (Figure 5.14 dark red) shows similarities in the ratio of the B800:B850 peaks but the difference in the 797 nm 802 nm peak intensities. This may indicate a change in the peptide composition of the B800-850a LH2 complex type.

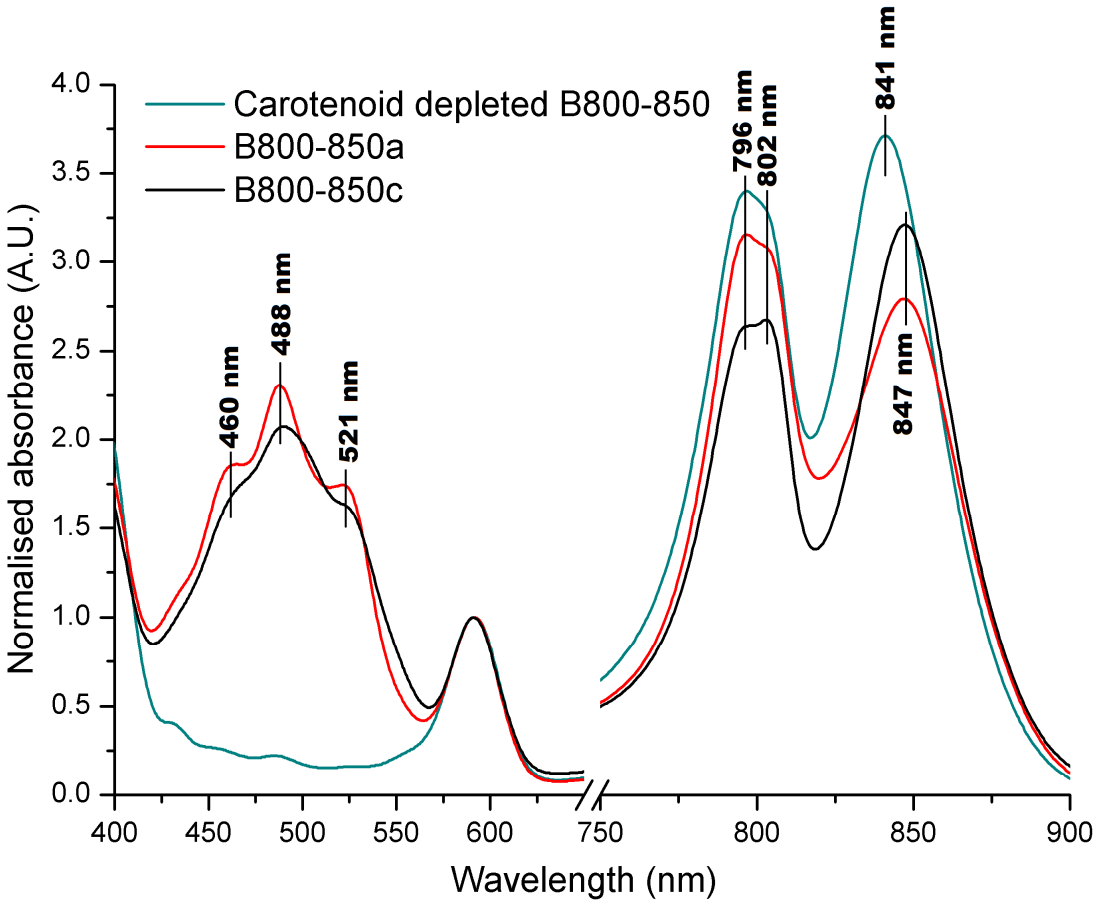

Figure 5.14 Normalised absorption spectra comparing the standard purified B800-850a and B800-850c LH2 complexes against the carotenoid depleted B800-850a LH2 complex.
The standard B800-850a LH2 complex produces peaks at 847 nm and 796 nm in the NIR, and two peaks at 488 nm and 521 nm with a shoulder at ~460 nm produced by the carotenoids present. The standard B800-850c LH2 complex produces a peak at 847 nm and 802 nm in the NIR and a single peak at 488 nm with two shoulders at ~ 460 nm and ~525 nm. The carotenoid depleted B800-850 LH2 complex type produces peaks at 841 nm and 796 nm in the NIR and produces no discernable peaks between 450-550 nm that would indicate there are very few, if any, coloured carotenoids present within the LH2 complex.

Circular dichroism was used to determine whether there was any carotenoids, colourless or otherwise, bound within the LH2 complexes (135). The CD spectrum of the visible part of the spectrum of the B800-850 LH2 from untreated cells (Figure 5.15 red) shows a broad maximum at ~ 350 nm with a shoulder at ~ 370 nm, which relate to the Soret peak, and a peak at 590 nm produced by the Qx band of the BChl (179). The other peaks are due to the carotenoid complement present and consist of two minima at 408 nm and 452 nm with a shoulder at ~ 473 nm followed by maxima at ~ 502 nm and 528 nm.

In the CD spectrum of the carotenoid depleted B800-850 LH2 complex (Figure 5.15 blue) from cells treated with DPA there are maxima at 336 nm and 398 nm with a minimum at 368 nm. There is a small maximum at 584 nm that relates to

the Qx band. In the absence of carotenoid, the soret peaks are expected to centre at 405 nm, 374.5 nm with a shoulder at ~ 352 nm (179), which are similar to the values observed here. Previous work was unable to identify whether phytoene was present due to the CD peaks being obscured by the soret bands (179). This CD spectrum suggests that there are negligible levels of coloured carotenoid present but cannot confirm the absence of any phytoene.

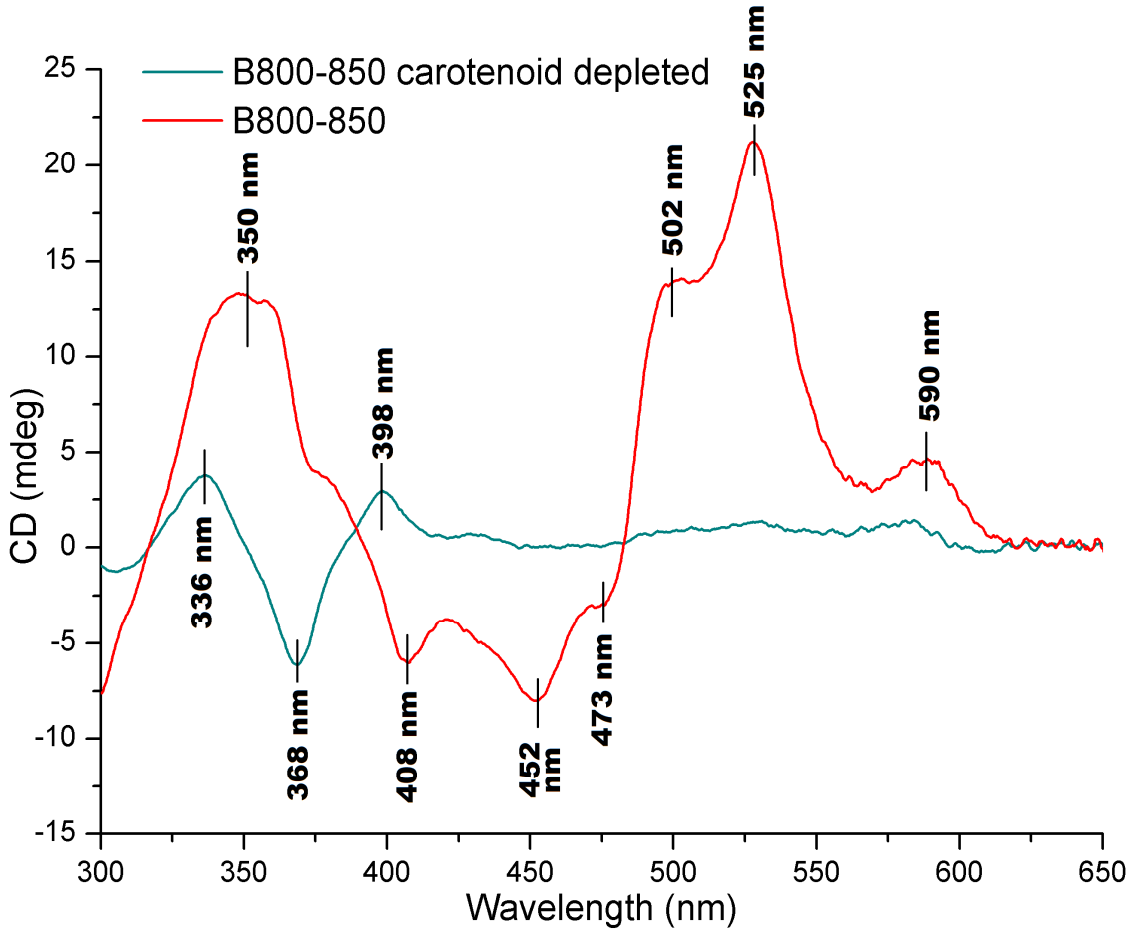

Figure 5.15 Circular dichroism spectra of the carotenoid region of carotenoidless B800-850a and standard B800-850 LH2 complexes from *Alc. vinosum*.
The standard B800-850 LH2 complex (red) produces a broad maximum at ~ 350 nm relating to the soret peak, followed by minima at 408 nm, and 452 nm with a shoulder at ~ 473 nm. There is a maximum at 525 nm with a shoulder at ~ 502 nm, followed by a small peak at 590 nm, which relates to the Qx peak. In the carotenoid depleted B800-850 LH2 complex (blue) there are distinct maxima at 336 nm and 398 nm with a minimum at 368 nm that correspond to the Soret peak. There are no other discernible peaks observed.

5.2.5 Tandem MS-MS of the carotenoid depleted B800-850 LH2 complex type from *Alc. vinosum*

The changes observed in the NIR region of the absorption spectrum of the B800-850a LH2 complex type from SHL30 growth conditions suggest the LH2 complex

type produced may shift over fully to a B800-850c LH2 complex type. To determine whether this is the case tandem MS-MS mass spectroscopy was performed with Dr Bill Mullen (as described in Methods and Materials section 2.9). The polypeptides identified were the α1, α2, ß1, ß2, ß3, and ß6 (Table 5.1) as observed in the standard B800-850a LH2 complex type (Chapter 4 section 4.2.4). The ß5 peptide observed in the standard B800-850a LH2 complex type was not observed. The ß5 peptide was observed as not fragmenting well during experiments on the standard B800-850a LH2 complex, however even if the threshold for peak identification was lowered for the carotenoid depleted B800-850a LH2 complex type the ß5 was not observed. This would indicate that the small differences in the Qy band of the B850 are due to changes in the beta peptides incorporated into the LH2 complex.

Table 5.1 The peptides identified by tandem MS-MS mass spectroscopy from the carotenoid depleted B800-850a complex and their modifications.
* are peptides observed in some form in other LH2 complex types but with or without the modifications observed in the B800-850a LH2 complex type.

Peptide	Sequence	MH+ [Da]	Modification	Observed in
A1	MAIEFMGYKPLENDYKFWLVVNPATWLIPTLIAVALTAILIHVVAFDLEGQGWHAPAAEAVEAAPAAQ	7402	none	B800-850 and B800-840p
A1-1	AIEFMGYKPLENDYKFWLVVNPATWLIPTLIAVALTAILIHVVAFDLEGQGWHAPAAEAVEAAPAAQ	7271	N/C term trunc	B800-850 and B800-840p
A1-4	MAIEFMGYKPLENDYKFWLVVNPATWLIPTLIAVALTAILIHVVAFDLEGQGWHAPAAEAVE	6893	C term trunc	B800-850
A1-4	AIEFMGYKPLENDYKFWLVVNPATWLIPTLIAVALTAILIHVVAFDLEGQGWHAPAAEAVE	6762	N/C term trunc	B800-850
A1-4.2	AIEFMGYKPLENDYKFWLVVNPATWLIPTLIAVALTAILIHVVAFDLEGQGWHAPAAEAV	6633	N/C term trunc	B800-850 and B800-840p
A1-5	MAIEFMGYKPLENDYKFWLVVNPATWLIPTLIAVALTAILIHVVAFDLEGQGWHAPAA	6464	C term trunc	B800-850 and B800-840p
A1-5	AIEFMGYKPLENDYKFWLVVNPATWLIPTLIAVALTAILIHVVAFDLEGQGWHAPAA	6393	N/C term trunc	B800-850 and B800-840p
A1-6	MAIEFMGYKPLENDYKFWLVVNPATWLIPTLIAVALTAILIHVVAFDLEGQGWHAPA	6333	C term trunc	B800-850 and B800-840p
A1-6	AIEFMGYKPLENDYKFWLVVNPATWLIPTLIAVALTAILIHVVAFDLEGQGWHAPA	6262	N/C term trunc	B800-850 and B800-840p
A2	MSDVAKPKNPEDDWKIWLVVNPATWLMPIFYALLVLAIAVHAVVFSVGLGWQ	5848	none	All LH2 complexes*
A2	SDVAKPKNPEDDWKIWLVVNPATWLMPIFYALLVLAIAVHAVVFSVGLGWQ	5717	N term trunc	All LH2 complexes
B1	MADMKSLSGLTEQQAKEFHEQFKVTYTAFVGLAALAHLFVIAANPWW	5296	none	All LH2 complexes*
B2	MAEQSLSGLTEQQAKEFHEQFKVTYTAFVGLAALAHLFVIAANPWW	5179	none	All LH2 complexes*
B3	MASLSGLTDQQAKEFHEQFKVTYTAFVGLAALAHLFVIAANPWW	4907	none	All LH2 complexes*
B3	ASLSGLTDQQAKEFHEQFKVTYTAFVGLAALAHLFVIAANPWW	4776	N term trunc	All LH2 complexes*
B6	MNGLTEQQAKEFHAQFKVTYTAFVGLAALAHLMVLANNPWF	4607	none	B800-820 LH2 complex

5.3 Deletion of the phytoene desaturase (CrtI) gene

The use of DPA to inhibit carotenoid biosynthesis and create carotenoid depleted LH2 complexes confirmed what had previously been observed in *Alc. minutissimum*, that the B800-850 LH2 complex type from *Alc. vinosum* is stable enough to exist without carotenoid in all carotenoid binding pockets. DPA in high concentrations is toxic to cell growth and is degraded by white light therefore cells must be grown behind a red filter (section 5.2). The size of the red filter reduces the volume of cells that can be cultured at any one time and could potentially have effects on phytochromes that regulate the light-harvesting machinery (64). The creation of a carotenoid mutant through DNA 'knock-out' would remove these limitations and consistently produce fully carotenoidless LH2 complexes. This can be done by replacing the CrtI gene within the *Alc. vinosum* genome with an insert lacking the functional gene.

5.3.1 Creation of the blunt CrtI$^-$ insert

The genome of *Alc. vinosum* identified two potential CrtI genes that code for the phytoene desaturase enzyme, which forms the conjugated double bond system of the carotenoid (Introduction section 1.4). Creating a CrtI$^-$ mutant by 'knocking out' the phytoene desaturase (CrtI) genes will create a mutant unable to form coloured carotenoids but that should still be able to produce light-harvesting complexes.

Genomic DNA was extracted from *Alc. vinosum* as per (142) to source the template DNA for the 'knock-out' (Methods and Material section 2.12.1). Primers were designed by Dr Sarah Henry (Methods and Material section 2.12.2) to complement the upstream (US) and downstream (DS) sections of the DNA around the CrtI gene. These primers were used for the PCR-driven overlap extension technique (143) to create a CrtI$^-$ insert (as described in methods and materials section 2.12.2). The US and DS sections have overlapping, complementary 3' ends that allow them to anneal to each other. The complementary section codes for a start and a stop codon, this will replace the CrtI gene in the insert, meaning that no protein is coded for at all.

The US and DS PCR products initially amplified well, but the US segment began to produce low to negligible levels during PCR. A gradient PCR with different annealing temperatures over eight tubes was performed (as described in methods and materials section 2.12.2). To determine the annealing temperature that produced the best amplification, PCR products were analysed by gel electrophoresis (as described in methods and materials section 2.12.3). An agarose gel of the US PCR products show bands at ~ 500 bp from the PCR reactions between 50 - 68 ℃ (Figure 5.16). The band is the correct size to be the US segment (480 bp). The brightest bands were from PCR products annealed at 64.9 ℃ – 57 ℃. This is the ideal annealing temperature range. In light of this information the standard annealing temperature during the PCR cycles was maintained at 60 ℃.

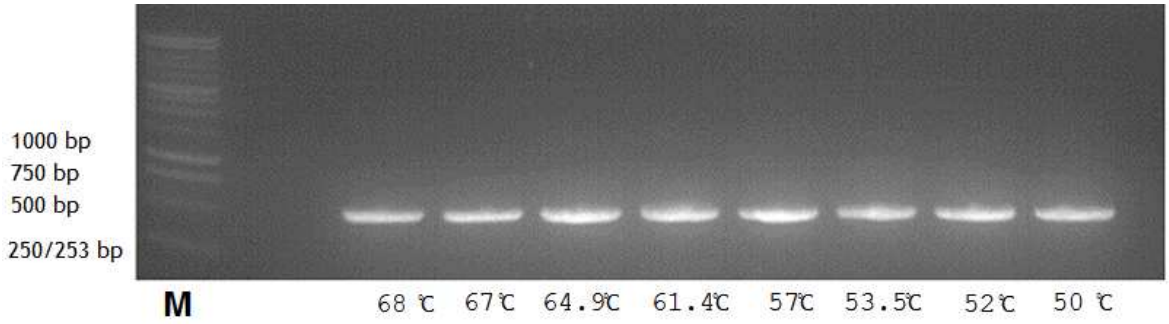

Figure 5.16 PCR products of the upstream segment of the CrtI⁻ insert after a gradient PCR performed.
Different tubes were subjected to different annealing temperatures, with denaturation and polymerisation stages of 98 ℃ and 72 ℃. The annealing temperature gradient across the tubes ran from 68 ℃ to 50 ℃, with temperatures of 68 ℃, 67 ℃, 64.9 ℃, 57 ℃, 53.5 ℃, 52 ℃, and 50 ℃ for 30 seconds. The expected product was 480 bp in size and was observed as amplified under all annealing temperatures. The PCR products from annealing temperatures between 64.9 ℃ – 57 ℃ had the brightest bands, and thus the highest amount of DNA.

Once the US and DS sections were amplified at sufficient concentrations as observed by bright bands at ~ 480 bp and ~ 300 bp on an agarose gel (Figure 5.17 A) they were ligated together using the splice, overlap, extension (SOE) method. The SOE method involves cycles of denaturation and annealing in the absence of DNA polymerase to bind the complementary overlap sections of the upstream and downstream primers. Phusion polymerase (Biolabs) and nucleotides were added to the mix and a standard PCR method was run (98 ℃, 60 ℃, 72 ℃) thus extending the DNA construct into a complete blunt ended CrtI- insert. After purification using an agarose gel a single bright band at ~ 780 bp was observed confirming the ligation of the two sequences together (Figure 5.17 B).

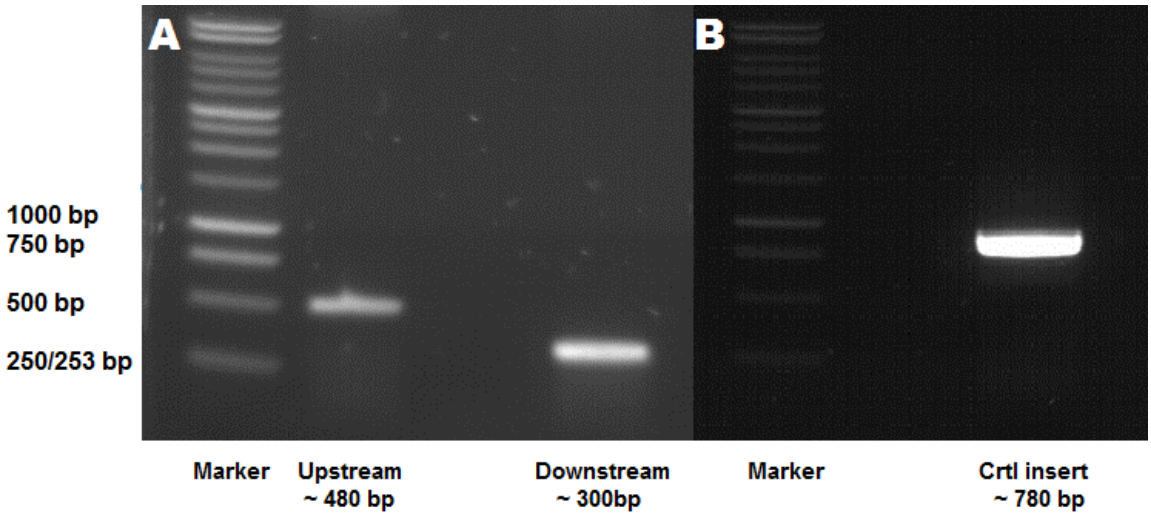

Figure 5.17 PCR products of the separate upstream and downstream segments of the CrtI⁻ insert (A) and the CrtI⁻ insert (B).
The upstream (US) segment observed after PCR was ~ 500 bp (480 bp) and the downstream (DS) segment was 250-500 bp (300 bp) which were within the correct range of sizes for each segment. Following the extraction of the US and DS segments they were amalgamated into a full CrtI⁻ insert through the use of splice, overlap, extension (SOE) method followed by PCR. There was a single band of 750-1000 bp after the SOE and PCR was performed, which is the correct range for the CrtI⁻ insert (780 bp).

5.3.2 Cloning of the blunt CrtI⁻ insert into the pJET1.2/blunt vector and creation of CrtI⁻ with 'sticky ends' by restriction digests

Agarose gels confirm that the CrtI- insert is the correct size, but it must be sequenced to ensure there have been no substitutions during PCR. The CrtI⁻ insert is blunt ended and so was cloned into the pJET1.2/blunt vector (Figure 5.18 A) (Thermo scientific), as per the manufacturer's instructions. The pJET1.2-CrtI⁻ vector was then used to transform *E.coli* strain DH5α cells using heat shock treatment and grown overnight on LB agar plates (as described in Materials and Methods section 2.12.4). After incubation six transformed colonies were observed (Figure 5.18 B) each of which were used to inoculate 5 ml of LB/ampicillin media that was grown overnight at 37℃. Plasmids were extracted using the Thermo Scientific miniprep kit and sent for sequencing. Colony six was found to contain the correct 780 bp insert and was taken on for further processes.

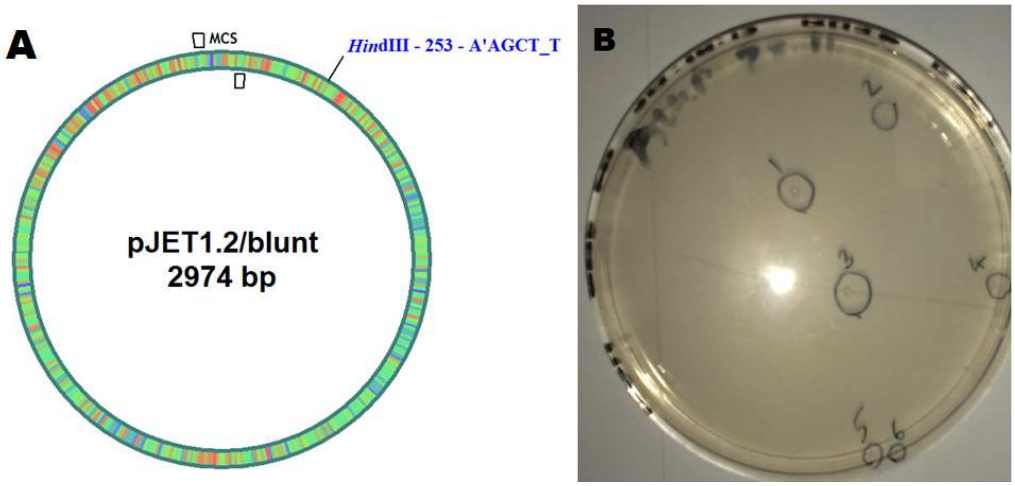

Figure 5.18 Schematic diagram of the pJET1.2/blunt (Thermo Scientific) cloning vector (A) and six *E.coli* strain DH5α colonies on a LB agar plate (B).
A: The pJET1.2/blunt vector schematic shows the multiple cloning site (MCS) where the blunt ended insert is incorporated into the vector. Also shown is the restriction site of HindIII present at position 253 within the vector. This restriction site is also found within the CrtI$^-$ insert (not shown). Vector was visualised and annotated using pDraw. B: LB agar plate enriched with 100 mM ampicillin with pJET1.2/blunt-CrtI$^-$ transformed DH5α colonies after growth overnight at 37 ºC. There were six transformed colonies identified that were circled and numbered.

5.3.3 **Ligation of the CrtI$^-$ insert into the pK18mobsacB vector**

The CrtI$^-$ insert must then be extracted and to be incorporated into the final pK18mobsacB vector (144), in order to do this both the vector and the CrtI$^-$ insert requires ‘sticky ends’. The pk18mobsacB vector contains HindIII and EcoRI restriction sites (Figure 5.19) and so these were incorporated into the CrtI$^-$ via the primers. The external primers for the SOE method incorporated two restriction sites into the CrtI$^-$ insert, an EcoRI restriction site at the 5’ end and a HindIII restriction site at the 3’ end.

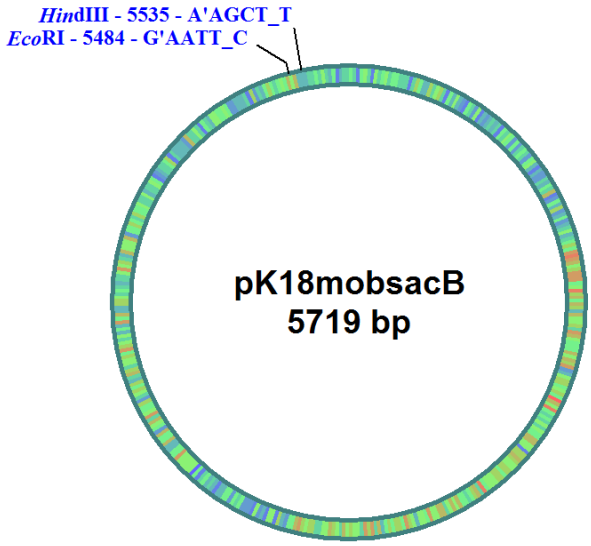

Figure 5.19Schematic diagram of the pK18mobsacB cloning vector showing the HindIII and EcoRI restriction sites.
After restriction digests with HindIII and EcoRI enzymes, the vector will contain 'sticky ends' suitable for incorporation of the CrtI$^-$ insert. The DNA cut out from the vector by restriction cleavage is 51 bp. Vector was visualised and annotated using pDraw.

The pJET1.2-CrtI$^-$ vector was simultaneously digested with both EcoRI and HindIII (as described in Methods and Materials section 2.12.5) to produce a CrtI$^-$ insert with 'sticky ends'. The digestion products were visualised by gel electrophoresis and three bands were observed, at ~ 750 bp, 2500-3000 bp, and 3000-4000 bp (Figure 5.20). The smallest band at ~ 750 bp is most probably the 780 bp insert and so was excised and then extracted using a gel extraction kit (Thermo Scientific). The band at 2500-3000 bp is most probably the pJET1.2 vector without the CrtI$^-$ insert (2974 bp) while the band at 3000-4000 bp is probably the uncleaved pJET1.2 vector still containing the CrtI$^-$ insert (3706 bp). The insert was then ready to be incorporation into the pK18mobsacB vector.

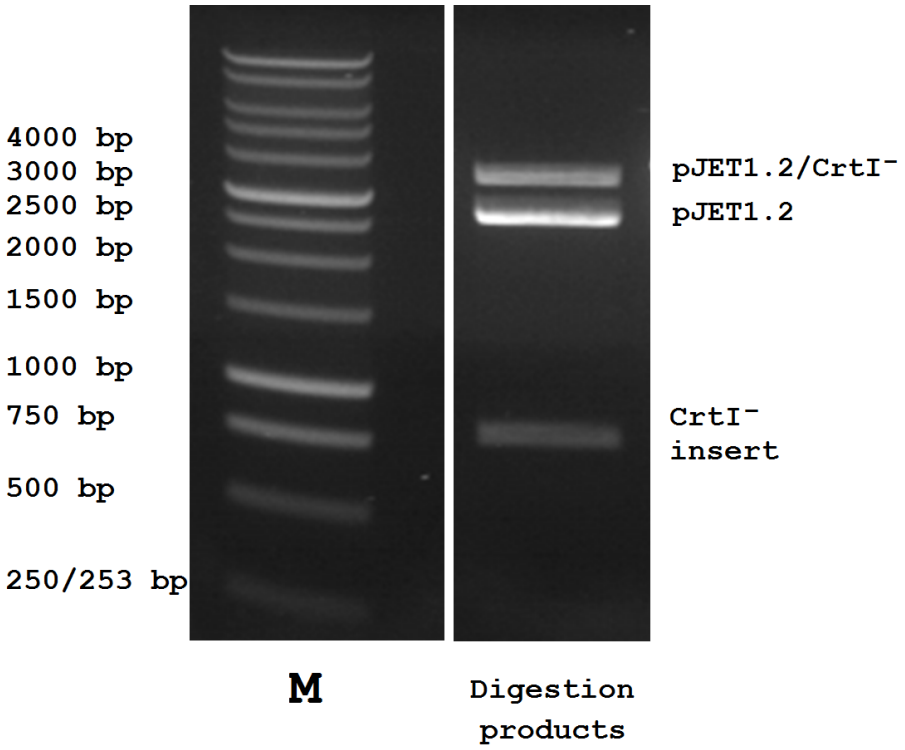

Figure 5.20 pJET1.2-CrtI⁻ digestion products after digests with HindIII and EcoRI. Three digestion products were observed, at 750 bp-1000 bp, 2500-3000 bp, and 3000-4000 bp. The 750 bp – 1000 bp band is within the correct range to be the CrtI⁻ insert (780 bp). The two other bands observed were the pJET1.2 without the CrtI⁻ insert (2974 bp) and uncleaved pJET1.2-CrtI⁻ (3706 bp).

To prepare the pK18mobsacB vector for incorporation it was PK18mobsacB vector was digested overnight with HindIII and EcoRI to prepare it for the CrtI⁻ insertion. Figure 5.21 shows a single, bright band present after EcoRI and HindIII digestion of pK18mobsacB suggesting there are ample amounts of vector and that digestion was effective as the presence of additional bands would be indicative of supercoiled, liner, and circular DNA. A faint band can be seen at the bottom of the gel that may be the excised DNA, although this fragment is only 51 bp and most probably ran off the gel.

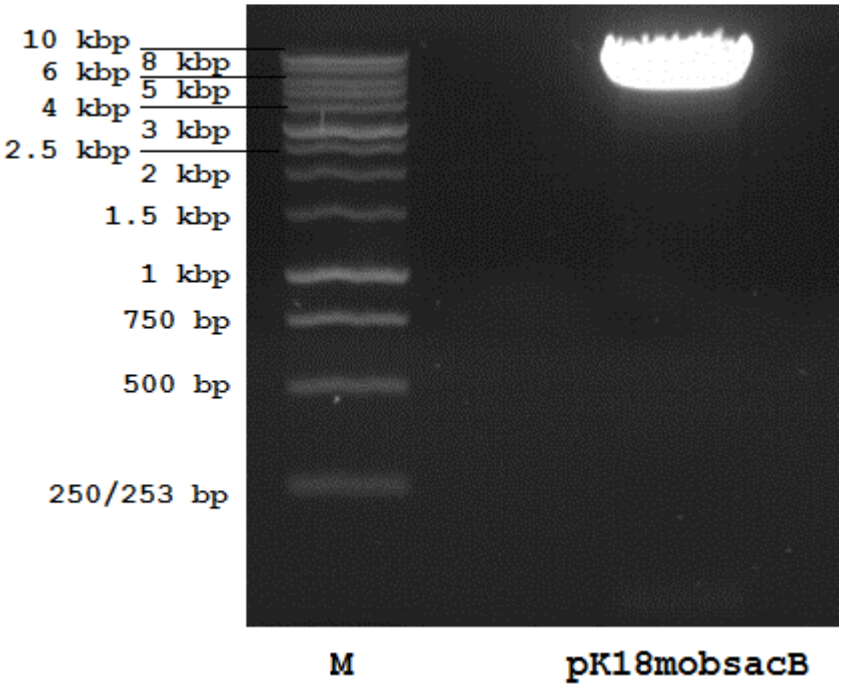

Figure 5.21Digestion product after restriction digests of pK18mobsacB with HindIII and EcoRI overnight at 37 ºC.
One band was observed, at 5000 bp -6000 bp. The band is within the correct range to be the cleaved pK18mobsacB vector (5669bp) however the 1 % agarose (w/v) gel is unlikely to separate the cleaved (5669 bp) from the uncleaved vector (5719 bp). A faint band is observed at the bottom of the gel that might be the excised 51 bp DNA, although it is likely that this DNA ran off the end of the gel.

The CrtI$^-$ insert was then ligated into the pK18MobsacB vector and was then used to transform JM109 cells using heat shock treatment. Transformed cells were then plated onto LB plates enriched with kana, 6 ul 1 M IPTG, 40 ul 20 mg/ml X-GAL to induce the lac operon (145), and grown overnight at 37℃. At this point in the process issues arose as the colonies that were produced on the LB plate after overnight incubation were very small and numerous so determining the colour of the individual colonies was very difficult, although they appeared to be white. Several colonies were picked and used to inoculate 5 ml of LB/kana (30 µg/ml kana), and incubated overnight at 37℃. These cultures failed to grow, even when incubated for longer. Transformations of JM109 cells were repeated with freshly ligated pK18mobsacB-CrtI$^-$ and the plated on LB/kana (30 µg/ml) and incubated overnight at 37℃. Numerous but small colonies were observed so the plate was left for an additional 6 hours in an attempt to produce larger colonies, however no additional growth occurred. When the colonies were used to inoculate 5 ml LB/kana (30 µg/ml kanamycin) no growth occurred.

These issues with creating transformants may be due to the CrtI$^-$ insert self ligating instead of ligating into the vector. The products of the ligation were separated on a 1 % agarose gel to confirm the absence of a CrtI$^-$CrtI$^-$ ligation product. After analysis using gel electrophoresis (Figure 5.22) a single band was observed between 6000 – 8000 bp. This band will consist of both ligated pK18mobsacB-CrtI$^-$ vector (6499 bp) as well as unligated vector (5719 bp) as the 1 % agarose (w/v) gel poorly separates such large DNA products. Any insert should be visible at 780 bp and any self ligated insert that would be expected at ~ 1500 bp. The absence of a band at 780 bp indicates either high incorporation of the CrtI$^-$ insert into the pK18mobsacB vector or that the concentration of insert is too low.

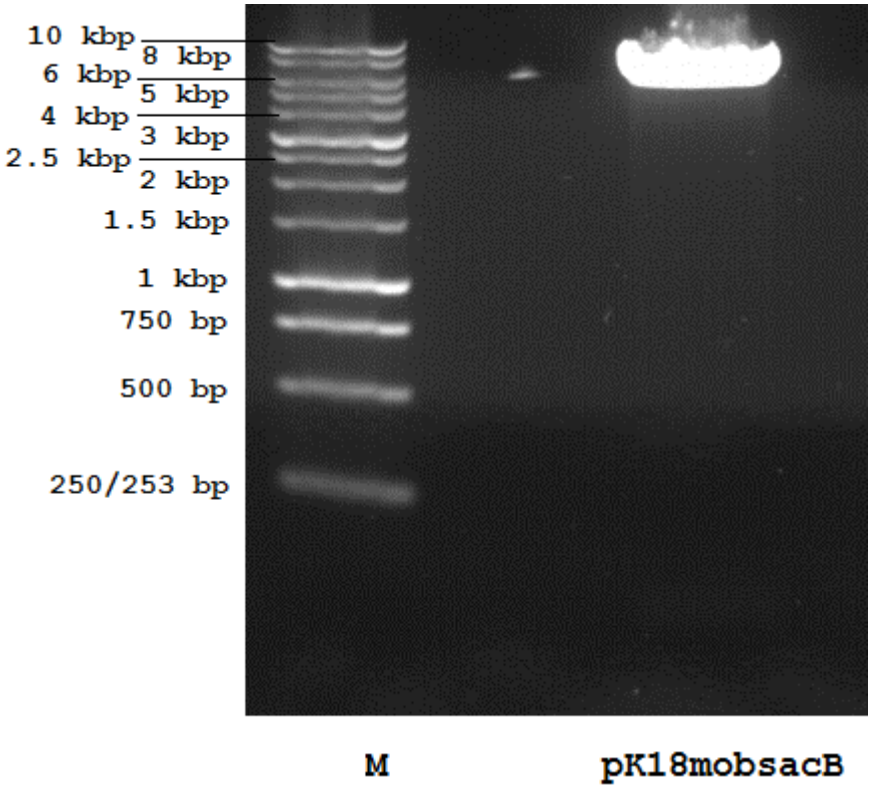

Figure 5.22 Ligation products of the pK18mobsacB vector with the CrtI$^-$.
One ligation product was observed at 6000 bp-8000 bp. The band is most probably both the CrtI$^-$ insert ligated into the pK18mobsacB vector (6499 bp) as well as the unligated pk18mobsacB vector (5669 bp). There was no band at 1560 bp that indicates the insert is not self ligating. There is no band at 780 bp suggesting the CrtI$^-$ insert concentration may be too low or that there is a high level of incorporation into the vector.

A potential problem highlighted is the low level of CrtI$^-$ insert present, as this would result in a low yield of transformed pK18mobsacB. Sequential and simultaneous digests of the pJET1.2-CrtI$^-$ vector were compared to determine whether the yield of CrtI$^-$ insert reclaimed from the pJET1.2 plasmid could be

improved (as described in Methods and Materials section 2.12.5). The pJET1.2-CrtI$^-$ construct only contains the EcoRI restriction site, incorporated within the CrtI$^-$ insert, and so was digested first with EcoRI for 90 min. Gel electrophoresis was used to purify the DNA and observe the level of DNA present (Figure 5.23). A bright band observed between 3000 bp - 4000 bp, suggesting a high amount of pJET1.2-CrtI$^-$. This band will consist of both the cleaved and uncleaved vectors as there is no difference observed in the size of the DNA fragment. This DNA was excised and reclaimed using a Thermo Scientific gel extraction kit and digested overnight at 37℃ with HindIII.

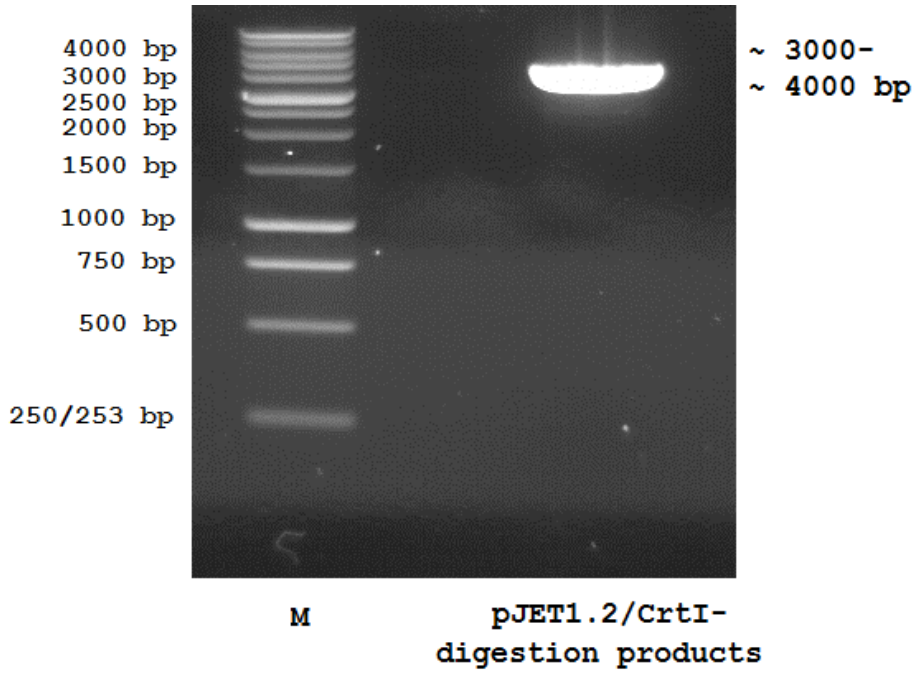

Figure 5.23Digestion product after EcoRI restriction digests of pJET1.2-CrtI- for 60 min. A single digestion product was observed at 3000 bp-4000 bp. The band is within the correct range to be the once cleaved pJET1.2-CrtI- vector or the uncleaved vector (3706 bp).

The pJET1.2 vector contains a HindIII restriction site in addition to the restriction site present within the CrtI$^-$ insert. This will result in competition for the HindIII enzyme and so the digestion time was extended to overnight. The products of HindIII digestion were run on a 1 % agarose gel to assay the amount and size of the DNA present (Figure 5.24). Three DNA bands were observed between 250 bp -500 bp, 750 bp – 1000 bp, and 2500 bp – 3000 bp. The band at ~3000 bp is the appropriate size to be the empty pJET1.2 vector (2974 bp) and the empty vector without the region of DNA between the MCS and the HindIII restriction site (2721 bp). The bands at ~ 780 bp and ~ 250 bp are the CrtI- insert and the region of DNA between the HindIII restriction sites, respectively. The

DNA bands observed at ~ 3000 bp and ~780 bp were much fainter than those observed after EcoRI digestion suggesting the level of DNA was greatly reduced after the gel extraction.

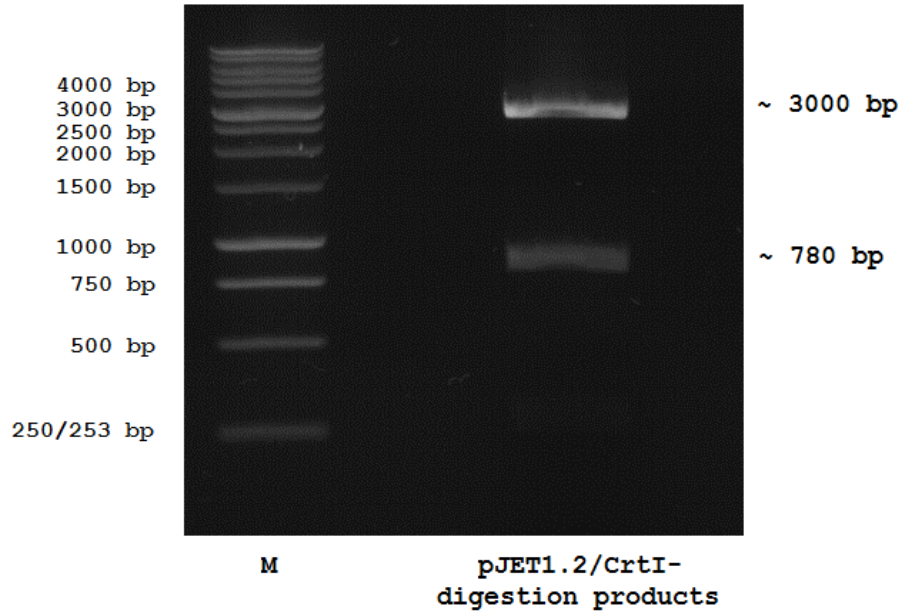

Figure 5.24 Digestion products after the second restriction digest with HindIII of once cleaved pJET1.2-CrtI^{-}.
Three digestion products were observed, at 2500 bp- 3000 bp, 750-1000 bp, and 250-500 bp. The band observed between 2500 bp-3000 bp is within the correct range to be the empty pJET1.2 vector (2974 bp). The band between 750-1000 bp is within the correct range to be the 'sticky ended' CrtI- insert (780 bp). The faint band between 250-500 bp is in the correct range to be the part of the vector between the multiple cloning site and the HindIII restriction site present within the pJET1.2 vector (253 bp).

This was compared to simultaneous digests of the pJET1.2-CrtI^{-} vector with both HindIII and EcoRI that were run overnight at 37℃ (Figure 5.25). Three bright bands were observed at ~ 2500 bp, ~ 1500 bp, and ~ 750 bp and a single dimmer band at ~ 250 bp. The band at ~ 2500 bp is the empty pJET1.2 vector (2721 bp) with the CrtI^{-} excised as well as the ~ 250 segment between the CrtI- HindIII restriction site and the restriction site found on the pJET1.2 plasmid. The band at ~ 1500 bp is the CrtI^{-} insert still attached to the 253 bp section of DNA (1033 bp) between the two HindIII restriction sites. The ~ 750 bp band is the CrtI^{-} insert (780 bp). The faint band at ~ 250 bp is the segment of DNA between the two HindIII restriction sites. There is no band present at ~4000 bp that would indicate uncleaved pJET1.2-CrtI^{-} vector.

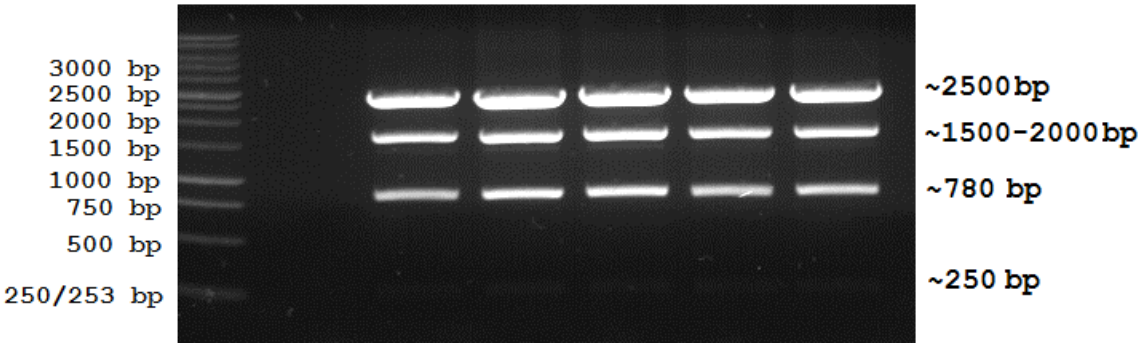

Figure 5.25 Digestion products after simultaneous restriction digests of pJET1.2-CrtI⁻ with EcoRI and HindIII overnight at 37 ºC.
Four bands were observed at 250-500 bp, 750-1000 bp, ~ 1500 bp, and ~ 2500 bp. The band at ~ 2500 bp is within the correct range to be the empty pJET1.2 vector without the fragment between the two HindIII restriction sites (2721 bp). The band between 750-1000 bp is within the correct range to be the CrtI⁻ insert (780 bp). The band at ~ 1500 bp is within the range of the CrtI⁻ insert attached to the DNA segment between the two HindIII restriction sites. The faint band at ~ 250 bp is the section of DNA between the two HindIII restriction sites.

This suggests that the sequential digests work effectively in ensuring that both HindIII sites are cleaved unlike during simultaneous digests. The issue with the sequential digests appears to be the loss of DNA during the gel extraction process. A Thermo Scientific Nanodrop 1000 spectrophotometer was used to confirm the levels of DNA present after extractions as well as to assay the purity of the DNA acquired. During gel extraction, multiple elution washes of 10 µl were performed to assay the impurities as well as the concentration of DNA. The nanodrop accurately records the absorbance in the UV in volumes of 1 nl, and so is an effective and less wasteful way to assay DNA samples for purity and concentration. The ideal concentrations should be ~ 50 ng insert in a 3:1 ratio to the vector to ensure interaction and ligation. Nucleotides, single stranded and double stranded DNA and RNA absorb at 260 nm, protein absorbs at 280 nm, while some carbohydrates, guanidine HCl and cyclic compounds such as phenol absorb at 230 nm. Impurities in the DNA sample effect upstream processes such as ligation and so ratios between the 260/230 and 260/280 are useful to determine purity. Sambrook (145) states that any value over 2.0 for the 260/280 ratio is of a sufficient purify for most upstream processes (142). Additionally, the 260/230 ratio must be above ~1.8 to ensure that upstream processes are unaffected by impurities. It was found that the 260/280 values averaged > 2 in the first elution wash. The 260/230 values were < 0.2 implying a high level of impurities absorbing at ~230 nm. The concentrations of DNA were observed were < 50 ng.

An alternative gel extraction kit (Qiagen) was used and the same low DNA concentrations and ratios were observed, implying the issue does not originate from the kit but due to issues in the sample.

The binding buffer elution and wash buffer elution steps were collected and the absorbance at 230 nm, 260 nm, and 280 nm recorded using the nanodrop to determine whether the DNA was not binding effectively and was being washed off before the elution wash. As the binding buffer contains guanidine isothiocyanate, which absorbs at ~260 nm, it is difficult to determine whether the DNA was washed off at this early stage. The 260 nm values for each of the washes was <0.4 and probably related to guanidine isothiocyanate being washed off as the value is lower after each wash. The elution washes were performed with heated elution buffer (70℃) that was incubated on the column for 5-10 min before the elution spin. The first elution showed the highest concentration of DNA. Sodium acetate pH 5.2 was added to ensure the binding buffer pH was optimum for DNA binding to prevent DNA being prematurely washed off with the binding buffer, however there was no improvement in the 260 nm absorption values observed in the elution wash.

Mini-preps were repeated and DNA eluted in volumes of 10-20 ul to increase DNA concentration without reducing yield too greatly. Ligations were repeated but the previous results of small colonies that failed to reach turbidity after media inoculations was observed each time. Due to time constraints the creation of the CrtI$^-$ "knock-out" was unable to be completed. The CrtI$^-$ insert should be recreated with a new set of primers and potentially an alternative vector could be used for subcloning.

5.4 Carotenoid extraction through the use of solvents

Previous studies created carotenoidless complexes by extracting the carotenoids out of the already formed LH1 complexes using a benzene wash (32, 121), resulting in the removal of up to 90 % of the carotenoids present (68). Benzene is highly toxic and not all complexes were resilient enough to remain intact after a benzene wash, so toluene was used as an alternative. Small percentages of more polar solvents were added to compensate for the less polar nature of toluene

with regards to benzene, and used to wash 1 mg of freeze dried *Alc. vinosum* membranes (as described in Methods and Materials section 2.13).

Alc. vinosum membranes from cells grown under sulphide, low light, 30℃ growth conditions were used as the base material for carotenoid extraction. Total carotenoid content was determined by washing 1 mg of membranes with methanol and then acetone to remove all carotenoids. It was observed that acetone only achieved total carotenoid extraction (confirmed by a blue pellet) after a methanol wash. The pellet observed after all of the different solvent mix washes stayed red pigmented and did not go blue suggesting the presence of carotenoid in the membranes and complexes.

The absorption spectra of the supernatant from acetone washed *Alc. vinosum* membranes were recorded and the average taken to determine the full carotenoid content from 1 mg of membranes. This was used as the benchmark for 100 % carotenoid extraction. The absorption spectra of the supernatant containing the extracted carotenoids from the different solvent mix washes were recorded and the average determined to identify the level of carotenoid extraction. Toluene extractions were found to extract 56.76 % ± 1.93 % of the total carotenoid content of the membranes (Figure 5.26 black line). Toluene/Diethyl ether mixes of between 1 % and 10 % diethyl ether showed negligible differences in the level of carotenoid content extracted (52.37 % ± 0.55 % to 52.21 % ± 2.28 %). At 5 % diethyl ether there was a reduction in the amount of carotenoid extracted (44.65 % ± 1.25 %) than observed at 1 % or 10 % diethyl ether (Figure 5.26 green data points).

In toluene/acetone mixes the level of carotenoid extracted increased from 55.32 % ± 3.02 % at 1 % acetone (v/v) to 55.58 % ± 3.31 % at 5 % acetone (v/v) and 64.87 % ± 3.31 % at 10 % acetone (v/v) (Figure 5.26 blue data points). It appears that a percentage acetone beneath 10 % produces negligible effects on the level of carotenoid extraction.

The toluene/ethyl acetate mix showed a similar trend to the toluene/acetone washes, showing an increase in carotenoid extracted of 55.20 % ± 4.56 % at 1 % ethyl acetate (v/v) to 60.80 % ± 2.75 % at 5 % ethyl acetate (v/v) and 66.56 % ± 1.56 % at 10 % ethyl acetate (v/v) (Figure 5.26 red data points). This suggests

that the extraction of carotenoids may be more sensitive to small increases in ethyl acetate than acetone.

The level of carotenoid extracted using 10 % acetone (v/v) and 10 % ethyl acetate (v/v) is only a small amount (~ 8 %) more than extracted when using 100 % toluene and is of a similar amount to the extractions with acetone without a methanol wash beforehand (Figure 5.26 purple line). This suggests that 10 % acetone or 10 % ethyl acetate in toluene could be used to extract carotenoids but examination of the residual pellet will determine the effects of these solvents on the light-harvesting complexes.

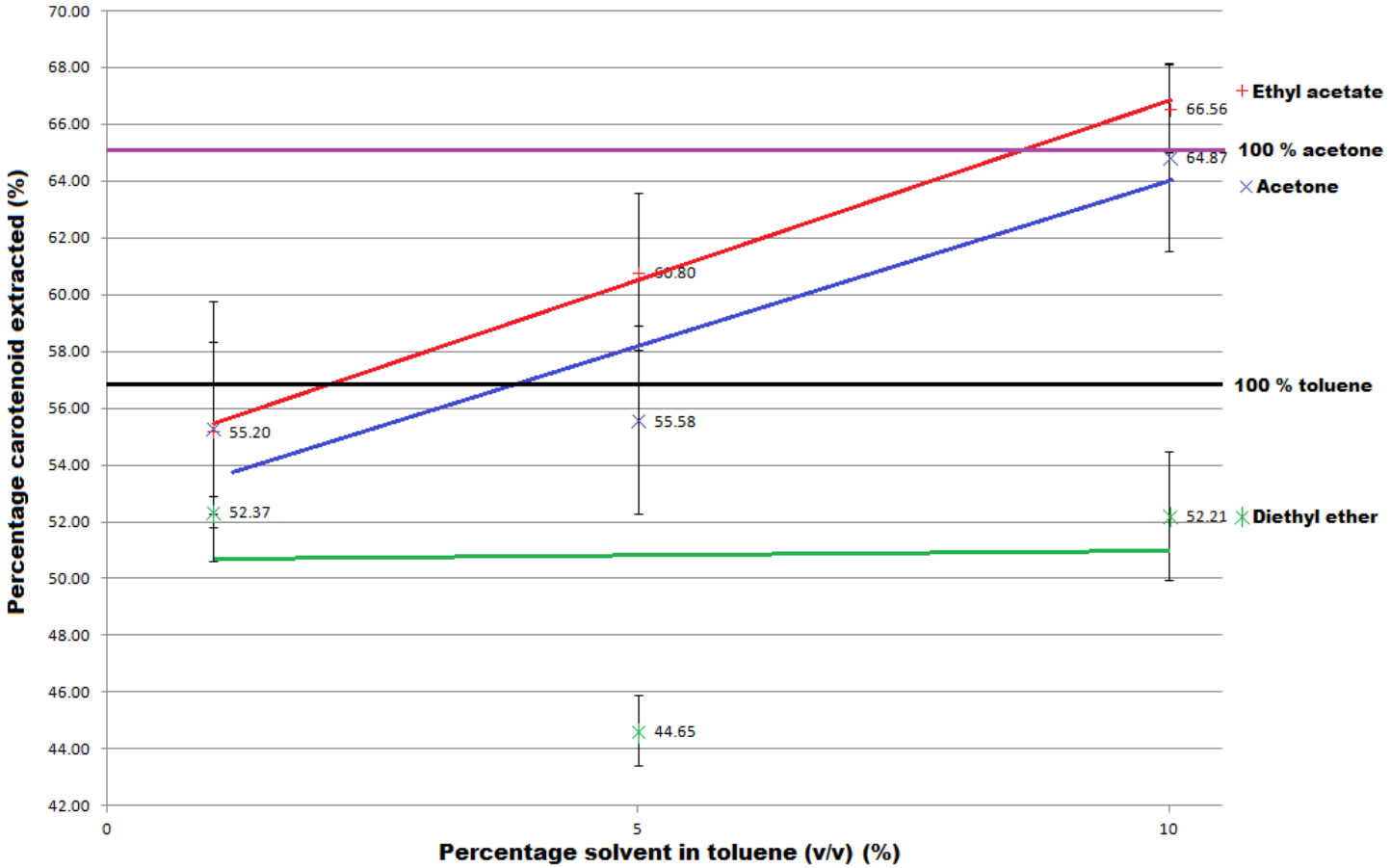

Figure 5.26 Graph showing the average percentage removal of carotenoid by different toluene-solvent mixes at 1 %, 5 %, and 10 %.
The percentage carotenoid removed by a 100 % toluene is 56.76 ± 1.93 % (black line) however 100 % acetone with no methanol wash extracts 65.91 ± 2.69 % (purple line). The percentage carotenoid extracted in different percentages of ethyl ether (red data points) is 55.20 ± 4.56 % (1 %), 60.80 ± 2.75 (5 %), and 66.56 % ± 1.56 % (10 %). The percentage carotenoid extracted in different percentages of acetone (blue data points) is 55.32 % ± 3.02 % (1 %), 55.58 % ± 3.31 % (5 %), and 64.87 % ± 3.31 % (10 %). The percentage carotenoid extracted in different percentages of diethyl ether (green data points) is 52.37 % ± 0.55 % (1 %), 44.65 % ± 1.25 % (5 %), and 52.21 % ± 2.28 % (10 %). The trend observed in increasing percentages of acetone is the same as that observed in increasing concentrations of acetone. At both 10 % acetone and ethyl acetate the level of carotenoid extracted is equivalent to the level extracted with 100 % acetone. There is an improvement in the level of carotenoid extracted from 100 % toluene but only by 6 - 7 %.

The membrane pellets of the 100 % toluene wash as well as the acetone/toluene and ethyl acetate/toluene mixes were re-suspended in 20 mM TRIS-HCl, pH 8.0 and the absorption spectrum measured to determine the effect of the different solvent washes on the light-harvesting complexes present (as described in Materials and Methods section 2.13). As the diethyl ether/toluene mix was ineffective at extracting carotenoids, the absorption spectra of the re-suspended pellets were not included.

The absorption spectrum of the membranes from *Alc. vinosum* grown under sulphide, low light, 30℃ growth conditions produce absorption peaks at 807 nm, 822 nm, and 890 nm in the NIR (Figure 5.27 black). The B800 NIR absorption peak blue shifted to 802 nm and reduced in intensity after membranes were washed in 100 % toluene (Figure 5.27 purple), suggesting a potential loss of the B800 BChl. The absorption peak associated with the B820 BChl red-shifts by 2 nm to 824 nm, however the most substantial change is the blue shift of the LH1 absorption peak to 878 nm. The blue shift of the LH1 peak suggests a loss of the carotenoid as observed in previous studies (125).

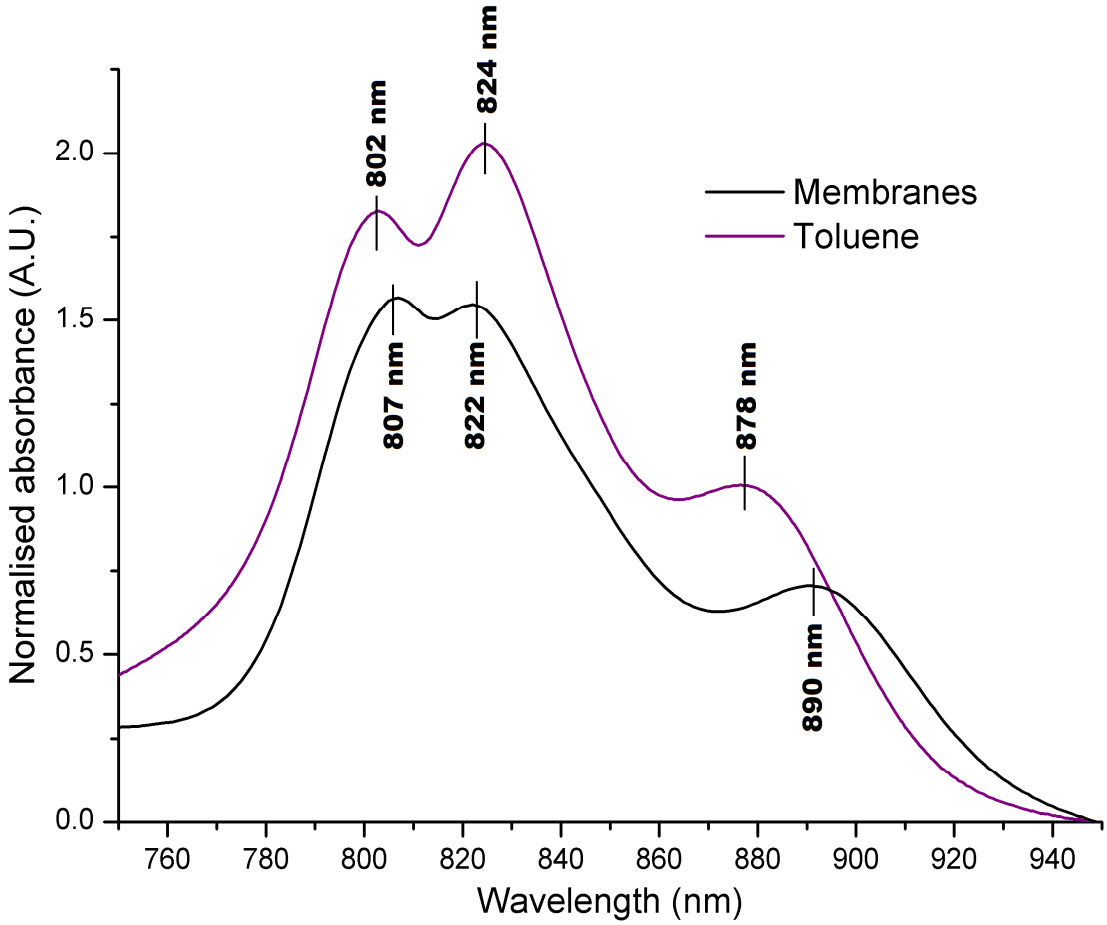

Figure 5.27 Normalised absorption spectra of membranes from *Alc. vinosum* cells before and after washing in 100 % toluene.
Membranes were prepared from *Alc. vinosum* grown in sulphide, under low light, at 30 ºC growth conditions. The standard SLL30 membranes (black) produce NIR absorption peaks at 807 nm, 822 nm, and 890 nm. After washing with toluene (purple) the membranes absorption peaks shifted to 802 nm, 824 nm, and 878 nm. The blue-shifting of the LH1 peak is indicative of the loss of carotenoids. The reduction in intensity and the blue shifting of the B800 peak suggests a loss of the B800 BChl.

Alc. vinosum membranes were washed in 1 %, 5 %, or 10 % acetone (v/v) in toluene and compared with standard membranes (Figure 5.28 black). The Qy absorption peaks observed after 1 % (Figure 5.28 dark red) and 5 % acetone (v/v) (Figure 5.28 red) washes were centred at 802nm, 824 nm, and 878 nm and were at similar intensities. However after the 10 % acetone wash there was a dramatic reduction in the 802 nm peak relative to the 824 nm peak. This suggests the loss of the B800 BChl.

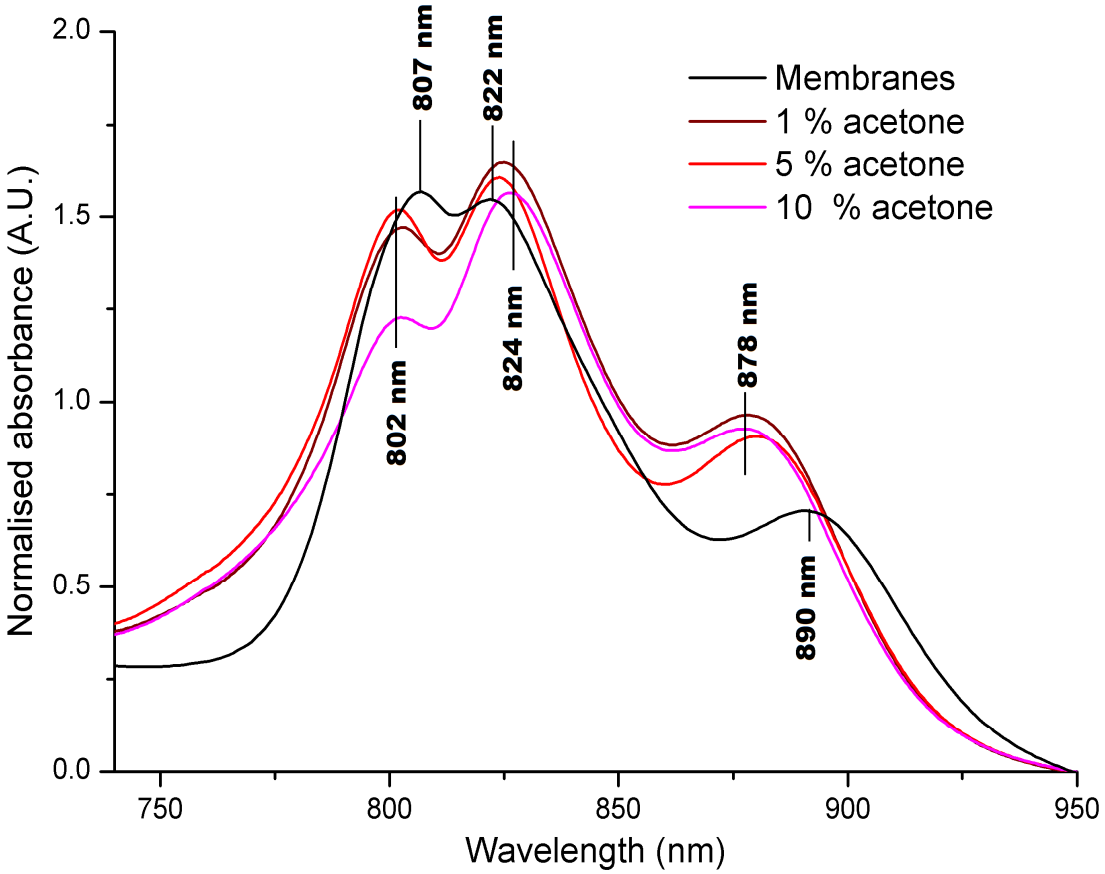

Figure 5.28 Normalised absorption spectra of membranes from *Alc. vinosum* cells before and after washing in 1 %, 5 %, and 10 % acetone in toluene.
Membranes were prepared from *Alc. vinosum* grown in sulphide, under low light, at 30 ºC growth conditions. The standard SLL30 membranes (black) produce NIR absorption peaks at 807 nm, 822 nm, and 890 nm. After washing with 1 % (dark red) and 5 % (red) acetone the absorption peaks shifted to 802 nm, 824 nm, and 878 nm. After washing with 10 % acetone in toluene (pink) the intensity of the 802 nm peak was greatly reduced relative to the 824 nm peak, and the LH1 associated peak blue shifted to absorption peaks shifted to 802 nm, 824 nm, and 877 nm. The blue-shifting of the LH1 peak is indicative of the loss of carotenoids. The reduction in intensity and the blue shifting of the B800 peak suggests a loss of the B800 BChl.

There was no substantial difference in the position of the NIR absorption peaks produced by *Alc. vinosum* membranes washed in 1 % (Figure 5.29 dark red), 5 % (Figure 5.29 red), and 10 % (Figure 5.29 pink) ethyl acetate (v/v). The NIR absorption peaks centre at 802nm, 824 nm, and 878 nm. The 802 nm absorption peak reduced in intensity but less substantially than observed in other solvent mixes.

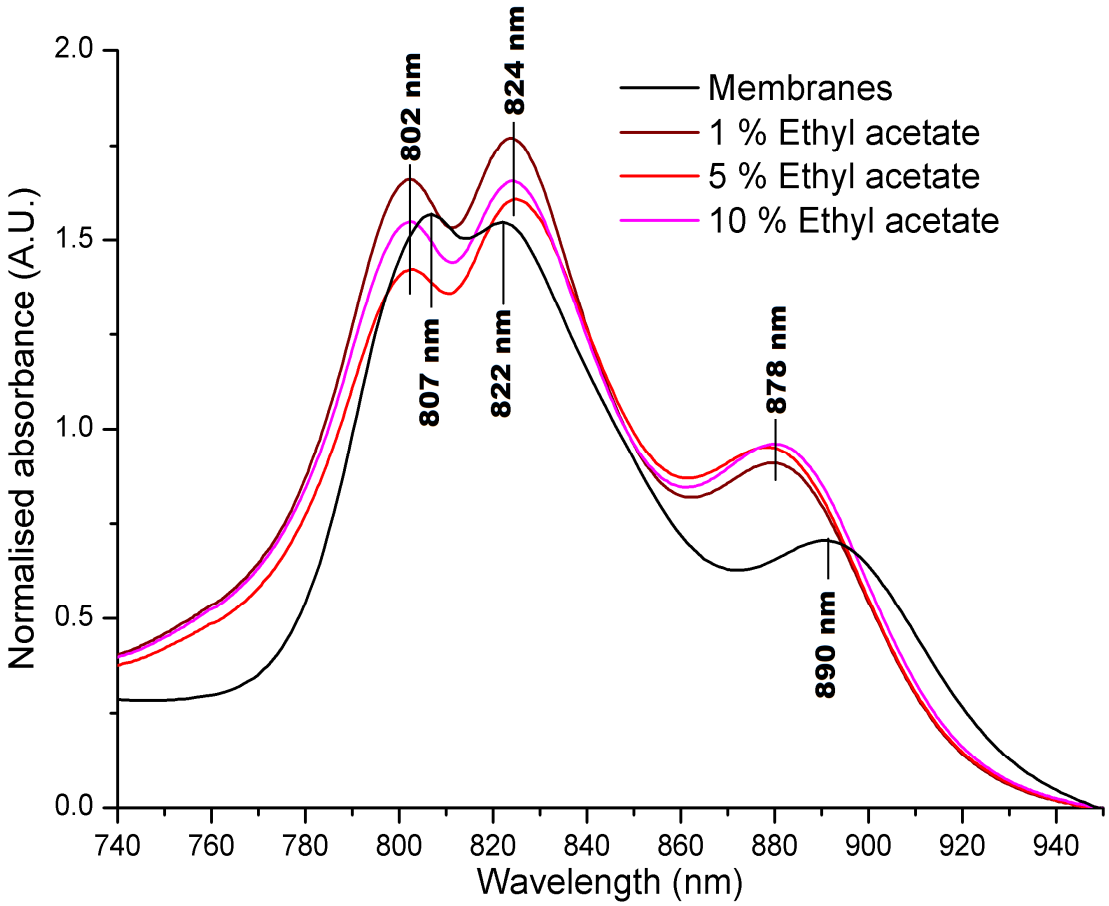

Figure 5.29 Normalised absorption spectra of membranes from *Alc. vinosum* cells before and after washing in 1 %, 5 %, and 10 % ethyl acetate in toluene.
Membranes were prepared from *Alc. vinosum* grown in sulphide, under low light, at 30 ºC growth conditions. The standard SLL30 membranes (black) produce NIR absorption peaks at 807 nm, 822 nm, and 890 nm. After washing with 1 % (dark red) and 5 % (red) ethyl acetate the absorption peaks shifted to 802 nm, 824 nm, and 878 nm. The blue-shifting of the LH1 peak is indicative of the loss of carotenoids.

5.5 Conclusions

DPA inhibition studies confirmed that *Alc. vinosum* can produce LH2 complexes in the absence of carotenoids, and the LH2 complexes produced are heavily carotenoid depleted. The B800-850 LH2 complex was produced in the absence of coloured carotenoids however there was preferential incorporation of carotenoids present into the B800-820 LH2 complex. Under growth conditions that usually produce B800-820 and B800-840 LH2 complex types, either very low inhibition was observed if the cells grew or if carotenoid incorporation was very low there was a red-shift of the dimeric BChl Qy peak. This suggests that carotenoid biosynthesis

inhibition is affecting the LH2 peptides that are expressed, either directly or indirectly.

The sulphide, high light, 30 ℃ growth conditions were identified as ideal for *Alc. vinosum* to produce nearly fully coloured carotenoid depleted B800-850 LH2 complex. Tandem MS-MS was used to determine the peptide composition of the carotenoid depleted B800-850a LH2 complex, finding that all the peptides from the standard B800-850a were observed with the exception of the β5.

The CrtI$^-$ 'knock-out' strain of *Alc. vinosum* was not completed within the time restraints of this project due to low yields of insert DNA during purification and complications in ligation into the final vector. To remedy this, new primers will be designed to create a new CrtI$^-$ insert. If this fails to produce a suitable yield, an alternative subvector will be used to amplify the insert for incorporation into PK18mobsacB. The creation of a carotenoidless *Alc. vinosum* mutant will allow large scale production of carotenoidless LH2 complexes. Additionally, this will allow the growth of *Alc. vinosum* under standard growth conditions without the use of a red filter. This will prevent any potential light effects on phytochrome regulation of production of the light-harvesting complexes.

Carotenoid extractions using toluene suggest that toluene is not able to extract the same amount of carotenoids present within the membranes as benzene. Benzene washes can extract up to 90 % of carotenoids present (68), whereas the highest level of carotenoid extraction was 66 % by 10 % ethyl acetate (v/v). The B800 peak of the LH2 complex, and the LH1 absorption peak blue shifted after washes with the toluene-solvent mixes however the LH2 peak associated with the B820 BChl did not shift substantially. This may indicate that the carotenoids were extracted predominantly from the LH1 complex and not the LH2 complex, which has been observed previously (68). The effects of the solvent washes on the stability of the light-harvesting complexes appear to be minimal, however the experiments must be repeated on purified complexes to confirm this.

Chapter 6 - Reversible dissociation of the carotenoidless B800-850 LH2 complex from *Alc. vinosum*

6.1 Introduction

This chapter aims to test that reversible dissociation can be performed on the carotenoid depleted B800-850 LH2 complex type from *Alc. vinosum* developed in this work (Chapter 5 section 5.2) using the reconstitution protocol developed for LH1 by the Loach group.

Reconstitution is a standard biochemical technique wherein a complex is taken apart and put back together again or created de novo from constituent parts. Alternative components can be substituted during the process, determining the importance of different structural elements to protein binding, function, and complex formation. This process has been successfully developed by the Loach group and applied to the LH1 complex from several different purple photosynthetic bacterial species (68, 122, 123, 125). The LH1 complexes were associated with non-native pigments and/or altered polypeptides substituted in place of native polypeptides. This process has been instrumental in elucidating important structural-function relationships due to the changes in function observed e.g. absorption maxima positions and intensities, energy transfer efficiencies, and formation of the complex.

The process of reversible dissociation of the LH1 complex has relied on the use of detergent such as octyl glucoside (OG) in high concentrations to dissociate a carotenoidless complex (32, 121-123). This process is then reversed by the dilution of detergent and addition of carotenoid that moves the equilibrium towards complex reformation (as outlined in Introduction section 1.4). Alternatively, the LH1 can be created from scratch (*de Novo*) with the separate isolated and purified components, e.g. BChl, alpha and beta polypeptides, and carotenoids. The components are then placed in conditions that favour complex formation.

Reconstitution has rarely been used successfully on an LH2 complex (127, 128) as most LH2 complexes cannot form in the absence of carotenoid. A carotenoid depleted B800-850 LH2 complex was developed previously in this work (Chapter 5 section 5.2) and provides an opportunity to perform reversible dissociation studies. Successful reconstitution studies on a carotenoid depleted B800-850 LH2 complex would prove that the process can work and future studies can work to optimise LH2 reconstitution.

6.2 Dissociation using detergents of both standard and carotenoid depleted B800-850 LH2 complexes

Reversible dissociation as a method of reconstitution involves the addition of an excess of detergent, usually OG, in order to pull the complex of interest apart. Upon dilution of the detergent the complex should begin to reform, initially the heterodimer subunits and then, upon a further reduction in detergent concentration, the full complex.

The carotenoid plays an important role in stabilising the LH2 complex, indicating that the presence or absence of carotenoid should affect the ability of detergent to disassemble the LH2 complex. The standard B800-850 LH2 complex was exposed to high concentrations of several detergents to identify whether the presence of carotenoids prevented dissociation, and if not whether the complex could be reformed after dissociation occurred (as described in Methods and Materials section 2.14.2). These experiments were then repeated on carotenoid depleted B800-850 LH2 complex types produced by *Alc. vinosum* in the presence of the carotenoid biosynthesis inhibitor DPA. These experiments will confirm whether the LH2 complexes can be reconstituted without needing to create a carotenoidless LH2. Additionally, the results will determine whether the carotenoid depleted B800-850 LH2 samples can be reversibly dissociation while still containing some coloured carotenoids.

Most previous work has used 3.5 – 5 % OG, depending on the concentration of light-harvesting complexes, to dissociate the carotenoid depleted complex (68, 121, 125)

added from a 20 % OG stock (32). Alternatively, Ghosh et al (131) used lauryldimethylamine oxide (LDAO) on the LH1 from *Rsp. rubrum* G9 to dissociate the complex, however LDAO has been implicated as too detrimental to the complexes to allow reformation after dissociation (126).

In order to detergent exchange the complexes into LDAO and OG they were purified in DM (as outlined in Methods and Materials section 2.5.2), as DM is easily dialysed out. The LH2 complexes from *Alc. vinosum* were detergent exchanged into the CMC of LDAO or OG.

Temperature affects on detergent have to be taken into consideration during reconstitution specifically in the case of the non-ionic detergent OG. There is an increase in the CMC of OG as temperature decreases (180). Reducing the temperature is thus used to move the LH2 complexes towards reformation, as has been done previously with reconstitution of the LH1 (68). It was established that, at room temperature, 0.6-0.8 % OG was the concentration of OG required to reform the subunit of the LH1 and reducing the concentration down to 0.3-4 % OG pushes towards whole complex reformation (121). The initial process of reforming the subunit is very quick while the reformation of the full complex takes longer, usually overnight (121).

Absorbance spectroscopy is effective at monitoring the status of the LH2 complexes, as when the detergent disrupts the structure it affects the binding of the pigments and thus the absorption spectrum. As the complex falls apart and the pigments are released into solution the Qy peaks of the BChl blue-shift towards the wavelength at which free, unbound BChl absorb (~780 nm). Absorption spectra of the B800-850 LH2 complex type were obtained at several stages of the process. The initial absorption spectrum was of the LH2 complex in buffer containing the CMC of the relevant detergent to determine the state of the complex before dissociation. A concentrated solution of detergent was added and the sample left at room temperature for an hour before the second absorption spectrum was recorded. If little to no difference was observed in the absorption spectrum the sample was left

at room temperature overnight (ON). The final spectrum was obtained to determine the level of dissociation that had occurred.

6.2.1 Detergent dissociation of the standard B800-850 LH2 complex using LDAO and OG

The stability of the standard B800-850 LH2 from *Alc. vinosum* was tested through the use of high concentrations of several detergents known to dissociate carotenoidless light-harvesting complexes, LDAO and OG.

The standard B800-850 LH2 complex was detergent exchanged into 0.1 % LDAO (v/v) from DM (Figure 6.1 black) causing the NIR absorption peaks to centre at 802 nm and 836 nm. After the detergent concentration was increased (Figure 6.1 blue) there was no change in the wavelength at which the absorption peaks centred after the increase in detergent concentration but there was a reduction in their intensity. The 802 nm reduced to a lower intensity relative to the other split B800 peak at 798 nm. A shoulder in the absorption at ~ 780 nm develops after an hour at 2 % (v/v) LDAO. A peak at ~ 780 nm is often associated with free BChl suggesting that some of the BChl are no longer bound within the protein scaffold. After the sample was left at room temperature overnight (Figure 6.1 red), the red-most absorption peak red shifted to 839 nm and there was a further reduction in the split B800 peaks. The absorption shoulder at ~780 nm increased in intensity and a peak at ~ 680 nm was observed. The peak at ~ 680 nm suggests the BChl are becoming oxidised. This presence of free BChl suggests that there is BChl loss from the LH2 however the relative stability of the position of the B850 peak suggests the complex is not dissociating.

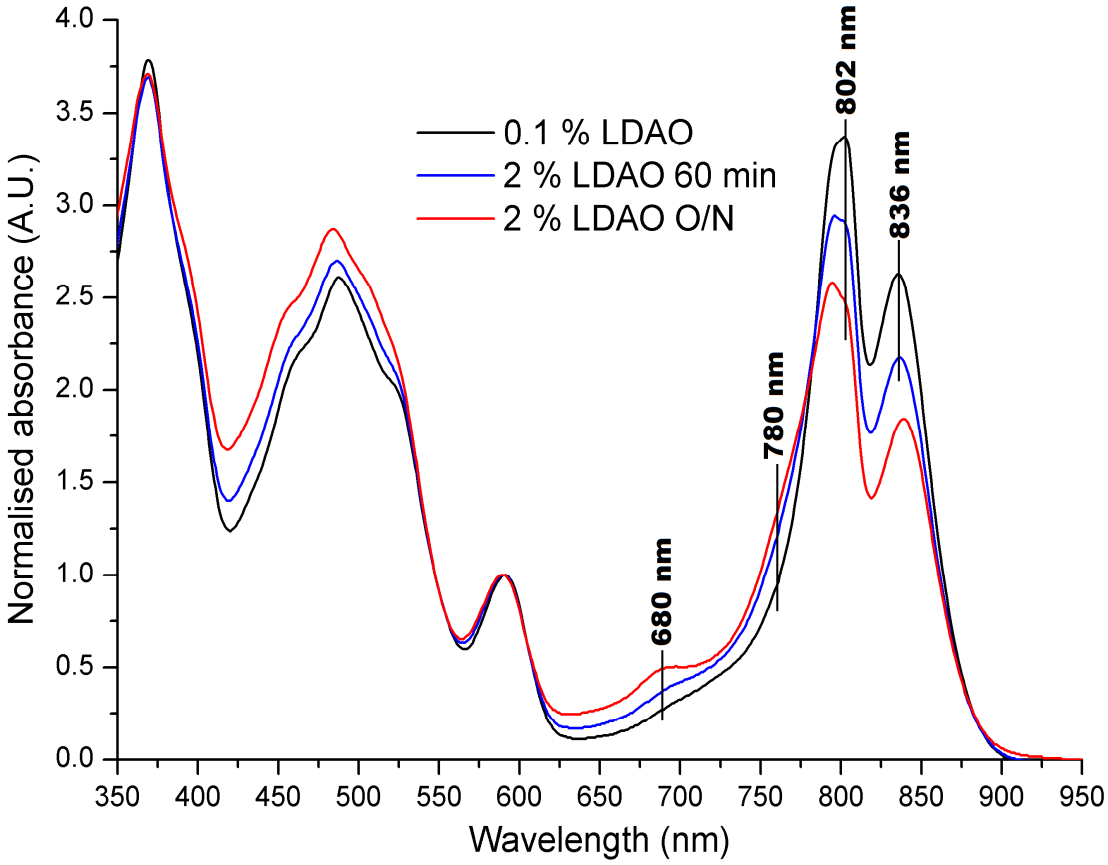

Figure 6.1 Normalised absorption spectra of the standard B800-850 LH2 complex from *Alc. vinosum* in 0.1 % LDAO and at 2% LDAO.
At 0.1 % LDAO (black) the peaks of the B800-850 LH2 complex centre at 802 nm and 836 nm. When the concentration of LDAO is increased to 2 % (blue) there is a loss in intensity of the Qy peaks and a shoulder develops at ~ 780 nm suggesting the presence of free BChl. The peaks are further reduced in intensity after the B800-850 LH2 has been left overnight (red). Additionally, a peak develops at ~680 nm, indicating the oxidation of the BChl.

Fresh B800-850 LH2 complex was detergent exchanged into OG to determine whether the standard LH2 complex would dissociate in OG. The absorption spectrum after detergent exchange into OG produced peaks in the NIR at 804 nm and 827 nm (Figure 6.2 black). The concentration of OG was increased to 5 % (w/v) (Figure 6.2 blue) and the position of the Qy peaks did not change however their intensity was reduced. After the sample was left overnight no further differences in the spectra were observed (Figure 6.2 red). This suggests the standard B800-850 LH2 complex is relatively stable in OG even at 5 % OG. None of the detergents tested successfully dissociated standard B800-850 LH2 complex, indicating that the presence of the carotenoid prevents dissociation.

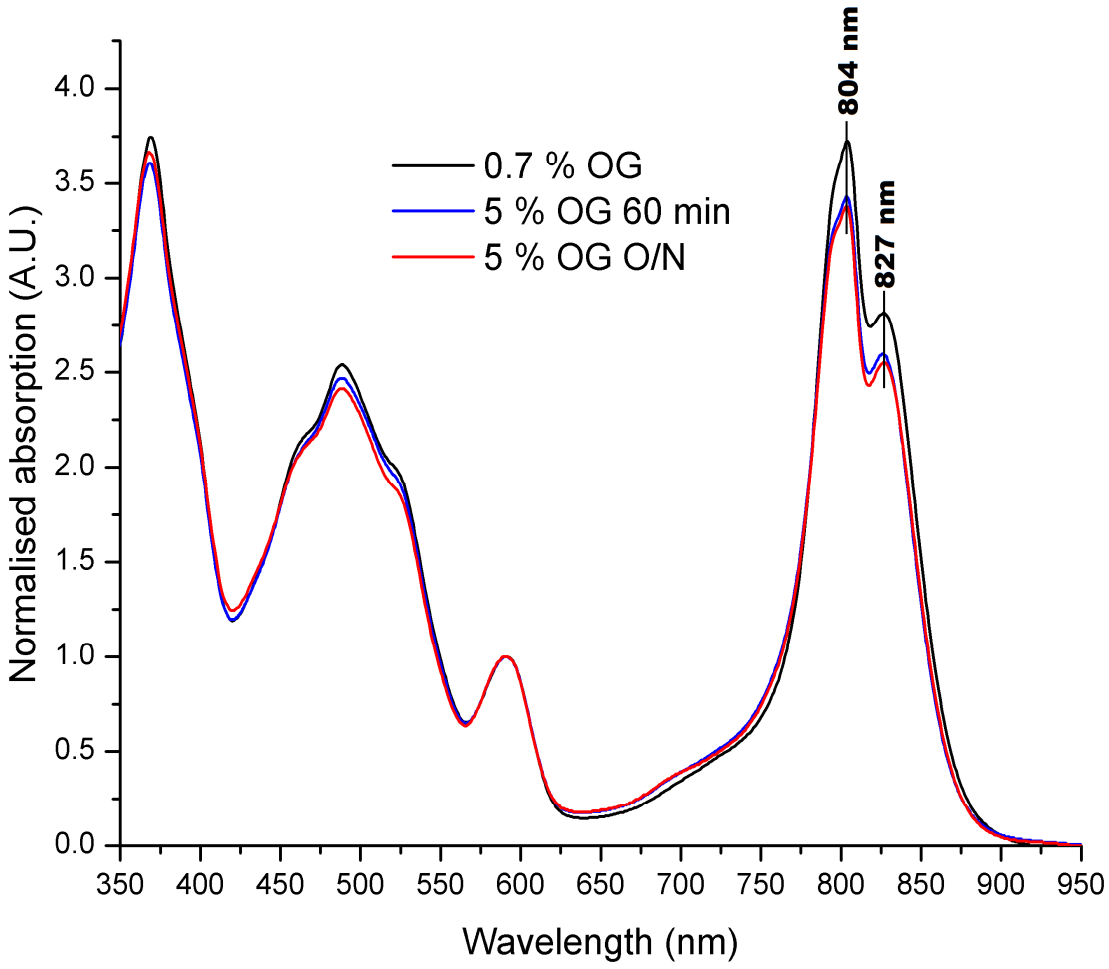

Figure 6.2Normalised absorption spectra of the standard B800-850 LH2 complex from *Alc. vinosum* in 0.7 % OG and at 5 % OG.
At 0.7 % OG (black) the peaks of the B800-850 LH2 complex centre at 804 nm and 827 nm. When the concentration of OG is increased to 5 % (blue) there is a reduction in the peak intensity but the peak positions don not change. The peaks do not change further if the sample is left overnight at 5 % OG (red). The peaks are further reduced in intensity after the B800-850 LH2 has been left overnight (red).

6.2.2 Reversible dissociation of the carotenoid depleted B800-850 using LDAO and OG

The stability of the carotenoidless B800-850 LH2 from *Alc. vinosum* was tested through the use of high concentrations of LDAO and OG. Upon dissociation, the detergent concentration was diluted back to the CMC in an attempt to reform the LH2 complexes.

The carotenoid depleted B800-850 LH2 complex was detergent exchanged into 0.1 % LDAO (v/v) and the Qy bands of the LH2 complexes centred at 794 nm and 832 nm

(Figure 6.3 green). The peak at 832 nm was dramatically lower than the B800 split peaks, and there is a shoulder in the absorbance at ~ 780 nm. The NIR absorption peaks observed are blue-shifted relative to the positions from the standard B800-850 in 0.1 % LDAO (v/v) by 2 nm for the 796 nm peak and by 4 nm for the B850 peak. This may indicate that the LH2 complexes were beginning to dissociate at low LDAO concentrations. The concentration of LDAO was increased to 2 % (Figure 6.3 blue) and the absorption peaks further blue shifted to peaks at 776 and 689 nm with a shoulder at ~830 nm. These values suggest the BChl are no longer bound to the proteins and are free in solution therefore the complexes are fully dissociated at 2 % LDAO (v/v). Only the peak at 689 nm increased after the sample was left at room temperature overnight (Figure 6.3 red). The concentration of the detergent was diluted down to 0.1 % LDAO (v/v) and the sample placed on ice to encourage reconstitution of the complex (Figure 6.3 red dotted line). After the sample was diluted back to 0.1 % LDAO (v/v) the Qy peak did not shift towards the red end of the spectrum. This implies the complex did not begin to reform. This suggests that dissociation with LDAO causes negative effects on the LH2 complex to the degree that dissociation is non-reversible.

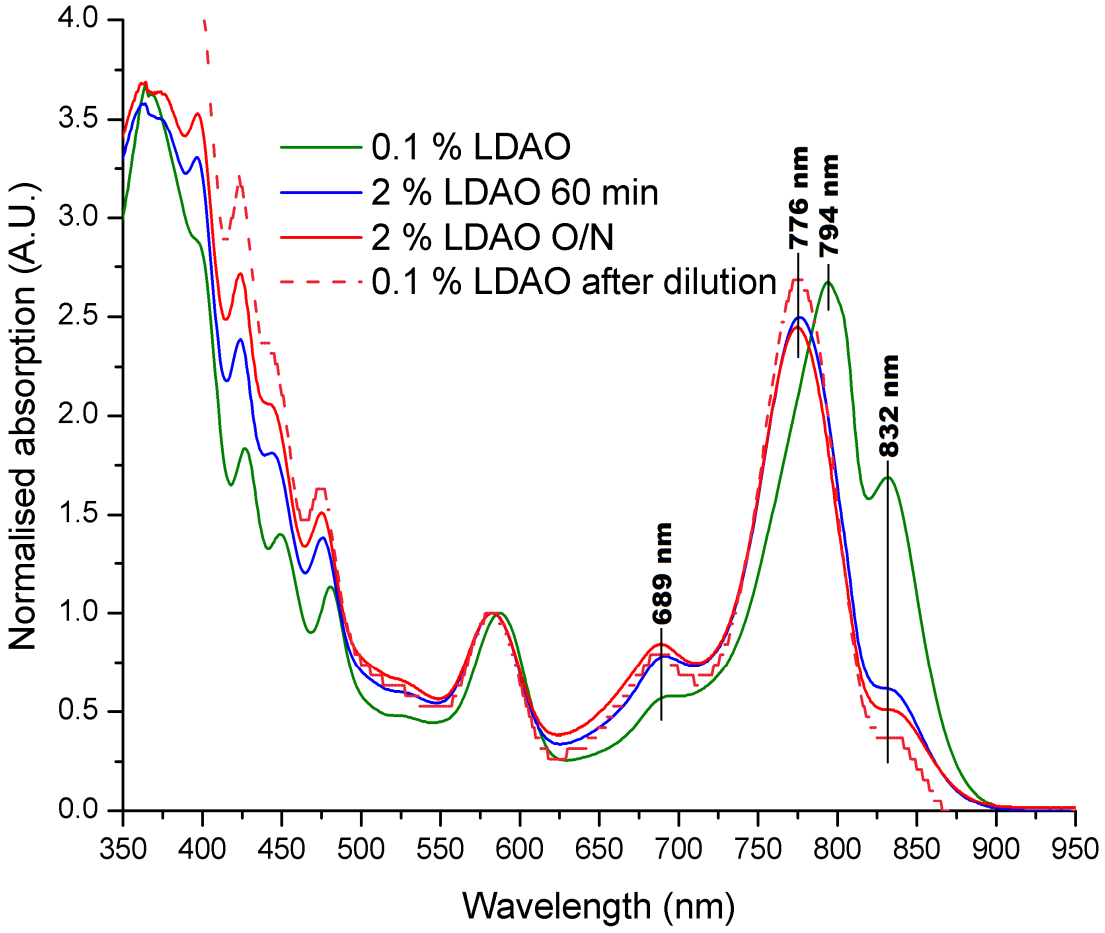

Figure 6.3 Normalised absorption spectra of the carotenoid depleted B800-850 LH2 complex from *Alc. vinosum* in 0.1 % LDAO and at 2% LDAO.
At 0.1 % LDAO (green) the peaks of the B800-850 LH2 complex centre at 794 nm and 832 nm. When the concentration of LDAO is increased to 2 % (blue) the peaks shift to 776 nm suggesting the presence of free BChl, and an increase of the peak at 689 nm indicating the BChl was oxidising. There was no change in peak position after the sample was left overnight (red) or when the concentration of detergent was diluted (red dotted line).

Reversible dissociation was repeated on the carotenoid depleted B800-850 LH2 complex using OG. The LH2 complex was detergent exchanged into 0.7 % OG (w/v) and the NIR absorption peaks centred at 804 nm with a shoulder at ~ 820 nm (Figure 6.4 green). The concentration of OG was increased to 5 % (w/v) (Figure 6.4 blue) and the absorption peaks blue shifted to a single peak at 792 nm with a shoulder at ~830 nm. After the sample was left overnight at room temperature (Figure 6.4 red) the peak blue shifted further to 788 nm. The position of the peak indicated the LH2 complexes had dissociated and so the detergent concentration was reduced. The NIR absorption spectrum showed a single peak at 805 nm after the concentration of

OG was diluted (Figure 6.4 dotted pink line). The red-shift of the Qy peak to 804 nm after OG dilution suggests the LH2 complexes are at least partially reforming; suggesting that dissociation with OG is reversible.

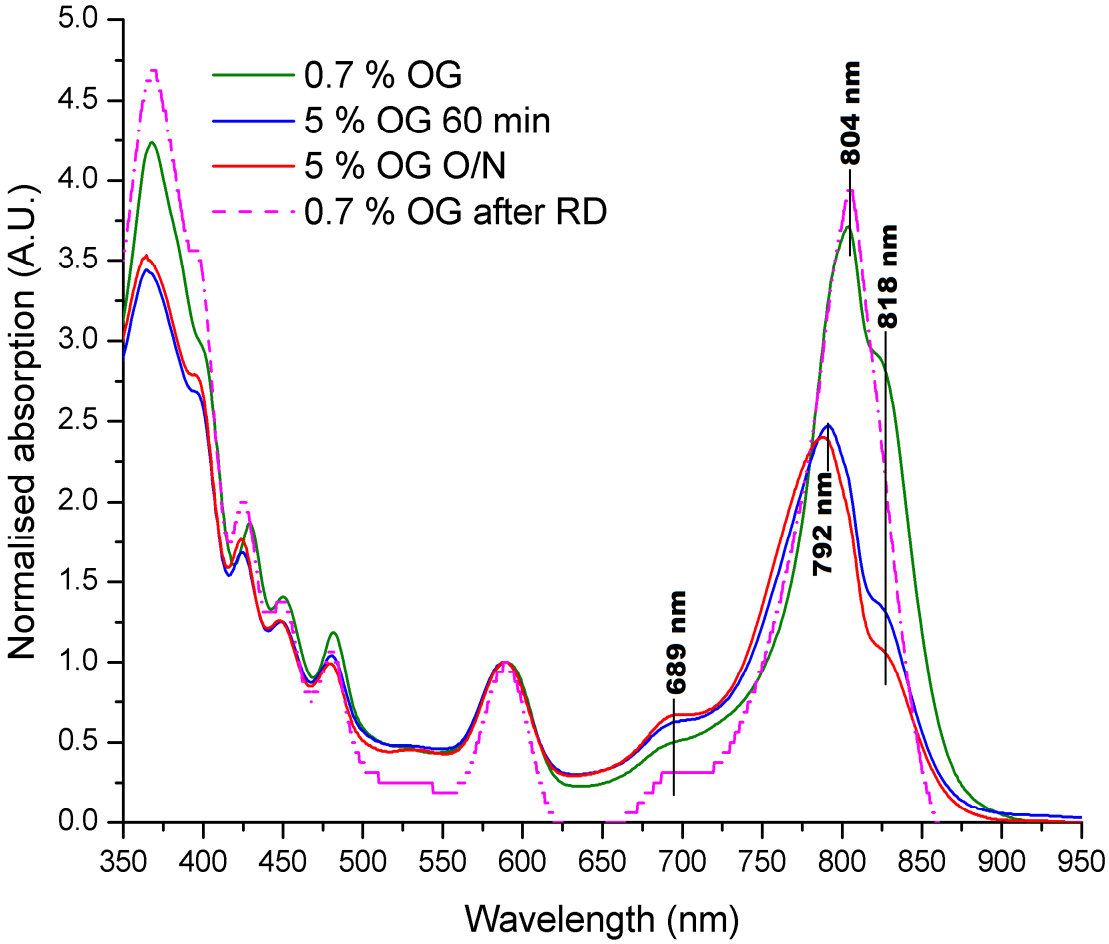

Figure 6.4 Normalised absorption spectra of the carotenoid depleted B800-850 LH2 complex from *Alc. vinosum* in 0.7 % OG and at 5% OG.
At 0.7 % OG (green) the peaks of the B800-850 LH2 complex centre at 804 nm with a shoulder at ~ 818 nm. When the concentration of OG is increased to 5 % (blue) the peaks shift to 792 nm suggesting the presence of free BChl, and a small increase of the peak at 689 nm indicating the BChl was oxidising. There was a small blue shift in the peak position after the sample was left overnight (red) to 788 nm. After the dilution of OG, the absorption peak red-shifted to 804 nm, however the absorption shoulder at ~ 818 nm failed to reform.

In the case of OG, full dissociation of all the complexes doesn't occur there is still a small shoulder present at ~830 nm. Previous work with OG (121) found that to remove the shoulder fully an excess of 20 % OG was needed. The benefits of this would be outweighed by the chemical changes that can occur on the BChl in the

presence of OG, namely the formation of 132-hydroxy-BChl that absorbs at 777 nm but is not able to reconstitute within the complex (32). The failure of the complexes to reform after reform in LDAO indicates that the detergent may be having a deleterious effect on either the proteins or the pigments, preventing the re-association.

6.3 Reversible dissociation of the carotenoid depleted B800-850 with carotenoid addition

The addition of carotenoid to dissociated LH1 is known to push the equilibrium towards complex reformation, and so carotenoid addition is used in conjunction with detergent dilution to re-associate the complex. Reversible dissociation was repeated using carotenoid depleted B800-850 LH2 complexes in OG, but with the addition of carotenoid (as described in Methods and Materials section 2.14.4). The addition of carotenoid should increase the yield of reconstituted complex by adding more structural stability. Previous work in this study (Chapter 4 section 4.3) has confirmed the carotenoids present within the LH2 complexes of *Alc. vinosum* are of the spirilloxanthin series (164). As the carotenoids of the spirilloxanthin series are naturally found in the LH2 complexes of *Alc. vinosum* the carotenoid binding site should be able to accommodate them easily. This should test the procedure without any carotenoid binding difficulties. Carotenoids were extracted as outlined in Methods and Materials section 2.14.1.

To test proof of concept these native carotenoids of the spirilloxanthin pathway (spirilloxanthin, lycopene, and rhodopin) were added to detergent dissociated carotenoid depleted LH2 complexes of *Alc. vinosum*.

RD with spirilloxanthin

Spirilloxanthin is one of the carotenoids identified in *Alc. vinosum* previously in this work (Chapter 4 section 4.3.2) as the second most prevalent carotenoid across all LH2 complex types (19 ±1% (164) or 6.0 ± 0.7 % (Magdong et al, 2015) in the B800-850 LH2 complex). Spirilloxanthin was extracted and purified from *Rsp. rubrum S1*

using a deactived alumina column (as described in Methods and Materials section 2.14.1). Carotenoid depleted B800-850 LH2 complexes from *Alc. vinosum* (Figure 6.5 green) were not carotenoidless but had a dramatically reduced carotenoid content. The NIR absorption peaks centre at 796 nm and 830 nm due to the effects of OG detergent. The LH2 complexes were dissociated and spirilloxanthin was added in as the detergent concentration was reduced. After the RD LH2 complexes were detergent exchanged into 0.02 % DDM (w/v) the B850 absorption peak (Figure 6.5 pink) red-shifted back to 838 nm with a single peak present at 796 nm for the split B800 peak. The ratio observed between the B800 and B850 Qy peaks is close to 1:1 in the reversibly dissociated sample. In the standard B800-850 LH2 complex, the Qy peaks centre at 847 nm and 796 nm in DDM (Figure 6.5 dark red) and the 847 nm peak is higher than the 796 nm peak. Whereas the fully carotenoidless LH2 complex (Figure 6.5 blue) produces absorption peaks at 841 and 796 nm. The absorption peaks of the RD LH2 complex do not red-shift as far as observed in either the standard LH2 complex or the carotenoidless LH2 complex suggesting that the complex is only partially reformed. The level of carotenoid observed is still much lower than that observed in the standard LH2 complex.

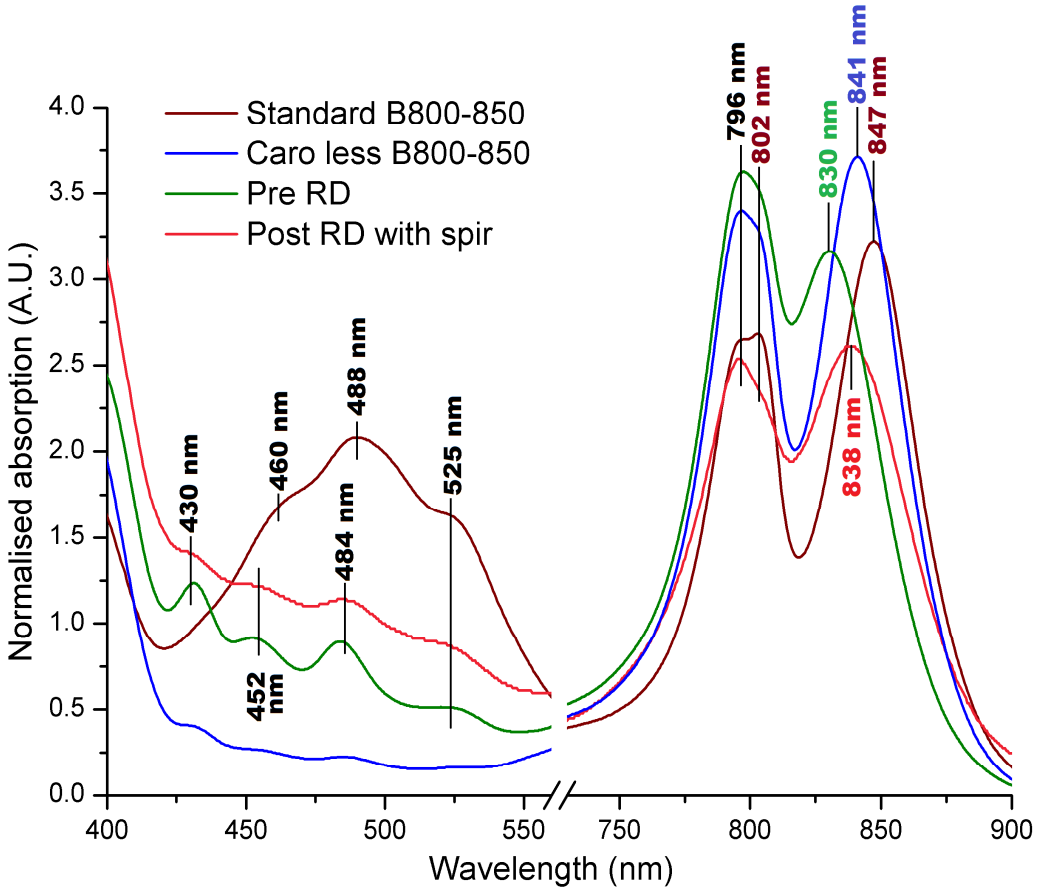

Figure 6.5 Normalised absorption spectra of the carotenoid depleted B800-850a from *Alc. vinosum* pre and post reversible dissociation with spirilloxanthin.
The standard B800-850 LH2 complex (dark red) in 0.02 % DDM (w/v) produces absorption peaks at 802 nm, 847 nm, and 488 nm with two absorption shoulders at ~ 460 nm and ~ 525 nm. The carotenoidless B800-850 LH2 complex (blue) in 0.02 % DDM (w/v) produces peaks at 841 nm and 796 nm. The carotenoid depleted B800-850 LH2 complex (green) in 0.7 % OG (w/v) prior to dissociation produced peaks at 796 nm, 830 nm, 431 nm, 452 nm, 484 nm, and a shoulder at ~ 526 nm. After reversible dissociation with spirilloxanthin and detergent exchange into 0.02 % DDM (red) the LH2 complex produces peaks at 838 nm, 796nm, 484 nm, with shoulders at ~ 430 nm, and ~ 525 nm. The carotenoid absorption peaks are higher after RD but there is more scattering than normally observed.

The post-RD LH2 complex was concentrated down and visually compared with the pre-RD carotenoid depleted B800-850 LH2 complex (Figure 6.6). The post-RD B800-850 LH2 complex was visibly red while the carotenoid depleted LH2 complex was green in colour. Potentially this may be due to free carotenoid pigments that are not within the LH2 complexes. Further purification by either sucrose density centrifugation or anion exchange would confirm the removal of any unbound carotenoids but the concentration of RD B800-850 LH2 complex was too low for either technique.

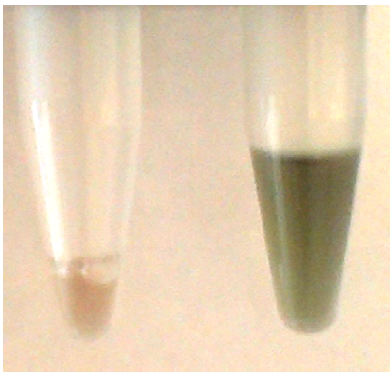

Figure 6.6 Visual comparison of the carotenoid depleted B800-850 LH2 complex before and after reversible dissociation with spirilloxanthin.
The pre-RD B800-850 LH2 complex was visibly green in colour, due to the low level of carotenoids present. After RD with spirilloxanthin the B800-850 LH2 complex was red/orange in colour indicating the presence of carotenoids in the sample. The volume and concentration of the sample was very low.

RD with lycopene

Previously in this work (Chapter 4 section 4.3.2), lycopene was identified as present in all the analysed LH2 complexes of *Alc. vinosum*, however lycopene makes up less than 5 % of the usual carotenoid complement (164). Reversible dissociation with lycopene will indicate whether the carotenoid binding sites have a level of exclusivity with regards to the carotenoids that are able to bind and may indicate whether differences in carotenoid composition are due to the binding pocket or simply the abundance of the carotenoid during LH2 complex formation. Lycopene was extracted and purified from tomato paste using an alumina column (as described in Methods and Materials section 2.14.1). The carotenoid depleted B800-850 LH2 complex was dissociated with 5 % OG overnight before the detergent was diluted to 1 % and lyocpene added (as described in Methods and Materials section 2.14.4). After reversible dissociation the LH2 complexes were detergent exchanged into DDM and purified by sucrose density centrifugation as lycopene is not dense enough to travel through the sucrose gradient. Only one band was observed in the sucrose density gradient, equilibrating at ~ 0.8 M sucrose (Figure 6.7) and this was of a yellow colour suggesting the incorporation of lycopene.

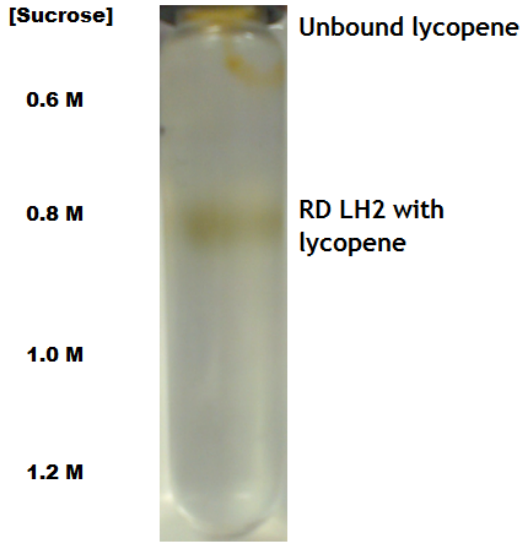

Figure 6.7Sucrose density centrifugation gradient of B800-850 LH2 complex reversibly dissociated with lycopene.
The sucrose concentrations of the sucrose density gradient are shown to the left of the tube. The RD B800-850 LH2 complex equilibrated to ~ 0.8 M sucrose and appeared as a yellow band, suggesting the incorporation of lycopene. Unbound lycopene did not move through the gradient.

The absorption spectrum of the purified RD B800-850 LH2 complex (Figure 6.8 pink) produces peaks at 797 nm and 843 nm in the NIR. The red-shift of the B850 Qy band is not to the extent of the standard B800-850 LH2 complex (Figure 6.8 dark red) at 847 nm. However, the red-shift of the B850 Qy RD B800-850 LH2 complex is further than that observed in the carotenoidless LH2 complex (Figure 6.8 blue). This suggests the incorporation of lycopene is causing the Qy peak to red-shift. The ratio of the B800 peak to the B850 peak is 1:1, indicating that the complex may only be partially reformed as in both the standard and carotenoid depleted LH2 complexes the B850 peak is substantially higher than the B800 peak. The pre-RD B800-850 LH2 complexes produces (Figure 6.8 green) peaks at 431 nm, 452 nm, 484 nm, and a shoulder at ~ 526 nm in the carotenoid region of the absorption spectrum. After RD with lycopene the peaks at 452 nm, 484 nm, and ~ 526 nm all increase in intensity but the peak at 431 nm does not. The three peaks that increase in intensity relate to lycopene, supporting the fact that the level of lycopene in the LH2 complexes has increased.

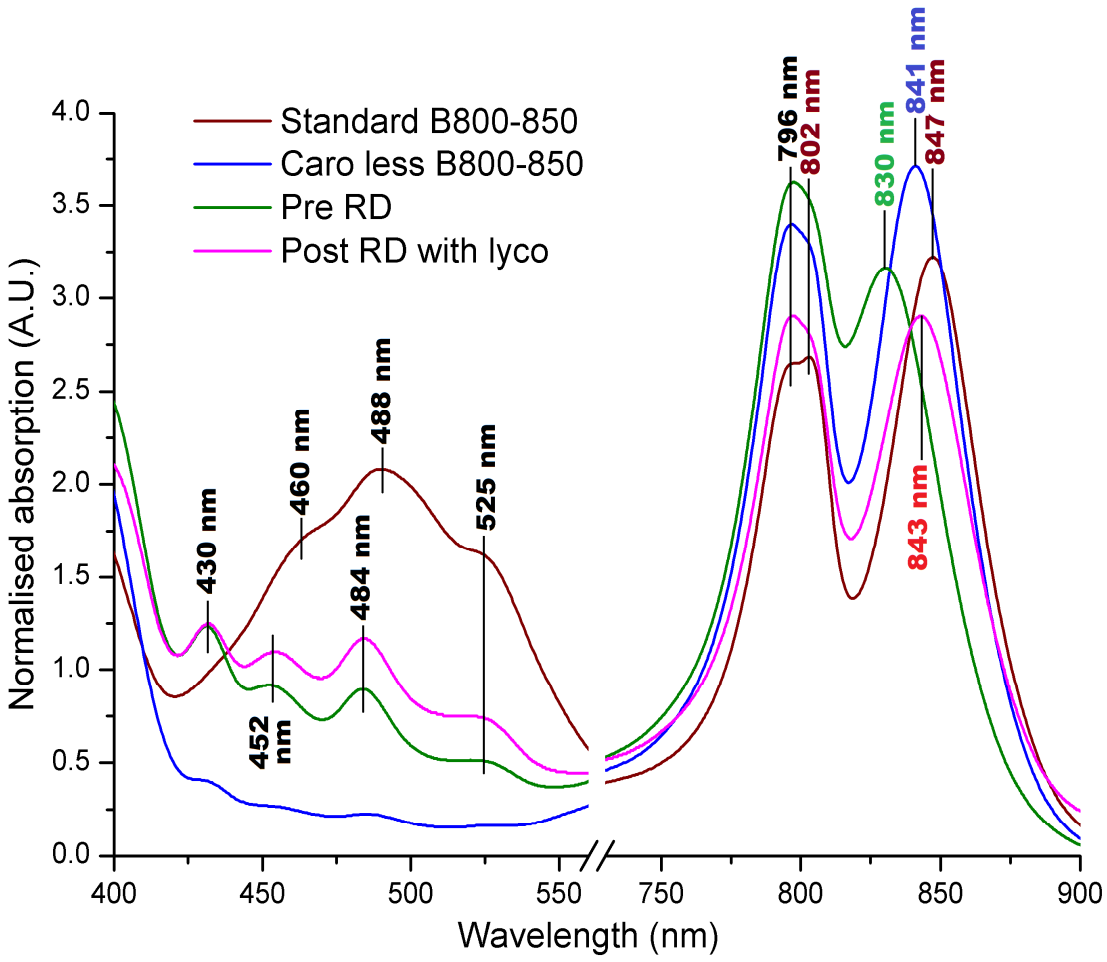

Figure 6.8Normalised absorption spectra of the carotenoid depleted B800-850a from *Alc. vinosum* pre and post reversible dissociation with lycopene.
The standard B800-850 LH2 complex (dark red) in 0.02 % DDM (w/v) produces absorption peaks at 802 nm, 847 nm, and 488 nm with two absorption shoulders at ~ 460 nm and ~ 525 nm. The carotenoidless B800-850 LH2 complex (blue) in 0.02 % DDM (w/v) produces peaks at 841 nm and 796 nm. The carotenoid depleted B800-850 LH2 complex (green) in 0.7 % OG (w/v) prior to dissociation produced peaks at 796 nm, 830 nm, 431 nm, 452 nm, 484 nm, and a shoulder at ~ 526 nm. After reversible dissociation with lycopene and detergent exchange into 0.02 % DDM (pink), the LH2 complex produces peaks at 843 nm, 797 nm, 461 nm, 452 nm, 484 nm, and ~ 526 nm. There is an increase in the carotenoid peaks at 452 nm, 484 nm, and 526 nm after RD indicating an increase in the level of carotenoid present.

To confirm that the carotenoids observed in the absorption spectrum of the RD B800-850 are incorporated within the LH2 complex the fluorescence emission spectrum was obtained (as described in Methods and Materials section 2.6). The fluorescence emission of the carotenoid depleted B800-850 LH2 complex (Figure 6.9 green) before reversible dissociation produces an emission peak at ~850 nm at an intensity of ~ 4000 counts with a small shoulder at ~ 810 nm. After reversible

dissociation with lycopene (Figure 6.9 red) the emission spectrum the peak profile was similar, centring at ~ 850 nm with a shoulder at ~ 810 nm however the intensity was much higher at ~ 12,000 counts. The increase in energy transfer indicates a larger amount of carotenoids are able to be excited and transfer the energy to the BChl. As energy transfer from the carotenoids to the BChl can only occur within van der Waals distance, the emission from the BChl suggests the carotenoids are bound close to the BChl thus within the protein scaffold. The correct position of the emission peak implies the BChl seem to be properly bound but this would need to be confirmed by a technique such as CD (121).

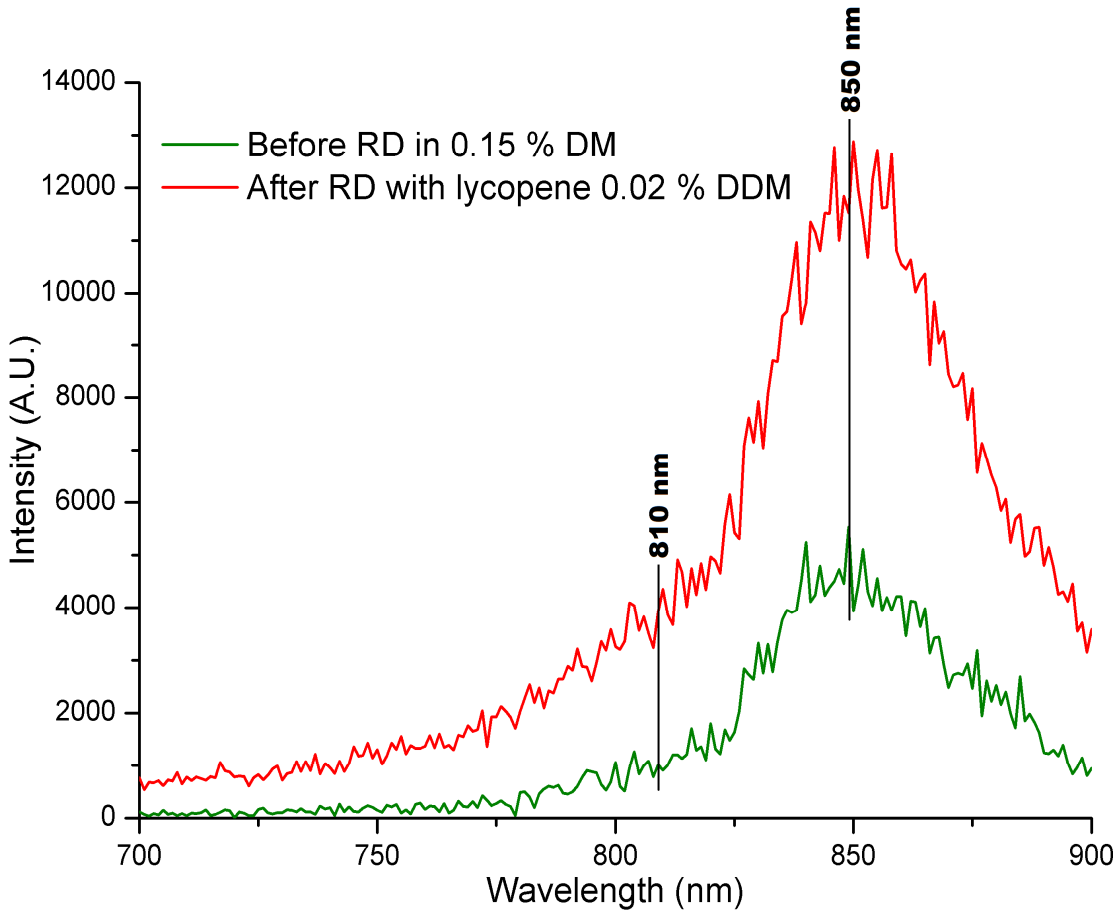

Figure 6.9Fluorescence emission spectra of the carotenoid depleted B800-850a from *Alc. vinosum* pre and post reversible dissociation with lycopene.
The carotenoid depleted B800-850 LH2 complex (green) in 0.7 % OG (w/v) prior to dissociation produced a peak at ~ 850 nm with a shoulder at ~ 810 nm. After reversible dissociation with lycopene and detergent exchange into 0.02 % DDM (red), the LH2 complex produces peaks at the same wavelengths but of a higher intensity, up to ~ 12,000 counts from ~ 4000.

RD with rhodopin

Rhodopin was used as the reconstitution carotenoid as it is the most abundant carotenoid present in the LH2 complex types of *Alc. vinosum* and will determine whether the limitations are due to the current protocol. Rhodopin was extracted and purified from *Alc. vinosum* membranes (as previously described in Methods and Materials section 2.14.1). The process of reconstitution and purification with sucrose density gradients was repeated as per the lycopene RD studies. The absorption peaks in the NIR from the B800-850 LH2 complex after RD (Figure 6.10 pink) with rhodopin observed centre at 843 nm and 797 nm as observed in the LH2 complexes reversibly dissociated with lycopene. The position of the Qy from the B850 BChl is blue-shifted relative to the standard B800-850 LH2 complex (Figure 6.10 dark red) however it is red-shifted relative to the carotenoidless B800-850 LH2 complex (Figure 6.10 blue). The carotenoids peaks of the carotenoid depleted B800-850 LH2 complex (Figure 6.10 green) centre at 431 nm, 452 nm, 484 nm, and a shoulder at ~ 526 nm. After RD the peaks at 452 nm, 484 nm, and ~ 526 nm increased in intensity indicating an increase in the level of carotenoid present.

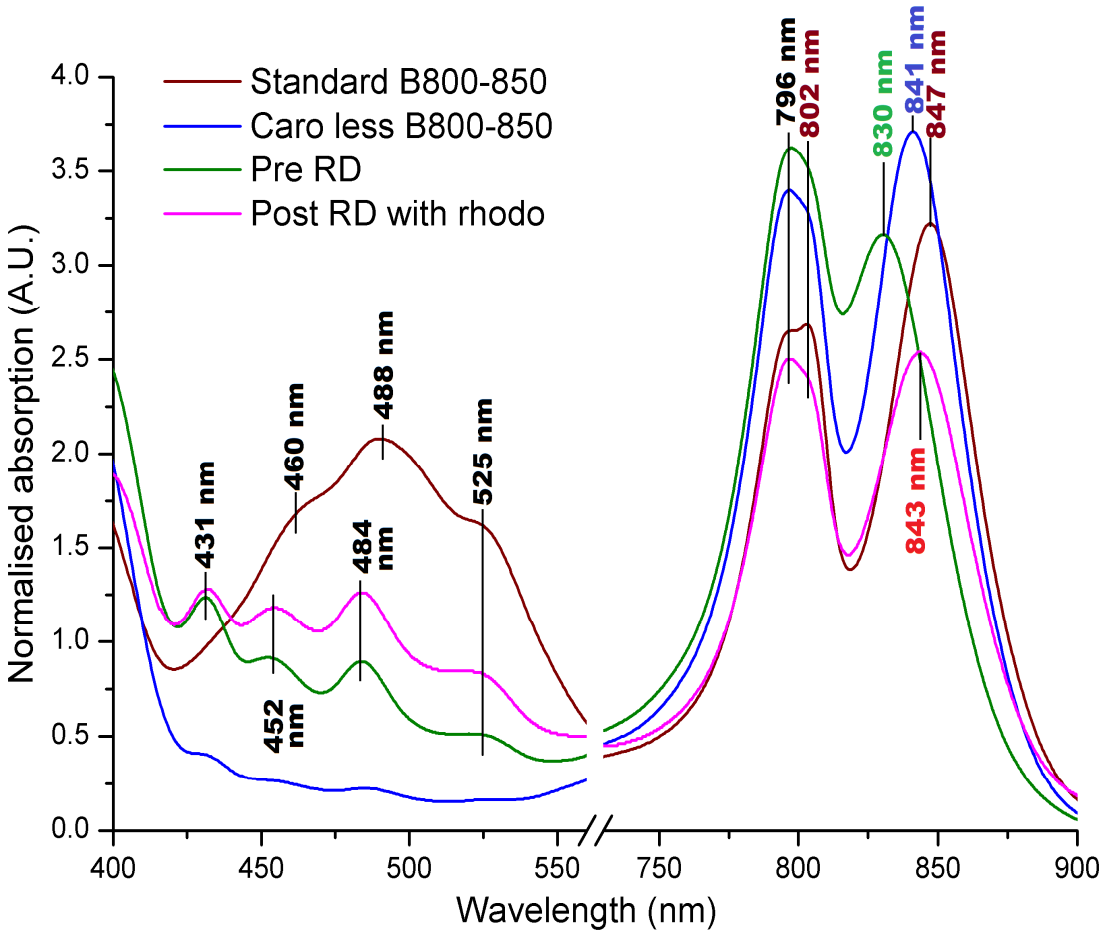

Figure 6.10 Normalised absorption spectra of the carotenoid depleted B800-850a from *Alc. vinosum* pre and post reversible dissociation with rhodopin.
The standard B800-850 LH2 complex (dark red) in 0.02 % DDM (w/v) produces absorption peaks at 802 nm, 847 nm, and 488 nm with two absorption shoulders at ~ 460 nm and ~ 525 nm. The carotenoidless B800-850 LH2 complex (blue) in 0.02 % DDM (w/v) produces peaks at 841 nm and 796 nm. The carotenoid depleted B800-850 LH2 complex (green) in 0.7 % OG (w/v) prior to dissociation produced peaks at 796 nm, 830 nm, 431 nm, 452 nm, 484 nm, and a shoulder at ~ 526 nm. After reversible dissociation with rhodopin and detergent exchange into 0.02 % DDM (pink), the LH2 complex produces peaks at 843 nm, 797 nm, 461 nm, 452 nm, 484 nm, and ~ 526 nm. There is an increase in the carotenoid peaks at 452 nm, 484 nm, and 526 nm after RD indicating an increase in the level of carotenoid present.

Emission fluorescence was recorded to determine whether the carotenoids had been incorporated into the LH2 complexes. The level of energy transfer in the carotenoid depleted B800-850 LH2 complex (6.11 green) was observed at ~ 850 nm at an intensity of ~ 4000 counts with a small shoulder at ~ 810 nm. After reversible dissociation (6.11 red) the fluorescence emission peak position did not change position however the intensity increased to ~ 13,000 counts. This increase of 8-9000

counts is similar to but slightly higher than observed after reversible dissociation with lycopene.

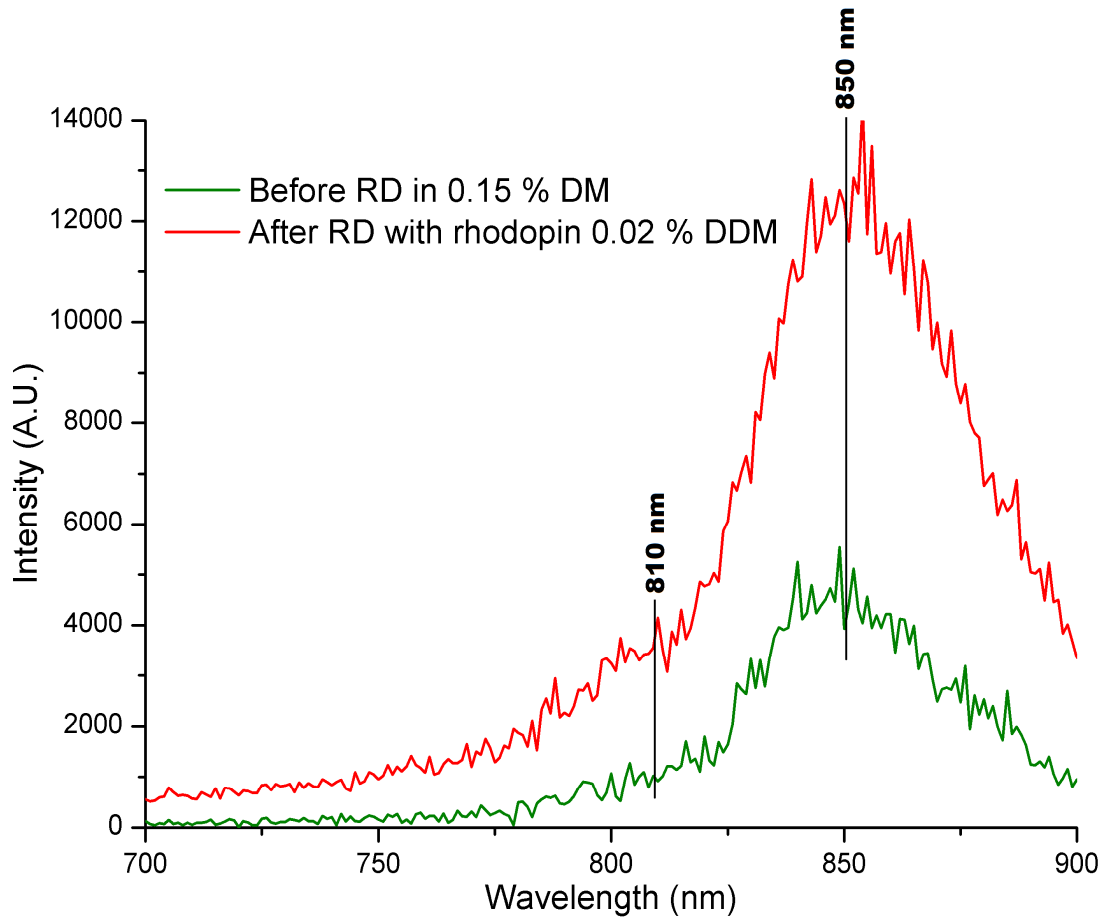

Figure 6.11 Fluorescence emission spectra of the carotenoid depleted B800-850a from *Alc. vinosum* pre and post reversible dissociation with rhodopin.
The carotenoid depleted B800-850 LH2 complex (green) in 0.7 % OG (w/v) prior to dissociation produced a peak at ~ 850 nm with a shoulder at ~ 810 nm. After reversible dissociation with rhodopin and detergent exchange into 0.02 % DDM (red), the LH2 complex produces peaks at the same wavelengths but of a higher intensity, up to ~ 13,000 counts from ~ 4000.

Comparison of reversibly dissociated B800-850 LH2 complexes with either lycopene or rhodopin

The level of carotenoid incorporation into the B800-850 LH2 complex type was similar between the purified LH2 complexes. To determine whether there was a substantial difference in the level of incorporation of lycopene or rhodopin differential spectra were created. The absorption spectrum of the carotenoid depleted B800-850 LH2 complex type was subtracted from the reversibly

dissociation B800-850 LH2 complex absorption spectrum. The difference in the carotenoid region after lycopene reversible dissociation (Figure 6.12 blue) shows an increase of 0.3 A.U. at the 485 nm carotenoid peak. However, the difference in the carotenoid region after rhodopin reversible dissociation (Figure 6.12 red) shows an increase of 0.4 A.U. at the 485 nm carotenoid peak. This may suggest a slightly higher incorporation of rhodopin than lycopene.

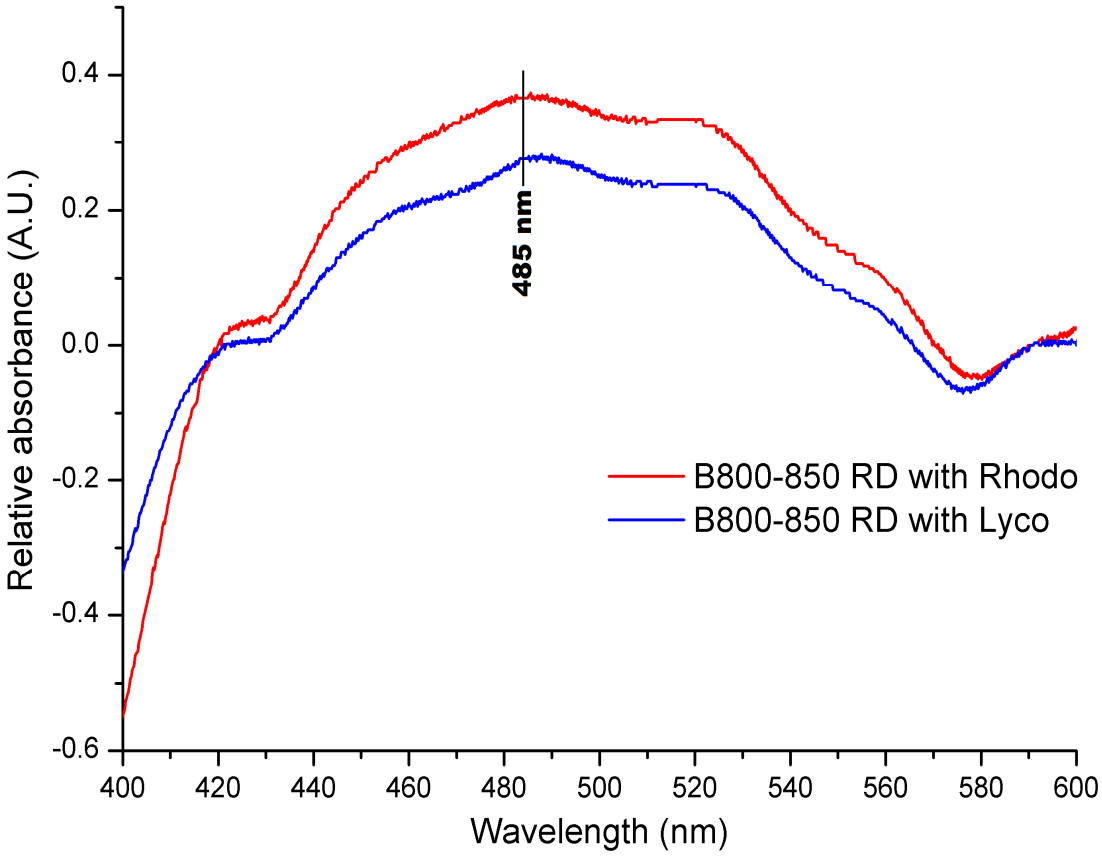

Figure 6.12 Differential absorption spectra of the carotenoid region of the B800-850 LH2 complex reversibly dissociated with either lycopene or rhodopin.
The B800-850 LH2 complex reversibly dissociated with rhodopin (red) produced an increase in absorbance at 485 nm by 0.4 A.U. The B800-850 LH2 complex reversibly dissociated with lycopene (blue) produced an increase in absorbance at 485 nm by 0.3 A.U. This indicates a slightly higher incorporation of rhodopin in reversible dissociation.

There appears to be little or no difference in the level of incorporation of the different carotenoids into the reversibly dissociated LH2 complexes of *Alc. vinosum*. This suggests a limitation in the technique either in the process, or the lack of fully carotenoid depleted LH2 complexes. The increase in the absorption spectrum in the

carotenoid region has the same line profile after reversible dissociation with both lycopene and rhodopin. This is due to the fact that lycopene and rhodopin contain the same chromophore.

6.4 Preliminary *De Novo* reconstitution

Initial results from the reversible dissociation suggested that this process can work with the LH2 complexes from *Alc. vinosum*. This was pushed further in a preliminary experiment to discern whether *de novo* creation of the LH2 complex from individually purified components could be effective (as described in Methods and Materials section 2.14.5.2). Figure 6.13 shows the spectra of the spirilloxanthin (red), BChl (green) and the reconstituted sample in 0.7 % OG after it was left at 4℃ overnight (blue). An absorption peak at 680 nm developed in the reconstituted sample after reconstitution overnight indicating a high level of oxidised BChl. After reconstitution, the peak of free BChl at 777 nm broadens to include a shoulder at ~ 850 nm. This suggests either the re-formation of the LH2 complex type or formation of BChl dimers (121). The small amount of reconstituted sample was run down a 1g De52 sepharose anion exchange column (Whatman) at 4℃ in order to separate free pigments and reversibly dissociated sample. The pigmented sample settled on top of the resin and failed to elute even with 2 M NaCl elution buffer. This indicated that the peak at ~ 850 nm observed was most probably BChl dimers and that the process of reconstitution had not been successful.

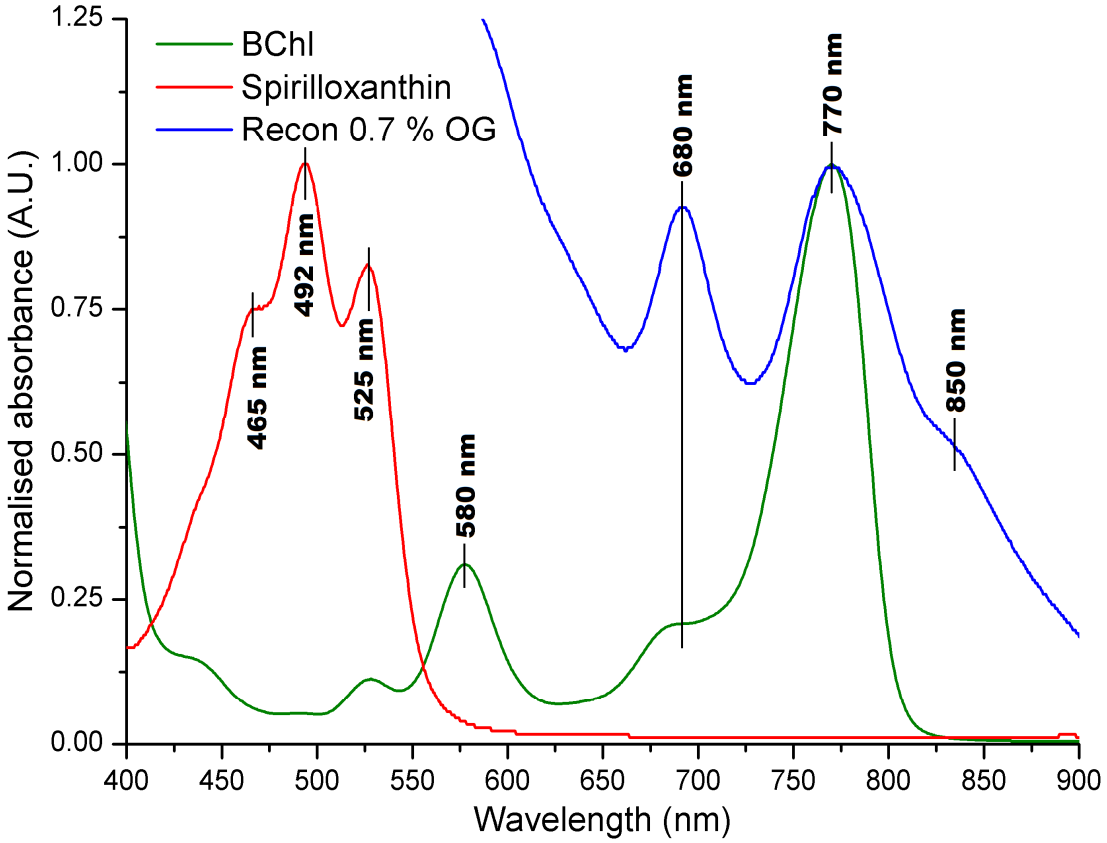

Figure 6.13 Normalised absorption spectra of de novo reconstitution of the B800-850 LH2 complex with the spectrum of spirilloxanthin and BChl.
The absorption spectrum of spirilloxanthin (red) in acetone produced three peaks at 465 nm, 492 nm, and 525 nm. The absorption spectrum of the free BChl (green) in methanol produced peaks that centred at 770 nm (Qy) and 580 nm (Qx). After the peptides, BChl, and carotenoid were mixed and left to reconstitute the absorption spectrum produced peaks at 680 nm, 770 nm, and a shoulder at ~ 850 nm. The absorption shoulder at ~ 850 nm is potentially reconstituted BChl or dimeric BChl free in solution. Spectra were normalised at their highest peak to 1.

6.5 Conclusions

The carotenoid depleted B800-850 LH2 complex produced under carotenoid biosynthesis conditions by *Alc. vinosum* is able to be reversibly dissociated using OG but not LDAO. The process of reversible dissociation was able to incorporate separately isolated and purified native carotenoids; lycopene, rhodopin, and spirilloxanthin. The level of carotenoid incorporation was the same regardless of the carotenoid incorporated. This suggests that the limitation is not due to differences in the carotenoid but in the reversible dissociation protocol. A fully carotenoidless B800-850 LH2 complex may be more successful as residual

carotenoids within the LH2 complex may inhibit the full dissociation of the LH2 complex. The attempt at de Novo reconstitution from constituent parts was unsuccessful, potentially due to aggregation of the BChl. Other factors may include incorrect ratios of the alpha peptides to beta peptides as the extraction technique preferentially extracts alpha peptides. Further work would require purification of the individual peptides using HPLC. Alpha and beta peptides can then be combined in a 1:1 ratio, as observed in the standard LH2 models (62, 63, 80) and during peptide composition analysis in chapter 4 of this work. The peptides can be combined in appropriate compositions identified to recreate the different LH2 complex types. Once the *de Novo* reconstitution protocol is optimized and the native complexes can be reconstituted alternative peptide compositions can be tested. This can be used to analyse and deduce the basis for the variation between the changes in the Qy absorption bands as well as deducing whether there are two B800 BChl binding sites.

Conclusions and future outlook

The energy from our local star showers the planet Earth with a huge amount (4.3 x 10^{20} J per hour (181) of renewable energy. This stream of solar energy could provide the means to help fulfil human energy requirements if it could be effectively harvested and harnessed. Current energy demand shows the human race meeting 70 % of current energy demands by burning fossil fuels (181). This has multiple effects not least of which being the change to the climate as sequestered carbon re-enters the atmosphere. These resources are finite and will ultimately run out and need to be replaced by alternatives, such as solar energy that can fill the energy shortfall. Multiple organisms in nature have evolved the process of photosynthesis to harvest the abundant solar energy and convert it into chemical energy. Understanding how these processes proceed *in vivo*, and how the proteins and pigments function in their respective roles of light-harvesting and absorption 'tuning' will aide in the development of man-made artificial photosynthetic systems. Understanding how how pigments are bound within natural systems and how this affects how they absorb and transfer energy is essential for creating new pigments and incorporating them into artificial light-harvesting systems.

Reconstitution has been an effective tool in understanding key structural features within the LH1 complex (32, 68, 121-123, 125) of purple photosynthetic bacteria. This understanding can be applied in the development of artificial light-harvesting systems. The LH2 complex is built on a similar modular principle to the LH1 complex however due to the inability of the LH2 complex to form in the absence of carotenoids there has only been one successful LH2 reconstitution study (127). As the LH2 complexes from *Alc. vinosum* were postulated as able to form in the absence of carotenoids, work was conducted to identify potential LH2 reconstitution candidates to develop a potential new system for reconstitution.

This work contributed to multiple publications and the development of the understanding of the LH2 complexes of *Alc. vinosum* in light of recent genomic (10)

and LH2 structural understanding (62, 63, 80, 99). The different LH2 complex types were identified and the complexes characterised with some of their defining features elucidated. This was to create an adequate knowledge base to identify a suitable carotenoidless reconstitution LH2 complex candidate and perform preliminary reconstitution experiments.

It was long established that *Alc. vinosum* produces different NIR absorption spectra depending on the growth conditions it was grown under (6, 109, 110, 146, 153). Further work determined that these variations were due to *Alc. vinosum* producing three LH2 complex types, the B800-820, B800-840, and B800-850 under different growth conditions (182).

Peptide analysis confirmed previous biophysical studies (113) that all the LH2 complexes are heterogeneous, with the highest levels of heterogeneity in the B800-820 and B800-840 LH2 complex types. Due to the high level of heterogeneity and limited number of peptides, all of the LH2 complex types share peptides with each other. Determining whether the different LH2 complex types are distinct or form a continuum is convoluted. It was noted that during anion exchange the elution peaks for each of the LH2 complex types were not discrete, with progressive fractions showing a red-shift in the position of the dimeric BChl Qy absorption peaks. This indicates that between the different LH2 complex types produced under the same growth conditions there are multiple intermediate LH2 complexes formed. It would appear that there is a continuum of LH2 complexes between the B800-820, B800-840, and B800-850c LH2 complex types.

This work has been able to identify the growth conditions that produce the different LH2 complex types and improve the purification protocol for each. Anion exchange chromatography identified LH2 complex subtypes of the B800-850 and B800-840 LH2 complex types; the B800-840h, B800-840p, B800-850a, and B800-850c LH2 complex types. The peptide composition difference between the B800-840h and B800-840p LH2 complex subtypes was not explored as part of this work but the peptide composition of the B800-850c and B800-850a LH2 complex subtypes were compared by tandem MS-MS and MALDI-TOF. The ß5 and ß6 peptides were observed

in the B800-850a LH2 complex subtype and not in the B800-850c. As there is high conservation between the different beta peptides, this change in composition would be unlikely to effect the anionic interactions. This may indicate a role of the beta peptides in binding the BChl (80) but also in 'tuning' the B850 Qy band between different LH2 complex subtypes. Unusually, the α3 was not observed in the B800-850a although it has been observed in all other LH2 complex types (164). Potentially, this may indicate that the α3 peptide does not fragment well during analysis however this must be confirmed. Alternatively, the lack of an α3 peptide may form the basis of the difference between the two B800-850 LH2 complex subtypes. This would be unusual as the α3 peptide is a component of all the LH2 complex types analysed as part of this work. The tandem MS-MS data must be repeated to ensure that all the peptides are being extracted and identified. Once the absence of the α3 is confirmed, percentage composition can be determined and further deductions made on the contribution from the different alpha and beta peptides on the BChl 'tuning'.

The basis of the blue-shift of the B850 BChl Qy absorption band from the B800-850 to the B800-820 LH2 complex type appears, in part, to be the same as that observed in the LH2 complexes from other species, namely *Rps. acidophila* (62, 99), and *Phs. Molischianum* (80, 94). The blue shift is due to the loss of a hydrogen bond donor residue at the position +11 relative to the conserved histidine on the alpha peptides. Only one alpha peptide, α5, contains a phenylalanine at the relevant position to result in a loss of hydrogen bonding and is found in the B800-820 LH2 complex type. The α6, found in the B800-820 and B800-840, may not form a hydrogen bond or may form an alternative hydrogen bond due to a tyrosine at position + 10 preceding a tryptophan at position + 11. The other α peptides of *Alc. vinosum* contain a glycine at position +10, which alternatively may indicate that a glycine at position +10 may be integral to the hydrogen bond formation from the tryptophan. In the absence of a glycine, steric hindrance may prevent the bond formation. This could be further analysed through mutagenasis studies to substitute the tyrosine for the glycine and see whether this red-shifts the B840 BChl Qy absorption band of the B800-840 LH2 complex.

This work contributed to the determination of the origin of the split B800 peak observed in all the LH2 complex types from *Alc. vinosum* (168). Both the peaks within the B800 split peak had been identified as produced from within the same LH2 complex due to the speed of energy transfer from the 796 nm peak to the 802 nm peak (113). Confirmation of the heterogeneity of the LH2 complex types and analysis of the peptides showed that there are two potential B800 BChl binding sites observed in all the LH2 complex types, two aspartic residues or a single aspartic acid residue following an asparagine or glutamine residue (164). These differences in the B800 binding site were postulated as the basis for the split B800 peak. Single molecule spectroscopy performed in collaboration with this work (168) confirmed the high level of heterogeneity within the B800 binding sites as well as the larger ring size of the LH2 complexes of *Alc. vinosum* in comparison to the current LH2 structures (115).

Previous EM work identified two ring sizes in the purified LH2 complex types; a dodecamer or 13-mer and something larger than a nonamer (115). Further work determined that that 13-mers were not electronically favourable and that the potential ring sizes were 8, 9, 10, or 12-mers (119) suggesting that the LH2 complex types from *Alc. vinosum* were most likely dodecamers. This work did not find any indicators that the ring size of the different LH2 complex types identified varied substantially enough to be visualised in purification methods such as size exclusion chromatography. This indicates that *Alc. vinosum* grown under the growth conditions covered in this work only produces LH2 complex types of a single ring size. Small angle neutron scattering or analytical ultracentrifugation could be used to potentially discern the ring size of the different LH2 complex types.

The fluorescence excitation spectrum of the split B800 peak of the B800-850 LH2 complex was reconstructed well using Monte Carlo simulations that factored in potential excitonic coupling between the two binding populations of the B800 BChl. Excitonic coupling of the BChl is observed clearly in the CD spectrum of the LH2 complex types. Previous NIR CD data gathered of the B800-850 LH2 from *Alc. vinosum* (141) observed a negative minimum followed by a small maximum and then

a large maximum before a large minimum, indicating there was no excitonic coupling of the B800 BChl. New data acquired in this work of the LH2 complex types in DDM as opposed to LDAO showed a sigmoidal profile for the B800 double peaks for all three LH2 complex types from *Alc. vinosum*. In data collected previously in this work (Chapter 3, section 3.2.3) LDAO was observed as possibly degrading the 796 nm peak, explaining the loss of the excitonic coupling of the B800 BChl. To confirm the excitonic coupling of the B800 BChl, further work should include hole burning spectroscopy as if the BChl are excitonically coupled both peaks should bleach when a hole is burnt in one peak.

Collaborations within this work illuminated the small but consistent variation within the carotenoid composition of the different LH2 complex types, which showed an increase in the level of carotenoids with longer chain chromophores in the low light LH2 complexes. It was not clear whether the differences in carotenoid composition were due to preferential binding of certain carotenoids by the LH2 complex types or due to different growth conditions upregulating spirilloxanthin. Further work would include sourcing the B800-840 LH2 complex types from low light growth conditions and using HPLC analysis to determine the carotenoid composition and whether there is an increase in the long chain chromophores in other LH2 complex types.

Once the standard LH2 complex types could be produced consistently and the peptide and pigment composition determined, work towards a carotenoidless LH2 complex began. Previous work had used carotenoid biosynthesis inhibition successfully with *Alc. vinosum* (134) and on the relative *Alc. minutissimum* (135). *Alc. vinosum* grew well enough in the presence of DPA and successfully produced carotenoidless LH1 and carotenoid depleted LH2 complexes. Curiously, under high levels of carotenoid biosynthesis inhibition there is a change in the LH2 complexes produced when *Alc. vinosum* is grown under growth conditions that do not produce a B800-850 LH2 complex type. All of the LH2 complexes that were highly carotenoid depleted produced LH2 complexes with strongly red-shifted dimeric BChl Qy peaks, producing “B800-850-like” LH2 complex types when usually a B800-820 or B800-840

LH2 complex should be produced. This occurred in the LH2 complexes produced in both low light and high light grown cells. This indicated that either there were direct effects from the DPA on the regulation or production of the alpha and beta peptides, or that the loss of the carotenoid from the LH2 complex types caused *Alc. vinosum* to shift to producing a B800-850 LH2 complex type. This indicates that the B800-850 LH2 complex is a more structurally stable LH2 complex type than the B800-820 or B800-840. This may be an adaptation for the bacterium to be able to grow at 40℃, as the B800-850c is the only LH2 complex produced under these growth conditions. The B800-850c LH2 complex from *Alc. vinosum* is very similar to the LH2 complex from its thermophilic relative, *Thr. Tepidum* (160). This may indicate that the B800-850 LH2 complex is a more thermostable LH2 complex. To explore this further, thermostability studies using CD on both the B800-820 and B800-850 LH2 complex types would indicate if there are any differences in the stability of the complexes. The carotenoid depleted B800-850a LH2 complex was identical in peptide composition to the standard B800-850a LH2 complex type with the exception that the β5 peptide was absent. This suggests the changes in the ratio of the two BChl Qy absorption bands in the absorption spectrum relate to the loss of the β5 peptide.

The overall aim of this work was to develop a protocol for LH2 reconstitution, and to ascertain whether the LH2 complexes of *Alc. vinosum* were suitable reconstitution candidates. The production of a carotenoid 'knock-out' strain of *Alc. vinosum* was not completed within this work, but through the use of carotenoid biosynthesis inhibition, carotenoid depleted B800-850 LH2 complexes were purified and prepared for reversible dissociation trials. Due to time constraints the protocol could not be optimized, however successful reversible dissociation experiments indicated that the native carotenoids could be reincorporated into the carotenoid depleted LH2 complex types of *Alc. vinosum*. After reversible dissociation only a small level of carotenoid was incorporated regardless of the carotenoid used for reconstitution. However this confirmed the B800-850 LH2 complex from *Alc.vinsoum* as suitable for the development of a reconstitution protocol.

Appendices

Appendix 1

***Alc. vinosum* growth media**

Sodium thiosulphate medium (6)

Solution 1	
Sodium Chloride (NaCl)	60 g
Potassium dihydrogen orthophosphate (KH_2PO_4)	1 g
Dipotassium hydrogen orthophosphate (K_2HPO_4)	1 g
Ammonium Chloride (NH_4Cl)	2 g
Calcium Chloride ($CaCl_2.2H_2O$)	0.33
Magnesium Chloride ($MgCl_2.\ 6H_2O$)	2.033
Make up to 1 L	
Solution 2	
Sodium Thiosulphate ($Na_2S_20_3$)	6 g
Sodium Hydrogen Carbonate ($NaHCO_3$)	8 g
Make up to 1 L	
Solution 3	
Ferrous sulphate ($FeSO_4\ \ .7H_20$)	1.6 g
EDTA	3 g
Make up to 1 L and store in cold room	
Final solution	
Solution 1	1 L
Solution 2	1 L
Solution 3	8 ml
Adjust final pH to 7.8	

Sodium sulphide medium (5)

Solution A

KH_2PO_4	34g
NH_4Cl	34g
KCl	34g

pH to 7.0 and make up to 1 L

Solution B

EDTA	3.0g
$FeSO_3$	1.1g
$CoCl_2$	190mg
$MnCl_2$	50mg
$ZnCl_2$	42mg
$NiCl_2$	24mg
Na_2MoO_4	18mg
H_3BO_3	300mg
$CuCl_2$	2mg

pH to 6.0 and make up to 1 L

Solution C

Vitamin B12	2 mg

Make up to 1 L

Solution D

Na_2S	1.2 g

Make up to 10 ml

Solution A	10 ml
Solution B	1 ml
Solution C	1 ml
Solution D	1.5 ml

Made up to 1 L with deionised water

Appendix 2

LB recipe

Typtone	10 g
Yeast extract	5 g
NaCl	10g

Components were dissolved in 1 L of deionised water and autoclaved at 121-124℃. For LB agar plates 1.5 % (w/v) agar was added before autoclaving.

Reference List

(1) Clayton RK. Photosynthesis: physical mechanisms and chemical patterns. Cambridge: Cambridge University Press; 1980.

(2) Wisniak J. Phlogiston: The rise and fall of a theory. Indian journal of chemical technology 2004;11:732-43.

(3) Dworkin M. Sergei Winogradsky: a founder of modern microbiology and the first microbial ecologist. FEMS Microbiology Reviews 2011;36:364-79.

(4) van Niel CB. On the morphology and physiology of the purple and green sulphur bacteria. Hopkins Marine Station of Stanford University, California; 1931.

(5) Hayashi H, Morita S. Near-infrared absorption spectra of light harvesting bacteriochlorophyll protein complexes from *Chromatium vinosum*. Journal of Biochemistry 1980;88:1251-8.

(6) Malik KA. A modified method for the cultivation of phototrophic bacteria. Journal of microbiological methods 1983;1:343-52.

(7) Pfennig N. *Rhodopseudomonas acidophila*, sp. n., a new species of the budding purple nonsulphur bacteria. Journal of Bacteriology 1969;99(2):597-602.

(8) Angerhofer A, Cogdell RJ, Hipkins MF. A spectral characterisation of the light-harvesting pigment-protein complexes from *Rhodopseudomonas acidophila*. Biochimica et Biophysica Acta 1986;848:333-41.

(9) Henderson R. The structure of the purple membrane from *Halobacterium halobium*: Analysis of the X-ray diffraction pattern. Journal of Microbiology 1974;93:123-38.

(10) Weissgerber T, Renate Zigann, David Bruce, Yun-juan Chang, John C.Detter, Cliff Han, et al. Complete genome sequence of *Allochromatium vinosum* DSM 180. Standards in genomic sciences 2011;5:311-30.

(11) Kilby BA. The photosynthetic bacteria. New York and London: Plenum Press; 1978.

(12) Firsow NN, Drews G. Differentiation of the intracytoplasmic membrane of *Rhodopseudomonas palustris* induced by vairations of oxygen partial pressure or light intensity. Archives of microbiology 1977;115:299-306.

(13) Schumacher A, Drews G. Effects of light intensity on membrane differentiation in *Rhodopseudomonas capsulata*. Biochimica et Biophysica Acta 1979;547:417-28.

(14) Niederman RA. Membrane development in purple photosynthetic bacteria in response to alterations in light intensity and oxygen tension. Photosynthesis research 2013;116:333-48.

(15) Madigan MT, Jung DO. An overview of Purple Bacteria: Systematics, Physiology, and Habitats. In: Hunter CN, Daldal F, Thurnauer M, Beatty JT, editors. The Purple Phototrophic Bacteria.Dordrecht: Springer; 2009. p. 1-15.

(16) Remsen C. Comparative Subcellular Architecture of Photosynthetic Bacteria. In: Clayton RK, Sistrom WR, editors. The Photosynthetic Bacteria.New York and London: Plenum Press; 1978. p. 31-60.
(17) Pierson BK, Sands VM, Frederick JL. Spectral irradiance and distribution of pigments in a highly layered marine microbial mat. Applied and environmental microbiology 1990;56(8):2327-40.
(18) Berg JM, Tymoczko JL, Stryer L. Biochemistry. Sixth ed. New York: W.H. Freeman and Company; 2007.
(19) Brandt U, Trumpower B. The protonmotive Q cycle in mitochondria and bacteria. Critical reviews in Biochemistry and Molecular Biology 1994;29(3):165-97.
(20) Axelrod HL, Abresch EC, Okamura MY, Yeh AP, Rees DC, Feher G. X-ray structure determination of the cytochrome C2: Reaction centre electron transfer complex from *Rhodobacter sphaeroides*. Journal of Molecular Biology 2002;319:501-15.
(21) Mitchell P. Coupling of phosphorylation to electron and hydrogen transfer by a chemi-osmotic type of mechanism. Nature 1961;191:144-8.
(22) Abrahams JP, Leslie AGW, Lutter R, Walker JE. Structure at 2.8 A resolution of F1-ATPase from bovine heart mitochondria. Nature 1994;370:621-8.
(23) Drews G. Structure and functional organisation of the light-harvesting complexes and photochemical reaction centres in membranes of phototrophic bacteria. Microbiological Reviews 1985;49(1):59-70.
(24) Sturgis JN, Tucker JD, Olsen JD, Hunter CN, Niederman RA. Atomic Force Microscopy of native photosynthetic membranes. Biochemistry 2009;48(17):3680-98.
(25) Turro NJ, Ramamurthy V, Scaniano JC. Principles of molecular photochemistry: An introduction. University Science Books; 2009.
(26) Van der Meulen DL, Govindjee. Is there a triplet state in photosynthesis? Journal of scientific and industrial research 1973;32(2):62-9.
(27) Scheer H. Chlorophylls. In: Renger G, editor. Primary process of photosynthesis - Part 1. Principles and applications.Cambridge: The Royal Society of Chemistry; 2008. p. 101-29.
(28) Scheer H, Svec WA, Cope BT, Studier MH, Scott RG, Katz JJ. Structure of bacteriochlorophyll b. Journal of American chemical society 1974;96(11):3714-6.
(29) Gest H, Favinger JL. *Heliobacterium chlorum*, an anoxygenic brownish-green photosynthetic bacterium containing a "new" form of bacteriochlorophyll. Archives of microbiology 1983;136:11-6.
(30) Fujita Y, Bauer CE. The light-independent protochlorophyllide reductase: a nitrogen-like enzyme catalyzing a key reaction for greening in the dark. In: Kadish KM, Smith KM, Guilard R, editors. The Porphyrin Handbook: Chlorophylls and bilins: biosynthesis, synthesis, and degradation.San Diego: Academic Press; 2003. p. 109-53.
(31) Katz JJ, Strain HH, Harkness AL, Studier MH, Svec WA, Janson TR, et al. Esterifying alcohols int he chlorophylls of purple photosynthetic

bacteria. A new chlorophyll, baceriochlorophyll (gg), all-trans-Geranylgeranyl bacteriochlorophyllide a. Journal of the American chemical society 1972;94(22):7938-9.
(32) Parkes-Loach PS, Michalski TJ, Bass WJ, Smith U, Loach PA. Probing the bacteriochlorophyll binding site by reconsititution of the light-harvesting complex of *Rhodospirillum rubrum* with bacteriochlorophyll a analogues. Biochemistry 1990;29:2951-60.
(33) Telfer A, Pascal A, Gall A. Carotenoids in Photosynthesis. In: Britton G, Liaaen-Jensen S, Pfander H, editors. Carotenoids.Berlin: Springer; 2008. p. 265-309.
(34) Cogdell RJ, Howard TD, Isaacs NW, McLuskey K, Gardiner AT. Structural factors which control the position of the Qy absorption band of bacteriochlorophyll a in purple bacterial antenna complexes. Photosynthesis research 2002;74:135-41.
(35) Fowler GJS, Sockalingum GD, Robert B, Hunter CN. Blue shifts in bacteriochlorophyll absorbance correlate with changed hydrogen bonding patterns in light-harvesting 2 mutants of *Rhodobacter sphaeroides* with alterations at a-Tyr-44 and a Tyr45. Biochemistry 1994;299:695-700.
(36) Sturgis JN, Robert B. The role of chromophore coupling in tuning the spectral properties of peripheral light-harvesting protein of purple bacteria. Photosynthesis research 1996;50:5-10.
(37) Young A, Britton G. Carotenoids in photosynthesis. First ed. London: Chapman & Hall; 1993. p. 282-3.
(38) Andersson PO, Gillbro T, Ferguson L, Cogdell RJ. Absorption spectral shifts of carotenoids related to medium polarizability. Photochemistry and photobiology 1991;54(3):353-60.
(39) Cogdell RJ, Frank HA. How carotenoids function in photosynthetic bacteria. Biochimica et Biophysica Acta 1987;895:63-79.
(40) Lang HP, Hunter CN. The relationship between carotenoid biosynthesis and the assembly of the light-harvesting LH2 complex in *Rhodobacter sphaeroides*. Biochemical Journal 1994;298:197-205.
(41) Griffiths M, Sistrom WR, Cohen-Bazire G, Stanier RY. Function of carotenoids in photosynthesis. Nature 1955;176(4495):1211-4.
(42) Cogdell RJ, Howard TD, Bittl R, Schlodder E, Geisenheimer I, Lubitz W. How carotenoids protect bacterial photosynthesis. Philosophical Transactions of the Royal Society 2000;1345-9.
(43) Hashimoto H, Fujii R, Yanagi K, Kusumoto T, Gardiner AT, Cogdell RJ, et al. Structures and functions of carotenoids bound to reaction centres from purple photosynthetic bacteria. Pure Applied Chemistry 2006;78(8):1505-18.
(44) Slouf V, Chabera P, Olsen JD, Martin EC, Qian P, Hunter CN, et al. Photoprotection in a purple phototrophic bacterium mediated by oxygen-dependent alteration of carotenoid excited-state properties. Proceedings of the national academy of science of the united states of america 2012;109(22):8570-5.
(45) Frank HA, Cogdell RJ. Carotenoids in photosynthesis. Photochemistry and photobiology 1996;63(3):257-64.

(46) Kakitani Y, Akahane J, Ishii H, Sogabe H, Nagae H, Koyama Y. Conjugation length dependence of the T1 lifetimes of carotenoids free in solution and incorporated into the LH2, LH1, RC and RC-LH1 complexes: possible mechanisms of triplet-energy dissipation. Biochemistry 2007;46:2181-97.
(47) Magdaong NM, LaFountain AM, Greco JA, Gardiner AT, Carey A, Cogdell RJ, et al. High efficiency light harvesting by carotenoids in the LH2 complex from photosynthetic bacteria: unique adaptation to growth under low-light conditions. The journal of physical chemistry 2014;118:11172-89.
(48) Polivka T, Sundstrom V. Ultrafast dynamics of carotenoid excited states- from solution to natural and artificial systems. Chemical Reviews 2004;104:2021-71.
(49) Ostroumov EE, Mulvaney RM, Anna JM, Cogdell RJ, Scholes GD. Energy transfer pathways in light-harvesting complexes of purple bacteria as revealed by global kinetic analysis of two-dimensional transient spectra. Journal of Physical Chemistry 2013;117:11349-62.
(50) Borland CF, Cogdell RJ, Land EJ, Truscott TG. Bacteriochlorophyll a triplet state and its interactions with bacterial caroteniods and oxygen. Journal of photochemisty and photobiology, B: Biology 1989;3:237-45.
(51) Frank HA, Young AJ, Britton G, Cogdell RJ. The Photochemistry of Carotenoids. Dordrecht: Kluwer; 1999.
(52) Krinsky NI. Non-photosynthetic functions of carotenoids. Philosophical Transactions of the Royal Society 1978;284:581-90.
(53) Foote CS, Denny RW. Chemistry of singlet oxygen. VII. Quenching by B-carotene. Journal of the American chemical society 1968;90(22):6233-5.
(54) Hirayama O, Nakamura K, Hamada S, Kobayasi Y. Singlet oxygen quenching ability of naturally occurring carotenoids. Lipids 1994;29(2):149-50.
(55) Okamura MY, Steiner LA, Feher G. Characterization of reaction centres from photosynthetic bacteria. I. Subunit structure of the protein mediating the primary photochemistry in *Rhodopseudomonas spheroides* R-26. Biochemistry 1974;13(7):1394-403.
(56) Deisenhofer J, Epp O, Miki K, Huber R, Michel H. Structure of the protein subunits in the photosynthetic reaction centre of *Rhodopseudomonas viridis* at 3 A resolution. Nature 1985;318:618-24.
(57) Deisenhofer J, Michel H. The photosynthetic reaction centre from the purple bacterium *Rhodopseudomonas viridis*. Bioscience reports 1988;9(4):383-419.
(58) Hess S, Chachisvilis M, Timpmann K, Jones MR, Fowler GJS, Hunter CN, et al. Temporally and spectrally resolved subpicosecond energy tansfer within the peripheral antenna complex (LH2) and from LH2 to the core antenna complex in photosynthetic purple bacteria. Proceedings of the national academy of science of the united states of america 1995;92:12333-7.

(59) Walz T, Jamieson SJ, Bowers CM, Bullough PA, Hunter N. Projection structures of three photosynthetic complexes from *Rhodobacter sphaeroides*: LH2 at 6 A, LH1 and RC-LH1 at 25 A. Journal of Molecular Biology 1998;282:833-45.
(60) Roszak AW, Howard TD, Southall J, Gardiner AT, Law CJ, Isaacs NW, et al. Crystal structure of the RC-LH1 core complex from *Rhodopseudomonas palustris*. Science 2003;302:1969-72.
(61) Niwa S, Yu L, Takeda K, Hirano Y, Kawakami T, Wang-Otomo Z, et al. Structure of the LH1-RC complex from *Thermochromatium tepidum* at 3.0 A. Nature 2014;508:228-32.
(62) McDermott G, Prince SM, Freer AA, Hawthornwait-lawless AM, Papiz MZ, Cogdell RJ, et al. Crystal structure of an integral membrane light-harvesting complex from photosynthetic bacteria. Nature 1995;374:517-21.
(63) Prince SM, Papiz MZ, Freer AA, McDermott G, Hawthornthwaite-Lawless AM, Cogdell RJ, et al. Apoprotein structure in the LH2 complex from *Rhodopseudomonas acidophila* strain 10050: modular assembly and protein pigment interactions. Journal of Molecular Biology 1997;268:412-23.
(64) Evans K, Fordham-Skelton AP, Mistry H, Reynolds CD, Lawless AM, Papiz MZ. A bacteriophytochrome regulates the synthesis of LH4 complexes in *Rhodopseudomonas palustris*. Photosynthesis research 2005;85:169-80.
(65) Gabrielsen M, Gardiner AT, Cogdell RJ. Peripheral complexes of purple bacteria . In: Hunter N, Daldal F, Thurnauer M, Beatty J, editors. The purple phototrophic bacteria. Springer science; 2009. p. 135-53.
(66) Aagaard J, Sistrom WR. Control of synthesis of reaction centre bacteriochlorophyll in photosynthetic bacteria. Photochemistry and photobiology 1972;15:209-25.
(67) Bauer CE, Bird TH. Regulatory circuits controlling photosynthesis gene expression. Cell 1996;85:5-8.
(68) Chang MC, Meyer L, Loach PA. Isolation and characterisation of a structural subunit from the core light-harvesting complex of *Rhodobacter sphaeroides* 2.4.1 and *puc*705-BA. Photochemistry and photobiology 1990;51(4):873-81.
(69) Feick R, Drews G. Protein subunits of bacteriochlorophylls B802 and B855 of the light-harvesting complex II of *Rhodopseudomonas capsulata*. ZEITSCHRIFT FUR NATURFORSCHUNG C-A JOURNAL OF BIOSCIENCES 1978;34:196-9.
(70) Kiley PJ, Donohue TJ, Havelka WA, Kaplan S. DNA sequence and In vitro expression of the B875 light-harvesting polypeptides of *Rhodobacter sphaeroides*. Journal of Bacteriology 1987;769(2):742-50.
(71) Rucker O, Kohler A, Behammer B, Sichau K, Overmann J. *Puf* operon sequences and inferred structures of light-harvesting complexes of three closely related *Chromatiaceae* exhibiting different absorption characteristics. Archives of microbiology 2012;194:123-34.

(72) Cogdell RJ, Isaacs NW, Freer AA, Arrelano J, Howard TD, Papiz MZ, et al. The structure and function of the LH2 (B800-850) complex from the purple photosynthetic bacterium *Rhodospeudomonas acidophila* strain 10050. Progess in biophysics and molecular biology 1997;68(1):1-27.
(73) Francia F, Wang J, Venturoli G, Melandri BA, Barz WP, Oesterhelt D. The reaction centre-LH1 antenna complex of *Rhodobacter sphaeroides* contains one PufX molecule which is involved in dimerisation of this complex. Biochemistry 1999;38:6834-45.
(74) Sener M, Hsin J, Trabuco LG, Villa E, Qian P, Hunter CN, et al. Structural model and excitonic properties of the dimeric RC-LH1-PufX complex from *Rhodobacter sphaeroides*. Chemical physics 2009;357:188-97.
(75) Qian P, Papiz MZ, Jackson PJ, Brindley AA, Ng IW, Olsen JD, et al. Three-dimensional structure of the *Rhodobacter sphaeroides* RC-LH1-PufX complex: dimerisation and quinone channels promoted by PufX. Biochemistry 2013;52:7575-85.
(76) Cogdell RJ, Lindsay G, MacDonald W, Reid GP. The subunit structure of the B800-850 light-harvesting pigment protein complex from *Rhodopseudomonas sphaeroides* strain 2.4.1. Biochemical Society Transactions 1979;7:184-7.
(77) Youvan DC, Ismail S. Light-harvesting II (B800-850 complex) structural genes from *Rhodopseudomonas capsulata*. Proceedings of the national academy of science of the united states of america 1985;82:58-62.
(78) Tichy H, Oberle B, Stiehle H, Schiltz E, Drews G. Genes downstream from *pucB* and *pucA* are essential for formation of the B800-850 complex of *Rhodobacter capsulatus*. Journal of Bacteriology 1989;171(9):4914-22.
(79) Tichy H, Albien K, Gad'on N, Drews G. Analysis of the *Rhodobacter capsulatus puc* operon: the *pucC* gene plays a central role in the regulation of LH2 (B800-850 complex) expression. The EMBO Journal 1991;10(10):2949-55.
(80) Koepke J, Hu X, Muenke C, Schulten K, Michel H. The crystal structure of the light-harvesting complex II (B800-850) from *Rhodospirillum molischianum*. Structure 1996;4(5):581-97.
(81) Cranston LJ, Roszak AW, Cogdell RJ. Crystallisation and preliminary X-ray diffraction analysis of the peripheral light-harvesting complex LH2 from *marichromatium purpuratum*. Acta Crystallographica 2014;F70:808-13.
(82) Cogdell RJ, Crofts AR. Analysis of the pigment content of an antenna pigment-protein complex from three strains of *Rhodopseudomonas sphaeroides*. Biochimica et Biophysica Acta 1978;502:409-16.
(83) Gall A, Henry S, Takaichi S, Robert B, Cogdell RJ. Preferential incorporation of coloured-carotenoids occurs in the LH2 complexes from non-sulphur purple bacteria under carotenoid-limiting conditions. Photosynthesis research 2005;86:25-35.
(84) Cogdell RJ, Isaacs NW, Howard TD, McLuskey K, Fraser NJ, Prince SM. How photosynthetic bacteria harvest solar energy. Journal of Bacteriology 1999;181(13):3869-79.

(85) Cogdell RJ, Gall A, Kohler J. The architecture and function of the light-harvesting apparatus of purple bacteria: from single molecules to *in vivo* membranes. Quarterly reviews of biophysics 2006;39:227-324.
(86) Fowler GJS, Visschers RW, Grief GG, van Grondelle R, Hunter CN. Genetically modified photosynthetic antenna complexes with blueshifted absorbance bands. Nature 1992;355:848-50.
(87) Sturgis JN, Robert B. Pigment binding-site and electronic properties in light-harvesting proteins of purple bacteria. Journal of Physical Chemistry 1997;101:7227-31.
(88) Sturgis JN, Jirsakova V, Reiss-Husson F, Cogdell RJ, Robert B. Structure and properties of the bacteriochlorophyll binding site in peripheral light-harvesting complexes of purple bacteria. Biochemistry 1995;34:517-23.
(89) Iwata K, Hayashi H, Tasumi M. Resonance Raman studies of the conformations of all-*trans* carotenoids in light-harvesting systems of photosynthetic bacteria. Biochimica et Biophysica Acta 1985;810:269-73.
(90) Koyama Y. Structures and functions of carotenoids in photosynthetic systems. Journal of photochemisty and photobiology, B: Biology 1991;9:265-80.
(91) Sturgis JN, Niederman RA. Organisation and assembly of light-harvesting complexes in the purple bacterial membrane. In: Hunter N, Daldal F, Thurnauer M, Beatty J, editors. The purple phototrophic bacteria. 2009. p. 254-73.
(92) Saleh MH, Tan B. Separation and identification of Cis/Trans carotenoid isomers. Journal of Agricultural and Food Chemistry 1991;39:1438-43.
(93) Gardiner AT, Cogdell RJ, Takaichi S. The effect of grown conditions on the light-harvesting apparatus in *Rhodospeudomonas acidophila*. Photosynthesis research 1993;38:159-67.
(94) Sauer PRR, Lottspeich F, Unger E, Mentele R, Michel H. Deletion of a B800-850 light-harvesting complex in *Rhodospirillum molischianum* DSM119 leads to "Revertants" expressing a B800-820 complex: insights into pigment binding. Biochemistry 1996;35:6500-7.
(95) Mascle-Allemand C, Duquesne K, Lebrun R, Scheuring S, Sturgis JN. Antenna mixing in photosynthetic membranes from *Phaeospirillum molischianum*. Biochemistry 2010;107(12):5357-62.
(96) Deinum G, Otte SCM, Gardiner AT, Aartsma TJ, Cogdell RJ, Amesz J. Antenna organization of *Rhodopseudomonas acidophila*: a study of the excitation migration. Biochimica et Biophysica Acta 1991;1060:125-31.
(97) Gardiner AT, Takaichi S, Cogdell RJ. The effect of changes in light intensity and temperature on the peripheral antenna of *Rhodopseudomonas acidophila*. Biochemical Society Transactions 1992;21.
(98) Heinemeyer E, Schmidt K. Changes in carotenoid biosynthesis caused by variations of growth conditions in cultures of *Rhodopseudomonas acidophila* strain 7050. Archives of microbiology 1983;134:217-21.
(99) McLuskey K, Prince SM, Cogdell RJ, Isaacs NW. The crystallographic structure of the B800-820 LH3 light-harvesting complex from the

purple bacteria *Rhodopseudomonas acidophila* strain 7050. Biochemistry 2001;40:8783-9.
(100) Tadros MH, Waterkamp K. Multiple copies of the coding regions for the light-harvesting B800-850 alpha and beta polypeptides are present in the *Rhodopseudomonas palustris* genome. The EMBO Journal 1989;8(5):1303-8.
(101) Brotosudarmo THP, Kunz R, Böhm P, Gardiner AT, Moulisova V, Cogdell RJ, et al. Single-molecule spectroscopy reveals that individual low-light LH2 complexes from *Rhodopseudomona palustris* 2.1.6. have a heterogeneous polypeptide composition. Biophysical journal 2009;97:1491-500.
(102) Tadros MH, Katsiou E, Hoon MA, Yurkova N, Ramji DP. Cloning of a new antenna gene cluster and expression analysis of the antenna gene family of *Rhodopseudomonas palustris*. European Journal of biochemistry 1993;217:867-75.
(103) Evans MB, Hawthornwaite AM, Cogdell RJ. Isolation and characterisation of the different B800-850 light-harvesting complexes from low- and high-light grown cells of *Rhodopseudomonas palustris*, strain 2.1.6. Biochimica et Biophysica Acta 1990;1016:71-6.
(104) Nishimura Y, Shimada K, Yamazaki I, Mimuro M. Energy transfer processes in *Rhodopseudomonas palustris* grown under low-light conditions. Heterogeneous composition of LH2 complexes and parallel energy flow pathways. FEBS 1993;329(3):319-23.
(105) Gall A, Robert B. Characterisation of the different peripheral light-harvesting complexes from high- and low-light grown cells from *Rhodopseudomonas palustris*. Biochemistry 1999;38:5185-90.
(106) Moulisova V, Luer L, Hoseinkhani S, Brotosudarmo THP, Collins AM, Lanzani G, et al. Low light adaptation: Energy transfer processes in different types of light harvesting complexes from *Rhodopseudomonas palustris*. Biophysical journal 2009;97:3019-28.
(107) Tharia HA, Nightingale TD, Papiz MZ, Lawless AM. Characterisation of hydrophobic peptides by RP-HPLC from different spectral forms of LH2 isolated from *Rps. palustris*. Photosynthesis research 1999;61:157-67.
(108) Vredenberg WJ, Amesz J. Absorption bands of bacteriochlorophyll types in purple bacteria and their response to illumination. Biochimica et Biophysica Acta 1966;126:244-53.
(109) Mechler B, Oelze J. Differentiation of the photosynthetic apparatus of *Chromatium vinosum*, strain D. I. The Influence of growth conditions. Archives of microbiology 1978;78(118):91-7.
(110) Bril C. Studies on bacterial chromatophores: I. reversible disturbance of transfer of electronic excitation energy between bacteriochlorophyll types in *Chromatium*. Biochimica et Biophysica Acta 1959;39:287-96.
(111) Cusanovich MA, Kamen MD. Light-induced electron transport in *Chromatium* strain D: I. Isolation and characterisation of *Chromatium* chromatophores. Biochimica et Biophysica Acta 1967;153:376-96.
(112) Hendley DD. Endogenous Fermentation in *Thiorhodaceae*. Journal of Bacteriology 1955;70:625-34.

(113) Niedzwiedzki DM, Bina D, Picken N, Honkanen S, Blankenship RE, Holten D, et al. Spectroscopic studies of 2 spectral variants of LH2 from *Allochromatium vinosum*. Biochimica et Biophysica Acta 2012;1817:1576-87.
(114) Cogdell RJ, Scheer H. Circular dichroism of light-harvesting complexes from purple photosynthetic bacteria. Photochemistry and photobiology 1985;42(6):669-78.
(115) Kereiche S, Bourinet L, Keegstra W, Arteni AA, Verbavatz J, Boekema EJ, et al. The peripheral light-harvesting complexes from purple sulphur bacteria have different 'ring' sizes. FEBS Letters 2008;582:3650-6.
(116) Kennis JTM, Streltsov AM, Vulto SIE, Aartsma TJ, Nozawa T, Amesz J. Femtosecond dynamics in isolated LH2 complexes of various species of purple bacteria. Journal of Physical Chemistry 1997;101:7827-34.
(117) Schmidt K. Die carotenoide der thiorhodaceae II. Carotinoidzusammensetzung von Thiospirillum jenense Winogradsky und *Chromatium vinosum* Winogradsky. Archiv fur mikrobiologie 1963;46:127-37.
(118) Noguchi T, Hayashi H, Tasumi M. Factors controlling the efficiency of energy transfer from carotenoids to bacteriochlorophyll in purple photosynthetic bacteria. Biochimica et Biophysica Acta 1990;1017:280-90.
(119) Cleary L, Chen H, Chuang C, Silbey RJ, Cao J. Optimal fold symmetry of LH2 rings on a photosynthetic membrane. Proceedings of the national academy of science of the united states of america - biophysics and computational biology 2013;110(21):8537-42.
(120) Miller JF, Hinchigeri SB, Parkes-Loach PS, Callahan PM, Sprinkle JR, Riccobono JR, et al. Isolation and characterisation of a subunit form of the light-harvesting complex of *Rhodospirillum rubrum*. Biochemistry 1987;26:5055-62.
(121) Parkes-Loach PS, Sprinkle JR, Loach PA. Reconstitution of the B873 Light-harvesting complex of *Rhodospirillum rubrum* from the separately isolated a- and b-polypeptides and bacteriochlorophyll a. Biochemistry 1988;27:2718-27.
(122) Davis CM, Bustamante PL, Loach PA. Reconstitution of the bacterial core light-harvesting complexes of *Rhodobacter sphaeroides* and *Rhodospirillum rubrum* with isolated alpha and beta-polypeptides, bacteriochlorophyll a, and carotenoid. The journal of biological chemistry 1995;270(11):5793-804.
(123) Pandit A, Visschers RW, van Stokkum IHM, Kraayenhof R, van Grondelle R. Oligomerisation of Light-harvesting I antenna peptides of *Rhodospirillum rubrum*. Biochemistry 2001;40:12913-24.
(124) Pandit A, van Stokkum IHM, Georgakopoulou S, van der Zwan G, van Grondelle R. Investigations of intermediates appearing in the reassociation of the light-harvesting 1 complex of *Rhodospirillum rubrum*. Photosynthesis research 2003;75:235-48.

(125) Heller BA, Loach PA. Isolation and characterisation of a subunit form of the B875 light-harvesting complex from *Rhodobacter capsulatus*. Photochemistry and photobiology 1990;51(5):621-7.
(126) Loach PA, Parkes-Loach PS. Structure-Function relationships in bacterial light-harvesting complexes investigated by reconstitution techniques. In: Hunter CN, Daldal F, Thurnauer M, Berg JM, editors. The Purple Phototropic Bacteria. Springer Science; 2009. p. 181-98.
(127) Todd JB, Parkes-Loach PS, Leykam JF, Loach PA. *In vitro* reconstitution of the core and peripheral light-harvesting complexes of *Rhodospirillum molischianum* from separately isolated components. Biochemistry 1998;37:17458-68.
(128) Toropygina OA, Makhneva ZK, Moskalenko AA. Reconstitution of okenone into light harvesting complexes from *Allochromatium minutissimum*. Biochemistry 2005;70(11):1231-7.
(129) Fiedor L, Scheer H. Trapping of an assembly intermediate of photosynthetic LH1 antenna beyond B820 subunit. The journal of biological chemistry 2006;280(22):20921-6.
(130) Clayton RK. Absorption spectra of photosynthetic bacteria and their chlorophylls. In: Gest H, San Pietro A, Vernon LP, editors. Bacterial photosynthesis.Yellow Springs, Ohio: The Antioch Press; 1963.
(131) Ghosh R, Hauser H, Bachofen R. Reversible dissociation of the B873 light-harvesting complex from *Rhodospirillum rubrum* G9. Biochemistry 1987;27:1004-14.
(132) Drews G, Leutiger I, Ladwig R. Production of Protochlorophyll, Protophcophytin, and Bacteriochlorophyll by the Mutant A la of *Rhodopseudomonas capsulata*. Archives of microbiology 1971;76:349-63.
(133) Jensen SL, Stanier RY, Cohen-Bazire G. Inhibition of carotenoid synthesis in photosynthetic bacterium. Nature 1958;181:250-2.
(134) Bril C. Studies on bacterial chromatophores: II. Energy transfer and photooxidative bleaching of bacteriochlorophyll in relation to structure in normal and carotenoid-depleted *chromatium*. Biochimica et Biophysica Acta 1962;66:50-60.
(135) Makhneva Z, Bolshakov M, Moskalenko A. Heterogeneity of carotenoid content and composition in LH2 of the purple sulphur bacterium *Allochromatium minutissimum* grown under carotenoid-biosynthesis inhibition. Photosynthesis research 2008;98:633-41.
(136) Britton G, Liaaen-Jensen S, Pfander H. Carotenoids: Natural functions. Berlin: Birkhauser.; 2008.
(137) Moskalenko AA, Makhneva ZK. Light-harvesting complexes from purple sulphur bacteria *Allochromatium minutissimum* assembled without carotenoids. Journal of photochemisty and photobiology, B: Biology 2011;108:1-7.
(138) Serrano W, Amann R, Rossello-Mora R, Herbert RA, Fischer U. The genus *Allochromatium* (*Chromatiales Chromatiaceae*) revisited: A study on its intragenic structure based on multilocus sequence analysis (MLSA) and DNA-DNA hybridisation (DDH). Systematic and Applied Microbiology 2011;34:590-4.

(139) Law CJ, Cogdell RJ. The effect of chemical oxidation on the fluorescence of the LH1 (B880) complex from the purple bacterium *Rhodobium marinum*. FEBS Letters 1998;432:27-30.
(140) Pucheu NL, Kerberm NL, Garcia AF. Isolation and purification of Reaction Centre from *Rhodopseudomonas viridis* NHTC 133 by means of LDAO. Archives of microbiology 1976;109:301-5.
(141) Georgakopoulou S, Frese RN, Johnson E, Koolhaus C, Cogdell RJ, van Grondelle R, et al. Absorption and CD Spectroscopy and Modeling of Various LH2 Complexes from Purple Bacteria. Biophysical journal 2002;82:2184-97.
(142) Sambrook J, Russell DW. Preparation and analysis of Eukaryotic genomic DNA. Molecular cloning A laboratory manual. Third ed. New York: Cold Spring Harbor Laboratory Press; 2001. p. 6.4-6.11.
(143) Heckman KL, Pease LR. Gene splicing and mutagenesis by PCR-driven overlap extension. Nature Protocols 2007;2(4):924-32.
(144) Schafer A, Tauch A, Jager W, Kalinowski J, Thierbach G, Puhler A. Small mobilisable multi-purpose cloning vectors derived from the *Escherichia coli* plasmids and pK18 and pK19: selectrion of defined deletions in the chromosome of *Corynebacterium glutamicum*. Gene 1994;145:69-73.
(145) Sambrook J, Russell DW. Plasmids and their usefulness in molecular cloning. Molecular Cloning A Laboratory Manual. Third ed. New York: Cold Spring Harbor Laboratory Press; 2001. p. 1.123-1.129.
(146) Thornber JP. Photochemical reactions of Purple Bacteria as revealed by studies of three spectrally different carotenobacteriochlorophyll-protein complexes Isolated from *Chromatium*, strain D. Biochemistry 1970;9(13):2688-98.
(147) Goodwin TW, Osman HG. Studies in carotenogenesis 9. General cultural conditions controlling carotenoid (spirilloxanthin) synthesis in the photosynthetic bacterium *Rhodospirillum rubrum*. Biochemistry 1952;53:541-6.
(148) Tonn SJ, Gogel GE, Loach PA. Isolation and Characterization of an Organic Solvent Soluble Polypeptide Component from Photoreceptor Complexes of *Rhodospirillum rubrum*. Biochemistry 1977;16(5):877-85.
(149) Edelhoch H. Spectroscopic determination of tryptophan and tyrosine in proteins. Biochemistry 1967;6(7):1948-54.
(150) Pace CN, Vajdos F, Fee L, Grimsley G, Gray T. How to measure and predict the molar absorption coefficient of a protein. Protein Science 1995;4:2411-23.
(151) van der Rest M, Gingras G. The pigment complement of the photosynthetic reaction centre isolated from *Rhodospirillum rubrum*. The journal of biological chemistry 1974;249(20):6446-53.
(152) Clayton RK, Clayton BJ. B850 pigment-protein complex of *Rhodopseudomonas sphaeroides*: Extinction coefficients, circular dichroism, and the reversible binding of bacteriochlorophyll. Proceedings of the national academy of science of the united states of america - biological sciences 1981;78(9):5583-7.

(153) Hayashi H, Nozawa T, Hatano M, Morita S. Circular Dichroism of bacteriochlorophyll a in light harvesting bacteriochlorophyll protein complexes from *Chromatium vinosum*. Biochemistry 1981;89:1853-61.
(154) Papiz MZ, Prince SM, Howard T, Cogdell RJ, Isaacs NW. The structure and thermal motion ofthe B800-850 LH2 complex from *Rps. acidophila* at 2.0 A resolution and 100 K: New structural features and functionally revelant motions. Journal of Molecular Biology 2003;326:1523-38.
(155) Parson WW. The role of P870 in bacterial photosynthesis. Biochimica et Biophysica Acta 1968;153:248-59.
(156) Brotosudarmo THP, Collins AM, Gall A, Roszak AW, Gardiner AT, Blankenship RE, et al. The light intensity under which cells are grown controls the type of peripheral light-harvesting complexes that are assembled in a purple photosynthetic bacterium. Biochemistry 2011;440:51-61.
(157) Weissgerber T, Dobler N, Polen T, Latus J, Stockdreher Y, Dahl C. Genome-wide transcriptional profiling of the purple sulphur bacterium *Allochromatium vinosum* DSM 180 during growth on different reduced sulphur compounds. Journal of Bacteriology 2013;195:4231-45.
(158) Bioedit a user-friendly biological sequence alignment editor and analysis program for Windows 95/98/NT. Nucl. Acids. Symp. Ser. 41:95-98). [computer program]. 1999.
(159) Mulvaney RM. Studies of light harvesting complexes from purple photosynthetic bacteria. University of Glasgow; 2013.
(160) Sekine F, Horiguchi K, Kashino Y, Shimizu Y, Yu L, Kobayashi M, et al. Gene sequencing and characterisation of the light-harvesting complex 2 from thermophilic purple sulphur bacterium *Thermochromatium tepidum*. Photosynthesis research 2012;111:9-18.
(161) Wagner-Huber R, Brunisholz RA, Bissig I, Frank G, Suter F, Zuber H. The primary structure of the antenna polypeptides of *Ectothiorhodospira halochloris* and *Ectothiorhodospira halophilaa*. European Journal of biochemistry 1992;205:917-25.
(162) Wang Z, Shimonaga M, Muraoka Y, Kobayashi M, Nozawa T. Methionine oxidation and its effect on the stability of a reconstituted subunit of the light-harvesting complex from *Rhodospirillum rubrum*. European Journal of biochemistry 2001;268:3375-82.
(163) Wang Z, Shimonaga M, Suzuki H, Kobayashi M, Nozawa T. Purification and characterisation of the polypeptides of core light-harvesting complexes from purple sulphur bacteria. Photosynthesis research 2003;78:133-41.
(164) Carey A, Hacking K, Picken N, Honkanen S, Kelly S, Niedzwiedzki D, et al. Characterisation of the LH2 spectral variants produced by the photosynthetic purple sulphur bacterium *Allochromatium vinosum* . Biochimica et Biophysica Acta 2014;1837:1849-60.
(165) Wang Z, Shimonaga M, Kobayashi M, Nozawa T. N-terminal methylation of the core light-harvesting complex in purple photosynthetic bacteria. FEBS Letters 2002;519:164-8.
(166) K.Schmidt. Die carotenoide der thiorhodaceae II. Carotinoidzusammensetzung von Thiospirillum jenense Winogradsky

und Chromatium vinosum Winogradsky. Archiv fur mikrobiologie 1963;46:127-37.

(167) Magdaong NM, LaFountain AM, Hacking K, Niedzwiedzki D, Gibson GN, Cogdell RJ, et al. Spectral heterogeneity and carotenoid-to-bacteriochlorophyll energy transfer in LH2 light-harvesting complexes from *Allochromatium vinosum*. Photosynthesis research 2016.

(168) Lohner A, Carey A, Hacking K, Picken N, Kelly S, Cogdell RJ, et al. The origin of the split B800 absorption peak in the LH2 complexes from *Allochromatium vinosum*. Photosynthesis research 2015;123:23-31.

(169) Hofmann C, Ketelaars M, Matsushita M, Michel H, Aartsma TJ, Kohler J. Single-molecule study of the electronic couplings in a circular array of molecules: Light-Harvesting-2 complex from *Rhodospirillum molischianum*. Physical review letters 2003;90(1):1-4.

(170) Sauer K, Cogdell RJ, Prince SM, Freer AA, Isaacs NW, Scheer H. Structure-based calculations of the optical spectra of the LH2 bacteriochlorophyll-protein complex from *Rhodopseudomonas acidophila*. Photochemistry and photobiology 1996;64(3):564-76.

(171) Koolhaus MHC, van der Zwan G, Frese RN, van Grondelle R. Red shift of the zero crossing in the CD spectra of the LH2 antenna complex of *Rhodopseudomonas acidophila*: a structure based study. Journal of Physical Chemistry 1997;101:7262-70.

(172) Olsen JD, Sturgis JN, Westerhuis WHJ, Fowler GJS, Hunter CN, Robert B. Site-directed modification of the ligands to the bacteriochlorophylls of the light-harvesting LH1 and LH2 complexes of *Rhodobacter sphaeroides*. Biochemistry 1997;36:12625-32.

(173) Naveke A, Lapouge K, Sturgis JN, Hartwich G, Simonin I, Scheer H, et al. Resonance Raman spectroscopy of metal-substituted bacteriochlorophylls: Characterisation of Raman bands sensitive to bacteriochlorin conformation. Journal of Raman spectroscopy 1997;28:599-604.

(174) Collins AM, Qian P, Tang Q, Bocian DF, Hunter NC, Blankenship RE. Light-harvesting antenna system from the phototrophic bacterium *Roseiflexus castenholzii*. Biochemistry 2010;49:7524-31.

(175) Parkes-Loach PS, Majeed AP, Law CJ, Loach PA. Interactions stabilising the structure of the core light-harvesting complex (LH1) of the photosynthetic bacteria and its subunit (B820). Biochemistry 2004;43:7003-16.

(176) Goodwin TW, Osman HG. Studies in carotenogenesis: General cultural conditions controlling carotenoid (spirilloxanthin) synthesis in the photosynthetic bacterium *Rhodospirillum rubrum*. Biochemical Journal 1953;53(4):541-6.

(177) Moskalenko A, Toropygina OA, Zhuravleva ZA, Erokhin YE. Effect of carotenoids on the interaction between pigment-protein complexes in membranes of the sulphur photosynthetic bacterium *Chromatium minutissimum*. Doklady Biochemistry and Biophysics 2001;381:423-6.

(178) Theiss C, Leupold D, Moskalenko AA, Razjivin AP, Eichler HJ, Lokstein H. Femtosecond spectroscopy of native and carotenoidless purple-

bacterial LH2 clarifies functions of carotenoids. Biophysical journal 2008;94:4808-11.

(179) Georgakopoulou S, van der Zwan G, Olsen JD, Hunter CN, Niederman RA, van Grondelle R. Investigation of the effects of different carotenoids on the absorption and CD signals of light-harvesting 1 complexes. Journal of Physical Chemistry 2006;110:3354-61.

(180) da Graca Miguel M, Eidelman O, Ollivon M, Walter A. Temperature dependence of the vesicle-micelle transition of egg phosphatidylcholine and octyl glucoside. Biochemistry 1989;28:8921-8.

(181) Cogdell RJ, Brotosudarmo THP, Gardiner AT, Sanchez PM, Cronin L. Artificial photosynthesis - solar fuels: current status and future prospects. Biofuels 2010;1(6):861-76.

(182) Kramer H, Amesz J. Antenna organisation in the purple sulphur bacteria *Chromatium tepidum* and *Chromatium vinosum*. Photosynthesis research 1996;49:237-44.